AD-A085 478 ROYAL AIRCRAFT ESTABLISHMENT FARNBOROUGH (ENGLAND) F/G 17/7
CONTRIBUTIONS TO THE UK MICROWAVE LANDING SYSTEM RESEARCH AND D--ETC(U)
MAY 79 J M JONES
UNCLASSIFIED RAE-TR-79052-VOL-1 DRIC-BR-73155 NL

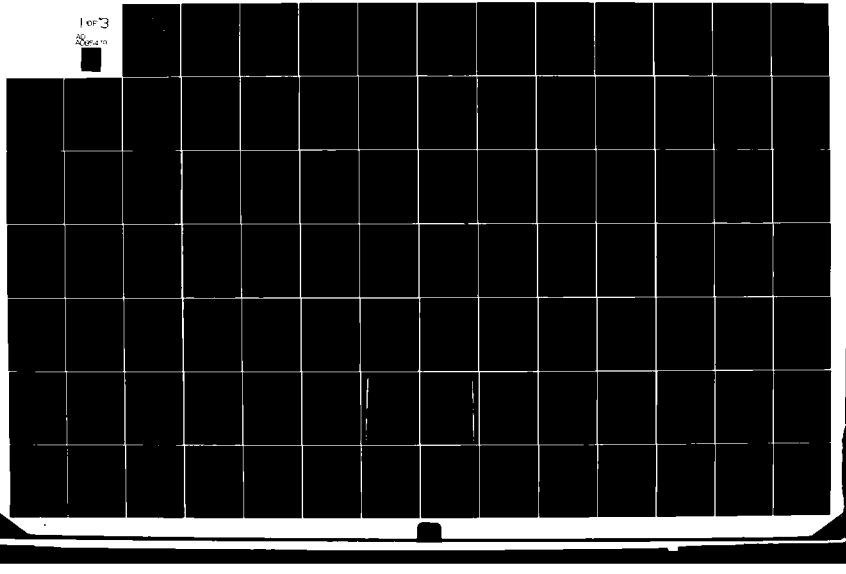

ROYAL AIRCRAFT ESTABLISHMENT

*

Technical Report 79052

May 1979

CONTRIBUTIONS TO THE UK MICROWAVE LANDING SYSTEM RESEARCH AND DEVELOPMENT PROGRAMME 1974 TO 1978

by

J.M. Jones

VOLUME 1

*

Procurement Executive, Ministry of Defence
Farnborough, Hants

UDC 621.396.933.23 : 527.6 : 621.396.962.23 : 621.391.826.2 : 621.3.029.64

ROYAL AIRCRAFT ESTABLISHMENT

Technical Report 79052

Received for printing 15 May 1979

CONTRIBUTIONS TO THE UK MICROWAVE LANDING SYSTEM RESEARCH AND DEVELOPMENT PROGRAMME 1974 TO 1978

by

J. M. Jones

SUMMARY

In support of the UK MLS programme, Doppler Microwave Landing System (DMLS) equipment operating on both frequency division and time division multiplex formats has been extensively evaluated by means of analysis, ground and flight tests and hybrid simulation. The results of this programme have shown that the use of the Doppler technique leads to simple and reliable equipment with performance well inside the operational requirements. In particular, a full understanding of the possible environmental effects on system performance at 5 GHz has been obtained.

Departmental Reference: Rad-Nav 79

LIST OF CONTENTS

79052

Pages 4 and 140 are left blank intentionally

LIST OF CONTENTS (concluded)

1 INTRODUCTION

1.1 General background

During the period from April 1974 to April 1978 the Microwave Landing System (MLS) Group of RN2 Division was totally committed to supporting the United Kingdom submission of the Doppler Microwave Landing System (DMLS)[1] to the International Civil Aviation Organisation (ICAO). Table 1.1 provides an overview of the significant events in this period, while Appendix A provides a more detailed diary.

At the All Weather Operations Divisional Meeting held in Montreal during April 1978, delegates from 71 States voted to recommend the adoption of the Time Reference Scanning Beam System proposed by USA and Australia as the future ICAO approved microwave aid. The voting was 39 for TRSB and 24 for DMLS with eight abstentions. As a result of this vote, development of DMLS has ceased. The objectives of issuing a comprehensive report at this stage are as follows:

(a) To ensure that the results of the R & D programme are properly documented and freely available to all interested parties, since the UK submission document[1], which contains much of the data, is not generally available.

(b) To highlight information obtained which is generally applicable to DMLS and TRSB.

(c) To identify ways in which the DMLS technique can be significantly improved, since it may find other applications where very high accuracy angle measurements are required.

1.2 Report structure

From Table 1.1 and Appendix A it can be seen that the reporting period falls naturally into three parts:

(i) The period from early 1974 until April 1976 covering the installation and testing of the DMLS frequency division multiplex system. Results from this system provided the main supporting information for the UK submission to ICAO.

(ii) The period from April 1976 to June 1977 covering the basic testing of the time division multiplex system, which was a practical realisation of the actual system proposed by the UK.

(iii) The period from June 1977 to April 1978 covering the evaluation of the TDM system at a range of airports and comparative trials with TRSB.

4 - Blank

Table 1.1

MLS programme overview

1974		
	April	- Start of FDM DMLS trials
	September	- London meeting AWOP WGA
	October → December	- USA internal system evaluation
1975		
	January	- USA internal choice of TRSB
	February	- Melbourne meeting AWOP WGA
	December	- Nominal date for full system submissions to ICAO
1976		
	February	- Braunchweig meeting AWOP WGA end of FDM DMLS trials
	May	- Washington meeting AWOP WGA TDM DMLS installed at Bedford
	July	- Hague meeting AWOP WGA
	November	- London meeting AWOP WGA
1977		
	March	- Montreal AWOP 6
	June	- Start of DMLS typical airport trials
1978		
	April	- Montreal AWOD meeting

Following a description of the basic DMLS technique, the first two periods are dealt with chronologically. The report gives only a survey of the information obtained from trials at operational airports, full details being given in individual site reports[2-9].

In reading this Report it should be remembered that it is not intended to provide a complete description of all the UK work on MLS. The main areas of RAE technical responsibility were:

(a) System analysis;
(b) Flight and ground trials;
(c) Data reduction and analysis;
(d) Hybrid simulation and multipath analysis.

In order to present a self-contained document the actual DMLS equipments are described in some detail.

1.3 Operational requirement

The basic coverage requirements for the MLS are illustrated in Fig 1.1, these have been derived directly from the ICAO Operational Requirement (OR).

The OR did not define system accuracy in detail and, as such, actual quantified requirements were generated at the Melbourne meeting of Working Group A (WGA) in February 1975. The following sections are a *direct reproduction* of the relevant sections of the Melbourne report, since these accuracy values became the yardstick against which system performance was judged.

1.3.1 Approach azimuth accuracy

At touchdown the accuracy of the total system for C/STOL aircraft should be such that twice the standard deviation of positional error in the across-track direction should not exceed 8.6 m (28 ft). Of this, the landing system should contribute only a fraction. In addition, the new landing system should meet or exceed the cross-track accuracy requirements for a Category III ILS.

Allowing a 2σ error of 6.1 m (20 ft) leaves a 2σ error of 6.1 m (20 ft) for wind gusts, autopilot errors and other non-landing system errors. Since the proportion of bias and noise effects the acceptability of the signal, the two are specified separately, in approximately equal parts (see Table 1.2).

Since runways up to 4200 m (14000 ft) should be accommodated, and assuming the azimuth facility to be positioned 300 m (1000 ft) beyond the stop end of the runway, the guidance error (2σ) shall be less than 0.076°; of this, the bias shall be less than 0.054°, and the noise (2σ) less than 0.054°.

Table 1.2

Error specification, full capability system

	Bias (2σ)		Noise (2σ)		Guidance error (2σ)		Distance to error window (ft)	Total error allowable degradation (1)		
	ft (3)	deg	ft (3)	deg	ft (3)	deg		W/distance (2)	With Az angle	With El angle
Azimuth	14	0.054	14	0.054	20	0.076	15000	Linearly to 0.15° at 20 n mile along CL	1.5:1 in angle from CL error at ±40° Az	2:1 in angle from 9° to 15° elevation
Elevation	1.4	0.07	1.4	0.07	2.0	0.10	1145	None	None	Bias - proportional to angle above 4°. Noise - none
DME	-	-	-	-	40	-	15000	10:1 at 20 n mile	None	None
Flare (5)	1.4		1.4		2.0 (4)			Not specified	None	
Missed approach azimuth	0.11			0.11		0.15		None	None	None

(1) Degradation varies linearly between the limits indicated. Proportionality between bias and path following noise shall be maintained.
(2) R = slant range. Range is measured from elevation reference datum.
(3) Measured at error window; azimuth figures hold throughout the roll-out zone.
(4) The linear errors hold throughout the touchdown zone.
(5) The flare errors include contributions of all equipments necessary to compute height.

Preliminary analysis of flight path performance requirements for all these operations has been undertaken. This suggests that, provided performance of the quality required for automatic landing can be achieved when the ground elements providing guidance in the across-track direction, *eg* for azimuth, are situated as far away as the upwind end of a long runway [of the order of 4200 m (14000 ft) from the touchdown region] then the across-track information will be sufficiently accurate to support all other operations in the approach sector.

Present navigational aid capability should be matched in the terminal area by the landing system. A representative 2σ figure is 180 m (600 ft). Thus a reasonable requirement is the following: angular accuracy can degrade by about 2:1 with range to 0.15° by 1.5:1 in azimuth from the runway centreline, and by 2:1 in elevation from 9° to 15°. Degradation of angular error should be linear with the parameter varied (range, azimuth, elevation).

For azimuthal guidance, coverage should be available down to 1 m (3 ft) [above the runway]. For runways not supporting autoland, azimuth guidance is needed only down to the minimum guidance altitude (MGA).

1.3.2 Missed approach azimuth accuracy

The most stringent accuracy requirement will probably be associated with separation of simultaneous departures from parallel runways. While this has not been firmly established, suggested requirements can be derived from the accuracy requirement of the approach azimuth at 10 n mile. This gives 0.15° for the path following error (2σ).

1.3.3 Vertical guidance

Elevation accuracy

Twice the standard deviation of positional error in the along-track direction should not exceed 180 m (600 ft) for the total aircraft system for C/STOL aircraft at touchdown. Of this, the landing system should be a small portion. Additionally, the elevation accuracy at threshold should support autoland capability whether using radio altimeter, inertial guidance, or landing system flare function. Matching radio altimeter performance, the elevation function should provide 2σ accuracy at threshold of 0.61 m (2.0 ft). Assuming a placement of elevation equipment 350 m (1150 ft) from threshold, the guidance error requirement (2σ) is 0.100°, bias should be less than 0.07°, and noise less than 0.07° (2σ). This is substantially better than present Category III ILS requirements.

The angular bias tolerance can degrade proportionally to angle above 4° up to 0.38° (15°). However, to maintain flyability, noise tolerances should not be relaxed.

Flare accuracy

As in the case of elevation, flare guidance should match the radio altimeter in accuracy in the flare and landing zone. Since the relevant parameters are height and height rate rather than angle, the errors should be specified in these parameters. For an aircraft executing a landing, the guidance error (2σ) should be less than 0.61 m (2.0 ft) (1.4 ft bias, 1.4 ft noise). Control motion noise should be quite small for stability.

Rate noise should be such as to permit safe landings using rate of descent derived from landing system equipment.

Vertical guidance coverage near touchdown

The OR is interpreted to mean that elevation guidance shall be available down to the 1:50 inclined surface except that for the reduced system it need not be provided below the MGA.

Flare guidance shall be available down to an antenna height of 2.4 m (8 ft) above the runway surface throughout the touchdown zone.

1.3.4 Distance information

DME accuracy

The system is expected to provide distance information which, along with elevation guidance, will be accurate enough to permit determination of decision height and also permit precise timing of the delivery of aircraft to threshold, to provide acceptable accuracy of touchdown in the along-track direction, to provide course softening, and to provide information on runway distance remaining for use during roll-out. Preliminary studies of these requirements suggest that the accuracy required from the distance information will be determined by its use in conjunction with elevation information to provide flare-out guidance.

For the reduced system the basic DME having a 2σ accuracy of 180 m (600 ft) is considered adequate. For the full capability system an accuracy of 12.2 m (40 ft) is believed to be necessary if used for flare guidance. For certain applications a relaxation may be permissible and is to be determined at a later date. The precision DME can have an accuracy relaxation of 10:1 at maximum range, and still allow sufficiently accurate computation of lateral and vertical position using landing system data.

Table 1.3

Error specification, reduced capability system

	Bias (2)		Noise (2)		Guidance error (2)		Distance to error window (ft)	Error allowable degradation (1)		
	ft	deg	ft	deg	ft	deg		With distance	With Az angle	With El angle
Azimuth	28	0.16	28	0.16	40	0.23	10000	Linearly to 0.5^{o} at 10 n mile	2:1 angle from CL error at $\pm 20^{o}$ azimuth	None
Elevation	7	0.10	7	0.10	10	0.14	4000	None	None	None
DME	-	-	-	-	600 (2)	-	10000	None	None	None

(1) Degradations vary linearly between the limits indicated.

(2) This accuracy allows decision height determination only, for a 2.5^{o} glidepath.

1.3.5 Summary of accuracy requirements

The guidance errors for the full capability system are summarised in Table 1.2.

The guidance errors for the reduced capability system are summarised in Table 1.3.

1.4 Scope

This Report concentrates on the development of the azimuth and elevation angle systems as these form the foundation of MLS. There has been general agreement among proposing States that the distance information requirements would be met by compatible modification to the standard L-band DME; work in this area is reported separately.

The Report uses basically SI units with the exception of use of feet for height and nautical miles for range. It should be noted that all system performance plots were made to an agreed format for the ICAO evaluation; where information is taken from ICAO documentation feet is retained. This also applies to the definition of ground test points.

2 THE DOPPLER MLS TECHNIQUE

This section describes the basic concept of the Doppler system. An analysis is given of the signal coding and its generation by the ground station. This leads to a brief description of the typical signal in space in a practical environment and is followed by an overview of the application of signal tracking systems to optimise the rejection of multipath.

2.1 The Doppler signal coding

The Doppler signal in space is precisely defined in all its characteristics by simple timing and frequency relationships in the transmitting system. This feature allows precise mathematical derivations of the signal in space, thus giving the ground and airborne equipment designer a well defined interface.

The angle defining technique used in the Doppler MLS is based upon the measurement of the frequency shift observed in the airborne reception of a radio signal transmitted from a moving ground-based source. The value of the observed frequency shift depends on the wavelength of the radiated signal, the speed of the source and the angle of the line of propagation to the observer with respect to the plane normal to the line of source movement. Referring to Fig 2.1, the Doppler frequency shift F_D is given by

$$F_D = \frac{V \sin \theta}{\lambda} \quad .$$

Typically, at 5000 MHz (λ = 6 cm) and with a speed V = 900 m/s, the Doppler shift will be close to 250 Hz at $\theta = 1^{\circ}$.

At typical transmission frequencies, the stability of reasonable ground and airborne oscillators (0.0001% and 0.0005% respectively) and the effects of Doppler shift due to aircraft motion will introduce frequency errors in the received signal that are comparable to the frequency coding. These effects can be eliminated by radiating a spatially invariant reference signal at a frequency which is precisely offset from that of the moving source. The offset frequency is chosen to facilitate the airborne processing, thus the angle coded frequency is readily measured with respect to this accurately known offset F_0 . These concepts are illustrated in Fig 2.2.

Clearly, the source of radiation can only move over a finite distance in a practical system. Distances of 30 to 120λ would be typical. Furthermore, effective source velocities of around 1000 m/s clearly cannot be achieved by simple linear physical movement of the source. The simplest way of synthesizing a linear physical movement is to move the source in a series of small fixed steps by commutating the signal along an array of radiating elements.

Fig 2.3 is a diagrammatic representation of a collinear Doppler array and reference antenna showing the far field propagation geometry. Consider a scan from left to right, the received reference signal is

$$\exp j\omega_R\left(t - \frac{R_1}{C}\right) \quad ,$$

where ω_R is the reference signal angular frequency, R_1 the distance of the aircraft from the reference antenna, and C the velocity of propagation.

The received array signal from the rth element is

$$\exp j\left[\omega_{A_1}\left(t - \frac{R_2}{C} + \frac{r-1}{E-1}\frac{\ell}{C}\sin\theta\right) + \alpha\right]$$

during the time interval

$$(r - 1)\frac{\tau}{E} < t < r\frac{\tau}{E} \quad ,$$

where τ is the duration of a one-way single scan, E the number of elements, ℓ the length of the array, R_2 the range from first element, and ω_{A_1} the array angular frequency on the first scan. In the receiver these two signals are fed to a linear detector, with reference predominating, to give a difference frequency signal of the form

$$\exp j\left[\left(\omega_{A_1} - \omega_R\right)t - \omega_{A_1}\left(\frac{R_2}{C} - \frac{\omega_R}{\omega_{A_1}}\frac{R_1}{C}\right) + \frac{r - 1}{E - 1}\ell \sin\theta + \alpha\right] \quad .$$

The difference between ω_{A_1} and ω_R is less than 0.001%, so that we may take $\omega_R/\omega_A = 1$. Further, we may write

$$R_1 - R_2 = d \sin\theta = D\lambda \sin\theta$$

and

$$\omega_{A_1} = \frac{2\pi C}{\lambda} \quad ,$$

so that

$$\omega_{A_1}\frac{R_1 - R_2}{C} = 2\pi D \sin\theta \quad ,$$

giving a difference frequency expression of the form

$$\exp j\left[\omega_0 t + 2\pi D \sin\theta + \frac{r - 1}{E - 1} 2\pi L \sin\theta + \alpha\right] \quad ,$$

where $\omega_{A_1} - \omega_R = \omega_0$, the angular offset frequency, and $\ell = L\lambda$. The Fourier transform of this signal is

$$\exp j\left[2\pi D \sin\theta + \frac{r - 1}{E - 1} 2\pi L \sin\theta + \alpha\right] \int_{(r-1)(\tau/E)}^{r(\tau/E)} \exp j\omega_0 t \exp(- j\omega t)dt \quad ,$$

which, by the relationship

$$\sin x = \frac{\exp jx - \exp(- jx)}{2j} \quad ,$$

reduces to

$$\frac{\tau}{E} \exp j\left[2\pi D \sin\theta + \alpha + \frac{r-1}{E-1} 2\pi L \sin\theta + (r - \tfrac{1}{2}) \frac{\tau}{E} (\omega_0 - \omega)\right] \overbrace{\frac{\sin\left(\frac{1}{2} \frac{\tau}{E} (\omega_0 - \omega)\right)}{\frac{1}{2} \frac{\tau}{E} (\omega_0 - \omega)}}^{P(\omega)} ,$$

..... (2-1)

where the last factor is $P(\omega)$ and gives the spectral shaping due to the finite rectangular dwell on each element.

Summing the transforms from each element gives

$$\frac{\tau}{E} \exp j\left[\alpha + 2\pi D \sin\theta - \frac{2\pi L \sin\theta}{E-1} - \frac{\tau}{2E} (\omega_0 - \omega)\right] P(\omega) \sum_{r=1}^{r=E} \exp jr\left[\frac{2\pi L \sin\theta}{E-1} + \frac{\tau(\omega_0 - \omega)}{E}\right],$$

which becomes $\tau P(\omega) Q(\theta\omega) \exp j\gamma_1$,

where
$$Q(\theta\omega) = \frac{\sin \frac{1}{2}E \left[\frac{2\pi L \sin\theta}{E-1} + \frac{\tau(\omega_0 - \omega)}{E}\right]}{E \sin \frac{1}{2} \left[\frac{2\pi L \sin\theta}{E-1} + \frac{\tau(\omega_0 - \omega)}{E}\right]} \qquad (2\text{-}2)$$

and

$$\gamma_1 = \alpha + 2\pi D \sin\theta + \frac{2\pi L \sin\theta + \tau(\omega_0 - \omega)}{2}$$

(*ie* a phase term). The product $P(\omega)Q(\theta\omega)$ reduces to

$$R(\theta\omega) = \frac{\sin \frac{1}{2}[2\pi L \sin\theta + \tau(\omega_0 - \omega)]}{\frac{1}{2}[2\pi L \sin\theta + \tau(\omega_0 - \omega)]} \qquad (2\text{-}3)$$

for $E \to \infty$, *ie* a single continuous scan, giving

$$R(\theta F) = \frac{\sin \frac{1}{2}[2\pi L \sin\theta - 2\pi\tau(F - F_0)]}{\frac{1}{2}[2\pi L \sin\theta - 2\pi\tau(F - F_0)]} . \qquad (2\text{-}4)$$

Fig 2.4a shows the received difference signal waveform for a continuous linear source movement and Fig 2.5a shows the signal spectrum, a single line at

$$F_0 + \frac{V \sin \theta}{\lambda} \quad . \tag{2-5}$$

Fig 2.4b shows the received difference signal waveform for a continuous linear movement over a finite distance of L wavelengths. The difference frequency signal now has a spectral distribution given by $R(\theta F)$, which is a maximum when

$$2\pi L \sin \theta - 2\pi\tau(F - F_0) = 0 \quad ,$$

ie when

$$F = F_0 + \frac{L \sin \theta}{\tau} = F_0 + \frac{V \sin \theta}{\lambda} \quad . \tag{2-6}$$

This signal spectrum is shown in Fig 2.5b. The effect of the limited scan length is to produce a continuous signal spectrum with a peak value associated with the receiver angular position and a width which is inversely proportional to the length L of the scan.

Fig 2.4c shows the received difference signal waveform for a commutated source movement. A single scan now has the spectral distribution shown in Fig 2.5c given by

$$P(F)Q(\theta F) \quad ,$$

where, from equation (2-1),

$$P(F) = \frac{\sin \frac{1}{2} \frac{\tau}{E} (F - F_0) 2\pi}{\frac{1}{2} \frac{\tau}{E} (F - F_0) 2\pi} \tag{2-7}$$

and, from equation (2-2),

$$Q(\theta F) = \frac{\sin \frac{1}{2}E \left[\frac{2\pi L \sin \theta}{E - 1} - \frac{2\pi\tau(F - F_0)}{E} \right]}{E \sin \frac{1}{2} \left[\frac{2\pi L \sin \theta}{E - 1} - \frac{2\pi\tau(F - F_0)}{E} \right]} \quad , \tag{2-8}$$

where E is the number of elements in the array.

The function $P(F)$ is the spectral distribution resulting from the finite rectangular dwell on each element. The function $Q(\theta F)$ has a maximum of unity when

$$\tfrac{1}{2}\left[\frac{2\pi L \sin\theta}{E-1} - \frac{2\pi\tau(F-F_0)}{E}\right] = \pm n\pi \quad , \tag{2-9}$$

ie

$$F - F_0 = \frac{EL\sin\theta}{(E-1)\tau} \pm \frac{nE}{\tau} \quad .$$

The required solution is obtained for $n = 0$ giving

$$F = F_0 + \frac{EL\sin\theta}{(E-1)\tau} \quad . \tag{2-10}$$

Comparing this equation with (2-6), it can be seen that the effective array length is increased by a factor $E/(E-1)$ and this must be allowed for in calculating system sensitivity.

The multiple solutions to equation (2-9) give rise to frequency grating lobes which must be kept out of the desired range of Doppler frequencies by suitable choice of E and L. Choice of too large an element spacing can also give rise to normal spatial grating lobes. From Fig 2.5c it can be seen that the spectral 'splatter' associated with the frequency grating lobes can be reduced by controlling $P(F)$. In the figure, the function $P(F)$ is shown for a hard switched pulse, but ideally $P(F)$ would be rectangular, just covering the required range of frequencies. Practical considerations force a compromise somewhere between this ideal and the simple $(\sin x)/x$ type of distribution of the hard switched case.

2.2 Signal format considerations

Basic design factors

From Fig 2.5c we can see that the multiple responses of the function $Q(\theta F)$ limits the range of unambiguous coding frequency available for a given number of elements and scan time. The frequency spacing between the maxima of $Q(\theta F)$ is E/τ. The code frequency at $\sin\theta = 0$, *ie* $\theta = 0^\circ$, is F_0 and the maximum unambiguous range of code frequency is $F_0 \pm (E/2\tau)$. Thus, for a given coverage and coding sensitivity, different array lengths can be employed by keeping $E/2\tau$ a constant.

For reduced coverage the number of elements can be reduced and an out of coverage indication signal and some radiation pattern shaping will be employed to suppress the unwanted responses in the term $Q(\theta F)$ and any conventional spatial grating lobes.

The other main design parameter is the offset frequency F_0 . Use of too high an offset frequency is wasteful in terms of spectrum utilisation. Choice of too low an offset would result in fold back through zero frequency, putting unwanted responses in the angle code band. In general the offset frequency should be at least 2.5 times the largest value of E/τ .

It is general practice in the Doppler azimuth system to design the signal format for a coding range of $1 > \sin\theta > -1$, *ie* $\pm 90^{o}$, and to limit the maximum operational sector in the airborne receiver thus ensuring complete unambiguity of the information in the forward sector of the array.

This section has presented detailed formulae describing the total signal in space. The basic design parameters can be summarised in terms of the 'end fire' Doppler frequency which is given by

$$\frac{V}{\lambda} = F_e = \frac{EL}{(E-1)\tau} \quad ,$$

from equation (2-10). Thus, we have the following simple relationships:

Effective aperture = $F_e\tau$ (wavelengths)

Coding sensitivity = $F_e \frac{\pi}{180}$ Hz/deg on boresight

Doppler frequency is $F_e \sin\theta$

4 dB beamwidth is $\frac{180}{\pi F_e \tau}$

3 dB beamwidth is $\frac{160}{\pi F_e \tau}$

Commutation frequency is $\frac{F_e}{\text{element spacing}}$.

Angle function multiplexing

Unlike the conventional VHF ILS, where the azimuth (localiser) and elevation (glide path) signals are in totally separate RF bands and utilise separate receiver systems, it is inherent in the MLS proposal that a number of angle functions, *eg* approach azimuth, elevation, missed approach azimuth, etc, be multiplexed onto the one channel using a single receiver system. The multiplexing possibilities are frequency division (within the available channel width), time

division or a hybrid of these two. The UK DMLS programme has utilised equipments operating in both FDM and TDM formats and the format details are discussed in sections 3 and 5.

Scan formats

Independent of the form of multiplexing used, there are a number of ways of organising the basic angle signal transmission within a given angle measurement slot. Although full angle position information is contained in one scan of the array, it has been normal practice to make an individual angle measurement from the average of a number of sequential scans. Historically this originated from the use of simple counting processors that needed a longer count period to give the required measurement resolution. Within a set of scans a number of arrangements are possible and those which have been employed in the UK programme are illustrated in Fig 2.6:

(a) a set of unidirectional scans, Fig 2.6a;

(b) a set of bidirectional scans, Fig 2.6b. This uses a simple interchange of the reference and array frequencies to maintain the correct sense of difference frequency from alternate scans with minimum spectrum occupancy;

(c) a set comprising a block of scans in one direction followed by a block in the opposite direction, Fig 2.6c.

The prime reason for use of a non-unidirectional set of scans, *eg* (b) or (c), is to minimise the effects of interfering signals. The choice of scan sequence also has a bearing on the effects of differential Doppler shifted multipath signals, this is examined in section 6. The interchange of reference and array signals for opposite scan directions maintains the correct sense of Doppler code in the difference frequency output of the receiver detector.

Commutated reference techniques

The analysis in section 2.1 has assumed use of a single fixed reference transmission and an associated commutated array. The basic process of commutation is to apply a staircase of phase steps to the received array signal which in turn appears at the receiver detector output as a phase staircase on the video difference frequency; this is illustrated in Fig 2.7a.

Clearly, the required phase staircase on the difference frequency can also be generated by a combination of small phase steps in the reference signal and larger steps in the main array signal. Fig 2.7b illustrates the concept where

the main array has been thinned by a factor of 4, but by introducing a four-element commutated reference array the signal at the receiver processor is unaffected. This technique can result in significant savings in the array networks. Of course, you do not get something for nothing. Because of the thinning in the main array, grating lobes are produced from this array, the ambiguity of these is, of course, resolved by the reference commutation. The grating lobes are, therefore, not operationally significant, unless energy from one is reflected back into the receiver when it would appear as a multipath signal virtually indistinguishable from the wanted array signal. On many sites the probability of such a situation is effectively zero and main array thinning with a commutated reference is a practical proposition.

2.3 Ground system basic requirements

The basic requirements for the ground system can be summarised as follows, with reference to Fig 2.8:

(a) Generation of two stable RF frequencies (in terms of receiver channel width) with an accurate fixed difference frequency F_0 .

(b) A linear array of radiating elements with element radiation patterns to suit the required system coverage.

(c) A method of commutating one of the RF signals along the array.

(d) A fixed reference element for radiating the reference RF signal.

(e) Means of identification of the system.

(f) Accurate and stable system monitoring.

The two types of ground transmitter system used in the UK DMLS programme are described in detail in sections 3 and 5. There are two main points to be noted at this stage: firstly, the basic signal generation requirements are very simple, the actual angle code generation being a process of switching, which is ideally suited to reliable digital techniques; and secondly, each element in the array is energised in turn, making it very easy to check the individual amplitude and phase on-line to form the basis of simple high integrity monitoring.

2.4 Doppler signal processing

Provided that the ground system meets the signal generation requirements outlined in sections 2.1 and 2.2, the received signal in a 'clean' environment would be as illustrated in Fig 2.9a for the azimuth system and Fig 2.9b for the elevation system. The presence of the second component in the elevation case is due to ground reflection of the commutated signal.

In a practical situation many other signal components will be present due to reflections from objects lying within the system angular coverage, and the received azimuth signal, for example, will look something like that shown in Fig 2.10.

The Doppler signal processor used in the airborne receiver has therefore to fulfil the following tasks:

(a) To acquire the direct signal spectra.

(b) To lock on and track the correct signal.

(c) To continuously validate that the tracked signal is the correct one.

(d) In the elevation system, to reject all signals with angle codings associated with ground reflections.

(e) To make an accurate frequency estimate of the position of the *peak of the direct signal spectrum* and hence provide an accurate measurement of angle position with minimal residual errors.

Two basic forms of processor have been used in the UK DMLS programme:

(i) the sine/cosine frequency tracker, which was used in the performance evaluation of the FDM system; and

(ii) the correlation processor which is used in the airborne processors for the TDM system.

Both systems operate on the assumption that the largest persistent signal in the system coverage is the correct signal and both systems follow the general form of operation outlined below.

On initial acquisition, the system code coverage is examined to determine the largest signal, and a narrow frequency measurement cell matched to the width of the signal is located on the signal identified, see Fig 2.11. Whilst the acquired signal is tracked and measured, the coverage is continuously examined; if the tracked signal remains the predominant signal the system confidence builds up to a maximum value. When a high level of confidence has been achieved, the receiver will track the wanted signal through periods when a multipath signal exceeds the wanted signal. Such a situation may occur during the final landing phase when on a humped runway the wanted azimuth signal may be severely attenuated in the touchdown region. (See report of DMLS trials at Manchester Airport[5].)

If the system confidence falls to zero, or no persistent signal is found on initial acquisition, the processor will continue in the search mode until a consistent signal arises.

The ground reflected signal in elevation systems may be rejected by use of a sector filter or by restricting the processor to utilise only signals with a positive angle code.

The individual processors are described in more detail in sections 3 and 5 and the multipath performance of the correlation processor used with the TDM format is examined more closely in section 6.

3 BASIC DATA COLLECTION FOR ICAO SUBMISSION - THE FDM SYSTEM

Although the UK DMLS submission to the ICAO was based upon a Time Division Multiplex (TDM) realisation, all the supporting test data available at the submission date (December 1975) was obtained from the Frequency Division Multiplex (FDM) feasibility demonstration system. This section describes the signal format and equipments used for these tests. The section also serves to introduce the general test facilities and data processing used on all the DMLS trials at Bedford.

3.1 FDM signal format

The Doppler MLS used for feasibility demonstration was designed to operate in the lower half (5000 MHz to 5125 MHz) of the 250 MHz band allocated for aeronautical navigation. For the trials a channel frequency of 5008 MHz was used. This choice of frequency band was dictated by the desire to use small wavelengths to give electrically large apertures, whilst not using too high a frequency, where weather effects become significant, RF power requirements become excessive and technology more expensive.

Data rate

Prior to the demonstration programme, a number of studies were carried out to determine the required data rate for the various elements of the new landing guidance system. The values recommended and used for the feasibility demonstration were as follows:

(a)	angle guidance (except flare)	not less than 5 Hz
(b)	flare angle guidance	not less than 10 Hz
(c)	ranging information	not less than 5 Hz .

Sub-system signal multiplexing

For the feasibility demonstration a hybrid frequency division multiplex/ time division multiplex (FDM/TDM) format was used. Each 600kHz channel was split into four sub-channels as shown in Fig 3.1. One of these sub-channels, the TDM, was designed to have three facilities time multiplexed onto it. The use of a Ku-band (15 GHz) channel for flare angle guidance was also proposed. However, during the demonstration programme, the TDM sub-channel only carried the missed approach azimuth signal and the Ku-band channel was not implemented. The feasibility demonstration elevation system was evaluated in the elevation and flare role.

Detail design factors

The two factors that determined the detailed design were the data rate and the system quantization. With the original angle processors using direct zero crossing counters, the quantization of frequency measurement was expected to be half the inverse of the measurement period, *ie* 2.5 Hz for a 200 ms measurement period (more advanced processors are not quantization-limited in this manner). Previous studies had suggested that an angular quantization of 0.02^{o} around antenna boresight would be adequate. The resulting broadside sensitivity was then:

$$\frac{2.5}{0.02} = 125 \text{ Hz/deg} .$$

For the feasibility demonstration programme it was decided that the prototype approach azimuth antenna would be retained and this determined the aperture of the antenna. It was also recognised that a whole number of scans in a measurement period was desirable. The number of scans (N) in a measurement period is a function of array length, broadside sensitivity and the measurement period, and is given by:

$$N = \frac{\text{broadside sensitivity} \times \text{measurement period} \times 57.3}{\text{array length}} .$$

With a sensitivity of 125 Hz/deg the value of N for the approach azimuth antenna would have been 12.3. Accordingly, a value of N = 13 was chosen resulting in an actual broadside sensitivity of 135 Hz/deg. This value of sensitivity was used for all the angle functions. The array lengths and resulting scan rates are shown in Table 3.1.

Table 3.1

Scan rates (feasibility phase)

Facility	Array length (λ)	Data period (ms)	Scans in period	Rate (Hz)
Approach azimuth	117.42	200	13	65
Missed approach azimuth	57.78	100/200	13/26	65
Elevation	90.27	200	17	85

For each azimuth sub-system frequency allowance was made for full coding coverage to $\pm 90^{\circ}$ requiring an information bandwidth of

$$\pm (135 \times 57.3) = \pm 7.73 \text{ kHz} .$$

For the elevation system a design coverage of $+20^{\circ}$ was chosen with coding allowance up to 30° giving a nominal information bandwidth of 4.36 kHz.

The offset frequency was chosen to be a multiple of the antenna switching rate for each sub-system at two to three times the 0° to 90° information bandwidth to avoid foldback of switching harmonics in the receiver detection process. This resulted in an offset frequency of 24.96 kHz for the azimuth systems and 14.96 kHz for the elevation system.

All angle facilities employed the frequency interchange method of providing array and reference frequencies. In this method (Fig 3.2), the reference and commutated frequencies were interchanged at the end of each scan. Thus, generation of only two frequencies was required and bandwidth was conserved.

The frequency utilisation for the azimuth sub-channels is shown in Fig 3.3 and for the elevation channel in Fig 3.4.

The frequency allocations within the channel are shown in Fig 3.1 and Table 3.2. The guard bands catered for the estimated maximum inter sub-channel interference levels and include allowance for an overall frequency stability of ±0.0006% allocated as:

(a) Ground sub-system ±0.0002%;

(b) Doppler shift due to aircraft motion 0.00003%;

(c) Airborne sub-system ±0.00037%.

Table 3.2

Bandwidth allocation

	Occupied bands	(kHz)
1	Data	15
2	Azimuth sine	60
3	TDM (missed approach azimuth with elevation and azimuth-derived cosine)	60
4	Elevation sine	15
	The following guard frequency bands were used:	
1	Lower channel edge to lower TDM edge	90
2	Between TDM and elevation sine	132.5
3	Between elevation sine and data	110
4	Between data and azimuth sine	87.5
5	Between azimuth sine and upper channel edge	30
	Total bandwidth required per channel	600

Function identification

A substantial integrity benefit of an FDM format is that each sub-system occupies a unique frequency position in each channel. This was considered to have sufficient integrity to render further sub-system identification unnecessary.

3.2 The FDM ground equipment

Background

Ground equipment, built, installed and tested for the feasibility demonstration phase of the UK MLS programme comprised:

(a) An approach azimuth array and transmitter (STL).

(b) A missed approach azimuth array, transmitter and monitor (STL).

(c) An elevation array, transmitter and monitor (Plessey).

(d) A data transmitter (RAE).

The transmissions from these systems were integrated into the hybrid FDM/TDM signal format described in section 3.1. A critical parameter with respect to an FDM system was the spectral splash between adjacent sub-systems and considerable effort was addressed to economic techniques for minimising spectrum spread. Two different UK companies were involved in the ground equipment

programme. The azimuth transmitters and arrays were based upon the prototype system first installed in June 1972 [11], which was designed and built by STL. In fact, the prototype approach azimuth long array and commutator system was used directly for the feasibility demonstration programme approach azimuth system.

The feasibility demonstration elevation system was a new design of array and transmitter by the Plessey Company and incorporated a variety of internal monitoring and field monitoring concepts for evaluation. A 90λ aperture was chosen for this system, so that performance in both the basic elevation and flare angle role could be evaluated.

The following sections describe the details of the various installations, the primary system parameters being summarised in Tables 3.3 to 3.6.

Table 3.3

Approach azimuth system parameters

RF frequency	5007.94 MHz
Long array length	117.42λ
Long array elements	64 elements Spacing 1.8638λ
Short array length	1.397λ
Short array elements	4 elements Spacing 0.4659λ
Azimuth coverage	±60° nominal
Elevation coverage	+1° to +20° nominal
Offset frequency	24.96 kHz
Bi-directional scan rate	32.5 Hz
Coding sensitivity	135 Hz/deg
Reference radiated power	4 W
Commutated radiated power	500 mW

Table 3.4

Missed approach azimuth system parameters

RF frequency	5007.52 MHz
Long main array	57.77λ
Elements	32 spaced 1.8636λ
Long standby interleaved array	57.77λ
Elements	32 spaced 1.8636λ
Basic reference short array	1.397λ
Elements	4 spaced 0.4659λ
Azimuth coverage	$\pm 60^{\circ}$ nominal
Elevation coverage	$+1^{\circ}$ to $+20^{\circ}$ nominal
Offset frequency	24.96 kHz
Bi-directional scan rate	32.5 Hz/65 Hz
Coding sensitivity	135 Hz/deg
Reference radiated power	3.5 W
Commutated radiated power	500 mW

Table 3.5

Elevation system parameters

RF frequency	5007.69 MHz
Commutated array	90.155λ
Elements	96 spaced 0.949λ
Azimuth coverage	$\pm 40^{\circ}$ nominal
Elevation coverage	$+1^{\circ}$ to $+20^{\circ}$ nominal
Offset frequency	14.96 kHz
Bi-directional scan rate	42.5 Hz
Coding sensitivity	135 Hz/deg

Table 3.6

Data system parameters

RF frequency	5007.815 MHz
Radiated power	1 W
Modulation	FM,PM or AM

3.2.1 Approach azimuth system

The 120λ approach azimuth system was installed on the extended centreline at a distance of 79 m (260 ft) beyond the west (09) end of the test runway at RAE, Bedford. This test site and the trials facilities are described in Appendix B. The actual transmitter installation is shown in Fig 3.5.

(a) Antenna array installation

The antenna array of overall length 9.15 m (30 ft) and with a ground plane 1.22 m (4 ft) from front to rear was mounted on five metal stands which were joined together by a steel tube structure. The stands were supported on a paving stone surface and the array was anchored to the ground by a system of guy wires. The array was levelled laterally by adjustable feet and a forward tilt of 0.5° was set, to allow for water drainage. The array was set to have its axis orthogonal to the runway centreline by theodolite measurements, the final setting being achieved by siting a receiving antenna on the runway centreline near the opposite end of the runway and physically adjusting the array to give a zero readout on the Doppler MLS receiver. The radiating elements of the array were 1.42 m (4.6 ft) above ground level. This height was chosen on the basis of earlier propagation measurements[11], which investigated the effect of the humped runway profile on signal level near threshold.

The array aperture was sealed by melamine sheet and dry air was circulated over the radiating elements.

(b) Transmitter installation

The transmitter was housed in a wooden weather proof cabinet standing immediately behind the antenna array. The cabinet had thermostatically controlled heating and ventilation. The cabinet was lower than the antenna array and caused no obstruction problems. The cabinet was anchored to the ground to prevent it being overturned by aircraft jet efflux.

(c) Design details

For the approach azimuth facility a lower coverage limit of 1 m along the runway and 1° elevation beyond threshold was adopted with an upper limit of $+20^{\circ}$ and an azimuth coding coverage of $\pm 60^{\circ}$. The effective scan aperture which generated the bearing information was approximately 119λ at a frequency of 5008 MHz giving an equivalent beamwidth of 0.5° on boresight.

Instead of using a fixed reference and close element spacing on the long commutated array, the long array was 'thinned' using fewer elements at greater

separation and multi-element commutated reference was used to provide the compensating multiplicative 'filling', see section 2.2.

In addition to the economy in the number of elements and associated commutators, two further advantages resulted from the use of the commutated reference approach:

(a) blending was only necessary on a few elements and coupling problems had only to be solved for these elements rather than across a full array;

(b) the wide spacing on the long array allowed two antennas, operational and standby, to be interleaved in the same physical position.

Long array

This consisted of a row of 64 monopoles mounted in a feed horn along the back of a flat plate counterpoise. Element spacing was 1.8638λ at 5007.94 MHz. The required vertical radiation pattern was obtained by the use of the counterpoise and the shape of the horn. It was of simple construction and had a low profile which easily allowed co-siting with the ILS localizer. Although this form of antenna is not suitable for regions of heavy snowfall, it does provide a very simple and economic system for those many areas of the world which do not have snow. Satisfactory performance has been demonstrated under conditions of heavy rain.

Each monopole was fed in turn from a single transmitter, Fig 3.6, by a two-level switching system (commutator). The transmitter fed an eight-way switch each output of which fed a second level eight-way switch (Fig 3.6). The switches were driven from the transmitter logic with the switching speed of the second level being eight times that of the first level. In this manner a single pole, 64-way switch was achieved.

Short array

The short, or reference, array together with its commutator and blending modulator were integrated into one module which mounted directly on the horn/counterpoise assembly. It consisted of four monopoles with a spacing of 0.465λ mounted in a feed horn similar to that used for the long array. A complete scan of the short array occurred during the transmission period of each element of the long array, so that the element density of the long array was effectively quadrupled.

Blending to minimise spectrum splash was carried out on the short array only, there being two adjacent antenna elements radiating at any one time. The amplitude of the transmission from each element was varied as an approximation of cosine squared (raised cosine). The reference output of the transmitter was split into two channels designated 'odds' and 'evens'. Each channel was amplitude modulated and the output sampled, detected and compared with a reference waveform. The resulting error was used to control the modulator. In this manner the amplitude modulation was made to follow the reference waveform (an approximation to cosine squared) generated in the transmitter logic. The waveforms and phasing are shown in Fig 3.7.

Transmitter

The approach and missed approach transmitters, Fig 3.6, were identical in design and construction, the appropriate parameter values for individual use being selected by means of front panel switches. This allowed the same transmitter to be used for either facility, so improving the availability of trials equipment. The transmitter provided the C-band drives to the long and short (reference) arrays with the two frequencies being separated by the desired offset frequency. It also provided all the logic control signals to ensure the appropriate phasing in the RF generation chains and the associated commutator timing. The design of these transmitters was derived directly from that used in the previous prototype system.

The offset generator provided two outputs at approximately 5.19 MHz which differed by the offset frequency of 24.96 kHz precisely. One output was fed to the long array RF chain and the other to the short array RF chain. The feeds were interchanged, without phase discontinuity, on receipt of a control signal from the transmitter logic which indicated the change of scan direction on the long array.

Two identical chains were used to raise the signal frequency to 5008 MHz and the level to 10 W at the output of the travelling wave amplifiers (TWA). The short array chain fed directly into the blender commutator, but the long array chain incorporated a shaping modulator, similar to the blender, which rounded off the switching pulses to reduce the spectrum occupancy.

The transmitter logic provided drive signals to the long and short array commutators, the offset generator sideband control, the two RF modulators, the shaper and blender.

The transmitter, transmitter power supply, travelling wave amplifiers and travelling wave amplifier power units were free-standing pieces of equipment, see Fig 3.8.

The vertical and horizontal radiation patterns for a single monopole, mounted in the feed horn on the counterpoise, are shown in Figs 3.9 and 3.10 respectively. Fig 3.11 shows the phase and amplitude distribution for the long array.

The frequency stability of the 94.808MHz oscillator was within ±0.0004%. At the final 5 GHz output, this represented less than 0.00001%. The measured frequency stability of the 4.908 GHz source, over a temperature range of -10^{o} to $+70^{o}$C, was better than 0.0001%. Over a period of six weeks running at room temperature, the maximum ageing was 0.00002%.

Monitoring and test facilities

Power level and commutation monitoring were built into the approach azimuth transmitter. A simple field monitor was provided, consisting of a horn antenna, detector and dc amplifier. The relative power radiated from each element could be checked remotely. The Doppler code frequency output from the detector was available for feeding to a conventional counter. The monitor antenna was mounted off centreline some 30 m (100 ft) from the array.

3.2.2 Missed approach azimuth sub-system

The missed approach azimuth sub-system was installed on the extended runway centre line at a distance of 152 m (500 ft) beyond the east end (27) of the test runway. The general installation is shown in Fig 3.12. The facility was of similar design to the approach azimuth and the transmitters were identical. However, a number of special facilities were provided for trials purposes:

(a) Standby operation using an interleaved array.

(b) Array configuration flexibility to allow for the assessment of various element spacings, array lengths and reference conditions.

(c) Controllable fault conditions to study the reaction of monitoring systems.

Antenna

The antenna was basically a shorter version of the approach azimuth array being 7 m long (23 ft). The array was again mounted on stands at a height of 1.12 m (3.6 ft) above ground.

The electrical length of the long array was a nominal 60λ, utilising 64 elements at a spacing of 0.93λ. This together with a flexible short array of four elements allowed a number of different commutation systems to be selected:

(a) Single 60λ array with 0.93λ spacing and a two-element blended reference.

(b) As (a), but with a fixed reference.

(c) A 30λ version of (a) or (b).

(d) Two interleaved 60λ main and standby arrays with 1.86λ spacing and separate four-element blended reference arrays.

To allow for this flexibility three-level commutation was used.

3.2.3 Elevation sub-system

The 90λ aperture elevation sub-system was sited 670 m (2200 ft) from the east end and 153 m (500 ft) to the south of the test runway. The installation is shown in Fig 3.13. The siting was chosen so that system performance in the elevation role could be evaluated with respect to a false runway threshold and performance in the flare angle guidance role could be evaluated with respect to the actual runway threshold. The ground in front of the array was essentially flat and had a high reflection coefficient, giving a stringent situation for low angle measurement. Whereas the azimuth equipments were basically first generation designs, the design of the elevation system was based upon the following features.

(a) An optimised transmitter design suitable for azimuth and elevation and a range of array lengths;

(b) The use of full power broadband switches;

(c) New antenna element structure with optimised radiation patterns;

(d) Integral, internal and external monitoring capabilities;

(e) A structure capable of withstanding the full environmental conditions.

Antenna assembly

The elevation antenna consisted of two arrays, the commutated long array and a non-commutated reference array. Both arrays used the same basic element.

The individual elements in each antenna consisted of a transition from semi-rigid coaxial line to a non-standard cross-section waveguide which feeds a flared

horn. Each horn radiated in a space bounded by parallel plates. The vertical radiation patterns of the elements were controlled mainly by the parallel plate region which restricted radiation to a nominal $\pm 20^{\circ}$ in elevation.

The radiation pattern in azimuth was controlled by a pair of flared plates which ran the whole length of the antenna. The azimuth and elevation patterns for an element are shown in Figs 3.14 and 3.15.

The long commutated array consisted of 96 fed elements with the odd elements fed from one commutation network and the even elements from a second network. The division into odd and even was for the purpose of blending the energy transfer from element to element. The array was terminated at each end with eight unfed elements to normalise end effects.

The short reference array had 40 elements of which 13 were active. These were fed by a network of ring couplers to produce a $\sin x/x$ amplitude distribution and a phase distribution resulting in a sectorial elevation radiation pattern with the lower edge at 0°, see Fig 3.16.

Each 48-way commutator network was achieved by three-level switching:

(i) 3 way;
(ii) 3 times 4 ways;
(iii) 12 times 4 ways.

Each switch consisted of a five-port module (one input and four output) with interconnection between switches by 50 ohm matched cables ensuring that the nominal path lengths to all elements from the input were equal, physically and electrically.

The actual switching module was a 50 ohm stripline circuit utilising shunt mounted PIN diodes. Two switching diodes were used in each arm. In each output arm of the 24 modules of the third bank, a third diode was provided which was forward biased with a low current to provide a good match to energy coupled into the element when the arm was turned off. A low power switching diode was used to isolate the reverse bias voltage of 40 V from this matching diode. Fig 3.17 shows the electrical circuit of one of the final element feed four-way modules. The typical insertion loss of a switch module is shown in Fig 3.18, this includes strip line and connector losses. Isolation as a function of frequency is shown in Fig 3.19.

Transmitter details

The transmitter was housed in a trailer which was sited adjacent to the array. The RF connections to the antenna were by waveguide. All cable connections were routed through a dry air duct which was fed from a dehumidifier housed in the trailer. This operated in a semi-closed loop cycle such that the antenna system within the radome was fed with dry air at slightly higher than ambient pressure.

A block diagram of the transmitter is shown in Fig 3.20. The basic signal relationships were generated at a nominal frequency of 15 MHz. The offset frequency of 14.96 kHz was derived from a master clock and was used as the reference in a phase lock system to obtain two output frequencies at 15 MHz and 15.01496 MHz.

These two signals were interchanged between reference and array channels on up and down scans to maintain the baseband 'Doppler shift' in one sense. Phase cycling at 5 Hz was applied to the array channel using a single sideband modulator; signal frequency was then increased to 190 MHz. This stage was followed by up conversion to C-band using a common local oscillator having a stability of ±0.0001%.

The output from the reference TWT amplifier was fed direct to the reference array distribution network. The output from the commutated array TWT amplifier was fed to a blending function modulator which provided two outputs of cosine-squared envelope shape and in antiphase. These outputs were fed to the odd and even commutator channels. The blending modulation was performed by a combination of variable ratio power splitters (VRPS). Theoretically this gives a lossless system. Practical imperfections introduced some loss, but this technique gave a much higher efficiency than the more conventional PIN diode modulator arrangements.

Flexibility in commutation logic was obtained by allocating each element a sequential 8-bit word address. The commutation process was then controlled by a stepped 8-bit word generator and scan turn round was initiated by the recognition of the hard-wired addresses of the end elements. Thus a change in array length was accommodated by providing the new end element addresses.

Monitoring facilities

The elevation transmitter and antenna had a comprehensive set of monitoring and diagnostic facilities. There were three basic types:

(a) Internal monitoring;

(b) Integral monitoring;

(c) Field monitoring.

The internal monitor measured such quantities as reference array and commutated array power levels and operated flag alarms at preset levels. A full listing is given in Table 3.7, which refers to the relevant points in Fig 3.20.

Table 3.7

Elevation facility monitoring functions

Sensor	Output/function
A	RF sample of even antenna elements
A'	Detected sample of even antenna elements
B	RF sample of odd antenna elements
B'	Detected sample of odd antenna elements
C	RF sample of even or odd + reference (depends on optional connection)
D	Detected sample of even + odd + reference
E	RF sample of reference forward power
F	RF sample of reference reverse power
G	Alternative RF sample of reference reverse power
H	RF sample of commutated power at TWT output
I	RF sample of forward modulated even elements power
J	Detected sample of forward modulated even elements power
K	RF sample of forward modulated odd elements power
L	Detected sample of forward modulated odd elements power
M	RF sample of odd elements reverse power
N	RF sample of even elements reverse power
O	RF sample of reverse power at input to modulator
P	Scan changeover/frequency interchange phases in lock

The internal monitor information could be processed in a variety of ways, for example a faulty switch gives an increase in reverse power. This would be detected by sensors M or N and, by comparing with the commutation logic signal, the number and position of such faults could be presented. In this way single failures could be seen before system performance deterioration occurred.

The integral monitor sampled the RF signal at each element by means of coupling holes into a pair of waveguides running up the commutated array, one for odd and one for even elements. A composite signal was produced which was a complete representation of the commutated signal in space at an angle determined by the waveguide propagation constant. This signal was detected with respect to a sample of the reference (point D refers) and was fed to an angle processor. The processor angle output was recorded and compared with preset alarm limits.

The field monitor consisted of a remote RF detector fed from a slotted waveguide antenna mounted on a mast at a height of 7.1 m (23 ft) and 191 m (625 ft) from the elevation antenna. This is shown in Fig 3.21 (the Landrover and associated equipment was present for multipath repeater trials). The monitor elevation was at 2.13° with respect to the array centre. The baseband signal from the remote RF head was fed by cable to the transmitter where it was processed in an identical manner to the integral monitor signal.

3.2.4 Data sub-system

The feasibility demonstration format included a dedicated frequency sub-channel for data transmission. This channel was not specifically used for transmission of proposed 'DMLS data', but was directly used in support of trials measurements to transmit such information as:

(a) Scan synchronisation signals for the elevation sine/cosine processor;

(b) TDM timing for the TDM sub-channel;

(c) AGC measurements to determine multipath levels during flight tests.

Installation

The data transmitter could be housed in the equipment cabinets for approach or missed approach azimuth and in the elevation trailer for operation at the respective sites. For azimuth site transmissions, use was made of one of the 'dummy' elements at the end of the azimuth long arrays. For use at the elevation site, a slotted waveguide element giving ground level cut off was employed.

Transmitter details

The block diagram of the data transmitter, which was assembled, in the main, from commercial items, is shown in Fig 3.22. The frequency source was a phase locked klystron oscillator. The synchronising system was nominally set up to the data channel centre frequency, but by use of an external reference at a nominal 30 MHz the RF output could be set at any value within ±2 MHz of nominal, thus providing a test signal source for any sub-system. Frequency or phase modulation could be applied via the synchronising system.

The normal mode of operation was amplitude modulation, which was applied via a feed back loop around the 20W TWT amplifier; this loop also served to stabilise the output level. When used for the transmission of synchronising timing information the timing signal was first applied to the frequency shift

tone generator which then fed the amplitude modulator. The mean transmitter power output was 5 W which reduced to 1 W at the antenna as a result of cable losses.

3.3 DMLS FDM receivers

Three experimental receivers were used in the feasibility demonstration programme. Two receivers were developed by Plessey, known as P2A and P2B, and one by STL, known as type S. In each case a section of the receiver was devoted to the interface circuitry required specifically for ordering and formatting the output data to the digital recording system. The design philosophy for each receiver was to produce units giving ease of access to all circuits and constructed to permit simple introduction of modifications and developments in the light of experience. For both systems, the use of a physically separate RF head was adopted for maximum flexibility of equipment siting in the trials aircraft.

The P and S receivers incorporated different types of angle processor. At a very early stage in the trials programme it was evident that the sine/cosine system used in the S receiver was the superior technique and all field data presented to ICAO was taken with this receiver. The following description therefore is confined to the S type receiver.

The S receiver

The S receiver was divided into two physical units as illustrated in Fig 3.23:

(a) The RF unit housed in a short ½ ATR case.
(b) The IF/processor unit housed in a long ½ ATR case.

An outline block diagram of the receiver is shown in Fig 3.24. Operation was on the double superheterodyne principle and was designed to operate only on the single trials RF channel. Fixed frequency crystal-controlled local oscillators were used with the three angle sub-channels following a common path to the output of the second mixer. No data sub-channel was provided.

The measured performance of the RF/IF unit was

(a) dynamic range, -109 dBm to -39 dBm;
(b) noise figure, 12 dB;
(c) intermodulation products, -60 dB with two tone input of -40 dBm.

The sine/cosine frequency tracker

A block diagram of the sine/cosine frequency tracker is shown in Fig 3.25. With a sinewave input the voltage controlled oscillator (VCO) was driven to reduce $\Delta\phi$ to zero. A simple zero crossing counter was used to measure the VCO frequency which followed the angle coding of the input signal. Digital and analogue outputs were derived from the counter output. The angular resolution of the counter output was dependent on the coding factor, the count period and the division ratio 'n'. For example in the FDM system measuring for a 200 ms period (5 Hz up-date rate) the counter resolution was 2.5 Hz corresponding to 0.0185° for $n = 1$, as used for the two azimuth channels, and 0.00925° for $n = 2$ as used for the elevation channel.

When the sinewave input was replaced by a series of scans from a Doppler antenna there could be a phase transient at the end of each scan which could generate an error voltage in the feed-back loop. In practice the effects of this phase transient were minimised by performing the angle measurement over a continuous group of scans and rotating the phase transient over a range of π during the group of scans. This was implemented in the transmitters by advancing the starting phase of the offset frequency on alternate scans through π radians. The use of a scan synchronised gate in the feed-back loop, which opened for the duration of the transient peak, virtually eliminated any residual effects.

Signal acquisition was performed by operating the tracker in a broadband mode to centre on the largest signal present and then reducing the bandwidth to match that of the transmitted signal in the track mode. Simple signal validation was performed by comparison between signal amplitudes at the input to the tracker and the output of the low pass filter. With a suitable weighting applied, this gave a measure of the relative peak signal levels inside and outside the tracking bandwidth.

4 FDM SYSTEM TEST RESULTS

This section presents examples of typical test results from the FDM equipment. Samples of results are given for ground based static and dynamic tests and flight tests. The results shown are intended to give an indication of the overall system performance capabilities, the full set of ground and airborne data for all the ICAO test profiles being given in the UK ICAO submission document[1].

The ICAO state letter SP20/1-75/58 attachment B, dated 3 July 1975, laid down a common series of flight and ground tests to be conducted by all proposing states. These test requirements were actually formulated at the London meeting

of WGA in September 1974 and were updated at the Melbourne meeting of WGA in February 1975.

All the FDM system field trials were based on the airfield at RAE, Bedford. This site was chosen as having a representative runway length, being in a location relatively unaffected by airways and other airfields within the limits of the MLS test plan, and having good tracking facilities for assessing system accuracy. A full description of the test site, instrumentation and test aircraft is given in Appendix B, together with the summary of the ICAO test requirements.

In addition to standardising the actual field tests, the AWOP WGA formulated guidelines for data reduction techniques and statistical analysis. Appendix C describes the data recording techniques and outlines the methods of data reduction adopted at RAE.

4.1 Ground based accuracy measurements

4.1.1 Approach azimuth

Fig 4.1a and b summarises the approach azimuth test points surveyed on the airfield at Bedford. Fig 4.2 shows the result of a typical pole test at position F6, each point represents the mean and standard deviation of 10 seconds' worth of data. It should be noted that below a height of 35 ft there is no line of sight to the azimuth transmitter due to the runway hump*. Fig 4.3a shows the kinetheodolite track of a test van run, along the runway. Fig 4.3b shows the DMLS receiver output and Fig 4.3c shows the system error with the receiving antenna tracked by the kinetheodolites. The gaps in the trace were due to missing kine data and a large kine tracking error showed as the base line of the two station system was crossed at 3700 ft from the array. The azimuth system measurement quantization of 0.018° shows clearly.

The result from a set of static checks on the cross runway is shown in Fig 4.4, as the kine baseline effect coloured the results between -10° and -20° a balloon theodolite mounted at the azimuth array was used to measure the receiver angular position. The kine baseline effect shows clearly in the tracked test van run shown in Fig 4.5a and b. Both these measurements indicated a small sensitivity error which was attributed to an increase in array length due to temperature. These results are typical of the large amount of ground test data obtained and illustrate the high basic system accuracy.

* See plot of runway profile in Appendix B.

4.1.2 Missed approach azimuth

Fig 4.7a and b summarise the missed approach azimuth static test results. Fig 4.7 shows the result of a typical pole test at position B6. There was a mean bias of -0.03° due to array misalignment which was consistent with ground dynamic and flight tests. Fig 4.8a, b and c shows the results from a test run along the runway centreline. The missed approach azimuth results are very similar to those of the approach azimuth system. The system noise level being determined by measurement quantization and not antenna aperture. (Approach azimuth 119λ aperture, missed approach azimuth 60λ aperture.)

The static and dynamic measurements on the cross track were limited by aircraft geometry, results are shown in Figs 4.9 and 4.10a and b. The spread of the static bias errors was in sympathy with the dynamic error plot which showed the effects of multipath due to obstructing objects on the airfield. The large bias error at +16° was due to obstruction of the signals by the static ATC runway controller caravan.

General comments on the azimuth tests

Both pole tests showed a small variation in static error (bias) as a function of height, the maximum peak-to-peak variation being 0.02°, which corresponded to a physical displacement of 1.1 m (3.58 ft) at the test range of 3354 m (11,000 ft). The actual mean physical displacement of the test pole would have been very small and would not have given the bias errors seen in the tests. The signal seen at the receiving antenna was formed by two main components a direct signal and a ground reflected signal. If the ground between the transmitter and the receiver were completely level the angle coding on the two signal components would be the same, but in a practical environment the ground plane is rarely level and any crossfall results in the angle code on the ground reflected signal having a small displacement from the direct signal, giving rise to a small multipath error which varies in relative phase as a function of receiving antenna height. This effect is discussed in more detail with respect to the tracked radial flights. In the case of these static tests, the phase rotation over the height change 0 to 70 ft would have been very small at the test range of around 3354 m. The small weave seen as the height changed was most likely due to the fact that, as the mast was raised, the reflection point moved towards the transmitter and would therefore have given rise to a slowly varying ground reflection.

Similar small effects will be seen on the runway runs as the reflection point moves with the test van. On these runs, it should be noted that, at a range of 300 m, an angular movement of 0.01^{o} is equivalent to 50 mm and the limits of kinetheodolite tracking accuracy were reached, so that tracking errors became significant at shorter ranges. The ground reflection component also introduced small errors on the cross runway measurements as the signal reflection point travelled over the varying ground profile.

4.1.3 Elevation system

Fig 4.11 summarises the elevation static test points, whilst the position of the installation with respect to other local structures is shown in Fig 4.12. During the measurement programme typical ground reflection coefficients were measured for the surface local to the array; the results are given in Fig 4.13.

Fig 4.14 shows the result of a pole test at position E3. The elevation system quantization of 0.009^{o} is reflected in the very low standard deviation of system noise at each measurement point. The phase centre of the elevation array was 5 m (16 ft) above the local ground surface and 6 m (19 ft) above the ground surface at the E3 test point. To a first approximation the separation angle between the direct and ground reflected signal is given by $\tan^{-1}(2h/R)$, where h is height of test point above local ground, and R is range of test point. This assumes that the ground between the array and test point is essentially planar. This is a reasonable assumption for Bedford. The measured multipath response of the receiver gave an in-beam width of 1.2^{o} and this separation angle would occur at a nominal height of 17 ft. Above 17 ft the errors should be due to sidelobes of the ground reflected signal and, therefore, of low amplitude; below 17 ft height error amplitudes would increase as the main lobe of the ground reflected signal moved into the tracker width. Fig 4.15a and b show the results of two pole tests at E7 corresponding to the typical position of threshold with respect to an MLS elevation array. These two measurements were made 9 months apart and illustrate the stability of the test results. At the distance of E7, 342 m (1123 ft), main lobe effects should only occur at less than 11 ft height, so we are seeing only sidelobe effects.

4.2 Flight accuracy measurements

4.2.1 General

The flight measurements were divided into sections appropriate to the three sub-systems: approach azimuth, missed approach azimuth, and elevation.

The recommended test conditions were followed as closely as possible within the constraints imposed by local conditions, such as low flying restrictions, airways and other airfields. Height and range were dictated in many cases by the visibility requirements for the tracking system, and in particular, tracked runs up to 10000 ft in height and 20 n mile range were not achieved.

For each run on each sub-system up to three types (a, b, c) of plots are presented in order:

Plot a A plot of the angular flight path as tracked by the kinetheodolite system. This plot is frequently presented as a deviation from the nominal flight path angle.

Plot b A plot of the angular flight path as derived directly from the digital output of the DMLS receiver with *no* filtering, that is raw data.

Plot c For each data point a plot of the angular error between the DMLS data and the tracking data. These plots cover the total valid data recorded on each run even if this extends beyond the nominal design coverage of the system. All data points are presented unless inhibited by the receiver flag. In general, these plots also have lines indicating the bias and noise limits over the various flight segments as recommended by the AWOP WGA. (*NB:* In general either plot a or plot b is included to give the actual aircraft flight profile. Both plots are only included together if they illustrate a specific event.) On azimuth system orbital flights, plots a and b are combined, that is DMLS angle is plotted against kine angle and is identified as an a/b plot; this also applies to vertical ascent measurements in the elevation flights. Plots are therefore presented as Fig Na,b,c or Fig Na,c or Fig Na/b,c etc.

Data points are excluded when receiver flags are operative and are also censored when more than 0.2^{o} different from the mean of the preceding three points. Censored points are indicated by a 'T' symbol on the plots. Mean values M and standard deviation S_T with respect to that mean, have been calculated for the *total* DMLS errors in each flight *segment*. These values are quoted on the type C plots (*ie* the per data point error plots). The statistical analysis was restricted to the coverage limits given below, which were the design aims of the FDM equipment:

	Azimuth	Elevation
Approach azimuth	$\pm 60^{o}$	$+30^{o}$
Missed approach azimuth	$\pm 60^{o}$	$+30^{o}$
Elevation	$\pm 40^{o}$	$+20^{o}$

4.2.2 General comments on flight test results

The quantization level of the output of the DMLS feasibility demonstration receivers, that is the smallest digital angular step, was 0.01847^{o} for the approach azimuth and missed approach azimuth sub-systems, and 0.00923^{o} for the elevation/flare sub-system. The result of this difference in quantization is immediately apparent when comparing the noise on the error plots for azimuth with that for elevation. The azimuth error plots show an angular noise which is almost twice that seen on the elevation error plots, showing that most of the noise is due to the quantization chosen for the feasibility demonstration equipment.

The quantization levels quoted above are for the bore-sight of the array in question, and at an offset angle θ, the quantization is proportional to $1/\cos\theta$, so it is doubled at an offset angle of 60^{o}. The effective angular beamwidth of the system is also doubled. The result of this is seen in azimuth sub-system orbital flights when the noise due to quantization increases at large offset angles. In interpreting multipath errors, the increase in beamwidth with offset angle must be taken into account.

All the data presented is for the sine/cosine tracker, and not for the earlier types of decoder used in the DMLS experimental programme. A source of error which was present in all the ungated sine/cosine tracker results (all the azimuth data, and the ungated elevation data) was a cyclic error identified in the simulator measurements. The error has an angular spacing of half a beamwidth (0.25^{o} for approach azimuth, 0.35^{o} for elevation and 0.5^{o} for missed approach azimuth). The magnitude of the error was 0.05 beamwidths peak-to-peak (0.025^{o} for approach azimuth, 0.05^{o} for missed approach azimuth, and 0.035^{o} for elevation). The angular spacing and the magnitude of the effect was again dependent on offset angle, that is doubled at 60^{o} offset. This error contributed to the general noise of the system in an azimuth orbit, where the angle was changing rapidly and gave slower changes during azimuth radial flights and elevation orbital flights. This cyclic error was a result of using the sine/cosine tracker in an ungated mode (unsynchronised with the transmitter scan). Most of the elevation measurements were made in the gated mode using the data channel for a synchronising signal (Appendix B refers).

4.2.3 Explanation of numerical annotations on error plots

The error plots associated with individual flights have numerical annotations so that recurring phenomena, most of which are not attributable to the DMLS, can be explained by referring to the following notes.

The annotations are summarised below and are described in more detail later:

(1) Missing or invalid kinetheodolite data
(2) Tracking error local to kinetheodolite baseline
(3) Digital recorder errors
(4) Receiver flag operation
(5) Outliers due to receiver
(6) Gaps or errors due to transmitter malfunction
(7) Interfering aircraft or vehicle
(8) Timing synchronisation errors
(9) Ground reflection effects
(10) Azimuth aerial tilt errors
(11) Errors due to temperature effects on aerial arrays.

(1) Missing or invalid kinetheodolite data

This could be caused by cloud obscuration, by a change in aircraft heading resulting in obscuration of the tracking lamp or by a film reading error. The invalid kinetheodolite data was either missing entirely from the kinetheodolite data tape, or it was 'flagged' as invalid by indicating excessive $\dot{x}$, $\dot{y}$, $\dot{z}$ values.

(2) Tracking errors local to kinetheodolite baseline

The use of a pair of kinetheodolites for tracking meant that at points on the line joining them (the baseline), or on its extensions, there were positional uncertainties. These uncertainties were worst at ground level, for example for aircraft taxi runs along a runway, and were reduced at high elevation angles, such as during high level orbits. The angular directions which were likely to give kinetheodolite baseline errors are illustrated in Fig 4.16.

(3) Digital recorder errors

Dirt on the airborne digital recorder tape or on subsequently transcribed tapes could cause garbled data, which in the worst case could be unrecognisable to the computer programme, causing information gaps, or could produce outlier points. Such errors which were rare were detected by reference to the analogue recording.

(4) Receiver flag operation

The receiver flag operated when the signal had not been acquired, or re-acquired after a temporary drop in level or after disturbance by a large

interfering signal, as in some of the multipath tests. In the S type receiver, the flag was linked to the search and acquisition circuits and exhibited a flag on, flag off sequence each of length 2.8 s when the signal was invalid. This mode of operation led to some uncertainty in detecting the start and finish of valid data and could have led to loss of data in one case or inclusion of invalid data in the other case. Such a flag system was used in the feasibility demonstration equipment only and was not in the final proposal.

(5) Outliers due to receiver

Occasional outlier points were present on the error plots, which were also on the corresponding receiver analogue recording, but not in the alternative P type receiver plots. These were due to a receiver malfunction and were normally for one update value only. Outlier points more than 0.2^{o} distant from the mean of the preceding three points were indicated by a T on the plot and replaced by a mean value in the statistical computations.

(6) Gaps or errors due to transmitter malfunction

Occasional gaps or errors could be identified as originating at the transmitter, since they occurred on both receivers, and were accompanied by AGC drop outs on the analogue record. This type of fault only occurred on the elevation sub-system and was due to a faulty connector causing occasional loss of signal for short periods of several seconds.

(7) Interfering aircraft or vehicle

The flight trials were conducted in such a manner that other aircraft or vehicles were kept away from the vicinity of the DMLS transmitter antennas during the tracked runs. However, detectable interference by aircraft or vehicles did occasionally occur, and where noted by observers or aircrew, or inferred from AGC recordings, the incident is marked.

(8) Timing synchronisation errors

The FDM system of the feasibility demonstration equipment used the full 200 ms update period for measurements on each of the sub-systems. The kinetheodolite measurements, which were unsynchronised with the receiver measurements and were read once per second, have been interpolated to coincide with the end of a receiver measurement period, that is the time that the receiver output data stores were updated, in order to give realistic FDM results. This gave a timing delay of 100 ms between the centre of the DMLS measurement period and that of the associated kinetheodolite measurement. This resulted in MLS errors

which were proportional to rate of change of angle. The effect was most noticeable for results taken close to the transmitters, for example in the flare region, or almost overhead for a constant height radial. There were also occasional high rates of change during the turn-in manoeuvre.

(9) Ground reflection effects

Ground reflection effects on the elevation sub-system were small because of the effectiveness of the receiver sector filter and tracking filter. However, at elevation angles below 3°, small variations could be detected on the error plots for normal approaches, and for radial and orbital flights. At higher elevation angles such errors were not seen, because of lower ground reflection and the increasing separation angles.

Ground reflected signals had very little effect on the azimuth system when the ground and antenna were both horizontal. However, an effective lateral ground slope (*ie* ground plus antenna) of as little as 0.1° could give measurable errors with the simple ground plane antenna used in the DMLS feasibility demonstration equipment. Such an antenna gives only a small amount of vertical directivity and hence comparatively high ground reflected signals. An estimate of the combined effect of ground reflection loss and antenna radiation pattern attenuation at negative angles is shown in Fig 4.17. It can be seen that the ground reflected signal was at least 15 dB below the direct signal, for elevation angles greater than 6°. This corresponds to ranges less than 3 n mile for a 2000 ft constant height radial. The effect of lateral ground slope on the Doppler angle coding is illustrated in Fig 4.18. Ground slopes of 0.1° and 0.25° were considered, for 2000 ft radials at a series of radial angles. The calculated, peak-to-peak error for different levels of ground reflected signal is shown in Fig 4.19. Elevation angle and position of ground interference nulls during a 2000 ft radial are shown in Fig 4.20, for the approach azimuth and missed approach azimuth antenna heights. Each ground interference null corresponds to a maximum phase error condition. Measured ground slopes in front of the approach azimuth antenna are shown in Fig 4.21a. When associated with an antenna tilt of 0.1° (see note 10), the estimated and measured ground slopes were reasonably consistent for the approach azimuth antenna. (Note, the reflection region was approximately 9.2 m (30 ft) wide.) Measured ground slopes for the missed approach azimuth site are shown in Fig 4.21b.

(10) Azimuth antenna tilt errors

An azimuth antenna tilt from horizontal could contribute to ground reflection errors, as described in (9), and also give rise to direct errors. Thus, an antenna tilt β gives an azimuth angle ϕ' instead of the true angle ϕ (see Fig 4.22), where

$$\cos \phi' = \cos \phi \cos \beta + \sin \theta \sin \beta$$

and θ is the elevation angle (ϕ is the angle with respect to the array axis, the angle with respect to centreline is $(\pi/2) - \phi$). This gives a maximum error of β when $\theta = \phi$, that is on crossing the axis of the array. The approach azimuth radial flight error plots gave a positive error close to the transmitter consistent with an aerial tilt upwards to the south of the centreline of 0.10°. Subsequent measurements of the antenna confirmed an overall tilt of 8 minutes of arc (0.13°) in this direction. This tilt could have been removed in the middle of the tests, but it was decided not to remove it in order to preserve continuity in the measurement programme.

(11) Errors due to temperature effects on antenna arrays

The angular sensitivity of a DMLS commutated array is proportional to the physical length of the antenna. No allowance was made in the DMLS feasibility demonstration equipment for array length changes due to temperature. The fundamental relationship for calculating the positional angle θ from the Doppler technique is:

$$\sin \theta = \frac{\text{Doppler count}}{A} ,$$

where A is proportional to array length L. Thus

$$\delta\theta = \tan \theta \frac{\delta L}{L} \quad \text{rad}$$

$$= \tan \theta \, \alpha \delta T \quad \text{rad} ,$$

where α is the linear coefficient of expansion of the array, and δT is the temperature change.

The coefficient of expansion of duralumin, which was used in the construction of the azimuth antenna is $23 \times 10^{-6}/^{\circ}C$. Thus, taking a temperature difference of $18^{\circ}C$, at an offset angle of 50° we have $\delta\theta = 0.03^{\circ}$.

4.2.4 Approach azimuth system (120λ aperture)

(a) Radial runs

The test programme called for two sets of constant height radial runs:

(i) At a nominal height of 3000 ft from a range of 20 n mile and at azimuth angles of ±45°, ±40°, ±20° and 0°;

(ii) At a nominal height of 2000 ft from a range of 10 n mile and at azimuth angles of ±15°, ±10° and ±5°.

The tests extended over the period May to November 1975 and therefore gave an indication as to the stability of the system over an extended time. The maximum tracked range was 19 n mile and many of the runs had to be made at altitudes below 3000 ft because of cloud cover. Manual flying was used on all flights with no strict instructions for path following accuracy so that angular dependent errors, if any, should be evident. Typical results are shown in Figs 4.23 to 4.28 covering azimuth angles from -40° to +40°. The effects of ground reflections with a cross slope are clearly seen in Fig 4.27 and 4.28.

(b) Orbital runs

Fig 4.29 shows the result of an orbital run at a nominal range of 7.2 n mile from threshold and height of 2000 ft giving a mean elevation angle of 2.4°. An example of the performance at a higher elevation angle is given in Fig 4.30, which is for an orbit at a mean elevation angle of 7.5°. Both these orbits were flown in June using the Wessex at low speed. Fig 4.31 shows a typical result using the Andover at a speed of 157 kn in December; this result can be compared with Fig 4.29 and shows little change with aircraft type and time difference of 6 months. All the orbits show a slight sensitivity error. The temperature difference between 11 June (Fig 4.30) and 3 June (Fig 4.29) was some 10°C, but in terms of direct sunshine, which is more relevant to array heating, there were 13.6 h on 11 June and only 5 h on 3 June. The implied 18°C change in temperature given by the increase in sensitivity on 11 June was not unreasonable. Even with the high system quantization, the overall noise was well inside the WGA limits.

(c) Approach azimuth centreline approaches at 3° elevation

Examples of approach azimuth centreline runs are shown in Figs 4.32 to 4.34. The signal quality was very good, the system noise being limited by quantization.

4.2.5 Missed approach azimuth (60° aperture)

Fig 4.35 is an example of a constant height centreline radial. The effects of ground cross fall are clearly seen. Figs 4.36 to 4.39 show the results of orbital flights at 2.5°, 4.7° and 12.8° elevation. These plots show an increasing positive error in the angular range of +50° to +60°. This affect was caused by the sector filter used in the receiver, which gave a sharp cut off beyond ±40° since the MLS receiver was designed for a nominal ±40° missed approach sector. The corresponding negative error can be seen between +50° and +60°, but the effect is not so marked, since the cut off rate at this end was not so great. Also noticeable in the error plots are discrete errors at +32° and +46°. The former corresponded to a large steel lattice tower of 33 m (110 ft) height (2.64° elevation), while the latter corresponds to a basically wooden tower of height 15 m (50 ft) (2.5° elevation). The lower elevation orbits also showed longer period waves, which were attributed to ground reflection. The multipath effects on the high angle orbit, Fig 4.39, were very small, as would be expected.

The result of a 3° approach is given in Fig 4.40. During an approach the elevation angle with respect to the transmitter slowly decreases from near 3° to zero at landing. Between 3 and 5 n mile a ground reflection error is clearly visible which was related to the 1° crossfall around centreline in the ground in front of the missed approach azimuth array (see Fig 4.21b).

4.2.6 Elevation system (90° aperture)

(a) Radial runs

The typical performance of the elevation system for constant height radials on centreline and at -44° and +51° is shown in Fig 4.41 to 4.43. The centreline radial shows some errors due to ground reflection at ranges beyond 12 n mile (below 2.5° elevation) with the maximum error at 18 n mile with an elevation angle of 1.6°. The maximum elevation angle achieved was +19°. As the rate of change of angle increased with increasing elevation an increasing negative bias was seen consistent with the 100 ms average measurement delay in the FDM receiver. The radial flights at -44° and +51° show similar results. It should be noted that these were actually flown at a fixed radial to the azimuth site and therefore at short range the azimuth angle to the elevation site was very large, see Fig 4.43c. The lower elevation system quantization is clearly seen. The top elevation angle was determined by the rapid cut off in the reference pattern at +17.5°.

...rital runs

... low noise and wide azimuth coverage is clearly illustrated in the ... of Figs 4.44 and 4.45 at elevation angles of 3^{o} and 9.5^{o}. These ... show the system symmetry about the vertical axis and indicate an ... system bias of 0.015^{o}. The bias variations at wide negative angles are ... to small internal reflections within the array structure associated ... reference element which was mounted on the negative side of the array.

... Vertical ascent

... shows the result of a vertical climb made in a helicopter at a ... n mile. This again emphasises the low system noise level.

... 3^{o} approach runs

Examples of 3^{o} approaches are given in Figs 4.47 and 4.48. In Fig 4.48, ... the aircraft starts well below the 3^{o} line, the system errors are still ... small at 1.5^{o} elevation.

... 6^{o} approach

Fig ...49 shows the result for a typical approach of 6^{o}. At this high ... there was no measurable error due to ground reflections, there was a strong ... effect at very short range.

... ability tests

In addition to the information obtained with respect to long-term system ... from the ground and flight trials, a specific measurement of system ... was made over a 30-day period of simultaneous operation of the three ... Fig 4.50 shows the position of the measurement point indicating the ... paths for the signals from each sub-system. The receiver and tape ... were mounted in the test van with an antenna at a height of 30 ft on ... mast. The position of the antenna with respect to each sub-system ... in Table 4.1.

Table 4.

Test antenna position

Sub-system	Range m (ft)	Azimuth (deg)	Elevation (deg)
Approach azimuth	2933 (9620)	+2.99	+0.06
Missed approach azimuth	521 (1710)	+17.1	+0.98
Elevation	305.5 (1002)	zero	+0.72

It can be seen from the layout of runways and taxiways that both the azimuth systems were susceptible to perturbation by vehicle traffic, with the approach azimuth more so due to the low elevation angle of the propagation path. In fact, due to the runway hump, there was no line of sight to the approach azimuth. The digital recorder was programmed to take a sample of at least 25 updates at half hourly intervals. Each data sample was analysed for mean and standard deviation of error. On a daily basis, the mean error, standard deviation of mean error and extremes of mean error for the 48 samples were computed. System noise was quantified by computing the rms noise on a daily basis.

(a) Approach azimuth

The results for the approach azimuth system are shown in Figs 4.51 to 4.54. The mean bias, bias extremes and daily standard deviation were all contained within very narrow limits. The rms noise level was also very consistent and appeared to be determined solely by the system quantization of 0.0184^{o}. The results are particularly noteworthy due to the lack of line of sight propagation. The typical received signal level was around -95 dBm.

(b) Missed approach azimuth

The results for this system are shown in Figs 4.55 to 4.58. The mean error over the 30-day period showed the same order of long-term stability as for the approach azimuth system. The maximum daily excursion and the standard deviation of mean error on a daily basis were slightly greater than for the approach azimuth. This was attributed to the effects of temperature change on the system sensitivity, which will have a greater effect at the 17^{o} missed approach angle compared with, the 3^{o} approach azimuth angle at the monitoring site.

(c) Elevation system

The elevation results are shown in Figs 4.59 to 4.62. The mean error shows a positive step change on September 7 which occurred on re-positioning the antenna. The rms noise was about half that of the azimuth systems due to the lower measurement quantization.

4.4 Multipath field trials

The multipath tests detailed in the ICAO test requirements were made using a combination of reflecting screens, the repeater system and other aircraft as multipath sources. The results obtained were in general agreement with the performance predicted from receiver measurements using the hybrid simulator as a signal source. (The hybrid simulator and its use in the TDM mode is described in section 6.) As the multipath performance is a function of system aperture, signal format and signal processing technique, the FDM multipath test results were not strongly relevant to the performance of the TDM system. Furthermore, the field test results, because of the difficulties in quantifying the environment, did not play a significant role in the comparative performance evaluation in the ICAO programme. Accordingly, no data is presented in this section and the reader is referred to section 6 for a detailed presentation of the TDM system multipath performance based upon the use of the hybrid simulator.

4.5 System coverage

The long range coverage of the FDM system was evaluated by a series of constant height radial flights starting beyond 30 n mile from threshold. The measurements showed that a range of 20 n mile was obtained with a margin of 6 dB or more when referred to the BAC 1-11 above cockpit antenna feeding a receiver located in an equipment rack and not using a remote RF unit. Extrapolation of these results to the TDM system, which had different ground antenna gains and receiver threshold levels, indicated that the required range performance on a clear site could probably be met with a reasonable working margin for the test aircraft used. For field test results on the TDM system the reader is referred to section 7.

The measurements did highlight that overall system performance would be highly dependent on the airborne antenna installation and at C band quite wide variations could be expected between different types of aircraft.

It is highly probable that an above cockpit site on the majority of aircraft will give good performance when the aircraft heading is within $\pm 90^{o}$ of the direction of the ground station, but we must accept that on a large aircraft

with long cable runs the combination of cable loss and shadowing by the wings and fuselage may well cause loss of signal for an aircraft flying away from the ground stations. One solution to such a situation could be to use a second antenna mounted at the rear of the aircraft. This would introduce problems of feeder loss or require the use of a remote RF unit coupled with the introduction of an associated automatic form of antenna selection mechanism.

An alternative solution, which should be carefully considered, would be to use some RF amplification at the above cockpit antenna. Suitable field effect transistor modules now exist with noise figures around 6 dB and wide dynamic range, *ie* 1 dB compression point at +10 dBm. The use of such a unit with a gain of 20 dB associated with a receiver of 11 dB noise figure, and, say, a cable loss of 10 dB, would give an effective system noise figure referred to the antenna of 8 dB. In this case the use of an amplifier gives an additional signal margin of 13 dB compared to performance without the amplifier.

4.6 Overall conclusions of the FDM system trials

The prime overall conclusion from the FDM trials was that the DMLS technique had been fully proven in terms of being able to meet the system accuracy requirements. The equipment had shown that very simple ground systems gave very stable signals and emphasised the basic attraction of the simple digital commutation process.

Whilst the performance of the technique had been validated by this work, a number of shortcomings of the FDM signal format and equipment implementation had emerged and needed to be carefully considered in formulating the next stage of equipment development:

(i) The simple ground-plane antennas would not be suitable in a snow and ice environment.

(ii) The FDM signal format was inefficient in the use of available signal spectrum. In particular, the use of a separate data channel was not cost effective as even the simplest basic azimuth and elevation system would need some data capability.

(iii) All of the improved signal processing concepts being developed required scan timing information which was not inherent in the FDM format.

(iv) If all functions, including flare, were to be accommodated on one RF channel, the current channel width of 600 kHz would have to be increased and this was contrary to the pressures to reduce channel width and conserve frequency spectrum.

(v) The FDM format was totally inflexible in that, as no sub-system carried any function identity code, unused sub-systems could not be readily replaced by another sub-system.

(vi) The multichannel IF of an FDM receiver was expensive and the maintenance of sub-channel separation in the receiver complicated design and increased cost.

Irrespective of these limitations the basic equipment design philosophy embodied in the elevation system proved very successful and formed the basis of the next stage of equipment development.

5 THE TIME DIVISION MULTIPLEX SYSTEM

The decision to utilise a pure time division multiplex format for the system proposed to ICAO was based on a number of factors which emerged from comparison of the FDM work in the UK and the work on TDM systems in the USA prior to 1975. These factors may be summarised as follows:

(a) A TDM system makes more efficient use of available channel bandwidth.

(b) A pure TDM system gives maximum flexibility in choice of functions.

(c) A TDM system gives minimum airborne equipment costs and component count.

(d) In those circumstances where co-located azimuth and elevation systems are employed, one transmitter can operate both systems.

(e) Any question of sub-channel cross-talk that might occur in the FDM system is eliminated.

Against these factors, the simple function identity integrity of the FDM system is lost and, for a given transmitter power, a range loss of 6 dB occurs due to the wider processing bandwidth necessary for the TDM system.

The TDM system concept emerged from joint discussions between RAE, CAA and Plessey. The detailed format structure and equipment designs were predominantly of Plessey origin. The signal format, ground equipments and airborne receiver described in this section are those used in the UK trials programme to provide data for the ICAO evaluation. It should be noted that certain features differ

from the actual format and equipment descriptions contained in the UK proposal to ICAO. This arises from the continued analysis and development applied to the proposal after the TDM equipment was built.

5.1 The TDM signal format

This sub-section provides an overview of the format used in the trials equipment; full details are given in Ref 1. The improved spectrum utilisation of a pure TDM format resulted in the decision to reduce the angle system channel width to 300 kHz, enabling the 200 angle guidance channels to be provided in a 60 MHz band situated between 5031 and 5090 MHz.

The basic TDM format is summarised in Fig 5.1a and was based on an update rate of 10/s for flare angle and 5/s for basic azimuth and elevation functions. The basic 200 ms time frame also included provision for the following:

(a) up to 315 bit/s of primary and auxiliary data;
(b) a ground radiated test signal;
(c) an extra time slot for growth.

Each function was preceded by a data preamble, Fig 5.1b, which comprised

(i) 5 bits for receiver AGC stabilisation (A);

(ii) a 5-bit Barker code for synchronisation (B);

(iii) a 13-bit function identity (FI) including 5 parity bits;

(iv) one morse bit for facility identity (approach azimuth and missed approach azimuth only) (O).

In addition, the approach azimuth preamble contained 32 bits for primary data and 2 × 4 bits for out of coverage indication (OCI) amplitude comparison, which prevented use of angle data outside the guaranteed coverage limits, the elevation included 4 bits for high angle OCI, and the auxiliary data slot had provision for two 32-bit words.

The preamble and data bit allocations are given in Table 5.1. All data was transmitted as a differential phase shift keyed (DPSK) modulation of a data sub-carrier, offset from the reference by 41.6 kHz, see Fig 5.2.

The angle guidance functions used an offset frequency of 83.2 kHz and employed the frequency interchange arrangement as shown in Fig 5.2. A nominal information bandwidth of 170 kHz was required. The overall receiver channel bandwidth was 220 kHz, which included an allowance of ±25 kHz for frequency misalignment made up as follows:

(a) ground station ±0.0001% (±5 kHz);

(b) airborne local oscillator ±0.00033% (±16.5 kHz);

(c) aircraft velocity Doppler shift ±0.00007% (±3.5 kHz).

Table 5.1

Preamble bit allocations

Feature		Approach azimuth	Elevation	Flare	Missed approach azimuth	Test	Growth	Aux. data
AGC		5	5	5	5	5	5	5
Prefix		5	5	5	5	5	5	5
Function	Information	8	8	8	8	8	8	8
Identity	Parity	5	5	5	5	5	5	5
Morse bit		1	B	B	1	B	B	B
Primary Data	Information	26	-	-	-	-	-	-
	Parity	6	-	-	-	-	-	-
Aux. Data	Information	-	-	-	-	12	-	52
	Parity	-	-	-	-	-	-	12
OCI	Right	4	4	-	4	-	-	-
	Left	4						
No. of bits		64	27 + B	23 + B	28	35 + B	23 + B	87+B
Equivalent time m/s (including blank)		7.69	3.36	2.88	3.36	4.33	2.88	10.58

Bit period = 5 × 1 cycles of 41.6 kHz data subcarrier, = 0.120192 ms.
Max. total preamble time = 24.6 ms (2 off for flare).
B = blank.

Different angle functions had different durations, see Fig 5.3. The function lengths were unique and could be used to provide a check on the correct decode of function identity. The choice of function duration devoted the largest slot of 50 ms to elevation to ensure good motion averaging performance of in-beam multipath (see section 6 for details). In all cases the format provided for multiple scans over a range of apertures.

Typical parameters are given in Table 5.2.

Table 5.2

Aperture and scan parameters

Function	3 dB beamwidth (deg)	Nominal aperture (wavelengths)	Single scan time (ms)	No. of scans in slot time	Endfire Doppler frequency (kHz)
Approach Azimuth	0.47 0.94 1.88	108.34 54.17 27.08	5 2.5 1.25	6 12 24	21.67
Missed Approach Azimuth	0.94 1.88	54.17 27.08	2.5 1.25	9 18	21.67
Elevation	0.47 0.94 1.88	108.34 54.17 27.08	2.5 1.25 0.625	20 40 80	43.34
Flare	0.47 0.94	108.34 54.17	2.5 1.25	8 16	43.34
Test	Not applicable	Not applicable	1.25	18	Not applicable

Offset frequency = 83.2 kHz

The boresight coding sensitivities were 378 Hz/deg for azimuth systems and 756 Hz/deg for elevation systems. These coding sensitivities were maintained as a fixed system characteristic by adjusting the commutation rate to compensate for the changes in electrical length over the 60 MHz operating band. In this way the same physical array was used for all channels, although at the higher frequency channels the full physical length would not be used.

The angle system coverage was normally defined to the airborne receiver by part of the ground-to-air data. General ground system design philosophy was to provide guidance data beyond the limits of nominal coverage, thus providing for initial signal acquisition outside the nominal coverage sector.

At very wide azimuth angles on the azimuth system, a possibility of false information existed, arising from reflections of a within-coverage signal being of greater amplitude than the direct signal due to the fall off in the radiated power of the array elements at wide angles. To guard against this situation, an out of coverage indication (OCI) was provided in the data preambles to both the approach azimuth and missed approach azimuth. An OCI was also available for

suppression of high angle residual grating lobes that may occur in the elevation system. Basically, a short burst of the data (4 bits) was radiated from each OCI element, which provided a directional signal outside the coverage sector greater in amplitude than that of the normal data antenna. This is illustrated in Fig 5.4, angle information was only accepted by the receiver processor when the data signal was 1 dB or more greater than the OCI, see Fig 5.5. The system was not intended to give positive OCI everywhere outside the normal coverage. In much of the region to the rear of the antenna the data signal strength would have been inadequate for decoding so that no information would have been decoded at all.

5.2 The TDM ground equipment

For the TDM evaluation programme, only an azimuth and elevation system were deployed and the descriptions given in this section are therefore confined to these equipments in the form used for the main field trials. An inherent feature of the TDM system was that the azimuth and elevation transmitters were essentially similar, the transmitter design being based largely on the experience gained with the FDM elevation transmitter. All the TDM equipment was developed by Plessey. Table 5.3 summarises the basic azimuth and elevation system parameters.

5.2.1 Transmitter system

The transmitter, Fig 5.6, provided the necessary C-band signals together with logic drives to the switches making up the commutator. The transmitter controlled selection of antenna elements for data and angle modes, organised primary and auxiliary data and housed the monitor decoding and logic. The transmitter comprised three distinct sections, the IF unit, the RF unit and the timing unit.

IF unit The IF unit generated the reference carrier and a sideband displaced by 83.2 kHz during the angle mode or by 41.6 kHz during the data mode. The unit also contained the modulator which was used for phase cycling and DPSK respectively. Its two outputs drive the up-conversion mixers in the RF unit.

A block diagram showing the elements making up the IF unit and their interconnections is presented in Fig 5.7. The principal boards and their functions were (page 61):

Table 5.3

Ground sub-system parameters

	PARAMETER	AZIMUTH	ELEVATION
1.	Signal format	Time division multiplex (TDM) as defined in section 2.2 of UK submission to ICAO.	
2.	Channel No.	100	
3.	Radio frequencies	f_1 = 5061.000 MHz f_2 = 5060.9584 MHz f_3 = 5061.0416 MHz	
4.	Sub-carrier frequencies	Data ($f_3 - f_1$) = 41.6 kHz Angle ($f_3 - f_2$) = 83.2 kHz	
5.	End fire Doppler frequency	21.67 kHz	43.34 kHz
6.	Scan changeover frequency	400 Hz	800 Hz
7.	Commutation frequency	38.172 kHz	50.896 kHz
8.	Coding sensitivity at broadside	378.21 Hz/deg	756.43 Hz/deg
9.	No. of scans per up-date	12	40
10.	Single scan time	2.5 ms	1.25 ms
	ARRAY PARAMETERS		
11.	No. of active elements	109	64
12.	No. of commutator switches	32	22
13.	Element spacing at operating frequency	0.5675λ	0.8513λ
14.	Array length at operating frequency	54.483λ	54.483λ
15.	Blending function	sin/cos	sin/cos
16.	Operational coverage	Azimuth ±40° Elevation 1° to 20°	Azimuth ±40° Elevation 1° to 20°
17.	OCI	AZ control point ±43° (nominal)	
18.	Coverage-field monitor	±45° Range 100-200 m	0-15° Range 100-200 m
19.	Monitor output logic levels	Output '1' + 12 V (+ 0 V, − 5 V) Output '0' 0 V (+ 0.5, − 0 V) V Alarm condition = '1'	
	POWER SUPPLY		
20.	Mains	115 or 230 V, 50-60 Hz	115 or 230 V, 50-60 Hz
21.	Consumption	9 kW	9 kW

79052

Table 5.3 (concluded)

PARAMETER	AZIMUTH	ELEVATION
OPERATIONAL ENVIRONMENT		
22. Ambient temperature	$-35^{o}C$ to $+50^{o}C$	
(i) Main antenna array	Temp. $10^{o}C$ - $30^{o}C$ Humidity RH 9%-30%	
(ii) OCI	Temperature maintained above $10^{o}C$	
(iii) Field monitor antenna	Temperature maintained above $10^{o}C$	As azimuth
DIMENSIONS AND WEIGHTS		
23. Antenna		
(i) Main structure	Length 5 m Width 1.5 m Height 2.9 m Weight 1182 kg (inc. OCI)	Depth 0.5 m Width 0.4 m Height 5 m Weight 545 kg
(ii) Support legs		2 off 1.5 m × 1.5 m × 2.1 m
24. Transmitter cabin	Length 2.3 m Height 1.5 m Width 1.2 m Weight (inc. all equipment) 909 kg	As azimuth
25. Remote Control Unit (Located close to azimuth facility)	Length 0.7 m Height 1.1 m Width 0.6 m Weight 70 kg	

79052

(a) Offset frequency generator, which contained three crystal oscillators:

(i) 15,0000Hz reference oscillator;

(ii) 15,0832MHz voltage controlled oscillator, which was phase locked to the angle offset clock from the timing unit to generate the offset frequency;

(iii) 15,0416MHz voltage controlled oscillator which was phase locked to the data offset clock from the control unit.

(b) Data angle change-over switch, to switch between the data and angle oscillators in synchronism with the appropriate antenna selection.

(c) Scan change-over switch, which was used only in the angle mode to interchange the carrier/sideband roles ('reference'/'commutated' channels) of the 15 MHz and 15.0832 MHz signals at the end of each scan.

(d) Phase modulator, which served the dual purpose of encoding the data subcarrier with DPSK and modulating the angle sideband during the angle mode. The latter included the application of phase cycling, which altered the phase of the signal in the 'commutated' channel by a predetermined increment at the end of each scan. The sum of these phase increments over the entire scan period was 180^{o}. It was also used to apply a precise frequency increment to the angle sideband to provide test tones used in the ground radiated test function.

(e) Modulator drivers, which provided the two modulating inputs in the desired phase quadrature. This was reliably achieved by generating all the modulation inputs digitally and adding a digital increment equal to 90^{o} in one of the two feeds. Prior to the modulator, each input was transformed into its analogue form by independent digital to analogue converters. The accuracy and spectral purity of the modulating waveforms were ensured by making each digital step equivalent to a small phase increment and by filtering immediately after the digital to analogue converters.

(f) Up-conversion board, in which the two signals were mixed in separate balanced mixers with a 175 MHz local oscillator signal. The desired upper sideband was selected by passing the output from both mixers through separate 190MHz band-pass filters.

(g) 175MHz oscillator board, which consisted of a crystal oscillator, a frequency multiplying stage and an amplifier which provided the drive for both double balanced mixers on the up-conversion board.

(b) 190MHz amplifiers, which were two identical circuits that amplified the carrier and sideband/sub-carrier to drive the following RF unit at approximately 20 mW. Outside the sub-frame period, these amplifiers were gated off by the control unit to remove the RF drive.

The minor variations needed for other functions were readily accommodated within this basic design.

RF unit The two '190 MHz' inputs were up-converted in the RF unit by independently mixing with a stable C-band local oscillator which defined the channel frequency. The two signals were filtered and amplified before being routed to the appropriate array elements (Fig 5.8). The principal sub-units were:

(a) C-band source, which provided the local oscillator signal appropriate to the designated channel. A stability of ±0.0001% was ensured by phase locking to a crystal oscillator.

(b) Up-conversion system, which used identical double balanced mixers providing good isolation between input and output. This eased the requirements on the following filters which selected the upper sideband in the range 5030 to 5091 MHz.

(c) Power amplifiers, one for each sub-channel, provided the necessary power gain. Travelling wave tubes were used to provide 40 dB gain and 15 W output. Solid state amplifiers could be used where either lower range or smaller provision for attenuation due to rain is acceptable and in the longer term will meet the full requirement.

(d) Power blending circuits designed to give a smooth transfer of radiated power from one array element to the next during commutation of the signal along the array. This was achieved using complementary amplitude functions to modulate the RF signals in the odd and even sub-channels.

The amplitude modulator was implemented by a combination of variable ratio power splitters (VRPS) which gave two amplitude outputs (sin and cos in RF phase at any power split ratio.

Transmitter timing unit The timing unit (Fig 5.9) performed a number of functions:

(a) Slaved the start of the sub-frame period to the START signal generated at the executive control unit (ECU).

(b) Organised the sequence of operating modes during the sub-frame period.

(c) Controlled the routing of RF power during the three sub-frame modes.

(d) Clocked data out of the preamble memory at the correct rate. The data included OCI as a series of zeroes.

(e) Generated the data offset frequency for the preamble period.

(f) Generated the angle offset frequency.

(g) Controlled the rate at which the angle sideband was scanned across the commutated array.

(h) Controlled the period of each scan.

(j) Generated the blending waveforms, in synchronism with element switching, to blend the RF power at each commutated element in order to reduce spectrum splash.

The most important element in the transmitter timing unit was the master clock. This consists of a crystal clock operating at 4.16 MHz from which all the sub-system timing was derived (Fig 5.10). When the 'sub-frame start' signal was received from the ECU, all the clock dividers were set to zero, and then allowed to continue counting. The dividers determined, in sequence, the angle offset frequency of 83.2 kHz, the data offset frequency of 41.6 kHz, the data clock of 8.32 kHz, and the scan clock at 1600, 800, 400 and 200 Hz depending on the antenna aperture.

The synchronising 'sub-frame start' pulse triggered the operation via a function timer. The latter was a shift register which was clocked at 83.2 kHz and was set to count an interval of 200 ms. Should the 'sub-frame start' not appear, the function timer would start the sequence within 0.012 ms and would maintain the function position in the frame within 0.5 ms for at least 8 min.

The preamble data was stored in a programmable read only memory (PROM). In addition to standard Barker code, this was pre-programmed with the function identity and scan time of the specific installation. This data was clocked to the IF unit under the control of the data clock derived from the timing unit.

In the angle mode, the Doppler shift was proportional to both the transmitted frequency and the velocity of scan. Thus, in order to maintain a fixed coding sensitivity for all channels, the scan velocity must be inversely proportional to the transmitted frequency. It was preferable to have a fixed element spacing on the commutated array, which required the rate of switching between elements (stepping rate) to be inversely proportional to transmitted

frequency. For this reason the frequency of the stepping rate clock was selected to suit the assigned RF channel.

The stepping rate clock drove a binary number generator which was basically an 8-bit up/down counter. The 8-bit word at the output of the counter identified one even and one odd numbered antenna element and appropriate microwave switches were closed to route the RF power to those two elements.

Data The data associated with DMLS was organised into two main groups:

(a) primary data - that fixed and variable data which fully defined the geometry and current status of the DMLS installation in use and all relevant information on its environment;

(b) auxiliary data - additional capacity, fixed, variable or both, the use of which was undefined.

All data was grouped into 32-bit words including five address bits, 21 information bits and 6 parity bits. One primary word was included in each azimuth preamble. Auxiliary data was radiated in a separate auxiliary data time slot, which had its own unique function identity preamble, and was designed to contain two words. Auxiliary data could be transmitted from any angle facility containing the appropriate data module, but it was anticipated that the azimuth facility would be the most commonly used.

Immediately prior to each function period, the preamble was clocked into a shift register ready for transmission. This transmission was followed directly by the primary data.

The auxiliary data was handled in an identical manner, but was assembled at the transmitter with a preamble containing its own unique function identity. In the basic format, one auxiliary data time slot containing two 32-bit words occurred each up-date period.

Commutator The simplicity of the Doppler system stemmed from the ease with which the antenna was fed with the RF signal. The transmitter output was merely applied in the same phase to each antenna element in succession. This was accomplished by a multithrow microwave switch consisting of single pole four throw (1P4T) modules arranged in a branching tree with equal path lengths to all elements (Fig 5.11). The switching module consisted of a 50 ohm stripline circuit with shunted mounted PIN diodes tuned to optimise the 'ON' condition for low loss. Signals were allowed to pass from the input to any of the four outputs by supplying a bias of 100 mA to the branch leading to that output. Thus, only

those few switching elements which were on at any time consumed power from the bias supply. The switch module was similar to that used in the FDM elevation system.

The performance of the switching module was as follows:

Power handling	20 W working	(50 W maximum)
Isolation	>40 dB	(-40 V bias)
Insertion loss	<0.6 dB	(100 mA bias)
VSWR	<1.3:1	(wrt 50 ohm)
Phase matching	$\pm 2^{o}$	(between outputs)
Phase matching	$\pm 4^{o}$	(between modules)
Bandwidth	5.00 to 5.125 GHz	(all parameters)

The commutation was sub-divided into two sets of elements, odd and even. Two-phase blending was then used to smooth the phase progression of the signal along the array and hence to limit the amplitudes of the sidelobes of the signal. Table 5.4 shows the range of possible system apertures and the number of commutated elements using both fully filled arrays and alternative thinned arrays with a four-element commutated reference, see section 2.2.

5.2.2 The azimuth system antenna

The azimuth antenna built for the ICAO test programme was 54λ aperture with 96 commutated elements using a fixed reference and designed for a coverage of $\pm 40^{o}$, see Table 5.4. The array was assembled from a series of vertical slotted waveguide columns designed to provide a sharp cut off at low elevation angles to minimise ground reflections. This provided more independence of local site conditions compared with the ground plane antennas used in the FDM equipment, see section 3.

A typical element is shown in Fig 5.12. The coupling slots were I-shaped and were totally confined within the narrow wall, so that elements could be placed in direct contact if so desired. The coupling of energy into the slots is dependent on the ratio of L_1 and L_2, with $L_1 = L_2$ coupling is a minimum. The selection as to whether L_1 is longer than L_2 or vice versa for a given coupling is determined by the need to minimise the overall cross polarisation component (horizontal polarisation) in the radiated signal. This is equivalent to using alternate slopes in the equivalent shunt inclined slot waveguide element. The azimuth and elevation patterns of a single element are shown in Figs 5.13 and 5.14.

Fig 5.15 shows a view of the array on its mounting frame during assembly. The columns were assembled on a simple support frame to make up the 96-element

commutated array, a single reference and a four element data array. Fig 5.16 shows the fully assembled antenna as initially tested in its housing. The array radome consisted of a glass reinforced plastic (GRP) microwave window covered with an inflatable rubber skin designed to shed ice. As indicated in Appendix A and detailed in section 7, changes were made to the reference and data antennas and to the de-icing skin during the initial evaluation programme. These changes and the reasons for them are discussed in section 7.

5.2.3 The elevation system antenna

The design of the elevation array was derived from that used in the FDM equipment. For the TDM system, the same concept of horn elements feeding a parallel plate region was retained, but was implemented in a cheaper and lighter form of construction using metal spray and GRP. Figs 5.17 and 5.18 show the azimuth and elevation pattern of an individual element. Fig 5.19 shows the completed 54-wavelength elevation array before the radome was fitted. The reference and data antenna was the single slotted waveguide column attached to the side of the main aperture. As with the azimuth antenna, the elevation array radome was clad in an inflatable rubber skin for de-icing. As a result of measurements during the first part of the evaluation programme, a number of changes were made to the elevation system and these are discussed in section 7.

A view of the complete azimuth and elevation antennas co-located for tests at the Plessey factory before delivery is given in Fig 5.16.

5.2.4 Monitoring

Three basic types of monitoring were incorporated in the ground systems: internal monitoring, integral monitoring, and field monitoring.

Internal monitor Internal monitoring measured transmitter parameters to provide a check of system performance and primary parameters. It also provided diagnostic information to maintenance personnel for fault isolation.

The majority of the internal monitor sensors were contained within the RF portion of the transmitter and were principally concerned with monitoring signal power and impedance match (as shown by the reflected power) between the output of the power amplifier and the array. The RF sensors each consisted of a directional coupler, which extracted a sample of the monitored signal and was followed by a detector. Where a go/no go indication was required, the detector output was compared with a threshold level.

Table 5.4

Facility	Coverage (deg)	Array length λ	Bandwidth (deg)	Fully filled array: Number of active elements	Fully filled array: Number of switch modules	Thinned array with four-element reference: Number of active elements	Thinned array with four-element reference: Number of switch modules	System
Azimuth	±60	27	2	60	22	19	7	
		54	1	120	40	34	13	
		108	0.5	240	80	64	22	
	±40	27	2	48	18	16	6	Typical forward azimuth
		54	1	96*	32	28	11	
		108	0.5	192	66	52	18	
	±20	27	2	32	10	12	5	
				28	10			
		54	1	64	22	20	7	
				56	20			
		108	0.5	128	42	36	13	
				112	38			
Elevation	+30	27	2	32	10			
		54	1	64*	22			
		108	0.5	128	42			
	+15	27	2	16	6			Typical elevation
		54	1	32	10			
		108	0.5	64	22			
	+7.5	27	2	8	2			
		54	1	16	6			
		108	0.5	32	10			Flare

* Actual systems built and tested in UK Programme.

To ensure high integrity of the monitoring system, great care was taken to ensure that the monitor sensors were themselves highly reliable and that their inclusion did not reduce the reliability of the basic equipment. This was achieved using stripline directional couplers which only loosely coupled to the signal channel. These couplers were integrated into the basic design and manufacture, ensuring a monitor point of high stability and reliability. The power level on the detectors in the monitor sensors never exceeded one tenth of the level required to damage the detector, even under fault conditions. In some areas reliability was achieved through redundancy, *ie* by duplication of monitoring points or monitoring the same quantity in more than one way.

The internal monitor sensors for an azimuth facility transmitter are shown in Fig 5.20, while Table 5.5 details the monitored parameters for typical azimuth and elevation facilities.

Table 5.5

Internal monitor sensors

No.*	Parameters	Facility	
		Azimuth	Elevation
1	Sideband VSWR	✓	✓
2	Reference VSWR	✓	✓
3	C-band source supply	✓	✓
4	C-band source lock	✓	✓
5	Odd element VSWR	✓	✓
6	Even element VSWR	✓	✓
7	Reference forward power	✓	✓
8	OCI left forward power	✓	-
9	OCI right forward power	✓	-
10	Element fault	✓	✓

* Note: numbering refers to that shown in Fig 5.20.

A feature of commutated arrays is that the performance of each individual element can be examined by sampling the reflected power at the centre of each element dwell period. This is achieved either at a single point or at two points for blended systems. Failure of any element produces an increase in the reflected power for the duration of that element dwell period, so that in addition to the basic warning the number of faults can be counted and reported.

Integral monitor A measure of the power levels being transmitted and of the signal quality in both the data and angle modes was obtained by integral

monitoring sensors built into all DMLS arrays. The signals from the data reference and commutated arrays were combined in exactly the same way as in an airborne receiver and were examined by a monitor processor which was a simplified airborne decoder. A block schematic of the integral monitor is shown in Fig 5.21.

In the azimuth system, a waveguide manifold running along the back of the array took a small sample of the signal in one data element and from all the reference and commutated elements. These signals were sensed by a detector probe and passed via a wideband amplifier into the monitor processor. The data preamble was the first signal transmitted. Its power level was checked and the DPSK demodulator established bit synchronisation from the Barker code. The subsequent data stream was checked in a comparator against a duplicate of the transmitted data which was held in the monitor processor store. This contained the preamble in a hard wired form and the primary data in a temporary form which was updated, via the central monitoring control, prior to each time slot. A prefix alarm was flagged if the prefix was in error.

The synchronisation established from the Barker code was used to synchronise the independent monitor timer, which was then used to check the timing of all the sub-functions within the transmitter.

In the angle period, the signals from the individual commutated elements experienced different phase shifts as they passed along the waveguide. The result was equivalent to receiving the signal from a fixed angle in space and for azimuthal systems this angle was 31.8°.

The beat between the commutated and reference signals was detected and passed via the wideband amplifier into the angle section of the monitor processor. Power level was checked and the signal was decoded to confirm the expected 31.8° measurement. This provided a powerful test of the accuracy of the frequency generation and logic timing within the transmitter.

In elevation systems, the waveguide manifold only sampled the commutated array and its output was mixed with a sample from the reference signal which was radiated, along with data, from a separate element. In this case the angular equivalent of the resulting Doppler signal was 23.57°.

The coding limits, with which the measured values were compared, were stored in the form of digital words hard wired into the equipment. In the case of azimuthal systems fitted to transmit the ground radiated test signal, the test tone limits were also hard-wire programmed and were multiplexed into the

comparator circuit under the control of the function timing. In all cases the measurement accuracy was comparable with that of the airborne receivers, as similar angle processors were used.

Field monitor The DMLS field monitor provided the main check that both the radiated RF power and the angle coding were within limits. The unique feature of the system was that the single point monitor provided verification of the radiated signal quality throughout the angular coverage since, at all positions, each array element contributed in turn to produce a signal which was continuous during the function period.

A block schematic of the field monitor is shown in Fig 5.22. The field sensor consisted of a vertical column antenna followed, in turn, by a square law detector and a wideband amplifier which fed the detected signal back to the monitor processor. The components were mounted in a weatherproof housing which could be heated to meet local weather conditions. The sensors were identical for all functions with only the mounting arrangements differing.

As with the integral monitor, the signal from the field monitor was processed in a simplified airborne decoder but in this case without the data sub-channel. The power detector provided a measure of the radiated power and would activate an alarm if out of limits. If desired, for flexibility, the angle code limits could be set by thumbwheel switches on the front panel; otherwise they were hard-wire programmed.

5.3 The TDM airborne receiver

The main receiver unit, shown in Fig 5.23, was housed in a long $\frac{1}{2}$ ATR case with an associated separate control unit; a basic system block diagram is given in Fig 5.24. In contrast to the FDM receivers, a separate RF head was not used. The trials receivers were designed to accommodate all the functions shown in the basic format, Fig 5.1. In practice only the azimuth and elevation functions were fully implemented and tested. The basic characteristics are given in Table 5.6.

5.3.1 RF/IF section

A diagram of the RF/IF section is shown in Fig 5.25. The receiver was basically a triple conversion system with design provision for compatibility with a C-band DME system. Provision was made for the injection of internally generated test signals at RF and IF. Channelisation over 200 channels was made at the first local oscillator, which was generated from a frequency synthesizer.

Table 5.6

Airborne sub-system parameters

PARAMETERS

1.	Signal format	Time division multiplex (TDM) as defined in section 2.2 of UK submission to ICAO[1]
2.	Radio frequency	5031.0 MHz to 5090.7 MHz
3.	No. of channels	200
4.	Channel bandwidth	300 kHz
5.	Receiver sensitivity	The minimum receiver sensitivities are:- Data - 101 dBm Azimuth - 110 dBm Elevation - 112 dBm These figures are based on the following assumptions:- (a) Input signals are derived from a 1^{o} beamwidth system. (b) The signal level is that of the scan signal level. (c) The reference signal is at least 6 dB above that of the scan signal. (d) In the data function the carrier and sub-carrier levels are equal. (e) The input signal represents an angle displacement of not more than 10^{o} from the centreline of the system. (f) Sensitivity is defined as follows:- (i) Data: The signal level at which the system fails to decode correctly 5% of the data preambles. (ii) Angle: The signal level at which the 2σ angle noise level begins to exceed 0.1^{o} or that where acquisition ceases to be effective - whichever is the greater. (g) Receiver noise factor is 11.5 dB.

RF UNIT

6.	RF bandwidth (-1 dB points)	5030 MHz to 5156 MHz
7.	IF frequency	561 MHz
8.	RF/IF conversion gain	20 dB ±1½ dB with circulator
9.	RF image frequency rejection	60 dB minimum
10.	Damage protection level	300 W in band
11.	Noise figure	12.5 dB maximum
12.	1 dB gain compression input level	-27 dB minimum
13.	LO input frequency	900 MHz ±6 MHz channelled in 60 kHz steps
14.	LO input level (integral receiver)	+9 dBm ±2 dBm

79052

Table 5.6 (continued)

IF UNIT		
15.	All image responses shall be at least 65 dB down on the desired response.	
16.	2nd LO frequency	540 MHz
17.	2nd IF frequency	21 MHz
18.	3rd LO frequency	18 MHz
19.	3rd IF frequency	3 MHz
20.	IF bandwidth (nominal)	240 kHz
ANGLE DECODER		
22.	Outputs	
	(1) Analogue deviation signal	In accordance with ARINC 578 (except for variable gain output in azimuth)
	(2) Analogue flag signal	In accordance with ARINC 578
	(3) Digital bearing output	Via recording interface
	(4) Digital flag outputs	Via recording interface
23.	Coverage	
	(1) Forward azimuth	$\pm 60^{\circ}$
	(2) Elevation	0° to 25°
24.	Quantization of output	0.005° or better
25.	Time to acquire signal (in the absence of other signals)	1 s (nominal)
26.	Analogue output up-date rate	Once per function time slot
27.	Digital output up-date rate	5 Hz
CONTROL UNIT FACILITIES		
28.	Angle selection	
	(1) Forward azimuth	1° steps up to a maximum of $\pm 69^{\circ}$ from runway centreline
	(2) Back azimuth	1° steps up to a maximum of $\pm 49^{\circ}$ from runway centreline
	(3) Elevation 1	0.1° steps from 0° to 9.9°
29.	Frequency channel selection	0 to 199
30.	Self-test initiate switch	
31.	Self-test pass and fail lamps	
32.	Morse volume control	
33.	Power on/off switch	

Table 5.6 (concluded)

POWER SUPPLY		
34.	Input volts	28 V dc to BS 3G100, Grade B
35.	Outputs volts (regulated)	+5 V, +15 V, -15 V
OPERATIONAL ENVIRONMENT		
36.	Climatic	Operations range 0° - $+40^{\circ}$C Storage range -40°C - $+85^{\circ}$C
37.	Vibration	Region B, Category 2 conditions as defined by BS.3G100 Part 2, section 3.1
38.	Acceleration	Designed to meet normal acceleration Class 3, Grade C - Crash acceleration Class 13 Grade F as defined by BS.3G100 Part 2, section 3.6.
39.	Electro-magnetic interference	To meet the requirements of conducted and radiated interference as defined in BS.3G100 Part 4, section 2.
MECHANICAL CHARACTERISTICS		
40.	Receiver unit	
	(1) Dimensions	Long $\frac{1}{2}$ ATR box
	(2) Weight	9.5 kg
41.	Control unit	
	(1) Dimensions	RTCA cockpit racking standard with height, 112 mm and depth 75 mm
	(2) Weight	909 g

The final IF bandwidth was determined by the 3MHz IF filter, the previous IF filters providing the necessary image rejection. A fast acting AGC was applied round the final IF amplifier with a dynamic range of better than 75 dB.

5.3.2 Data decoder

In the TDM format, the critical operation was the positive identification of the function being radiated, so that the correct decoding circuits could be activated. The data preamble was transmitted on a discrete sub-carrier and started with a Barker code word to enable the receiver to match the bit and word timing of the following data. This code was followed by a function identity word which identified the function being transmitted and the scan length in use. The data decoder stored the preambles in a shift register, performed any required parity checks and controlled the timing of the angle processor.

The data appeared at the output of the RF/IF section as differential phase shift keyed (DPSK) modulation of a 41.6kHz sub-carrier at a rate of 8.32 kbit/s and passed into the decoder via a band-pass filter centred on 41.6 kHz (see Fig 5.26). Carrier recovery demodulation was used to derive the differential phase coded bit stream. The DPSK baseband signal from the comparator was turned into binary by generating half data-bit width pulses at each zero crossing. These were fed to the Barker sync correlator formed by a tapped 32-bit shift register, which established an 'average' bit transition time giving bit sync and message sync simultaneously. The timing sync was used to reset the divide-by-eight circuit to the appropriate phase. The data register was fed data which had been converted to binary by the bistable/exclusive-or gate combination.

Data bits were decoded in parallel from the 32-bit data shift register at a time controlled by timing pulses from the 76-bit timing register.

5.3.3 Monitoring and self test

The signal level of each of the three local oscillators was measured, the phase lock indication from the synthesizer was checked and the received signal level was monitored by checking the final IF amplifier AGC voltage. If any of these measurements or any of the power supply voltages were out of tolerance, the flag was operated. Monitoring of the angle decoder is discussed later.

The push-to-test facility provided an end-to-end check of the receiver on pressing a test button on the control unit. The test sequence is illustrated in Fig 5.27 and consisted of four basic stages:

(1) To ensure that the test was not corrupted by external signals, the synthesizer was tuned to channel 201 which was not allocated to any ground station.

(2) The RF unit conversion gain was checked with an injected high level oscillation signal. The signal was coupled to the receiver input, passed through the RF unit and down-converted to a frequency in the band 500 to 600 MHz (thus the oscillator could have a relaxed frequency tolerance). The amplified output appeared via the IF power splitter at the input to a detector. If the detected output was satisfactory, the RF unit conversion gain was correct and the oscillator was turned off.

(3) In stage 3, a 561 MHz crystal controlled signal was injected at low level modulated by signals generated in the data decoder. The signal appeared at the detector output as if it were a normal signal and the AGC voltage was checked to see that the IF sensitivity was correct.

(4) The detector output, which was coded with internally generated azimuth and elevation preamble codes and suitable angle frequency codes, was decoded in the normal way by the data and angle decoders and the decoded values checked.

If any part of the test failed, a red test-fail lamp was lit on the control unit, if the test was passed a green pass lamp was lit. It should be noted that the implemented test system was an example of what could be done. Other test techniques could be employed and automatic sequences considered.

5.3.4 Angle decoding - the correlation processor

Despite the high performance achieved using the sine/cosine tracker in the FDM trials, it did not use all the information available in the DMLS signal and was, therefore, not optimum. Alternative methods of processing were studied with the principal aim of making more complete use of the DMLS information and hence extending the decoding capability. Subsidiary objectives included the achievement of optimum filtering using single scan processing and the reduction of measurement quantization to entirely negligible proportions.

These studies led to the use of a correlation processor which provided a spectral analysis of the received signal. The principle of this form of Doppler processor is the correlation of the incoming signal against the in-phase and quadrature components of a locally generated signal for a given time, T .

This yields a relative measure for the spectral density of the input signal in relation to T at the local oscillator frequency.

In practice, the correlation of two signals involves multiplying them together and integrating the result over a time T. These integrated products for one or more local oscillator frequencies are then used to provide a precise measure of the wanted Doppler frequency. Various processing techniques may be used and one of the most simple is the sum and difference method of steering the local oscillator onto the received Doppler frequency. This is identical to monopulse radar tracking and can be implemented with a single local oscillator. More powerful measurement algorithms make use of different forms of taper across the scan and multiple local oscillators - all without the need for any extra hardware in the digital implementation.

In the following sections, the principles of the correlation processor are considered in more detail and the procedures for acquiring, validating and tracking the wanted signal are described. As an aid to understanding, an analogue version of the system is introduced first before dealing with the preferred digital implementation.

Simple principles of the correlation process. The correlation of the incoming signal $F(t)$ against the in-phase and quadrature components of the locally generated signal $e^{-j\omega t}$ for a time T, yields a relative measure of the spectral density $g(w)$ of the input signal over the time T. This process is simply a physical realisation of the Fourier integral,

$$g(\omega) = \int_{-\infty}^{\infty} F(t)e^{-j\omega t}dt \quad .$$

Since the input signal is only considered to exist over the period $\pm \tau/2$ (in the Doppler MLS this was the scan time),

$$g(\omega) = \int_{-\tau/2}^{\tau/2} F(t)e^{-j\omega t}dt \quad .$$

By correlating $F(t)$ against several locally generated frequencies, the full spectral density of the input signal can be established (the Fourier transform). Since the Fourier transform is a complete representation of the input signal in

the frequency plane, this process uses all of the available information. In fact there has been a simple transformation from the time frame to the frequency plane, from which it is easier to assess comprehensively the content of the input signal. Fig 5.28 is an illustration of the Doppler angle information in the two planes. It should be noted that the $\sin x/x$ function in the frequency plane is a continuous spectrum formed from a single scan.

A simple schematic form of a single frequency analogue correlator is shown in Fig 5.29. The input signal $F(t) = A \sin(2\pi f_0 t + \theta)$, is mixed with the in-phase $F_1(t)$ and quadrature $F_2(t)$ components of the local oscillator of frequency f, that is

$$F_1(t) = \cos 2\pi ft \quad \text{and} \quad F_2(t) = \sin 2\pi ft \ .$$

The products are integrated over the period T to yield the correlation terms I and Q, where

$$I = \int_{-\tau/2}^{+\tau/2} F(t) \cos 2\pi ft \, dt$$

$$Q = \int_{-\tau/2}^{+\tau/2} F(t) \sin 2\pi ft \, dt$$

$$I - jQ = \int_{-\tau/2}^{+\tau/2} F(t) e^{-j\omega t} dt$$

$$= \int_{-\infty}^{+\infty} F(t) e^{-j\omega t} dt \ ,$$

if the scan is treated in isolation, and this integral is, of course, the Fourier integral which was mentioned earlier.

Now $I - jQ$ may be rewritten as

$$G(\omega) = \frac{AT}{2j} e^{j\theta} \frac{\sin \pi T(f_D - f)}{\pi T(f_D - f)} + \text{a term in } (f_D + f) \ .$$

The folded frequency term $(f_D + f)$ is ignored in simple algorithms, with negligible error. The value $G(\omega)$ is the amplitude of the frequency f in the sin x/x function shown in Fig 5.28. The peak value of this term may be tracked to find $f = f_D$.

The ease of tracking using a single local oscillator is improved by subdividing the scan processing into two halves and performing separate sum and difference integrations. In this way the centre of the signal spectrum produces a zero in the difference signal and this is tracked, monopulse fashion, with the sum term normalising the difference signal.

Where near-beam or in-beam multipath signals intrude into the narrow matched filter provided by the correlation process, the spectrum is no longer symmetrical around the desired signal, and the simple tracking algorithms, which assume symmetry, will be in error. The performance in these circumstances can be greatly improved by sampling the spectrum of the incoming signal with several local oscillators, thereby establishing a measure of the different signals present and their relative positions.

To implement this procedure in analogue equipment, requires discrete local oscillators for each of the n sampling frequencies with separate sets of integrators for each. These multiple circuits lead to problems in accurately combining the stored values to perform the desired tracking algorithm. Furthermore, the phase relationship between the local oscillators is important and in an analogue implementation is difficult to control. Fortunately these problems of analogue implementation are removed by the use of digital techniques.

Digital correlation and processing system The digital version of the single frequency correlator is shown in Fig 5.30. A sampling procedure was used whereby the incoming signal was sampled in an analogue to digital converter (A/D). The local oscillator was generated digitally by taking equal phase steps at the sampling rate and the quadrature sine and cosine representations were formed using a read only memory (ROM). After multiplication, the equivalent of integration was achieved by accumulating the sample products.

The great advantage of this implementation was that the same circuitry could be used to generate and process several local oscillators with only a limited number of dedicated word stores for each.

Sampling A sampling frequency of approximately three times the highest expected Doppler frequency was used. This more than satisfied the sampling theorem and a simple filter gave adequate rejection of the image band. With the

currently proposed format, the information band extended from approximately 60 to 105 kHz. A sample period of 3.5 μs was chosen providing a sampling rate of approximately 285.7 kHz. Since the information band was fairly narrow, a four-pole band-pass filter could give at least 46 dB rejection of the image band for this sampling frequency.

Analogue to digital conversion As predicted by computer simulation, extensive practical experience showed that quantization of the input signal and of the local oscillator signals to 5 bits (4 bits + sign) gave adequate system linearity and good output noise results.

The A/D converter consisted of a series of comparators and operational amplifier rectifiers, one of each comprising one stage of the converter. This arrangement gave a very high speed conversion, because it was quasi-parallel in operation. The outputs from the comparators formed a Grey code, in which 1 bit at a time changed as the input varied. The Grey code was converted to binary with exclusive OR gates.

The local oscillator In the digital system this was represented by a frequency synthesizer in the form of a phase accumulator. The objective of this circuitry was to produce two digital words representing the sine and cosine of the local oscillator frequency at each sample period. This was achieved by using the relationship, frequency $f = d\phi/dt$, where $d\phi$ is the phase change in time dt . Every time increment dt , in this case 3.5 μs, a 16-bit word describing a fixed phase step $d\phi$ was added to a register. The value of $d\phi$ was set at the beginning of the scan time according to the frequency, f , required. The register could store a maximum phase of 2π , that is one cycle of frequency. As $d\phi$ continued to be added then integral cycles were lost. This is perfectly acceptable since

$$\sin(N2\pi + d\phi) = \sin(d\phi) \quad ,$$

and

$$\cos(N2\pi + d\phi) = \cos(d\phi) \quad ,$$

where N is an integer. The phase stored in the register is a sawtooth function with time, as illustrated in Fig 5.31.

The content of the register was converted to the sine and cosine representation in a look-up read only memory (ROM), which also performed the multiplying function. The starting phase could be adjusted by pre-setting the register accordingly. The multiplier system took the digitised sample of the input

signal from the A/D and the first 6 bits of the synthesizer output and produced two words, which were the products of the A/D output with the sine or cosine representation of the local oscillator respectively.

The integrator The integration process for the two products was carried out in two 'independent' accumulators, which shared an arithmetic logic unit (ALU). The ALU performed the accumulation of the new sample product with the value previously stored.

The sine and cosine registers, which could be two addresses in a single random access memory (RAM) were accessed sequentially, in sympathy with the multiplier operation, described above.

At the beginning of the scan, both registers were cleared, and the integration process took place throughout the scan until, at the end, the two registers contained the correlation coefficients related to the vector amplitude of the input spectrum at the locally synthesized frequency, f .

In the correlator built into the demonstration equipment the high speed of the logic allowed sufficient time in every sample period to perform these calculations for four different local oscillator frequencies. Each frequency had its own fixed $d\phi$ at the beginning of the scan period but they all used the same stored sample of the incoming signal.

Acquisition, validation, tracking and confidence The initial acquisition and the subsequent validation were carried out on a narrowband basis. For each function, the equivalent frequency band was divided into a set of contiguous narrowbands (angle bins). These were continuously examined, first to identify which bin contained the largest signal and then to confirm that this remained consistently the largest. This built up confidence that the desired signal was in this bin. Once this confidence was above the required level, the signal was considered to be acquired and the dedicated tracking frequency assigned the corresponding value.

Taking a $\pm 40^{o}$ azimuth system as an example, the full angle coverage was divided into 16 angle segments (bins), see Fig 5.32. The correlation process was used to make an assessment of the average energy in each of the 16 angle bins, this would be proportional to the largest signal in each bin. By using four separate correlation reference frequencies for each quarter of a scan, all 16 segments were examined in one scan. When a bin or pair of bins was identified as having a content which was higher than the average level in all bins by a factor of 2.2, interpolation of the frequency corresponding to this peak was

made, and the four homing bins were centred on this value. By interpolation of the outputs of the four homing bins, a fine estimate of the position of the signal was made and the angle tracker placed over the signal. Once this condition had been established, a trial track was initiated and confidence was built up that the tracked signal was correct. The confidence level remained high as long as it was consistently the largest signal present. With a good signal, track was initiated after one scan; for low signal levels several scans could be needed to establish the confidence necessary to initiate track. The angle tracker was associated with two tracked angle bins termed the long-term and short-term bins respectively. If the tracked signal vanished rapidly, *eg* due to false acquisition of a high level multipath that rapidly disappeared, the signal level in the short-term bin would collapse rapidly and the acquisition process would be initiated.

The long-term bin had an associated time constant comparable with that applied to the ordinary angle bins. A continuous amplitude comparison was made between the content of the 'long-term' tracked bin and the ordinary bins with an emphasis of between 1 and 2.5 dB applied to the tracked angle bin. If the long-term tracked angle bin content was exceeded by any of the ordinary bins, the acquisition process was initiated. This process permitted tracking through multipath signals of greater than unity for a period of time which was determined by the time constant associated with the angle bins and the degree that the multipath exceeded the emphasised level in the tracked bin. A feature of this system was a high level of immunity to 'bright flash' multipath and interfering signals which would not remain consistently in any one bin.

It was only when confidence in a new larger signal was established that the tracking frequency was changed to the position coincident with that signal. Any such change in the local oscillator frequency was performed at the end of a scan.

Normal tracking adjustment also took place at the end of each scan, when the spectral density $g(\omega)$ of the input signal was used to steer the tracked local oscillator frequency towards the wanted Doppler frequency. The rate of change of the input signal was very small compared with the pull-in range of the system.

Output quantization The quantization and output noise were similar for each of the MLS functions. For example, with a 54-wavelength elevation array and a scan time of 1.25 ms, the noise was assessed by numerical analysis to be approximately 1.5 Hz rms per scan. Over a measurement period of 40 scans (50 ms),

this resolved to [illegible] = [illegible] Hz. At 756.36 Hz, [illegible], this is equivalent to [illegible].

Multipath removal The basic correlation process provided an optimally matched filter which efficiently rejected out of beam multipath and, because of this optimal match, was superior to basic tracking filter systems. By making more use of the [illegible] (multiple antenna amplitude and phase) it is possible to reduce the [illegible] and near-beam multipath. The principal features might be used:

(a) [illegible] local oscillator frequencies;

(b) the sub-division of the scan into several sections by the use of separate accumulators which can be re-[illegible] to provide various taper functions.

As described previously, a simple sum and difference technique using two accumulators, each covering half of the scan, could be employed. The sum of the two accumulators yields the standard sin x/x (that is, sin πx/T) response (Fig 5.6(a)). The difference yields a response which has a null at the centre of the scan and the first nulls at the ±1/T points (Fig 5.6(b)). The output formed by dividing the difference by the sum provides a normalised error function which could be used to steer the tracking [illegible].

The multiple local oscillators and various [illegible] could be used to minimise the effects of in-beam and near-beam multipath [illegible] relatively simple processing.

Confidence checks The confidence checks available [illegible] considerable and extend beyond those usable by the analogue systems. Those employed in the trials equipment included validation, adequate [illegible] signal level, outlier test and coast timer.

The process of checking that the tracked signal was persistently the largest was readily accomplished using the acquisition routine outlined above. This was an improvement on the analogue systems, in that note was made continually of the size of signals across the whole band. This system was able to discriminate between different ratios of multipath to wanted signal, and was not captured immediately by the largest signal. It was also immune to multiple bright flashes.

79052

The signal level of the sum correlation at the tracking frequency was monitored to ensure that the decoder signal level was adequate. An internal flag inhibited the output if the signal level was inadequate.

A check on excessive angular movement is readily effected in digital form. This is the outlier test which was set to limit the maximum output change rate to 0.2° per update.

A coast timer was included to provide a fail-safe characteristic. Its implementation was a monostable with a relaxation time of typically 2 s, which was triggered by the logical AND of the following:

(a) function identity decode,
(b) adequacy of decoder signal level,
(c) outlier test.

One trigger pulse was obtained for each coincidence of the above. Therefore, under normal operation, the monostable was triggered every 200 ms. In the event of a failure of the angle OR data decoders exceeding 2 s, the coast timer flag was displayed.

Equipment implementation

General The correlation processor incorporated into the trials airborne receiver may be dealt with in three parts:

(a) the input section, comprising a band-pass filter and the analogue to digital conversion;

(b) the digital section, in which all the individual functions were implemented in a single central processing unit;

(c) the output section, providing the analogue and other interfaces to external equipment.

Input section

Band-pass filter The four-pole active filter used in this application was positioned at the geometric centre of the Doppler band and was 43.5 kHz wide. A Chebychev design for 1 dB pass-band ripple was used and gave 46 dB attenuation at the edge of the first image band.

Analogue to digital converter The analogue to digital converter consisted of a series of comparators and operational amplifier rectifiers, one of which ... one stage of the converter. This arrangement gave a very high ..., because it was quasi-parallel in operation. The normal 'bit

time' (the time taken for the conversion of each bit) in a conventional successive approximation system is usually made up of three main events:

(1) digital to analogue (D/A) converter settling time

(2) buffer amplifier settling time

(3) comparator settling time.

The specific A/D described here:

(a) Did not use a D/A.

(b) Had its comparators out of the direct signal path, such that for any number of conversion bits, the comparator needed only to be included once in the total conversion time.

(c) Although having amplifiers in cascade, permitted stages two, three, etc, to begin to slew as soon as the preceding amplifier output had begun to move. Thus, by the time the first stage rectifier had fully settled, the last stage rectifier was already approaching its final value, and because of its lesser significance, was less critical. The only part of the rectifier's response, which for each stage must be included in the total conversion time, was the propagation delay through the rectifier, which occurred before the output began to move in response to a step at the input.

The 4 bit + (plus) sign converter used two operational amplifiers in each rectifier. The converter was capable of tracking a 150 kHz sine wave, and responded to a full scale step at the input in approximately 700 ns.

The outputs from the comparators formed a Grey code, in which for a changing input, only 1 bit at the output changed at a time. This was a useful feature, in that it prevented gross misreading of the output due to skewing, therefore precluding the need for a static input signal. If a successive approximation A/D had been used, this condition would have required the use of a sample and hold circuit. The Grey code was converted to binary with exclusive OR gates.

The digital section The digital section of the decoder system was configured as a microcomputer set, driven by a programme, which was stored in read only memory (ROM). Inputs and outputs (I/O) were system clock, the associated data and control signals from the data decoder, D/A drive, and A/D output. The microcomputer set consisted of:

(a) A central processing unit (CPU), where the computation was performed.

(b) Memory, of which some was read/write or random access (RAM) and some was read only, where various system constants, look-up tables, etc, were stored.

It was a 16-bit machine, with an execution cycle of 250 ns. Add, subtract and shift (rotate) were direct instructions, and multiply, divide, were performed with high speed sub-routines. Trigonometric operations were performed either by direct look-up, or by interpolation between such look-up results. Note that processes such as arc sine transformation could be provided at no cost. The main steps in the programme flow diagram are shown in Fig 5.35.

Typically, 95% of each scan was used for the correlating process, with the remaining 5% used for the calculation process, acquisition, validation, etc. For the longer scan times, the calculation portion would remain constant, and thus more than 95% of the scan would be devoted to the correlating process.

The digital to analogue converter (D/A) The D/A converter used was of the stochastic type. The single chip consisted basically of an input store, a high speed random word generator clocked by a system clock of period τ, and a digital comparator.

Over a period of many τ, the mean value of the comparator output (called the stochastic output) reflects the digital input converted. The stochastic output was therefore used to switch precision reference voltages (either positive or negative) into an RC filter. The voltage at the capacitor was the D/A output.

6 THE DOPPLER SIMULATOR AND TIME DIVISION MULTIPLEX BENCH MEASUREMENTS

Early in the UK MLS programme it was realised that many essential system measurements could best be performed using a laboratory simulation. The results of such a programme, when correlated with actual trials results, could give a wide and detailed picture of system performance under the full range of possible operational conditions. It would have been difficult to obtain such a range of results in a realistic time scale from any practical series of field trials alone. The success of any hardware simulation programme depended on the use of fully realistic representations of the various system components. For example, a full representation of the MLS signal in space must be created, including all the signal sidelobe structure. The Doppler system, with its clearly defined signal structure, lent itself readily to an accurate and meaningful simulation. The adopted hybrid simulation technique allowed the actual circuitry of much of the transmitter and receiver to be included as an integral part of any test.

6.1 The commutated Doppler simulator

6.1.1 Description

The simulator represented the free space propagation path between ground antenna and aircraft by a series of RF cables. Propagation from an array of E elements was represented by E cables, one originating from each element. The difference in length of propagation path from each array element to the aircraft was represented by cutting the cables to different lengths as illustrated in Fig 6.1. The relationship between the simulated far field and commutated array far field is given by

$$\frac{L}{E-1} \sin\theta = \frac{I \times F}{c \times V_c} ,$$

where E is the number of array elements, L the length of the array in wavelengths, I the length difference between adjacent elements in the simulated array, V_c the cable velocity constant, F the frequency of operation in the cables, and c the velocity of light.

Thus, by using a variable frequency F , the relative phase delay across a cable net can be controlled. For a given set of system parameters $\sin\theta$ is proportional to frequency. Therefore, by choosing a suitable range of frequencies, the signals received by an aircraft moving over a range of θ could be represented. In the current system the following basic parameter values were used:

$$I = 1.25 \text{ m}$$

$$0.5 \text{ MHz} < F < 170 \text{ MHz}$$

$$\text{maximum number of elements} = 32$$

$$V_c = 0.66 .$$

The block diagram of the simulator is shown in Fig 6.2. The 'transmitter' was similar to the early stages of the transmitter used for azimuth trials, with an output frequency of 100 MHz. The simulator consisted basically of two identical signal paths, one representing the direct received signal and the other a multipath signal. The angle generated in each path was controlled by separate oscillators allowing a wide range of relative direct and multipath angles to be obtained. The basic simulator output signals at 100 MHz nominal were converted to 57 MHz using a separate stable local oscillator for each path. Using synthesizer and phase lock systems, these oscillators could be controlled

so that the frequency difference between them could be varied linearly over a range of at least ±2 kHz, to an accuracy of ±0.03 Hz, thus enabling full coverage over the range of multipath fading rates likely to be encountered by MLS at C-band. One of the local oscillators had a voltage control capability and could be programmed to represent the fading rate for typical multipath situations, *eg* lateral reflections from a large hangar with respect to the elevation system.

The 57 MHz signal was fed into a spectrum analyser, used as a receiver with no AGC, and the video output fed, via a band-pass filter, direct to the correlation processor of the DMLS receiver. The 57 MHz signal could also be converted to C-band, using a solid state C-band source as the local oscillator and a C-band waveguide hybrid-Tee as a balanced mixer.

The system offset frequency was derived from a frequency synthesizer allowing selection of any value in the range 10 kHz to 100 kHz, which included 83.2 kHz as used in the TDM format.

In TDM format the simulator could operate in the following modes:

(a) azimuth with either a 54λ or a 27λ array; or
(b) elevation with either a 54λ or a 27λ array.

For both (a) and (b) the array scanning could be bi-directional (alternate scans in opposite directions), uni-directional in either direction, or 'block' (first half of angle period uni-directional one way and uni-directional the opposite way during the second half of the angle period). This was realised by a combination of scanning logic circuits and a TDM format generator, the latter producing the angle period waveform and its preceding data period waveform. These waveforms controlled the output of the transmitter by means of RF switches in the reference and array outputs. During the data period the format generator produced the necessary signal encoding for AGC stabilisation, Barker code, function identification, etc, by means of DPSK. Facilities were also incorporated to enable the simulator to operate as a referenceless system during the angle period.

6.1.2 Simulator performance

Whilst the chosen simulator technique gave a very flexible high-performance tool, there were residual errors remaining in the simulation process.

In the field trials equipment there was a residual random amplitude distribution across the array elements due to differences between the distribution switches. The fast AGC system in the simulator array channels eliminated this

error from the simulation. The field trials equipments also had a small random phase spread across the array elements. The same effect was present in the simulator, which had a maximum phase spread across the 'array' of $\pm 15^{o}$ at the highest 'angle frequency' of 170 MHz, see Fig 6.3. This spread was similar to the values measured on the actual trials transmitters.

In the angle channels the use of only 32 elements in the simulated array limited the unambiguous operational coverage that could be simulated to the following:

(a) $\pm 16.7^{o}$ for a 54λ azimuth array

(b) $\pm 35.0^{o}$ for a 27λ azimuth array

(c) 0 to $+16.7^{o}$ for a 54λ elevation array

(d) 0 to $+35.0^{o}$ for a 27λ elevation array.

These limits are derived from the relation that the unambiguous code range is $f_0 \pm E/2\tau$, from equation (2-9), section 2.1, which gives limiting values for θ of $\sin^{-1}(\pm E - 1/2L)$. This of course corresponds to the situation where the phase jump between signals from adjacent elements is 180^{o}.

The main difference between the simulator and the trials system was the use of hard switching in the simulation with no blending. This introduced additional spectrum spreading which had no effect on the basic system performance, although it inhibited the use of the simulation for adjacent channel measurements. Fig 6.4 shows the basic signal spectrum produced by the array where the simulator was operating in the uni-directional scan mode representing a 54λ azimuth array (see also Fig 2.6a and section 2.2). The reference signal was set at +6 dB with respect to the array signal. Even with hard switching the signal splash at the centre of the adjacent channels was down to 50 dB. The simulated angle was set at -1^{o} and the multiple responses of the function $Q(\theta f)$ modified in amplitude by the envelope of $P(f)$ can be clearly seen. Fig 6.5 is a repeat of 6.4 on an expanded frequency scale. The skirt noise around the reference was generated by the transmitter, the skirt noise round the array signal was actually the resultant spectral distribution given by $Q(\theta f)P(f)$. Fig 6.6 is a repeat of 6.5 but with a -10 dB multipath signal present with a coding angle of -6^{o}, giving a separation from the wanted signal of 1890 Hz. Fig 6.7 is a further expansion of Fig 6.6, whilst Fig 6.8 shows a multipath at -3^{o}, *ie* 2^{o} separation angle. Fig 6.9 shows the wanted signal alone to the same expanded frequency scale.

6.2 Basic noise and accuracy measurements

For this test the receiver was driven from the test set, which produced a full set of DPSK and angle signals. In particular, the test set gave single sideband DPSK which was truly representative of the signal format, whereas the hybrid simulator used double sideband DPSK which had no effect on the multipath measurements, but was not a realistic signal for checking low level signal acquisition. The test set also produced the full set of approach, missed approach, elevation and flare signals in the format sequence, whilst the simulator only operated on one angle function at a time.

Fig 6.10 shows the video output from the receiver detector when driven by the test set at a signal level of -60 dBm on each function. One complete 200ms frame is shown (compare with Fig 5.1). No signal was transmitted in the growth slot resulting in a noise output from the detector. Fig 6.11 shows the end of the missed approach azimuth slot and the start of the elevation slot on an expanded time scale of 1 ms per division. At the end of the missed approach azimuth angle data there is a guard space. The start of the elevation preamble is accompanied by a large AGC transient which is accommodated by the uncoded 5 bit time period at the start of the preamble. The DPSK phase reversals can be clearly seen in the preamble before the elevation angle data. Clearly the guard space is unduly long and could be reduced to about 0.5 ms if reasonably accurate sub-system timing was maintained.

To reproduce representative long-range signal conditions, the missed approach and flare signals were inhibited and the tests were performed with azimuth and elevation signals of about equal level. For each angle function a plot was taken of angle output as a function of time for a range of RF signal levels; the results are given in Fig 6.12a&b for azimuth and elevation respectively. Shown in Fig 6.13a&b are the associated plots of function identity decode success. From these results a plot of FI decode success has been made, Fig 6.14.

The results show that the limit to usable signal was set by the DPSK FI system. When the decode success rate fell below 60%, the system flag showed intermittently, indicating periods when few decodes were made for at least 2 s. In this condition the actual angle output holds at the latest value; this effect occurred at a signal level of about -106 dBm.

In order to investigate the basic angle processor performance alone at low signal level, a measurement was made using the hybrid simulator as a signal

source with the necessary information normally derived from the FI preamble being hard-wired from the simulator into the angle processor. The results for the approach azimuth are shown in Fig 6.15. Consistent operation was maintained to below -110 dBm with flag operation due to low signal-to-noise ratio occurring around -114 dBm. In particular, it should be noted that at the higher signal levels the residual overall angle system noise was negligible showing that noise actually generated in the simulator could be ignored.

It should be noted that, in all the above signal level measurements, the absolute measurement accuracy could have an error of up to ±2 dB although the relative levels were to an accuracy of ±0.5 dB.

The typical dynamic output characteristic is shown in Fig 6.16 for a linear sweep of simulator angle with the receiver reference angle set to 3.0^{o}. The noise level is commesurate with the input signal level. The output plot is very linear but shows a small sensitivity change in the receiver D/A system between positive and negative angles with respect to the 3^{o} reference.

6.3 Basic multipath performance of different algorithms

In order to quantify the basic multipath performance, the simulator was set up typically as follows:

(a) Direct signal at a fixed angle, *eg* 3^{o}.

(b) Fixed multipath to direct signal ratio, *eg* -1, -3 dB.

(c) Low differential fading rate between direct and multipath signal, *eg* 0.2 Hz to slowly rotate the relative RF phase.

(d) Multipath separation angle varied from 0^{o} to an upper value at a sufficiently slow rate to fully define the peak envelope of error.

Basic error versus separation angle curves were obtained for three processor algorithms:

(1) The basic single frequency.

(2) Single frequency with an applied Taylor weighting to the received scan signal.

(3) A three-frequency algorithm combining the outputs of three single frequency correlation processes when the correlating frequencies are separated by a fixed value.

Typical curves for these three algorithms are shown in Fig 6.17a,b&c. Note that the multipath level in 6.17a is at -3 dB compared with -1 dB for curves 6.17b&c.

The basic single frequency processor, which was used in all flight trials up to November 1976, gave a narrow in-beam response with the first null at 1.6 beamwidth, but the amplitude of the sidelobes was high. In particular, for elevation system performance, a low sidelobe response above 5^{o} separation (corresponding to a 2.5^{o} glidepath) is desirable whilst this processor for -3 dB multipath could give peak-to-peak errors of 0.08^{o} at an elevation angle of 2.75^{o} (5.5^{o} separation).

A standard technique for minimising sidelobes to a low constant level is to apply a Taylor weighting to the received aperture scan. To do this in the existing processor the received scan was split into eight segments and each given an appropriate amplitude weighting. The plot in Fig 6.17b shows that a sensibly constant sidelobe level was obtained at the expense of some main beam broadening as would be expected. Unfortunately the simple process of splitting the received scan into eight sections (sub-arrays) introduced sidelobes at separation angles associated with the sub-array beamwidth. These responses arose from the need for small gaps between the segments in the current hardware implementation. With the Taylor weighting the processor only used about 94% of the scanned aperture, giving a sub-array beamwidth of $\underline{\Omega} = \tan^{-1} 8/0.94 \times 54 = 9.1^{o}$.

Fortunately, a more economical sidelobe reduction process was found using an algorithm combining the outputs of three frequency trackers; the overall result is shown in Fig 6.17c, where the sidelobe error associated with typical elevation glidepaths was very small. This algorithm was used in all flight tests after April 1977. With this tracker the first multipath null occurred at 2 beamwidth separation angle, the beamwidth being given by $\sin^{-1}(1/L_{EFF})$, where L_{EFF} was the actual array length used for correlation. In this tracker L_{EFF} was about 96% of the 54λ array, giving a beamwidth of 1.1^{o}, and a first null at 2.2^{o} separation angle.

All the multipath separation angle curves are 'anti-symmetrical' about the Y axis, although only the portion for positive separation angles has been plotted in each case. The locus of the peak errors is given by the condition where the RF phase of the multipath signal is either in-phase or 180^{o} out-of-phase with the direct signal. At high multipath levels the peak positive and negative errors are not equal in amplitude, but averaged over 360^{o} of relative phase in small steps the error will tend to zero due to the bath-tub shape of the error versus relative phase plot.

At lower multipath levels the in-phase and out-of-phase error envelopes are symmetrical and the error versus phase plot tends to be sinusoidal.

6.4 Basic multipath performance as a function of system aperture

Although the TDM trials equipment was built with a 54λ aperture, both the elevation and azimuth systems could be switched to use only the central 27λ of aperture with twice the number of scans per measurement period. This change in aperture was automatically identified to the airborne receiver as part of the sub-system FI code. Additionally, during the 1977 operational airport trials, it became apparent that the performance of other system apertures was well worth investigating. In order to avoid the necessity of additional transmitter modifications, one airborne processor was adapted to operate over scan lengths of 20 and 15λ in azimuth with the ground system operating at 27λ aperture. The scan-length times for 20 and 15λ azimuth were the same as 40 and 30λ elevation (elevation scan rate = 2 × azimuth rate), so that the same processor timing modification enabled elevation apertures of 39 and 30λ to be examined with the ground array operating in the 54λ mode.

Fig 6.18a,b&c show the basic elevation channel multipath performance for effective apertures of 54, 39 and 30λ (note vertical scale change between a and b, c). For all three apertures the first null is at 2 beamwidths, defined as $\sin^{-1}(1/L_{EFF})$, where L_{EFF} is

$$\frac{54 \times \text{actual receiver scan receiving time}}{T \times \text{scan time (1.25 ms)}} .$$

From these curves we can see that even apertures as low as 30λ should give acceptable performance for a 3^{o} glidepath providing the ground reflection is from level or falling ground, i.e giving separation angles of greater than 6^{o}. There is a distinct risk with an aperture of 30λ or less, however, that any forward scatter from objects sited in front of the array will give rise to large errors as the separation angle from such signals will be only 3^{o}. Fig 6.19 shows the performance of the nominal 27λ elevation aperture (effective aperture = 25λ). Here it is very clear that significant errors could arise from 0^{o} coded scatter at quite low levels, such effects can be seen on the flight trials using this aperture.

The basic multipath versus separation angle curves for the four azimuth system apertures are given in Fig 6.20a,b,c&d.

6.5 The effects of different multipath fading rates

6.5.1 General

In any practical environment, the differential fading rate between the multipath signal and the direct signal will lie in the range of 0 to upwards of 1000 Hz, depending on the situation geometry and the aircraft velocity vector.

The relation between these parameters is illustrated in Fig 6.21 for a typical azimuth and elevation situation, where α and ϕ are conical code angles.

Neglecting second order effects the signals received by the aircraft over the duration of one scan of the array can be written as

$$B \sin\left(\omega_r + \frac{2\pi v}{\lambda} \cos \beta\right)t \qquad \text{the direct reference signal} \quad (6\text{-}1)$$

$$A \sin\left(\omega_r + \omega_0 + \frac{2\pi v}{\lambda} \cos \beta + \frac{2\pi L}{\tau} \sin \alpha\right)t \qquad \text{the direct array signal} \quad (6\text{-}2)$$

$$\rho B \sin\left(\omega_r + \frac{2\pi v}{\lambda} \cos \theta\right)t \qquad \text{the multipath reference signal} \quad (6\text{-}3)$$

$$\rho A \sin\left(\omega_r + \omega_0 + \frac{2\pi v}{\lambda} \cos \theta + \frac{2\pi L}{\tau} \sin \phi\right)t \qquad \text{the multipath array signal.} \quad (6\text{-}4)$$

The relevant signals in the detector output are

$$BA \sin\left(\omega_0 + \frac{2\pi L}{\tau} \sin \alpha\right)t \qquad \text{the wanted code term} \quad (6\text{-}5)$$

$$\rho^2 BA \sin\left(\omega_0 + \frac{2\pi L}{\tau} \sin \phi\right)t \qquad \text{the multipath code term} \quad (6\text{-}6)$$

$$\rho BA \sin\left(\omega_0 + \frac{2\pi L}{\tau} \sin \phi + \frac{2\pi v}{\lambda} (\cos \theta - \cos \beta)\right)t \qquad \left.\begin{array}{r}\text{from multipath array}\\ \text{signal and the}\\ \text{direct reference}\end{array}\right\} \quad (6\text{-}7)$$

$$\rho BA \sin\left(\omega_0 + \frac{2\pi L}{\tau} \sin \alpha + \frac{2\pi v}{\lambda} (\cos \beta - \cos \theta)\right)t \qquad \left.\begin{array}{r}\text{from the multipath}\\ \text{reference and}\\ \text{direct array signal.}\end{array}\right\} \quad (6\text{-}8)$$

In general, there are two situations:

(i) The case where ϕ is separated by more than 2 beamwidths from α and the terms (6-6) and (6-7) have an effective code which puts them well out-of-beam with respect to the wanted signal. This is the normal situation for azimuthal reflections in the azimuth system.

79052

(ii) The case where ϕ is separated by less than 2 beamwidths from α and terms (6-6), (6-7) and (6-8) all give rise to in-beam components. This is the normal situation for azimuthal reflections in the elevation system.

6.5.2 Azimuth system

In the azimuth case terms (6-6) and (6-7) normally fall well outside the processor bandwidth, *i.e.* they are out-of-beam components. On the other hand, term (6-8) is separated from the wanted signal by only $(2\pi v/\lambda)(\cos\beta - \cos\theta)$ and, in general, forms an in-beam multipath component relative to the wanted signal. This component has become known as the reference scalloping term. Now the starting phase of the wanted coding term advances by $\omega_0\tau$ from scan to scan and the starting phase of the reference scalloping component will change by $(\omega_0 + 2\pi v/\lambda(\cos\beta - \cos\theta))\tau$ on each scan.

The resulting system error is determined by two factors. Firstly, the frequency term $2\pi v/\lambda(\cos\beta - \cos\theta)$, which gives the coding offset from the wanted term, and hence determines the peak error potential in terms of the multipath versus separation angle curve (Fig 6.33); and secondly, the relative starting phase between the direct and multipath signals given by $2\pi v/\lambda(\cos\beta - \cos\theta)\tau$, which determines the actual error on each scan within the envelope limits set by the multipath error versus separation angle curve.

Maximum errors occur when $(2\pi v/\lambda)(\cos\beta - \cos\theta)\tau = n\pi$ and the resulting envelope is sketched in Fig 6.22. If, as is generally the case, the relative starting phase changes from scan to scan, the resultant error averaged over the scans in the angle measurement period will be reduced; this effect is known as motion averaging.

Uni-directional scanning (54λ array, τ = 2.5 ms) Fig 6.23a shows the plot of error as a function of fading rate when this rate is advanced slowly from 0 to 500 Hz. At 0 Hz the effective coding offset is zero and the error is zero. As the frequency rises the error increases, but falls to a minimum at 33 Hz which is the reciprocal of the 30 ms azimuth angle measurement period. At a fading rate of 200 Hz the differential phase advance is π per scan and, although the peak error is of opposite sign on each scan, the asymmetry in the multipath curves, Fig 6.22, gives rise to an error envelope peak at this frequency. At a fading rate of 400 Hz the differential phase advance is 2π on each scan and the worst case peak envelope error given by Fig 6.22 will be seen, with error reduction from motion averaging minima at 400 ± 33 Hz, etc.

Bi-directional scanning (54λ array, τ = 2.5 ms) The error plot as a function of fading rate is given in Fig 6.23b. For bi-directional scanning, the reversal of the array and reference signals on alternate scans, which is necessary to preserve the correct sense of the detected code signal, causes a

reversal in the sign of the multipath error due to reference scalloping on each scan, all other factors being constant. Therefore, at low fading rates where the relative starting phase changes only slowly from scan to scan, the errors on alternate scans effectively cancel each other giving a very low resultant error. As the fading rate rises this cancellation becomes incomplete until at 200 Hz the starting phase change on each scan also reverses the error sign on alternate scans giving rise to peak system errors.

Block scanning (54λ array, τ = 2.5 ms) The third scan format used in trials was the so-called block scan consisting of six scans one way followed by six scans in the opposite direction (abbreviated as 6^{+-}). Each block of six uni-directional scans will have a peak response at 400 Hz with zeros at 400 ± 66 Hz due to averaging over the 15 ms block length. At 400 Hz the errors for each block will be equal in amplitude but of opposite sign due to the opposite scan direction. Thus at exactly 400 Hz a complete error zero is to be expected.

Comparison On the basis that high fading rates were likely to be less frequent and of less duration in an operational environment, the block scan (6^{+-}) was chosen as standard for trials purposes. It must be remembered that the error mechanism of reference scalloping was solely due to the use of a spatially invariant reference transmission. This is clearly illustrated by Fig 6.24 which shows the equivalent system performance with the multipath reference suppressed (which was easily done on the simulator). Only very small errors remain due to the sidelobes of the multipath array signal as can be seen by comparison with the plot having no multipath.

Techniques for practical implementation of a referenceless DMLS are discussed in section 9.

To complete the picture, Fig 6.25a&b show the effects of reference scalloping errors for the 27λ azimuth array. The scan length is now 1.25 ms giving peak error responses at 400 Hz for bi-directional scanning and either side of 800 Hz for block scanning.

Effect of high rate of change of scallop rate All the preceding measurements were made with a low rate of change of scalloping frequency in order to ensure that the peak envelope of error was obtained. In a practical environment scallop frequencies will not be fixed, but will vary as the aircraft proceeds along the approach path. Fig 6.26 shows an overlay of successive error plots for a rate of change of 26 Hz/s which is higher than most practical situations. It can be seen that the peak errors can still reach the envelope maximum given in

Fig 6.23c and it was therefore concluded that practical rates of change of scalloping would not affect the peak errors that may be seen.

6.5.3 Elevation system

The choice of elevation system aperture was such that ground reflected signals lay out-of-beam and in any case have very low fading rates and could be treated as a quasi-static situation. On the other hand azimuthal multipath as illustrated in Fig 6.21b could give rise to in-beam errors from terms (6-6), (6-7) and (6-8) derived in section 6.5.1. The error due to term (6-6) gives rise to a bias independent of fading rate. This is in general small due to the θ^2 term.

Fig 6.27a&b show a typical error versus fading rate plot with a multipath separation angle of 1°. Whilst Fig 6.28a&b show the same situation, but with the multipath reference inhibited.

At zero fading rate, the peak error due to term (6-7) is seen; as the fading rate rises this error is rapidly reduced by the very efficient motion averaging given by the 50 ms angle period with 40 scans. Averaging very effectively suppresses errors from both terms (6-7) and (6-8) until the fading rate approaches 800 Hz where peak errors due to reference scalloping, term (6-8), are seen.

6.6 Signal acquisition and validation

It is essential in any guidance system where a signal is acquired and tracked by a narrow guidance cell that the acquisition and validation system behaves in a logical and predictable manner. The tests in this section were designed to stress the signal acquisition and validation logic in the presence of a single specular multipath signal. The tests were made on the azimuth function.

Fig 6.29 illustrates the effects of applying an out-of-beam multipath at a range of different levels and at low fading rate where there will be no reference scalloping effects. Due to the designed enhancement of the tracked angle bin, there was no loss of track of the wanted signal up to multipath values of +2 dB. At higher levels track was lost and the multipath signal acquired after a time given by the validation programme time constant; this time as expected reduced as the multipath level increases.

Fig 6.30 illustrates the same test as above but now with a fading rate of 370 Hz, which gave a peak reference scalloping error for the 6^{+-} format. Setting

AD-A085 478 ROYAL AIRCRAFT ESTABLISHMENT FARNBOROUGH (ENGLAND) F/G 17/7
CONTRIBUTIONS TO THE UK MICROWAVE LANDING SYSTEM RESEARCH AND D--ETC(U)
MAY 79 J M JONES
UNCLASSIFIED RAE-TR-79052-VOL-1 DRIC-BR-73155 NL

2 OF 3
AD A085478

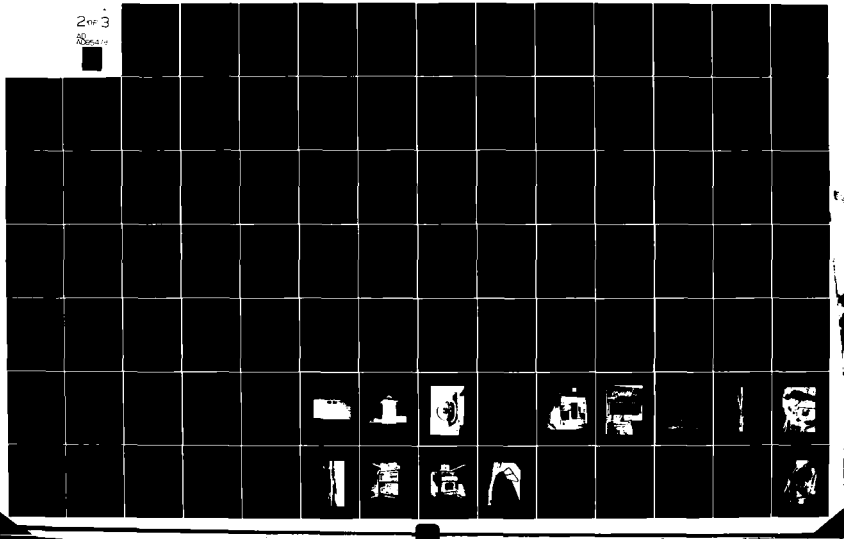

the signal very close to a multiple of 5 Hz gave rise to a very low alias frequency of the resultant error. The presence of the reference scalloping term distorted the spectrum of the wanted signal so that tracking of the wanted signal was lost for multipath levels greater than 0 dB.

Fig 6.31 illustrates the effects when a fading rate of 372.4 Hz was chosen which being half-way between 5 Hz alias frequencies resulted in maximum error swing between updates. Since this error swing was in excess of 0.2^{o}, it continually triggered the rate limiting circuits in the receiver output. Initially the rate limit operated to restrict the maximum error change per update to 0.2^{o} but continual operation of the rate limit caused loss of confidence resulting in removal of the rate limit and flag action. After about 2 s confidence rebuilds, the rate limit was reapplied and the sequence then repeats. At multipath levels greater than 0 dB, loss of tracking occurred after similar times to those seen in Fig 6.30.

Fig 6.32 is a repeat of the test illustrated in Fig 6.31 but with no multipath reference signal. This illustrates the improvement that might be expected with a reference-less system, see section 9; as would be expected the results were similar to those for low scallop rate multipath.

Part of the design philosophy of the validation logic was the recognition of sudden collapse of the tracked signals as might occur if the processor had initially acquired a multipath signal. Fig 6.33 illustrates the correct operation of this system where it is seen that the wanted signal was acquired within 2 s after the collapse of a previously acquired high level multipath signal.

6.7 Effects of propeller modulation

The adverse effects of propeller modulation on VHF ILS are well known and it was one of the basic design aims for MLS that the system should have a high immunity to propeller modulation. This section describes tests related to the reception of the DMLS signal through the zone of an aircraft propeller as might be frequently encountered on a single engined light aircraft.

The prime effect of reception of signals through the swept zone of a propeller is to cause an amplitude modulation of the received signal. The resulting amplitude variations depend on the following factors

(a) the horizontal aperture of the receiving antenna,

(b) the distance of the receiving antenna from the plane of the propeller,

(c) the distance of the receiving antenna from the axis of rotation of the propeller,

(d) the blade width on the line of optical obstruction.

Measurements of signal attenuation as a function of blade angle have been made with both a simulated and real propeller. Fig 6.34 illustrates the geometry for the real propeller tests, where L is the distance from the propeller plane and H is the height of the antenna above the axis of rotation. Fig 6.35 to 6.39 show typical results, whilst Fig 6.40 shows a similar result from FAA measurements.

From these and other results the following general conclusions may be drawn:

(1) The peak attenuation levels reduce as the distance from the propeller plane is increased; this is accompanied by an increase in propeller angle over which signal variations are seen.

(2) The duration of the attenuation falls as the distance from the axis of rotation is increased, as would be expected from simple geometry.

(3) With a real propeller there is asymmetry in the attenuation curve due to propeller shape.

(4) The angle over which effects are seen and the degree of attenuation is not altered significantly by small changes in the antenna horizontal aperture, *ie* when the aperture is smaller than the blade width.

DMLS is an amplitude/frequency coded system and is, therefore, fundamentally immune to basic amplitude or time variations in the total signal, such as those caused by propeller modulation, but effects will be seen if the increase in attenuation takes the signal below the receiver threshold.

Fig 6.41 shows the simple test arrangement used for simulated propeller modulation tests, simulated modulation was produced by modulating the signal with a PIN diode attenuator.

Typical attenuation patterns used are shown in Fig 6.42; these were based on the measured data in Figs 6.35 to 6.40 and represent a two-blade propeller where the peak attenuation lasts for a dwell angle of 22^{o} to 27^{o} and has an average value of -10 dB.

Fig 6.43 shows typical results obtained for the elevation system operating on a 54λ aperture using the waveform of Fig 6.42a with the propeller speed chosen to be close to a multiple of 5 Hz thus ensuring periods where an attenuation peak was synchronous with the elevation transmission.

As would be expected with signal levels well above the receiver threshold, the effects of propeller modulation are non-existent as the amplitude variations are corrected by the receiver fast AGC system and no information is lost irrespective of whether the blocking rate is synchronised with the signal format or not. As the signal level is reduced towards the threshold value (-106 dB m), two effects become apparent. Firstly, the angle output in the presence of propeller modulation shows an increase in noise level due to the degraded signal-to-noise ratio on array scans shadowed by the propeller; and secondly, function identity decodes are lost when the DPSK signal is attenuated below threshold. Therefore, with a regular signal format there can be loss of information when the signal is within P dB of the threshold and the propeller modulation is synchronous with the function preamble. (P is the attenuation level of the modulation.)

This synchronous condition can be avoided by incorporating a simple jitter in the signal format. Two examples of jitter are shown in Fig 6.44. There are other error mechanisms associated with propeller aircraft, *eg* reflections from the propeller in a multi engine aircraft. No specific measurements have been made, but the resultant amplitude variations in the received signal would be much smaller. The reflected signal will also contain a very slightly different angle code, but again the effects would be very small as the rotation of the propeller effectively phase cycles the reflected signal at high rate thus tending to average out any induced errors.

Another possible error mechanism will occur if a multipath signal is present which arrives at the aircraft antenna from a significantly different direction to the direct signal; this will be the case for much azimuthal multipath on both azimuth and elevation systems. With a non-jittered format the possibility arises of differential blockage of the direct and multipath signals which could in some cases effectively enhance the relative multipath level. A simple format jitter will minimise such effects.

No experimental work has been made on the effects of rotor modulation in helicopter installations. Direct signal blockage is most unlikely, but high levels of reflection off rotors are to be expected. If the receiving antenna

is sited to see signals off the rotor large amplitude variations in the resultant signal could occur giving rise to loss of signal at range.

7 FLIGHT TRIALS RESULTS OF THE TDM SYSTEM

This section presents a selection of typical results from the flight trials of the TDM azimuth and elevation systems at RAE Bedford during the period June 1976 to June 1977. The aim has been to present data showing all facets of the system performance encountered during this period. A number of initial problems were encountered and solved; these are looked at in some depth. It is worth noting that the equipment was conceived, designed and built in a period of 12 months from March 1975 to March 1976. The delay between initial factory tests at Cowes and installation at RAE Bedford can be attributed to the effort involved in preparing for ICAO meetings during this period.

The trials procedures and data processing followed those used for the FDM equipment tests, and details are given in Appendices B and C.

The field tests of the FDM system had clearly shown that information from tracked flight runs was much more productive in assessing overall system performance than ground based tests. Accordingly, only very superficial ground tests were made on the TDM system. Whilst the FDM system had given very good results with simple antennas, we were expecting the TDM implementation to give significantly lower quantization noise and more immunity from ground reflections in the azimuth system, due to the use of 20λ of vertical aperture in the azimuth antenna. No effects were expected from the reduction of azimuth aperture from 120 to 54λ, although the 54λ elevation system was expected to give larger errors due to ground reflection at low angles, ie below 2^{o}, compared with the 90λ FDM system.

The field trials of the TDM system at Bedford airfield can be conveniently split into two periods:

(a) June 1976 to November 1976;

(b) May 1977 to June 1977 after equipment modification.

7.1 Results prior to November 1976

7.1.1 General

For the first part of this test period, the azimuth and elevation equipments were installed in a co-located configuration abreast of the threshold of runway 27, see Fig 7.1, with timing synchronization by cable connection.

A summary of the flights in this period is given in Table 7.1. In early September the equipment was relocated to serve runway 27 in a split site configuration co-located with the Stan 37/38 VHF ILS, see Fig 7.1. In the split site configuration the azimuth system was placed 146 m (480 ft) beyond the end of the runway. In relation to the siting of the 120λ FDM azimuth antenna (which was removed prior to the TDM trials), the phase centre of the TDM array was a further 0.67 m (2.2 ft) below the crest of the runway hump. The elevation system was sited adjacent to the VHF ILS glidepath at a distance of 201 m (660 ft) from the runway centreline. In this position the array looked towards several ILS monitor masts which gave rise to small amounts of interference in parts of the coverage. A summary listing of the flights in this period is given in Table 7.2.

Table 7.1

TDM flights with DMLS at Bedford site 3 using Andover with omni-antenna

Flight No.	Date	TX		Profiles	Track	Comments
		Az	El			
AA44	9.6.76	54λ	54λ	R,A	Y	
AA45	10.6.76	54λ	54λ	R,A	Y	
AA46	29.7.76	54λ	54λ	R,A	Y	
AA47	29.7.76	54λ	-	A	Y	Repeater test
AA48	19.8.76	-	54λ	R,A	Y	
AA49	19.8.76	54λ	-	R,A	Y	
AA50	20.8.76	54λ	-	R,A	N	Digital recorder fault
AA51	20.8.76	54λ	-	O,A	Y	Bad tracking
AA52	23.8.76	54λ	54λ	R	Y	
AA53	23.8.76	54λ	54λ	R,A	N	
AA54	24.8.76	54λ	54λ	O,R,A	Y	
AA55	25.8.76	54λ	54λ	O,R,A	Y	
AA56	25.8.76	54λ	54λ	O,R,A	Y	
AA57	26.8.76	54λ	54λ	O,R,A	Y	

Notes: 1. No flights AA58/59.

2. Site 3 was a collocated site at threshold 27. All results affected by mismatch on radomes due to rubber de-icing boots.

3. A = approach; R = radial; N = no;
O = orbit; Y = yes.

Table 7.2

TDM flights with DMLS at Bedford site 2

Flight No.	Date	TX Az	TX El	Profiles	Track	Comments
		Andover XS646 omni				
AA60	17. 9.76	54λ	54λ	A	Y	
AA61	27. 9.76	54λ	54λ	O,R,A	Y	
		No flights AA62/63				
DA/AA64	4.10.76	54λ	54λ	O,R,A	Y	Kine problems
DA/AA65	5.10.76	54λ	54λ	O,R,A	Y	
		BAC 1-11 omni-antenna				
DB27	12.10.76	54λ	-	A	Y	Repeater tests
DB28	13.10.76	54λ	54λ	O,A	Y	
DB29	13.10.76	54λ	54λ	R	Y	
DB30	15.10.76	54λ	-	A	Y	RAE sync failure
DB33	22.10.76	54λ	-	R,A	Y	
DB34	22.10.76	54λ	54λ	A	Y	Repeater tests
DB35	26.10.76	54λ	54λ	A	Y	Repeater tests
DB36	27.10.76	54λ	54λ	A	Y	Repeater tests

Notes: 1. Site 2 Bedford. Azimuth approximately 300 ft in front of 27 ILS (Stan 37). Elevation at side of Stan 38 approximately 650 ft from centreline. Flights to investigate effects of de-icing boots and reference scalloping.

7.1.2 Typical azimuth results from co-located site (site 3)

Orbits The results of two-part orbital runs are shown in Figs 7.2 and 7.3. From Fig 7.2 three effects are apparent:

(a) an overall system bias of -0.23^{o},

(b) a large cyclic error, which was a function of azimuth angle,

(c) gaps in the error plot with large transient errors each side due to loss of kine synchronization information on the ground-to-air timing link.

These effects are repeated in Fig 7.3, where the negative bias has been removed in the data processing in order to see the full error excursion at wide angles. The bias error was due to a physical misalignment of the array and arose from the difficulty of aligning the 0^{o} line parallel to the runway

centreline. For the purpose of these initial trials, it was decided not to realign the array in the middle of the trials period.

The large cyclic error was traced to the mismatch introduced by the inflatable de-icing boot on the outer surface of the radome. This mismatch gave rise to a secondary signal which was then reflected from the array surface. The effect, illustrated in Fig 7.4, was to generate a secondary source, which appeared to lie behind the main array at a distance of twice the radome spacing. At $\theta = 0^{o}$, this image array was the same length as the main array, but, as θ increased, the effective length of the image was reduced due to the finite length of the reflecting surface given by the real array. The foreshortened image also had a phase lag on the direct signal given by

$$\frac{2a \cos \theta}{\lambda} 2\pi \quad \text{rad} \quad ,$$

where a was the spacing between the array and radome surface. The net overall result was to introduce a phase squint in the received signal, which increased, as θ increased, in a cyclic manner, giving rise to the errors seen. On the basis of a nominal antenna to rubber boot spacing of 275 mm (11 in), peak errors were to be expected at azimuth angles of ±4.6, ±19, ±27, ±33, ±38, ±43, ±47, ±51, ±55, ±59 and $\pm 62^{o}$. Bearing in mind the presence of second order effects, due to the positioning of the reference and data elements on one end of the array, the calculated positions of peak error were in good agreement with the flight results, particularly for negative angles. The obvious solution to this problem was to improve the radome match and reduce the spacing to a minimum (see later results).

Approaches Two examples of approach flight profiles on the system centreline at 3^{o} elevation and ending in a low overshoot are shown in Figs 7.5 and 7.6. Fig 7.5b shows a direct error plot with the large bias due to array misalignment. In Figs 7.5c and 7.6b the bias has been removed in the data processing. As would be expected the radome reflection had little effect on centreline and the basic low noise level of the TDM system compared to the FDM system is evident.

7.1.3 Typical elevation results from the co-located site

Orbits The results of two partial orbit runs are shown in Figs 7.7 and 7.8 at elevation angles of 3.3 and 10.7^{o} respectively. Both error plots show evidence of cyclic errors. As the elevation system radome also had a rubber

de-icing boot this was immediately suspect. However, the actual error mechanism was traced to energy being re-radiated by the waveguide column reference element sited alongside the commutated array. As the vertical aperture of this element was only 20", it gave rise to a much shortened image of the main array introducing an error vector which cycled in phase as a function of azimuth angle. The geometry is illustrated in Fig 7.9, which shows that the reference waveguide column stood slightly forward of the array aperture and was, therefore, probably illuminated both directly and by reflection from the radome.

Taking b as 100 mm, as measured from the array, the first order calculation gave error peaks (positive or negative) at -58, -33, -14, +3, +20, +40 and +72°. This was regarded as having sufficient agreement with the results from the orbital flights to have pin pointed the error mechanism. The proposed cure was to improve the radome and to add dummy waveguide columns to both sides of the array extending along the full height to give a totally symmetric situation

Radial flights Fig 7.10 shows the result from a typical radial run. At this time in the programme the correlation processor of the TDM receiver was a simple sum and difference tracker, which gave rather high sidelobes, for example from Fig 6.17a, -3 dB multipath at 5.5° separation (2.75° elevation) can give 0.08° peak-to-peak error. The effects of these sidelobes can be seen in Fig 7.10b, where a bend structure due to the ground reflected signal is apparent beyond 3.5 n mile range, ie below 5° elevation. The system performance above 5° was good up to 22.5° where the signal was lost due to the high angle cut-off in the waveguide column DPSK antenna and the sector cut-off of the array parallel plate region, see Fig 5.18.

3° approach The performance on a nominal 3° approach is shown in Fig 7.11. As would be expected from the evidence of the radial run, there is a significant bend structure due to ground reflection. The actual errors were somewhat greater than would be predicted from Fig 6.17a and it is possible that array phasing errors were contributing to increase the sidelobe levels.

7.1.4 Typical azimuth results from the split site (site 2)

Orbits Figs 7.12 to 7.16 show the results of part orbit runs with the radome removed from the array. It is immediately apparent that the large cyclic errors which were attributed to the rubber boot mismatch have been eliminated. The results are presented in order of increasing elevation angle from the azimuth site. At the lowest elevation angle, 2.1°, the large errors at +38°

were due to signal blockage by an old crash barrier supported by metal poles. The siting is shown in Fig 7.1; no effect was seen on the FDM azimuth orbits due to the siting of this array closer to the runway end. A small increase in elevation angle to 2.5° reduced the errors to a very low level. There was a small bias change between clockwise and anticlockwise runs; this was attributed to the 2.4 m longitudinal displacement of the MLS airborne antenna from the aircraft nose, which was used as a film reading point for orbital flights. For a nominal range of 13414 m (44000 ft) this would have given a bias difference of 0.025° between clockwise and anticlockwise orbits. The other feature of the results was that at the higher elevation angles longer period errors became evident; these were attributed to the effects of ground reflection. Due to the general slope of the ground at the Bedford azimuth site, the effective ground cross fall was quite large. The design coverage of the system was ±40°, signal coding was provided beyond this point.

Approaches Figs 7.17 and 7.18 show the results of typical 3° approaches along the runway centreline. The performance was very similar to that obtained from the co-located site. The noise level was significantly lower than that on the FDM system; in all other respects, however, the performance was very similar to that obtained with the 120λ FDM system. The long period weaves were attributed to the slope error seen on the low orbits at 0°, see Figs 7.14 and 7.15. This is discussed further in section 7.2.2.

Radials Fig 7.19 shows the result of a constant height radial flight at 0° azimuth angle. The cyclic error was due to reflection from the ground in front of the array which had a significant cross fall. This radial was flown at a nominal height of 5000 ft; the appearance of significant ground reflection errors at elevation angles up to 15° was somewhat unexpected, as the low angle cut-off due to the use of 20λ vertical aperture in the array was expected to give a significant performance improvement over the FDM equipment, see Fig 4.26c. The vertical radiation pattern of the FDM antenna is given in Fig 3.9 and that of the TDM antenna in Fig 5.14. The ground reflection protection factors for the two antennae are plotted in Fig 7.20; it can be seen that the waveguide column element gave significant improvement up to 3.5° elevation and virtually similar performance at 10°. The cross fall slope in front of the TDM array site averaged 1.5° at angles around zero azimuth; this was greater than that at either of the FDM azimuth sites. At 15° elevation the effective ground multipath code angle is $2 \times 1.5 \sin 15 = 0.77°$ and an effective multipath level of -27 dB would give the 0.04° cyclic error seen.

7.1.5 Typical elevation results from the split site

Orbits Figs 7.21 to 7.24 show the results of part orbital runs with the elevation array radome removed. It is clear that whilst the cyclic errors seen in Figs 7.7 and 7.8 were reduced, significant errors still remained. The discrete error at an angle of $+12^{\circ}$ was due to signal blockage by a wooden lattice tower, which subtended a maximum elevation angle of 4.1° with respect to the bottom of the elevation array. This tower caused interference on all orbits except that at 6.5° for which all elements of the array had a clear propagation path to the aircraft. The fact that the long-period errors decreased on the 6.5° orbit suggested that these were mainly due to ground reflection.

Approaches Fig 7.25 shows the result for a nominal 3° approach ending in a low overshoot. The system showed a small negative bias of 0.015° and the noise level was well inside the 2σ limits of $\pm 0.076^{\circ}$. Nevertheless, we would have hoped for lower noise from a 54λ array.

Radial The result from a typical radial flight is given in Fig 7.26. At low elevation angles the performance was similar to that seen at the co-located site, Fig 7.10. At the higher angles, above 10°, there was an increase in cyclic noise; there is no obvious explanation for this as at such high elevation angles we would expect multipath effects to be minimal. Nevertheless the system performance was well inside the requirements.

7.1.6 Equipment modification arising from trials results

The results obtained in this period showed that the TDM equipment had the potential to meet the performance required with adequate margins, but that to achieve it in a fully operational state would require a number of system modifications.

The equipment was returned to the factory at the beginning of November 1976 for modifications based on both the flight trials results and the proposal for trials in the USA during 1977 (these trials did not actually take place until 1978). The main modifications to the azimuth and elevation systems are listed below.

Azimuth

(a) Radome redesigned, with rubber de-icing boot removed, and placed in direct contact with the array face.

(b) Data carrier and data sideband separated and radiated from separate elements to optimise transmission efficiency (the signals had previously been combined in a coupler and radiated from a single element).

(c) Reference antenna modified to give 6 dB of azimuth emphasis on runway centreline to minimise the effects of reference scalloping.

(d) Provision made to operate the system as a 27λ aperture using the central half of the array.

(e) Array phasing checked.

(f) Optical azimuth alignment system fitted.

(g) Power supply distribution altered for operation on US 60 Hz supplies.

(h) Air conditioning flow to the array reduced.

(j) General mechanical changes to the transmitter housing.

Elevation

(a) Radome redesigned with rubber de-icing boot moved.

(b) Flares on edges of array removed to give a more rapid roll-off in the azimuth radiation pattern.

(c) Data carriers and data sub-carrier radiated from separate column elements, one on each side of the array.

(d) Alignment spirit levels fitted.

(e) Option of block scan sequence introduced.

(f) Option of 27λ aperture operation introduced.

(g) Air conditioning flow to the array reduced.

(h) Power supply distribution rearranged for 60 Hz operation.

Receiver Processor modified to three frequency tracker, see Fig 6.17c.

7.2 Results after equipment modification

7.2.1 Background (period May 1977 to June 1977)

After completion of the modification, but prior to full system trials, the elevation system was reinstalled temporarily at Bedford at the end of February 1977, with the intention of collecting data in time for the AWOP 6 meeting in

early March. The flight tests, which were completed in a period of five working days, are listed in Table 7.3. When the full merged error data became available about 5 days after completion, it was found that all the results had cyclic errors which were a periodic function of elevation angle. A typical example from a constant height radial flight is shown in Fig 7.27. This clearly illustrates a cyclic error of 0.06° peak-to-peak with an angular period of 1 beamwidth ($\sin^{-1}(1/54)$).

This error was traced to a missing bit in the data preamble radiated from the ground. In the elevation transmitter all the Barker codes, function identity and data bits were monitored, but a spare bit inserted between the end of the data and the start of the angle transmission was not. This was an oversight in the implementation; a slip in the logic timing caused loss of this spare bit which led to the angle transmission starting 120 μs early. This resulted in the timing of the processor in the airborne receiver being effectively 120 μs late, leading to the correlation period extending over the scan turn round. This gave rise to a cyclic error, which was zero at elevation angles where the path difference between the ends of the array was a whole number of wavelengths, and was a maximum at elevation angles where the path difference was an odd number of half wavelengths.

Table 7.3

TDM flights with DMLS at Bedford site 2 using Andover with omni-antenna

Flight No.	Date	Transmitter		Profiles	Track	Comments
		Az	El			
DA70	2.3.77	-	54λ	R,A	Y	Timing fault on transmitter
DA71	2.3.77	-	54λ	O,R,A	Y	
DA72	3.3.77	-	54λ	R,A	Y	
DA73	3.3.77	-	54λ	O,R,A	Y	
DA74	4.3.77	-	54λ	O,R,A	Y	
DA75	4.3.77	-	54λ	O,R,A	Y	
DA76	7.3.77	-	54λ	O,R,A	Y	

Note: A = approach R = radial
O = orbit Y = yes

The elevation timing fault was corrected and both systems were reinstalled at Bedford at the end of April 1977. A total of 15 flights were made in the period 18 May to 14 June after which the azimuth system was removed for installation on runway 07L at Brussels. Three further flights on the elevation system

alone were made prior to its transfer to Stansted on 19 July. The flights are summarised in Table 7.4. During some of the flights (DA05 to UT12) contractors were working on the runway with maintenance vehicles. In general, this restricted approaches to a minimum height of 300 ft and also introduced unquantifiable possible multipath errors into the results when work was near the transmitter end of the runway.

In general, each flight consisted of a variety of types of run. For the purpose of presentation, the results have been grouped generally in chronological order by type of run profile. For flights DA01 to UT06, problems were experienced with the kine frame number data and this prevented the merging of the DMLS and tracking data on many of the runs. This fault was cured after flight UT06.

The available results are listed in Tables 7.5 to 7.19; the results presented in the following sub-sections have been selected as representative of those listed.

7.2.2 Typical azimuth results from the 54λ array

General The error plots presented in this section have limit lines drawn to show the *overall* ICAO system B guidance error 2σ limits as derived from Table 1.2. Where a relaxation with range and/or azimuth angle is allowed, this has been applied to the overall limits. In all cases the individual noise and bias 2σ limits are 0.707 × the total guidance error 2σ limits.

Orbits The results from four tracked semi-orbital flights are shown in Figs 7.28 to 7.31. These orbits showed:

(a) A general system sensitivity error of about 0.08° total in $\pm 40^{\circ}$, *ie* 1.0008:1 coupled with a possible very small residual error from the modified radome, see Fig 7.32.

(b) A change in bias as a function of flight direction, which was due partly to the 2.4 m offset of the airborne antenna from the aircraft nose (tracking point) and partly due to small timing delays (about 30 ms) between the kine data and DMLS data.

(c) A mean system bias at 0° azimuth of $+0.025^{\circ}$ given by the average of the two curves, Figs 7.27 and 7.28, which were made at the same range and height but in opposite flight directions.

Table 7.4

TDM flights with DMLS at Bedford site 1
using Andover with omni antenna

Flight No.	Date	Transmitter		Profiles	Track	Comments
		Az	El			
DA/						
UA01	18.5.77	54λ	-	R,A	Y	
DA02	19.5.77	54λ	54λ	O,R,A	Y	
DA03	20.5.77	54λ	54λ	O,R,A	Y	
DA04	20.5.77	27λ	-	O,R,A	Y	
DA05	24.5.77	54λ	54λ	O,R,A	N	Coverage flight Contractors on runway
DA06	24.5.77	54λ	54λ	O	N	Coverage flight Contractors on runway
DA07	25.5.77	54λ	54λ	R,A	Y	Contractors on runway
DA08	26.5.77	54λ	54λ	O,A	Y	Tracking approaches only Contractors on runway
DA09	26.5.77	27λ	-	R,A	Y	Contractors on runway
DA10	27.5.77	54λ	54λ	O,R,A	Y	Contractors on runway
UT01/ UT11	27.5.77	54λ	54λ	A	Y	Contractors on runway
UT02/ UT12	31.5.77	54λ	54λ	R,A	Y	Contractors on runway
UT05	3.6.77	54λ	54λ	A	Y	No data kine fault
UT06	3.6.77	54λ	54λ	O,R,A	Y	Coverage orbits
UT07	14.6.77	Telecroscope v. kine flight				
UT19	18.7.77		54λ	A	Y	Azimuth removed for trials at Brussels and Stansted
DA14	19.7.77		54λ	O,R,A	Y	
DA15	19.7.77		54λ	A	Y	

Note: A = approach R = radial N = no
O = orbit Y = yes

79052

Table 7.5

Flight DA02 at Bedford on 19.5.77 using Andover with blade antenna

Run No.	Transmitter		Profile	DMLS plot	Error plot	Comment
	Az	El				
1	54λ	54λ	3° approach, low overshoot (50 ft)			Kine synch problem
2	54λ	54λ	3° approach touch and go	Az El	Az El	
3	54λ	54λ	Radial 3000 ft 40° left			Kine synch problem
4	54λ	54λ	Radial 3000 ft 40° left			Kine synch problem
5	54λ	54λ	Radial 3000 ft on centreline			Kine synch problem
6	54λ	54λ	Radial 3000 ft on centreline			Kine synch problem
7	54λ	54λ	Radial 3000 ft 40° right			Kine synch problem
8	54λ	54λ	Radial 3000 ft 40° right			Kine synch problem
9	54λ	54λ	Orbit 7 n mile at 1500 ft	Az El	Az El	
10	54λ	54λ	2° approach low overshoot			Kine synch problem
11	54λ	54λ	6° approach low overshoot			Kine synch problem

Table 7.6

Flight DA03 at Bedford on 20.5.77 using Andover with omni antenna

Run No.	Transmitter		Profile	DMLS plot	Error plot	Comment
	Az	El				
1	54λ	54λ	3° approach			Kine synch problem
2	54λ	54λ	Radial at 2000 ft 20° left	Az El	Az El	
3	54λ	54λ	Radial at 2000 ft 20° right	Az El	Az El	
4	54λ	54λ	Orbit 7 n mile and 1500 ft	Az El	Az El	
5	54λ	54λ	Orbit 4 n mile and 1500 ft			Kine synch problem
6	54λ	54λ	Radial at 2000 ft 30° left			Kine synch problem
7	54λ	54λ	Radial at 2000 ft 30° right	Az El	Az El	

Table 7.7

Flight DA04 at Bedford on 20.5.77 using Andover with omni antenna

Run No.	Transmitter		Profile	DMLS plot	Error plot	Comment
	Az	El				
1	27λ	-	3° approach	Az	Az	
2	27λ	-	Radial at 2000 ft 20° left	Az	Az	
3	27λ	-	Radial at 2000 ft on centreline			Kine synch problem
4	27λ	-	Radial at 2000 ft 20° right			Kine synch problem
5	27λ	-	Orbit 4 n mile at 1500 ft			Kine synch problem
6	27λ	-	1.5° approach to low overshoot	Az	Az	
7	27λ	-	2° approach to low overshoot	Az	Az	
8	27λ	-	3° approach to low overshoot			Kine synch problem

Table 7.8

Flight DA05 at Bedford on 24.5.77 using Andover with omni antenna

Run No.	Transmitter		Profile	DMLS plot	Error plot	Comment
	Az	El				
1	54λ	54λ	3° approach to 300 ft overshoot			
2	54λ	54λ	3° approach to 300 ft overshoot			
3	54λ	54λ	Coverage radial 30 n mile on centre-line at 3000 ft	Az		
4	54λ	54λ	Coverage radial 30 n mile 20° left at 3000 ft	Az		Coverage flight No kine
5	54λ	54λ	Coverage radial 30 n mile 30° left at 3000 ft	Az		
6	54λ	54λ	Coverage radial 30 n mile 20° right at 3000 ft	Az		
7	54λ	54λ	Coverage radial 30 n mile 30° right at 3000 ft	Az		

Contractors on runway

79052

Table 7.9

Flight DA06 at Bedford on 24.5.77 using Andover with omni antenna

Run No.	Transmitter Az	Transmitter El	Profile	DMLS plot	Error plot	Comment
1	54λ	54λ				Run aborted, ATC
2	54λ	54λ	Orbit 7 n mile 1500 ft			
3	54λ	54λ	Orbit 20 n mile 2500 ft N to S			Coverage flight No kine
4	54λ	54λ	Orbit 20 n mile 2000 ft S to N			

Contractors on runway

Table 7.10

Flight DA07 at Bedford on 25.5.77 using Andover with omni antenna

Run No.	Transmitter Az	Transmitter El	Profile	DMLS plot	Error plot	Comment
1	54λ	54λ	3° approach overshoot at 300 ft	Az El	Az El	
2	54λ	54λ	3° approach overshoot at 300 ft	Az El	Az El	
3	54λ	54λ	1.5° approach overshoot at 300 ft	Az El	Az El	
4	54λ	54λ	Radial at 2000 ft 5° left	Az El	Az El	
5	54λ	54λ	Radial at 2000 ft 10° left			Kine synch problem
6	54λ	54λ	Radial at 2000 ft 15° left			Kine synch problem
7	54λ	54λ	Radial at 2000 ft 5° right			Kine synch problem
8	54λ	54λ	Radial at 2000 ft 10° right	Az El	Az El	
9	54λ	54λ	Radial at 2000 ft 10° right	Az El	Az El	

Contractors on runway

Table 7.11

Flight DA08 at Bedford on 26.5.77 using Andover with omni antenna

Run No.	Transmitter		Profile	DMLS plot	Error plot	Comment
	Az	El				
1	54λ	54λ	3° approach low overshoot at 300 ft	Az El	Az El	
2	54λ	54λ	3° approach low overshoot at 300 ft			Kine synch problem
3	54λ	54λ	Orbit at 20 n mile and 10000 ft N to S	No kine		Coverage flights
4	54λ	54λ	Orbit at 20 n mile and 10000 ft S to N	No kine		
5	54λ	54λ	Orbit at 4 n mile and 2500 ft N to S	No kine		
6	54λ	54λ	Orbit at 4 n mile and 2500 ft S to N	No kine		
7	54λ	54λ	Orbit at 7 n mile and 3000 ft N to S	No kine		

Contractors on runway

Table 7.12

Flight DA09 at Bedford on 26.5.77 using Andover with omni antenna

Run No.	Transmitter		Profile	DMLS plot	Error plot	Comment
	Az	El				
1	27λ	-	2° approach low overshoot at 300 ft	Az	Az	
2	27λ	-	3° approach low overshoot at 300 ft			Kine synch problem
3	27λ	-	3° approach low overshoot at 300 ft	Az	Az	
4	27λ	-	3° approach low overshoot at 300 ft			Kine synch problem
5	27λ	-	4° approach low overshoot at 300 ft	Az	Az	
6	27λ	-	4° approach low overshoot at 300 ft	Az	Az	
7	27λ	-	5° approach low overshoot at 300 ft			Kine synch problem
8	27λ	-	5° approach low overshoot at 300 ft	Az	Az	
9	27λ	-	6° approach low overshoot at 300 ft	Az	Az	
10	27λ	-	6° approach low overshoot at 300 ft	Az	Az	
11	27λ	-	Radial at 2000 ft 30° left			Kine synch problem
12	27λ	-	Radial at 2000 ft 35° right	Az	Az	

Contractors on runway

Table 7.13

Flight DA10 at Bedford on 27.5.77 using Andover with omni antenna

Run No.	Transmitter		Profile	DMLS plot	Error plot	Comment
	Az	El				
1	54λ	54λ	3° approach 300 ft overshoot	Az El	Az El	
2	54λ	54λ	3° approach 300 ft overshoot	Az El	Az El	
3	54λ	54λ	Orbit at 4 n mile and 4000 ft	Az El	Az El	
4	54λ	54λ	Orbit at 4 n mile and 4500 ft	Az El	Az El	
5	54λ	54λ	Radial at 2000 ft 35° left	Az	Az	
6	54λ	54λ	Radial at 2000 ft 35° right	Az	Az	Kine faults at range 4-7 n mile

Contractors on runway

Table 7.14

Flight UT11 (UT01) at Bedford on 27.5.77 using Andover with omni antenna

Run No.	Transmitter		Profile	DMLS plot	Error plot	Comment
	Az	El				
1	54λ	54λ	3° approach with 300 ft overshoot	Az	Az	
2	54λ	54λ	3° approach with 300 ft overshoot	Az	Az	
3	54λ	54λ	3° approach with 300 ft overshoot	Az	Az	
4	54λ	54λ	3° approach with 300 ft overshoot			Kine synch problem
5	54λ	54λ	3° approach with 300 ft overshoot			Kine synch problem
6	54λ	54λ	3° approach with 300 ft overshoot			Kine synch problem
7	54λ	54λ	3° approach with 300 ft overshoot			Kine synch problem
8	54λ	54λ	3° approach with 300 ft overshoot			Kine synch problem
9	54λ	54λ	3° approach with 300 ft overshoot	Az	Az	
10	54λ	54λ	3° approach with 300 ft overshoot	Az	Az	

Contractors on runway
Elevation data not processed

79052

Table 7.15

Flight CT12 (CT02) (DA12) at Bedford on 31.5.77 using Andover with omni antenna

Run No.	Transmitter		Profile	DMLS plot	Error plot	Comment
	Az	El				
1	54λ	54λ	3° approach to 320 ft overshoot			Kine synch problem
2	54λ	54λ	3° approach to 320 ft overshoot			Kine synch problem
3	54λ	54λ	Radial 2000 ft on centreline	Az El	Az El	
4	54λ	54λ	Radial 2000 ft on centreline			Kine synch problem
5	54λ	54λ	Radial 10° right at 2000 ft	Az	Az	
6	54λ	54λ	Radial 10° right at 2000 ft			Kine synch problem
7	54λ	54λ	Radial 10° left at 2000 ft			Kine synch problem
8	54λ	54λ	Radial 10° left at 2000 ft	Az	Az	
9	54λ	54λ	3° approach to 50 ft overshoot	Az	Az	
10	54λ	54λ	3° approach to 50 ft overshoot	Az	Az	
11	54λ	54λ	3° approach to 300 ft overshoot	Az	Az	
14	54λ	54λ	3° approach	Az	Az	

Contractors on runway

Table 7.16

Flight UT06 at Bedford on 3.6.77 using Andover with omni antenna

Run No.	Transmitter		Profile	DMLS plot	Error plot	Comment
	Az	El				
1	54[illegible]	54[illegible]	Radial 20° right at 2000 ft			
2	54[illegible]	54[illegible]	Orbit 10 n mile at 1500 ft S to N		No kine	Coverage
3	54[illegible]	54[illegible]	Orbit 10 n mile at 2000 ft N to S		No kine	Coverage
4	54[illegible]	54[illegible]	Orbit 10 n mile at 2500 ft S to N		No kine	Coverage
5	54[illegible]	54[illegible]	Orbit 10 n mile at 3000 ft N to S		No kine	Coverage
6	54[illegible]	54[illegible]	3° approach to 50 ft overshoot	Az	Az	
7	54[illegible]	54[illegible]	3° approach to 50 ft overshoot	Az	Az	
8	54[illegible]	[illegible]	3° approach to 50 ft overshoot			Kine failed
9	54[illegible]	54[illegible]	3° approach to 50 ft overshoot			
10	54[illegible]	54[illegible]	3° approach to 50 ft overshoot			
11	54[illegible]	54[illegible]	3° approach to 50 ft overshoot			

Table 7.17

Flight UT19 at Bedford on 18.7.77 using Andover with omni antenna

Run No.	Transmitter		Profile	DMLS plot	Error plot	Comment
	Az	El				
1	-	54[illegible]	3° approach	El	El	Clean with some short range noise
2	-	54[illegible]	3° approach	El	El	Clean with some short range noise
3	-	54[illegible]	3° approach	El	El	Very windy
4	-	54[illegible]	3° approach	El	El	Kine errors 0 to 1 n mile, very windy
5	-	54[illegible]	3° approach	El	El	Kine errors at short range, very windy
6	-	54[illegible]	3° approach	-	-	Power supply to transmitter and kine failed
7	-	54[illegible]	3° approach	-	-	Power supply to kine failed
8	-	54[illegible]	3° approach	-	-	
9	-	54[illegible]	3° approach	-	-	

79052

Table 7.18

Flight DA14 at Bedford on 19.7.77 using Andover with omni antenna

Run No.	Transmitter		Profile	DMLS plot	Error plot	Comment
	Az	El				
1	-	54λ	3° approach	E1	E1	
2	-	54λ	3° approach	E1	E1	
3	-	54λ	Radial 20° left at 2000 ft	E1	E1	
4	-	54λ	Radial on centre-line at 2000 ft	E1	E1	
5	-	54λ	Radial 20° right at 2000 ft	E1	E1	
6	-	54λ	Orbit at 4 n mile and 1500 ft	E1	E1	
7	-	54λ	Orbit at 4 n mile and 3000 ft	E1	E1	
8	-	54λ	3° approach	E1	E1	
9	-	54λ	3° approach	E1	E1	
10	-	54λ	Radial 20° right at 2000 ft	E1	E1	
11	-	54λ	Radial on centre-line at 2000 ft	E1	E1	

Table 7.19

Flight DA15 at Bedford on 19.7.77 using Andover with omni antenna

Run No.	Transmitter		Profile	DMLS plot	Error plot	Comment
	Az	El				
1	-	54λ	2° approach	E1	E1	
2	-	54λ	3° approach	E1	E1	
3	-	54λ	4° approach	E1	E1	
4	-	54λ	5° approach	E1	E1	
5	-	54λ	6° approach	E1	E1	
6	-	54λ	7° approach	E1	E1	
7	-	54λ	8° approach	E1	E1	
8	-	54λ	9° approach	E1	E1	
9	-	54λ	9.9° approach	E1	E1	

(d) Very clear multipath effects at discrete azimuth angles. In particular, the presence of an old metal monitor box from the FDM equipment sited on centreline about 100 m in front of the array caused a significant error about the centreline. For an approach flight this would effectively give rise to a localised sensitivity error about the centreline.

(e) A general loss of the discrete multipath effects at higher angles to be replaced by signs of errors due to ground reflection (see results of constant height radial flights).

(f) The azimuth coverage limits of $\pm 40^{\circ}$ programmed into the processor were operating correctly.

There was no obvious reason why the orbit at 9.36° elevation, Fig 7.31 should have exhibited less apparent sensitivity error, but it may have been due to a fortuitous effect of ground tilt. The most likely source of the sensitivity error was expansion due to array heating. The array was assembled at a temperature of about 15°C, the weather in May 1977 was continually very hot and sunny and it is not unreasonable to assume that the array temperature might have reached around $\sim 50^{\circ}$C. With a typical coefficient of expansion for aluminium of around 23 parts per million per 1°C, a 35°C change in the array temperature would give the sensitivity error of 1.0008 seen in the trials results.

Radials The results from a series of radial runs at a constant height of 2000 ft and a range of azimuth angles are given in Figs 7.33 to 7.39. A plot of the elevation angle with respect to the azimuth site is given in Fig 7.40. In looking at the results it must be remembered that the upper design coverage of the azimuth array was $+20^{\circ}$. These radial flights show:

(a) On the -35° radial, at low elevation angles, there were large cyclic errors associated with the TDM field monitor. At higher angles, above 6°, a ground reflection error mechanism took over.

(b) On -20°, small errors were seen from ground reflections.

(c) On -10°, only very small ground reflection errors were in evidence.

(d) On centreline, ground reflection errors were small. The aircraft flight path at low elevation angles was very stable and little effect of the monitor box was either expected or seen.

(e) On $+10^{\circ}$, small effects of ground reflections were present.

(f) On $+20^{\circ}$, large cyclic errors were seen at elevation angles between $+5^{\circ}$ and $+10^{\circ}$, which were again consistent with the effects of reflection from ground with cross fall.

(g) On $+30^{\circ}$, very similar results to the $+20^{\circ}$ radial.

These results were generally consistent with the data obtained from the orbital runs. The radials at positive azimuth angles had a positive mean error at the longer ranges corresponding to lower elevation angles, whilst at increasing negative azimuth angles the positive bias became negative. All the radial runs exhibited an increasing positive error at shorter range, with increasing elevation angle. This appeared to be due to a small tilt in azimuth in the physical alignment of the array.

Approaches Examples of azimuth approaches are given in Figs 7.41 to 7.49. The runs took the form of a conventional approach ending in a low overshoot profile. The characteristics are listed in Table 7.20. The actual

Table 7.20

Azimuth approaches

Run No.	Fig No.	Approach angle	Overshoot height	Contractors on runway	Date
DA2/02	7.41	3°	T & G	no	19.05.77
DA7/01	7.42	3°	300 ft	?	25.05.77
DA7/3	7.43	1.5°	300 ft	?	25.05.77
DA10/2	7.44	3°	300 ft	?	27.05.77
UT11/3	7.45	3°	300 ft	?	27.05.77
UT12/9	7.46	3°	50 ft	?	31.05.77
UT12/10	7.47	3°	50 ft	?	31.05.77
UT6/06	7.48	3°	50 ft	no	03.06.77
UT6/07	7.49	3°	50 ft	no	03.06.77

elevation angles subtended at the azimuth transmitter for the various approaches starting from a constant height of 1500 ft are plotted in Fig 7.50. A study of the results leads to the following:

(a) As the centreline radial, Fig 7.36, showed very small effects due to ground reflection, the main source of error on the 3° approaches at ranges beyond threshold was the multipath from the old FDM monitor box. From the orbital plots at about 2° elevation and within $\pm 1^{\circ}$ of the centreline, effective sensitivity errors of up to $0.04^{\circ}/0.05^{\circ}$ per degree could occur depending on the exact RF phasing. Furthermore, from the orbital plots, when the aircraft was on the electrical centreline, ie about $+0.02^{\circ}$, no error due to the monitor base would be expected. This was generally true for all the 3° runs except UT11,

UT12 (Figs 7.45 to 7.47); on these runs the telescope tracker was also sited about 100 m in front of the array and may have introduced additional multipath effects (the tracker head of the telescope is a 0.3m diameter metal cylinder mounted about 3.5 m above ground). This probably accounted for the large errors at short range seen in particular on UT11 3, when the increasing elevation angle during the overshoot manoeuvre could have produced worst-case multipath phase conditions.

(b) All the results were within the AWOP CAT B requirements. In particular, all runs ending in a 50 ft overshoot or a touch and go gave very low error during the last mile and touch down zone.

(c) The approach at a nominal elevation angle of 1.5° gave a very small bend structure and low noise. This occurred because line of sight to the transmitter over the runway hump was maintained, whilst multipath from the monitor box was attenuated by the hump, see Fig 7.50.

The results were consistent with the operating environment. It is possible that a higher rate roll-off in the low angle elevation pattern of the array would have given more attenuation of the centreline multipath due to the old monitor, but the [illegible] ground profile in front of the array due to the runway hump was the main controlling feature, as this put the monitor box at a positive elevation angle with respect to the array.

7.2.7 Typical elevation results from the 34° array

General Early flight test results (DA01 to DA09) showed a larger amplitude beam bend structure at low elevation angles due to ground reflections than had been expected from the simulator tests. A subsequent check on the array phasing showed that there were discrete steps in the phase distribution along the array which would degrade the sidelobe performance; there was also a small phase slope across the array. The simple expedient of interchanging several of the feed cables and switches reduced the phase steps and slightly reduced the phase slope. This change applied to all flights from DA10 and is reflected in the results discussed below. All the flights listed in Tables 7.3 to 7.19 used the three-frequency receiver processor.

As with the azimuth results the limit lines drawn on the error plots are the overall ICAO system B guidance error 2σ limits, ± 0.1°. The separate resulting bias and noise limits are each 0.07° (2σ).

79032

Orbits The results from six tracked semi-orbital flights are shown in Figs 7.51 to 7.56. The results of Figs 7.53 onwards (flight DA10 onwards) were taken after changes to the array feed phase distribution had been made. These orbital results showed:

(a) On the early 3^{o} elevation orbits (Figs 7.51 and 7.52), cyclic errors due mainly to ground reflection, the effects of which were reduced by phasing changes (Fig 7.55).

(b) From the high angle orbits, some residual effects from internal reflections in the elevation antenna (Figs 7.53, 7.54 and 7.56).

(c) A general positive system bias with a mean value of about $+0.05^{o}$ in the later flights.

(d) A very low overall system noise level with some discrete multipath effects at lower elevation angles due to discrete obstructions.

(e) Very wide system azimuth coverage, in excess of $\pm 65^{o}$.

Radials Figs 7.57 to 7.62 show the results of radial flights at a nominal constant altitude of 2000 ft and azimuth angles of -20, 0, +10, +20 and $+30^{o}$.

The runs showed consistent performance with small errors due to ground reflection even down to 2^{o} in one of the later flights, DA14. The upper limit of coverage was around 22.5^{o} and, as previously, was determined by the data antenna. The small negative roll off in the error plot at high elevation angles was due to the high rate of change of angle and the inherent mean elevation time delay of 25 ms.

The results were consistent with the orbital data.

Approaches Typical results from nominal constant angle approaches are given in Figs 7.63 to 7.75. The earlier 3^{o} approaches (Figs 7.63 and 7.64) showed evidence of excessive ground reflection effects before the array phasing was improved, although the results were still well inside the limits, the main error being bias. Even at an approach angle of 1.5^{o}, Fig 7.65, the noise level was inside the 2σ limit of 0.070^{o}.

The results of flight DA15, Figs 7.67 to 7.75, provided the best example of the elevation system performance. Results are presented for approach angles from 2^{o} to 9.9^{o} elevation. At the higher approach angles there was an increasing positive bias as the range decreased. This arose from the fact that the MLS

airborne antenna was about 2.4 m aft and 2.4 m above the tracking lamp. The compensation applied in the data programme assumed nominal level flight, whereas at high approach angles the vertical separation of the antenna and lamp was increased by 2.4 $\sin\theta_m$. This introduced an increasing positive bias as the range reduced.

7.2.4 Coverage

The coverage of the TDM system was examined by a series of long range constant height radial runs and a series of orbital runs. None of these runs was tracked and the coverage assessment was therefore made from the raw data. The actual coverage flight profiles are given in Fig 7.76, from which it can be seen that the azimuth transmitter was used as the origin for all flights and this must be taken into account when assessing the data from the elevation system. The data plots also show the sub-system digital frame flag. This consisted of an ANDING of the sub-system overall flag and the valid FI flag.

Radial runs The results from the five radial runs are shown in Figs 7.77 to 7.81 in which the raw azimuth and elevation DMLS data is plotted against range from the azimuth site. The minimum range coverage for both systems was set by the high angle cut off for the ground system antennas ($+20^{o}$). The long range coverage was determined by loss of FI decodes due to low signal level. Fig 7.77c shows typical azimuth and elevation received signal level plots. The deep fades at ranges in excess of 25 n mile were probably, in this case, due mainly to aircraft manoeuvres, as both azimuth and elevation signals were similarly affected and the azimuth angle plot indicated a non linear flight path in the region. The azimuth system flagged at a level of -106 dB m, which agreed closely with the bench test results. On all the radials, good information was available to beyond 28 n mile from the azimuth transmitter (26 n mile beyond runway threshold) for both systems. Allowing for earth's curvature at 3000 ft height, the aircraft was at 1.14^{o} elevation (1:50) with respect to threshold at a range of 24 n mile from the azimuth; thus, at Bedford, which has little rising ground off the airfield, the requirement of coverage down to the 1:50 slope from threshold was met with a working margin.

Orbits Results of four part orbital runs, all at a range of 20 n mile, are given in Figs 7.82 to 7.85. Runs were made at nominal heights of 2000, 2500 and 10000 ft.

For the azimuth plots the DMLS angle is shown as a function of nominal angle derived from the aircraft navigation system. In order to see the short

term system noise detail, a pseudo-reference was derived from the first plot and used to normalise the MLS data to remove the rate term due to the orbital path, thus permitting the use of the control motion noise filter to examine the fine grain noise. The same procedure was applied to elevation data except that a fixed angle reference was used.

The results were very much as expected. At the lower heights the azimuth system showed the effects of discrete multipath sources seen in the tracked runs of section 7.2.2, while the elevation system showed relatively high noise (0.2^{o} peak to peak). The elevation system exhibited the very wide azimuth coverage inherent in the simple antenna design, whilst the azimuth data showed clear flag action at $\pm 40^{o}$ as programmed into the receiver for this test.

The two orbits at 10000 ft, Figs 7.84 and 7.85, exhibit predictable characteristics with a very low noise level for both systems.

7.2.5 Results from operation at 27λ aperture

Azimuth system Fig 7.86 shows the result from a constant height radial at 2000 ft and -20^{o}, which may be compared with Fig 7.34. The two runs were flown on the same day, so ground reflection conditions were essentially the same; the flight paths were also similar. The 27λ system gave about twice the error amplitude of the 54λ system. Now from the simulation curves, Fig 6.20a&b, up to separation angles of around 0.4^{o} the two apertures give similar errors for a given multipath level, and a significant difference is not apparent until separation angles are greater than 0.6^{o}. From this we can deduce the magnitude of ground cross fall angle for this radial. For example, at 1.5 n mile, i.e. 20000 ft from the array the 27λ cyclic error is 15/9 times the 54λ error, this implies an effective separation angle of about 1^{o}, which gives a ground cross-fall of

$$\theta = \frac{1.0}{2 \times \sin\left(\tan^{-1}\frac{2000}{20000}\right)} = 5^{o} \quad ;$$

this value is large, but quite possible over small zones.

Figs 7.87 to 7.89 show the results of approaches at angles of 3^{o}, 2^{o} and 1.5^{o} elevation to low overshoot. These may be compared with Figs 7.41 to 7.49; the 27λ performance was very similar to that of the 54λ array with very clean results at 2^{o} and 1.5^{o}.

79052

Elevation system The result of a constant height radial flight is shown in Fig 7.90. The error plot is characterised by:

(a) Significant short term noise below elevation angles of 4^{o}; and

(b) Large long period cyclic errors below elevation angles of 5^{o}.

An examination of the simulation result in Fig 6.19 shows that below 4^{o} elevation angle 0^{o} coded multipath produced by forward scatter from objects in front of the array (VHF ILS etc) falls inside the main lobe of multipath error. It is estimated from Fig 6.19 that a total multipath level of only -23 dB coded at 0^{o} is necessary to give the 0.1^{o} peak-to-peak noise seen at 3^{o}. The longer period cyclic errors are due to specular ground reflection. Typical reflection levels at $4\text{-}5^{o}$ elevation range from -3 to -6 dB for the test site, see Fig 4.13. From the error curve of Fig 6.19, cyclic errors due to ground reflection of the order of 0.12^{o} peak-to-peak at 4^{o} falling to 0.05^{o} peak-to-peak are to be expected. As the elevation angle increases the ground reflection error falls off as would be expected, but there is no obvious explanation for the increase in noise at about 15^{o} elevation.

Fig 7.91 shows the result of a nominal 3^{o} approach. The result was completely consistent with the simulator plot shown in Fig 6.19. It is clear that the 27λ elevation system (effective processing aperture of 24λ) did not give adequate protection to 0^{o} coded signals which could arise from scattering by ground installations.

7.2.6 Conclusions from the TDM system flight trials

The following general conclusions are drawn from the trials at Bedford:

(a) The performance of the 54λ aperture systems, although degraded by site effects, was within the ICAO system B limits.

(b) No error mechanisms were identified which were technique related.

(c) Although the Bedford azimuth site was clear of major obstructions, the significant ground slope close to the array was a major source of system error, even when using vertical directivity. The rate of cut off below 0^{o} could be increased with some benefit, but, more important, the cut-off skirt should be well down, e.g. -20 dB as opposed to the current level of -12 to -15 dB.

(d) If wide angle high accuracy coverage is to be achieved, internal antenna reflections must be minimised.

(e) Small metallic obstructions can cause significant errors.

(f) Although ground slope effects can give 'big' errors at higher elevation angles on the azimuth system, this form of error is minimum at zero elevation, i.e. in the final touchdown zone.

(g) The 27λ aperture systems behaved in a generally predictable manner.

The final assessment was that the system performance, allowing for known site effects, was up to expectation and that the overall design concept was basically sound. Accordingly the decision was made to proceed with a trials programme at operational airports to acquire data over a range of real environments, see section 8.

7.3 Additional field measurements

7.3.1 The effect of metallic poles near the azimuth system

The flight trials reported earlier showed that the performance of the azimuth system at low elevation angles could be signifcantly affected by quite small metallic structures situated close to the antenna. In order to quantify the effects of objects such as lighting poles, some simple field measurements were carried out. These were by no means exhaustive as they were fitted in during other trials, but they do give an indication of the effects to be expected.

The measurement set up is shown in Fig 7.92. The test van with a DMLS receiver was sited 1520 m (5000 ft) from the azimuth array on nominal centreline. A metal pole of length 10 ft mounted on a small trolley was then pulled across in front of the array and the resultant effects recorded in the van as a function of pole angular position with respect to the centreline. Tests were made with two pole diameters, 47 mm and 16 mm at ranges from the array of 30 m (100 ft) and 45 m (150 ft) and with the array operating in both 54λ and 27λ aperture modes.

The results from these tests are shown in Fig 7.93a&b. At a range of 30 m the pole was well inside the near field of both apertures. Peak-to-peak errors for 54λ aperture were very small and spread over a wide angular range. This was due to the considerable effective spectrum spread on the signal from the pole due to its short range from the array. For the 27λ aperture the errors were longer and more concentrated, within ±2 beamwidth of the centreline, due to the smaller spectral spreading from the shorter aperture and the greater error susceptibility for a given multipath level.

Increasing the range to 45 m reduced the pole illumination by 3 dB; for the 27λ aperture in particular larger errors were actually seen, but now virtually confined within ±2 beamwidth (±4°) as the effect of spectrum spread was also reduced. It was concluded that, if poles, *eg* monitors etc, had to be placed near

to and within coverage of the array, the effects could be minimised by putting the pole at very short range.

The 54λ aperture results were significantly smaller than effects seen during the tracked orbit flights. The main difference was that all the obstructions identified in the tracked trials were in excess of 100 m from the array and at small positive elevation angles. Clearly further work could be beneficial in this area.

8 FIELD TRIALS AT OPERATIONAL AIRPORTS

8.1 Background

The trials of the DMLS TDM system at operational airports conducted during 1977/78 were in specific response to ICAO State letter SD 23/1 - 77/127, in which the Council "encouraged proposers of MLS to carry out real trials at typical airports prior to the All Weather Operations Divisional meeting scheduled for April 1978". The airports visited in the trials programme were Brussels[2], Stansted, Gatwick[3], Kjevik (Norway)[4], Manchester[5], Berne[6,8], Tehran[9], John F. Kennedy[7] and Dorval (Montreal)[10].

The primary information from these trials was submitted to ICAO prior to the April meeting in a series of working papers. Each site also forms the subject of a separate RAE report, which is intended as a more permanent and widely available record of the work, and also looks at the results in more depth than the working papers. At three sites, Brussels, Kjevik and JFK, the US TRSB system was also tested in order to obtain directly comparable performance data.

8.2 Objectives

The trials at each site were conducted with the following basic objectives in mind:

(1) To demonstrate the ease of installation, siting and commissioning of DMLS and the ease of co-location with the existing ILS where relevant.

(2) To evaluate the propagation environment.

(3) To evaluate the overall system performance by a series of tracked approach flights.

(4) To evaluate the system coverage by a series of radial and orbital flights.

(5) To demonstrate the capability of DMLS to support full autoland operations with a simple auto-pilot system in conditions where adequate ILS performance would be difficult or impossible to obtain.

(6) To demonstrate the basic system reliability.

8.3 Summary of trials

Each trial was a combined exercise using the resources of RAE, CAA and Plessey. In general, RAE was responsible for the conduct of the measurement programme, which used both RAE and CAA aircraft, and carried out the data analysis and interpretation. The tracking system used for the accuracy measurements was the telescroscope infra-red system used by the CAA for flight calibration of UK ILS installations. This device gave an output in the form of angular deviation of a target lamp on the aircraft from a nominal reference plane within a range of $\pm 0.4^{\circ}$. Tracking was, therefore, restricted to conventional approach profiles for which aircraft angular movement could normally be kept small.

The basic features of each trial are summarised in Table 8.1.

8.4 Overall conclusions

The overall conclusions from this set of trials may be summarised as follows:

(1) At all sites the accuracy of the 54λ azimuth and elevation system was well inside the ICAO system B limits. No allowance was made for the fact that most test runways were shorter than that used to derive the B limits.

(2) At all sites the 27λ azimuth system also performed inside the system B limits, although with less margin than the 54λ azimuth.

(3) The system coverage at low elevation angles, $\leq 6^{\circ}$ or less, was very terrain dependant and, as would be predicted at C band, terrain blockage caused total loss of signal. No cases of false course were seen in any of the shadowed regions.

(4) The trials demonstrated the ease of installation of DMLS which typically took a four-man team 48 h.

(5) The equipment, although not built for portability, proved extremely reliable with no in-service failures in over 5000 h operation.

(6) No operationally significant errors attributable to the reference scalloping mechanism were seen at any site.

(7) The performance of the azimuth system could be affected by small reflecting objects close to the antenna, in particular non-symmetrical approach lighting arrays.

Table 8.1

Trials summary

Trials site	Arrival	Departure	Total runs	ILS colocated	Hours run	
	1977					
Brussels Runway 07L 3638 m × 45 m	Az only 14 Jun	2 Jul	135	No	406	54° and 27° apertures. Investigation of azimuth performance for comparison with computer simulations. Extensive multipath evaluation made. Performance well within ICAO system B limits; no multipath errors observed. Comparative TRSB data from trial in January 1978 very similar.
Stansted Runway 05 3048 m × 61 m	Az 11 Jul	14 Aug	38	El only	834	Main objective to site elevation in front of VHF ILS glidepath to give same nominal threshold height. No ill effects on VHF glidepath. First check runs on CAFU aircraft MLS installation.
	El 21 Jul	14 Aug			572	
Gatwick Runway 08 3098 m × 46 m	Az 17 Aug	2 Sep	33	Yes	402	Correct colocation with ILS. Az 54° and 27°; El 54°. Rising ground under approach path introduced some Az noise. Performance well within ICAO system B limits. Autoland comparison on DMLS and ILS. Low-angle long-range coverage terrain limited.
	El 22 Aug	2 Sep			268	
Kjevik Runway 22 1900 m × 45 m	Az 26 Sep	9 Oct	109	No	295	Az 54° and 27°; El 54°. Hilly terrain, offset azimuth, approach down narrow valley. Approach performance within ICAO system B limits. Low elevation coverage (+6°) very terrain restricted, no false courses, concise flag action in shadow regions. Comparative site with TRSB.
	El 26 Sep	9 Oct			293	
Manchester Runway 24 2804 m × 46 m	Az 23 Oct	10 Nov	74	Yes	326	Az 54°, 27°, 20° and 15°; El 54°, 39° and 30°. Severe hump in runway, large attenuation of azimuth at threshold with high level multipath also present. Performance within ICAO system B limits except for Az 15°. Performance better than existing Cat II ILS.
	El 23 Oct	10 Nov			326	
Berne Runway 32 1200 m × 30 m	Az 18 Nov	12 Dec	199	No	556	Az 54°, 27°, 20° and 15°. El 54°, 39° and 30°. Short narrow runway, mountain very close to approach path. Terrain severely limits low angle coverage, no terrain induced errors. Azimuth bend near threshold due to multipath from reciprocal approach lighting arrays. 54° azimuth and elevation performance within ICAO system B limits.
	El 18 Nov	12 Dec			556	
	1978					
Brussels Runway 07L	El only 5 Jan	12 Jan	29	No	280	Approaches down to 2° with shadowing Hercules in front of the array, approach accuracy and coverage to ICAO system B requirements. Comparative TRSB data, similar performance.
Tehran Runway 29L 4028 m × 61 m	Az 23 Jan	10 Feb	95	Yes	325	Very long humped runway. ILS glidepath out of service due to earth movements near array. Very low azimuth signal inside threshold. Azimuth bends due to cross-fall ground reflection. Autoland performance affected by turbulence on approach over town. No tracked flights.
	El 23 Jan	10 Feb			325	
JFK Runway 13L 3049 m × 46 m	Az 10 Mar	25 Mar	?	Yes	?	Significant elevation multipath and shadowing due to large hangar. Prime flying FAA CV580 with laser tracking, comparative TRSB data, very similar performance for both systems. Good example of high density site. Performance within ICAO system B limits.
	El 10 Mar	25 Mar	?		?	
Dorval Runway	Az 28 Mar	20 Apr	?	No	?	Comparative demonstrations for AWOP meeting, DMLS and TRSB co-sited on same runway. No comparative tracked flights.
	El 28 Mar	20 Apr	?		?	

(8) No effects were seen that could be classified as unique to DMLS, while on those sites from which comparative TRSB data was available the performance of the two systems was very similar.

9 A REFERENCE-LESS SYSTEM

9.1 Background

The use of a reference frequency transmission in the Doppler system was essential for the operation of the early type of processors, such as those used in the FDM system. The results of section 6 showed that the reference signal could give rise to large system errors if particular multipath situations occurred. Whilst it was questionable whether this error mechanism could be operationally significant, it was clearly very attractive to consider a system that did not use a reference transmission. This would then realise the full performance capabilities of the simple commutated coding, and at the same time greatly simplify the ground system, giving direct benefits in terms of cost, reliability and integrity.

The development of the correlation processor, which essentially operated on a single scan basis, provided the technique whereby a reference-less system might be implemented. This section outlines a possible system and presents some basic supporting measurements made with the hybrid simulator.

9.2 System outline

In the basic TDM signal structure, the received angle-coded signal was differenced in the receiver detector to obtain a signal, based upon the 83.2 kHz offset, which was free from the effects of ground and airborne oscillator drift and Doppler shift due to aircraft motion. Arising from the use of a reference during the angle transmission, it was decided to implement the function identity and data transmission as modulation on a sub-carrier offset by a 41.6 kHz from the same reference.

In the proposed reference-less system, the reference transmission would be totally removed. The function identity and data signals would be radiated as direct DPSK modulation of the carrier (carrier DPSK); this is now a well established technique which has been well tried in the TRSB system.

The method of obtaining the angle data is given in Fig 9.1. The receiver follows normal practice as far as the final IF, but, instead of the final IF feeding a detector, a further stage of frequency conversion would be employed to give a final IF centred around 90 kHz. This signal would then be applied

directly to the input of a correlation processor. With the transmitter operating in the bi-directional scan mode, the processor would be configured to search for, acquire and track alternate scans independently. As alternate scans contain opposite sense of angle code but the same errors due to frequency drift, etc, the actual angle information would be obtained by differencing the two measurements.

The system outlined above looks so attractive that one may well ask why it was not implemented in the UK programme. The simple answer was lack of time and effort. The basic correlation processor was not fully proven in dedicated hardware until late 1976. The reference-less system required search and acquisition over an additional bandwidth of ±25 kHz to cover the full range of airborne and ground system frequency tolerances. This, together with the need for total independence on alternate scans, called for a sizeable increase in the system storage and a small increase in the upper limit of operating frequency to around 136 kHz compared with the value of 105 kHz for the basic system.

The need to search over an additional bandwidth of ±25 kHz to allow for system frequency tolerances could be avoided by using the processor to measure the frequency of the DPSK signal prior to each angle transmission. This then defines the centre frequency of the angle transmission and reduces the search range to that originally needed for the system where a ground radiated reference was employed. If this approach were followed, it would also be logical to incorporate the DPSK decoding into the digital processor.

Although the differencing of alternate scans removes the effects of long-term drift, it is essential for satisfactory operation of the system that the short-term drift, $\delta\phi$ between scans, should be small compared with the desired smallest increment of frequency measurement. Some simple tests were carried out to investigate this area of performance of the existing equipment.

9.3 Feasibility tests

The system block diagram for these tests is given in Fig 9.2. As the existing receiver was not configured to separately track alternate scans, it was decided to introduce a pseudo reference at 20 MHz, f_0 the second IF frequency, which would alternate by 83.2 kHz on alternate scans in sympathy with the angle coded signal. This had the effect of maintaining a uniform sense of angle signal on the output of the final mixer centred on 83.2 kHz, whilst reversing the sense of all the drift terms hence giving rise to the same mathematical result as depicted in Fig 9.1. For odd scans the two signals at the detector input referenced to 20 MHz were:

$$\text{pseudo reference} = f_7 + f_1$$

$$\text{coded signal} = 83.2 + f_1 + f_2 + f_3 + f_4 + f_5 + f_6 + F_D \ ,$$

giving a detection output of $83.2 + F_D + (f_2 + f_3 + f_4 + f_5 + f_6 - f_7)$. For even scans the detection input signals reference to 20 MHz were:

$$\text{pseudo reference} = 83.2 + f_1 + f_7$$

$$\text{coded signal} = f_1 + f_2 + f_3 + f_4 + f_5 + f_6 + F_D \ ,$$

giving a detector output of $83.2 + F_D - (f_2 + f_3 + f_4 + f_5 + f_6 - f_7)$. As long as the system was set up such that $(f_2 + f_3 + f_4 + f_5 + f_6 - f_7)$ was less than ±1 beamwidth, i.e 378 Hz for the 54λ azimuth system, the correlation processor would accurately measure the frequency of each scan and give an average output value for the six bi-directional scan pairs in the 30 ms measurement period. Therefore, as long as the medium term frequency drift (i.e over a period of say 15 min) was within 378 Hz, this simulation gave a very good indication of the effects of very short-term drifts. In fact the simulation included effectively five short-term sources (f_2, f_3, f_4, f_5 and f_7) compared with the two sources to be expected in a normal transmitter. A simulation of a 54λ azimuth system was chosen, since this had the longest normal scan length, 2.5 ms and should be most sensitive to short-term frequency jitter.

Fig 9.3 shows the results obtained at a fixed angle measured over a period of 2.5 min. The top two traces are for uniscan operation and show the overall frequency drift of the oscillators in the system. The drift over a 2.5 min period was below 0.3° (120 Hz). The lower two traces show the basic noise when operating in the bi-directional mode in which drift effects should cancel out. The resultant noise level was somewhat higher than that given by the standard system (see Fig 6.15), but the rms level was still small at 0.005°. The most sensitive system element was found to be the voltage-controlled oscillator in the receiver frequency synthesizer. The control loop bandwidth of this oscillator was less than 600 Hz, which made the structure sensitive to mechanical vibration with frequency components above 600 Hz; the effects of tapping the oscillator housing are shown in Fig 9.3. No investigation of the effects of cyclic vibration were made although it would be expected that the VCO would be more sensitive to this.

Figs 9.4 and 9.5 show the basic error versus separation angle for multipath levels of -3 dB and -1 dB. The results, as expected, are effectively identical to those for the basic system, see Fig 6.20.

The performance as a function of relative fading rate is shown in Fig 9.6; note that the multipath level used is -1 dB, whereas all the comparative plots in section 6 were made at a level of -3 dB. The top plot shows the basic noise level with the direct signal only. The bottom plot shows the residual effects of the multipath signal for fading rates of 0-500 Hz. Some increase in noise was expected, as were small responses at 200 Hz and 400 Hz from sidelobes of the multipath signal; the responses at 100 Hz and 300 Hz were not expected. The simple test of removing the multipath signal, while leaving the fading system running, produced the middle plot, which shows that the responses at 100 Hz and 300 Hz were in the main due to cross talk in the phase-lock fading oscillator circuits of the simulator.

9.4 Conclusions

The tests demonstrated that a reference-less system is a practical proposition and that the full multipath rejection potential of DMLS can be realised in such a system.

In a practical implementation one of the main design criteria would be control of the short-term stability of the various signal sources in the system. The simulator tests have shown that the basic crystal and multiplier sources used in the transmitter were adequate, but the design of the VCO used in the receiver synthesizer should be such that it has a low response to mechanical vibration at frequencies outside the loop control bandwidth.

10 DESIGN DISCUSSION AND OVERALL CONCLUSIONS

10.1 Design factors

The overall UK DMLS programme including the series of trials at operational airports has enabled us to form a detailed understanding of the relevance of the basic system design parameters to different aspects of the overall operational environment. This section discusses these factors (comments about multipath assume no reference scalloping) and gives overall conclusions on the technical aspects of the programme.

10.1.1 Azimuth system

Antenna aperture One of the fundamental design decisions is the choice of horizontal aperture for the azimuth antenna. This will normally be based on

the requirement to keep all significant multipath sources in the out-of-beam region of the multipath response curve. In general, ICAO safety criteria ensure that large structures are a minimum distance from the runway and many people have therefore assumed that smaller apertures can be used on shorter runways. It has also been frequently assumed that the sole critical performance criteria is the lateral displacement error at touchdown and therefore on shorter runways greater angular errors can be tolerated. This of course neglects the overall performance degradation that could take place in the rest of the coverage. For example, if we accepted lateral displacement threshold performance as the sole criteria, the angular limit error (2σ) would be 0.076° for a 4270m (14000ft) runway and 0.15° for a 2285m (7000ft) runway. Although the lateral performance at threshold would be the same, the long-range performance would differ by 2:1. We should note that the OR interpretation states "that provided performance of the quality required for automatic landing can be achieved when the ground elements providing across-track direction, e.g. for azimuth, are situated as far away as the upwind end of a long runway (of the order of 4200 m (14000 ft) from touch-down region) then across-track information should be sufficiently accurate to support all other operations in the approach sector". We can see, therefore, that the OR does not give any real guidance on acceptable angular performance for full capability systems on shorter runways. Probably the most sensible interpretation is to take the lateral displacement errors as a function of range from threshold for the 4200m runway and then use those to derive angular limits for the shorter runway, this is illustrated in Fig 10.1 for 4200m and 2100m runways. This results in a somewhat unusual curve for the shorter runway which does have some practical meaning as shown later.

Aircraft moving on the ground, if they pass through the line of propagation from the ground array to the receiving aircraft, will in general give rise to errors which are proportional to system beamwidth both in amplitude and duration. For a given situation increasing the aperture reduces both amplitude and duration. The incidence of such effects will be greatest when the receiving aircraft is at a low elevation with respect to the azimuth station.

The presence of any small metallic obstructions close in front of the array can also give rise to beamwidth related errors. Examples of such obstructions are approach lighting arrays, power distribution boxes, small radar reference reflectors and even, in some circumstances, the MLS monitor. The effects of such structures depend on the symmetry with respect to the centreline, the distance from the array and the illumination by the array. Objects exactly

on centreline give no centreline error but do induce a localised sensitivity error which is proportional to beamwidth. Objects off centreline will give rise to slowly cycling errors on the approach if they lie within about 1.5 beamwidth of the centreline; this can include a large area. In general, the use of vertical aperture to give a low angle elevation cut-off in the vertical radiation pattern ensures that significant effects will only occur at low elevation angles. Unfortunately, this means that worst effects are likely to be seen during the last part of the approach to touch-down; here we can see that the short runway angular error curve as given in Fig 10.1 has a practical significance.

The final source of azimuth system errors is reflection from ground with a cross fall. In general, the effective separation angle of the reflected signal is small, particularly at low elevation angles. For very small separation angles, e.g. below 0.2^{o}, the multipath errors are virtually aperture independent as the error curves for all apertures start with similar slopes around zero separation angle. The best protection against this source of error is a sharp well defined low angle cut off in the vertical radiation pattern. There is a limit to the rate of cut off that can be obtained with acceptable vertical apertures, e.g. 1.2 m, and sites with large cross fall and upward sloping ground, such as at Bedford, provide the worst possible combination of conditions.

In the UK trials programme the 54 aperture system gave adequate performance on all sites with good margins, whilst on some sites smaller azimuth apertures gave rise to significant increases in system noise.

Beam shape, sidelobe levels The application of aperture amplitude weighting (in DMLS this is applied in the airborne processor) or an equivalent operation to reduce system sidelobe levels to a considerably low value is highly desirable as this largely removes the consideration of sidelobes as a critical performance factor, any residual errors due to reflections of sidelobes are generally further reduced by the effects of motion averaging.

Motion averaging In the azimuth system in-beam multipath signals will be associated with very low fading rates where motion averaging is ineffective. Out of beam multipath, e.g. from sidelobes, will only give measurable errors for very high multipath levels which will only be associated with good specular reflectors. In typical environments the situation geometry will be such that this type of signal will have an associated fading rate between 0 and 1000 Hz. The ideal motion averaging characteristic is one in which all frequencies above those needed for stable operation of the AFCS are attenuated. The continuous signal of the FDM system effectively provided this characteristic; on the other

79052

hand, the TDM system would need to sample at 2500 Hz to provide this ideal characteristic. The current compromise of averaging over a 30 ms measurement has proved satisfactory as significant attenuation of all signals above 25 Hz is obtained. However, some aliasing errors will still exist on some sites.

10.1.2 Elevation system

Antenna aperture The vertical aperture of the elevation array is determined primarily by the ground profile and obstruction in front of the array. If the ground is planar and free of significant scattering structures, the minimum acceptable aperture is that which gives adequate discrimination against the specular ground reflection for the lowest operational approach angle. From the simulation measurements for flat ground, a 27° aperture (22° effective) would be marginally adequate for a 3° approach. If conditions are not ideal, such as a rising slope on the ground or significant forward scatter of zero elevation signals from scattering structures, the 27° performance will be unacceptable. A logical design criteria would be to ensure that 0° coded signals which could arise from scatter or inclined surfaces, e.g. rising ground, are strongly discriminated against. This would imply using an aperture not less than 40° for consistent performance on a 3.0° minimum approach angle and larger apertures for lower approach angles. These requirements could be relaxed if some degree of vertical directivity were introduced into the individual array element patterns*. In civil operations the additional cost involved would probably not be worthwhile as vertical aperture in DMLS is relatively cheap.

The azimuth aperture of the antenna will be a compromise between the long-range wide azimuth coverage requirements and the desire to restrict illumination of any large structures, such as hangars, which may be relatively close to the elevation site at wider azimuth angles, e.g. runway 13L at JFK.

Beam shape - sidelobe levels The design aim here is the same as for the azimuth system, use an effective aperture distribution which results in consistent low sidelobe levels, i.e. below -20 dB. It is particularly important that the amplitude of the low number sidelobes is very small as the ground reflection coefficient associated with the angles of these sidelobes will be at its highest. In the elevation system we can also consider the use of asymmetric processing laws which give additional discrimination against ground reflected signals at the expense of discrimination against above beam multipath, which is very rare.

* The resulting increase in total system aperture might be better employed in a fully active mode.

Motion averaging In the elevation system ground reflected signals will have very low fading rates and are not sensitive to reduction in effect by motion averaging. On the other hand azimuthal reflected signals will in general have significant scalloping rates particularly at shorter ranges. The use of a 50 ms total measurement period for the elevation system gives significant reduction in error amplitude for fading rates above 15 Hz. The reduction in error amplitude due to motion averaging is an important feature of wide azimuth coverage systems as multipath from vertical surfaces will have in-beam angle codes due to the nature of the conical system geometry. In such situations the effects of multipath can only be controlled by a combination of azimuth pattern shaping and motion averaging.

10.1.3 Long range coverage

The trials at Bedford demonstrated adequate long range coverage with the trials aircraft used. Of course Bedford, in terms of the surrounding terrain profile, is a good site as the ground generally falls away off the airfield. Even on this site the signal level margins at 20 n mile were not large enough to guarantee coverage to all possible types of aircraft in all realistic orientations. One of the main facts emphasised by the trials at operational airports was that long range coverage (ie beyond 10 n mile) at low elevation angles was very dependent on terrain and local line-of-sight obstruction and it is only on a limited number of airfields that the OR will be met.

10.1.4 The design factors discussed above are summarised in Table 10.1.

10.2 Overall conclusions

The development programme has shown that the Doppler technique can be readily implemented in practical equipments to give overall system performance well within the ICAO operational requirements. The concept has been thoroughly evaluated in two signal formats in a wide range of full system trials and associated bench tests using hybrid simulation techniques.

One error mechanism (reference scalloping) which may be regarded as unique to the DMLS system, when implemented with a reference, has been shown to have little operational significance. Simple system changes which remove this mechanism have been demonstrated which would also lead to reduced ground system costs and increased reliability and integrity.

One of the main aims of the ICAO MLS development programme was to obtain a system which would be easier to install than ILS, give consistent performance,

work on sites where ILS did not and give extended high accuracy navigation capabilities in the terminal area.

DMLS has met all these requirements related to the provision of high accuracy angular information in azimuth and elevation.

At the same time the trials programme has shown that MLS is not immune from environmental effects and some of the sources of error to which 5000 MHz systems are sensitive are not relevant to VHF ILS.

Table 10.1

Design factor summary

Parameter	Sensitivity
Azimuth array azimuth aperture	Runway length : performance category : approach sector performance : ground movements : localised structures (lights etc)
Azimuth array vertical aperture	Performance category : near field ground profiles : threshold range
Sidelobe level	For consistent performance design for -20 dB or better
Motion averaging	Not a critical parameter for azimuth systems with low sidelobes
Elevation array vertical aperture	Minimum glidepath angle : terrain slopes : local structures : element vertical directivity
Azimuth aperture	Long range wide angle coverage *vs.* protection against azimuth reflections
Sidelobe level	Design for consistent low sidelobes better than -20 dB
Motion averaging	Very important in reduction of azimuth reflection effects choose update format to optimise performance
Long range coverage	Terrain profiles, aircraft antenna installation

Appendix A

DIARY OF EVENTS APRIL 1974 TO APRIL 1978

1974

9 April	Delivery of missed approach azimuth ground system
21 March	Delivery of Plessey 2A FDM receiver
10 April	Delivery of STL FDM receiver with simple self tuning filter
23 July	Delivery of approach azimuth ground system
28 August	Delivery of elevation ground system
9-13 September	Second meeting of AWOP Working Group A in London. Demonstration of DMLS to panel members at RAE Bedford
9 September	Delivery of Plessey 2B FDM receiver
September to December	USA - FAA internal evaluation of DMLS and scanning beam systems

1975

11 February	Sine/cosine tracker installed in elevation channel of STL receiver
February	FAA select TRSB as USA system proposal
24-28 February	Third meeting of AWOP Working Group A in Melbourne
10 March	Start of flight trials using digital recorder system
11 April	Installation of sine/cosine trackers in approach and missed approach azimuth channels of STL receiver
18 April	Start of fully instrumented accuracy flight trials of FDM system to fulfil data requirement for ICAO submission
November	UK final system proposal sent to ICAO (system submitted based on time division multiplex, data base provided by tests on frequency division multiplex system)

1976

9-20 February	Fourth meeting of AWOP Working Group A in Braunschweig
17-26 May	Fifth meeting of AWOP Working Group A in Washington
May	Doppler TDM ground equipment installed at RAE Bedford on co-located site
5-16 July	Sixth meeting of AWOP Working Group A in the Hague
September	TDM equipment relocated to normal azimuth and elevation sites
1-14 November	Seventh meeting of AWOP Working Group A in London. Demonstration of DMLS TDM system at Bedford
4 November	TDM equipment returned to Plessey for modification and refurbishing

1977

28 February to 18 March	Sixth meeting of AWOP in Montreal
1-10 March	TDM elevation system at Bedford for brief flight tests then returned to factory for completion of update
May	TDM azimuth and elevation systems installed at Bedford
May to June	Data collection flights for UK submission
13 June to 2 July	Trials of TDM azimuth system at Brussels National Airport[2]
July	Trials of TDM system at Stansted Airport
17 August to 2 September	Trials of TDM system at Gatwick Airport including autoland[3] checks
26 September to 9 October	Trials of DMLS TDM system at Kjevik Airport, Kristiansand[4], Norway
23 October to 10 November	Trials of DMLS TDM system at Manchester Airport[5]
18 November to 12 December	Trials of DMLS TDM system at Berne Airport[6,8]

1978

January	Trials of DMLS TDM. Elevation system at Brussels National Airport[2]
January	UK evaluation of Bendix basic narrow TRSB system at Kjevik[4], Kristiansand, Norway
January to February	Trials of DMLS TDM system at Mehrabad Airport, Tehran, Iran[9]
January to February	UK evaluation of Bendix basic wide TRSB system at Brussels National Airport[2]
March	Observation of trials of TRSB basic wide system at JFK Airport[7]
March	Trials of DMLS TDM system at JFK Airport, New York[7]
April	Demonstrations of DMLS TDM system at Dorval Airport, Montreal[10]
April	ICAO All Weather Operations divisional meeting, Montreal

Appendix B

TRIALS FACILITIES AND ICAO TEST REQUIREMENTS

B.1 Test site description

The site chosen for acquiring basic accuracy data on both the FDM and TDM DMLS systems was RAE Bedford.

The Bedford airfield was chosen as having a representative runway length, being in a location relatively unaffected by airways and other airfields within the limits of the MLS test plan, and having good tracking facilities for assessing system accuracy. The airfield was also a relatively clean environment in terms of buildings likely to give interfering multipath signals, and so the multipath level could be controlled by other means. A plan of the test site is shown in Fig B1.

B.1.1 Position of DMLS transmitters - FDM system

The main runway (09/27) has been used as the test runway and is 3200 m (10500 ft) long and 92 m (300 ft) wide. The DMLS approach azimuth transmitter was installed on the extended centreline approximately 76 m (250 ft) beyond the 09 end of the main runway, and the missed approach azimuth transmitter was installed 150 m (500 ft) beyond the 27 end of the main runway, again on the extended centreline. The elevation transmitter was installed 150 m (500 ft) to the south of the runway centreline, and approximately 660 m (2200 ft) from the 27 end of the runway. In this position, the elevation transmitter could be tested in the elevation role by using a false threshold, 300 m (1000 ft) in front of the transmitter, and in the flare role by using the true runway threshold.

B.1.2 Position of DMLS transmitters - TDM system

The three different siting positions used for the TDM system are shown in Fig B.1. For initial tests the equipments were co-located at G. For subsequent tests the azimuth equipment was sited on the extended centreline 142 m (467 ft) beyond the 09 end of the runway and the elevation equipment was sited beside the STAN 38 glide path 203 m (666 ft) from the runway centreline. For the final trials, to obtain direct comparison with the FDM 90λ elevation results, the TDM elevation was sited beside the FDM elevation 122 m (400 ft) to the south of the centreline and 640 m (2100 ft) from the 27 end of the runway.

B.1.3 Airfield buildings

The principle airfield building was the control tower, Fig B1, which was 12 m (40 ft) high by 18 m (60 ft) wide and was sited 450 m (1300 ft) from the runway centreline with the front face at an angle of 8^{o} to the centreline. Large hangars were at least 750 m (2500 ft) from the runway and none were orientated to put reflections into the main coverage. Buildings closer to the runway were 3.5 m (12 ft) maximum height and some of these were parallel to the runway.

B.1.4 ILS transmitter positions

The STAN 37 ILS localizer transmitter was sited 235 m (775 ft) beyond the west end of the test runway, and the STAN 38 ILS glidepath transmitter was sited 200 m (650 ft) to the south of the test runway and 275 m (900 ft) from threshold. Thus the DMLS approach azimuth transmitter lay between the ILS localizer and threshold, and the ILS glidepath transmitter lay between the DMLS elevation transmitter and threshold. This ILS installation was promulgated as a Cat II facility.

B.1.5 Ground static test points

A series of surveyed test positions were marked on the airfield in accordance with Attachment B to ICAO State letter SP20/1-75/53, dated 3 July 1975. The surveying was done by the Contraves kinetheodolite tracking cameras where possible, and, if line-of-sight was obstructed, a surveying theodolite was used to determine the azimuth or elevation angle with respect to the appropriate transmitter array centre. Paint marks were used on the concrete or tarmac surfaces, and concrete blocks were let into grass surfaces. For details see section B.6.5.

B.1.6 Airfield and local topography

The main feature of the Bedford airfield topography is illustrated in Fig B2. This shows the test runway profile in a section along the centreline. There was an obvious hump close to the west end of the runway, with the ground falling away some 8.5 m (28 ft) from the crest to the 27 threshold. Fig B.3 shows a B707 at a distance of 900 m from forward azimuth already partially screened by the hump.

The azimuth transmitter positions are shown in the same figure and it is clear that line-of-sight did not exist from the approach azimuth transmitter to positions lower than 10 m (30 ft) above the 27 threshold. In the forward

coverage zone there was a general fall in height with increasing distance from threshold, giving a mean ground slope angle of -0.2^{o}.

B.2 Tracking system

B.2.1 Kinetheodolite system[12]

The primary range tracking facility available at the Bedford airfield was optical, being a pair of kinetheodolites. These were positioned as shown in Fig B1, and gave tracking cover for the main runway 27 and the shorter runway 24. The spacing was 2401.60 m (7879.3 ft), the baseline crossing runway 27 at 1166.34 m (3826.6 ft) from the approach azimuth array and making an angle of 31.211^{o} with the runway centreline.

Being a single baseline system with no instrument redundancy, considerable reliance was placed on the accuracy of the cameras themselves and the stability of the mounting structure and its foundations. To provide complete airfield coverage the kinetheodolites were raised on 10m (30ft) high towers. Each kinetheodolite was mounted on a massive stressed concrete central column. A mechanically isolated brick support tower provides access to the operating platform. One of these towers is shown in Fig B4. The stability of the central support column was monitored against short and long term movements by inset spirit levels.

The kinetheodolite type was the Contraves EOTS model E-C having a rate-aided tracking servo. They were operated by an experienced crew employed particularly for this purpose. One of the cameras is shown in operation in Fig B5.

The kinetheodolite tracking facility included a dedicated computer installation and a film reading section. Reference objects, photographed before each run, were used to remove any range instrumentation error that may have occurred and corrections for bore sight tracking errors were applied; thus realising the full accuracy potential of the system, which is covered in detail in Appendix C.

B.2.2 Kinetheodolite tracking limitations

The accuracy of a two-instrument tracking system of this type obviously varies with the target position relative to the baseline running through the instruments. However, the region in which tracking accuracy was not adequate for DMLS evaluation was small and did not lie within a critical area of the DMLS coverage (see Appendix C).

Film reading eliminated operator tracking errors, which could become significant at short range, where very high angular tracking rates predominated. This could not altogether compensate where the tracking target was obscured by the bulk of the aircraft itself, such as when using a nose-mounted tracking lamp after the aircraft has passed a kinetheodolite site. The problem was minimised by careful location of the tracking target (usually a lamp) on the aircraft and by control of the flight paths used. A similar problem could occur in relating the tracking target position to that of the MLS receiving antenna. For example, the BAC 1-11 target was a nose-mounted lamp while the antenna was above the cockpit.

Fig B6 highlights the effect of uncompensated tracking point/DMLS receiving antenna displacement errors at short ranges.

Range limitation exists for any optical tracking device. This may be typically taken as 7-8 n mile maximum for conditions prevailing in southern England. Cloud layering provided only rare opportunities for tracking aircraft at high altitude (20000 ft) and the optical tracking system therefore normally limited accuracy tests to heights below 6000 ft.

B.3 Ground test facilities

B.3.1 Test van

For ground dynamic and static test measurements a test vehicle was required. This vehicle was based on a Ford transit van and was equipped with communications, tracking equipment, antennae and power sources. It is shown overall in Fig B7 and its interior in Fig B8.

The primary experimental power source was a 28V 60A engine-driven alternator, which fed a 28V dc bus-bar across which two series connected 12V 70A h batteries were floated. Power at 230 V, 50 Hz and at 115 V, 400 Hz was provided by solid-state sine wave inverters. For prolonged static vehicle positions, where engine use was not practical, an external mains supply was available.

The van carried both VHF and UHF communication transmitter/receivers, which served airfield communication requirements and provided tracking synchronisation links when required.

The vehicle interior was designed to carry a single aircraft type RADRAC in addition to two fixed equipment racks. Accommodated in the equipment racks were an 18 channel ultra-violet recorder with interface matching electronics for two DMLS receiver systems, and an X-Y plotting table. These allowed

recording and presentation of results in real time, providing immediate feedback of measurements to the operator. The RADRAC carried the DMLS receivers and additional analogue and digital recording systems as required. The van RADRAC was interchangeable with either of the aircraft RADRACs.

In addition to VHF and UHF communication antennae, the vehicle carried a general antenna mounting which could be orientated to look in any direction. This was designed to carry a variety of microwave antennae, such as the large horn seen in Fig B7, which was useful for investigations requiring some degree of directivity. A pneumatic mast operated by an electrically driven compressor was attached to the rear of the vehicle allowing DMLS antennae to be raised to 7 m (23 ft) above ground level.

B.3.2 Telescopic mast

For ground static tests, when heights in excess of those obtainable with the test van mast were required, a trailer mounted telescopic mast was used to a maximum height of 22 m (70 ft) above ground level. Two similar masts were used, one for general airfield measurements, and one to carry the antenna for the elevation sub-system field monitor. The trailer and mast are shown in Fig B9. Jacks were attached to each of the four trailer corners to provide a stable, level base. The mast was pneumatic, being operated by a compressor driven from a petrol engine mounted on the trailer.

B.4 Test aircraft

Apart from aircraft used as obstacles in shadowing and multipath measurements, three aircraft were used in the UK DMLS assessment programme at Bedford. These were a Hawker Siddeley Andover, a BAC 1-11 and a Wessex helicopter. All three aircraft were fitted as flying laboratories and carried the MLS RAE RADRAC equipment mounting system, so providing complete experimental equipment compatibility between aircraft. In each case the MLS guidance information replaced the signals from one of the standard VHF ILS navigation units fitted and was fed in the normal manner to displays and flight director. No smoothing time constant was added to the DMLS receiver guidance signals.

B.4.1 Andover C Mk 1

Description and performance The Andover, shown in Fig B10, was the UK military version of the Hawker Siddeley HS 748. This aircraft was propeller driven by two turbine engines and had STOL characteristics which allowed descents at approach glidepath angles up to 10°. A Smiths series SEP2C autopilot was fitted allowing localizer and glidepath autopilot coupling to an altitude of

200 ft with a minimum airspeed of 110 kn. On radial flights the aircraft was normally coupled to DMLS. Apart from autopilot restrictions runway approach airspeed could vary from 96 to 120 kn with a landing airspeed of 90 kn. Climb rates for the typical aircraft weights used were 7 min to an altitude of 5000 ft and 13 min to 10000 ft. The nominal turn radius for a bank angle of 15° was 1400 m (4500 ft). Normal in-circuit airspeed was 120 kn. Navigational aids fitted include ADF, VOR, ILS, Tacan, Doppler 72 and Decca Mk 19. A radio altimeter and weather radar were also installed.

The standard RAE RADRAC system was used to house experimental equipment in the cabin, Fig B11.

Antennae The Andover was fitted with two small dual horn C-band antennae, although only the vertically polarised horn of each pair was used for DMLS evaluation. The aperture of this horn was 5 cm by 7 cm; it had a gain of 8 dB over an isotropic radiator and radiation patterns of $\pm 40^{\circ}$ in azimuth and $\pm 25^{\circ}$ in elevation between -3 dB points. One of the horns was mounted in a blister below the nose radome, in close proximity to the 500W tracking lamp position, and one in the point of the tail. Mountings were provided for two DMLS RF units in the nose section, whilst there was provision for a further RF unit in the aircraft tail. Elevation and azimuth radiation diagrams for the nose-mounted horn are shown in Figs B12 and B13, tail horn radiation patterns being very similar.

A further C-band horn with an aperture of 10 cm^2 was mounted in the cabin skin to look to the port side of the aircraft. It was proposed to use this for coverage measurements.

During the aircraft overhaul in early 1975, a printed dipole antenna in a blade housing (designed by MEL for the Madge programme) was fitted to the cockpit roof. This antenna gave very wide azimuth coverage and was used as the prime antenna in all subsequent trials. The azimuth pattern was checked by flying a circle of 4 n mile radius, centred 14 n mile from the azimuth transmitter and at a height of 2500 ft. Fig B14a shows the aircraft track and actual received signal. Fig B14b shows the signal level corrected for variation of aircraft range from the transmitter. No other corrections have been applied, and the signal level shown will be dependent on the ground system radiation pattern, which will be subject to some ground reflection lobing at the lower elevation angles flown, $1.3\text{-}2.3^{\circ}$.

The full Andover antenna layout is shown in Fig B15.

B.4.2 BAC 1-11 (400 series)

Description and performance This aircraft, shown in Fig B16, was a typical modern medium-haul commercial transport powered by two tail-mounted engines and an auxiliary power unit. The Elliott/Bendix 2000 autopilot allowed coupled approaches down to an altitude of 200 ft in IMC, but these could be extended down to 50 ft in VMC.

Typical in-circuit airspeed for the BAC 1-11 was 155 kn. Approach airspeed was 135 kn with a landing speed of 125 kn. This aircraft had a climb rate of 2000 ft/min and a turning circle radius of approximately 1700 m (5500 ft) for an applied bank angle of 15°. The maximum approach glidepath angle was approximately 5°.

Navigational aids carried by the BAC 1-11 included VOR, ILS, Tacan, Decca Mk 19, Loran, TANS, ADF and Doppler 72. A radio altimeter and a weather radar were also fitted.

The dual RADRAC installation in the cabin, Figs B17 and B18, housed the DMLS receivers and recording equipment. Fig B17 shows a dual installation of the STL and Plessey FDM receivers.

Antennae The BAC 1-11 was fitted with three DMLS C-band antennae, two of which covered considerably more than 180° in azimuth and were, therefore, nominally referred to as 'omni-directional'. The omni-directional antennae were mounted on the cockpit roof, Fig B17, and on the underside of the tail. The third DMLS antenna was a horn, which was identical to those used on the Andover and Wessex and was mounted in the radome below the weather radar installation. No antenna was mounted specifically to look perpendicular to the aircraft's direction of flight as the tail and above-cockpit omni-directional antennae more than adequately covered this region for orbital measurements. These antennae were commercially available in the UK, the manufacturer producing three models according to the inclination of the surface on which they were to be used. The antenna layout for this aircraft is shown in Fig B20. Provision was made for an RF unit location in the radome and close to the tail antenna. The above-cockpit antenna fed direct to the RADRAC in the cabin via a low loss semi-rigid cable.

The omni-directional above-cockpit antenna radiation pattern in the horizontal plane was measured at 0° elevation angle and 14° elevation angle above the horizontal. The measurements were made in an RAE anechoic chamber at a frequency of 5000 MHz, with the antenna mounted on a ten-wavelength square

ground plane. The radiation patterns obtained are given in Figs B21 and B22, the inset diagrams on these figures referencing the measurements to the antenna position on the aircraft. Flight measurements to confirm the performance of this antenna, when used on the aircraft, yielded the radiation patterns given in Fig B23. The BAC 1-11 flew an 8 n mile radius orbit at an altitude of 10000 ft and a range of 25 n mile from the airfield (3.8^{o} elevation).

Although the relatively large orbit radius required signal level correction for range, it was chosen to allow the use of minimal aircraft bank angle to give direct comparison with Fig B21. Unfortunately, the large radius used makes the measurement dependent on the radiation pattern of the transmitter and the ground contouring. To overcome misleading effects of this nature, the aircraft received signal levels from both approach azimuth and elevation sub-systems were recorded. The two ground sub-systems were sited approximately 2600 m (8600 ft) apart and it is very unlikely that ground contouring would similarly modify both radiation patterns received by the aircraft.

B.4.3 Wessex II

Description and performance The Wessex II helicopter is shown in Fig B24. It was powered by two turbine engines which gave a normal in-circuit airspeed of 90 kn. The maximum climb rate with the aircraft typically loaded was 2000 ft/min up to an altitude of 2000 ft with a required forward airspeed of approximately 10 kn for aircraft control. The Wessex ceiling is normally 13500 ft, but the practical maximum usable altitude was 10000 ft. Navigation equipment carried included Tacan and Decca Mk 8. The autopilot was of limited capability and used solely for aircraft stabilisation.

The helicopter was an ideal vehicle for short range orbital studies. Having the capability of flying in controlled paths at airspeeds down to 20 kn allowed sufficient data to be collected from the DMLS for what would otherwise be prohibitively large cross-tracking rates. The Wessex was particularly useful for very low altitude measurements where noise abatement procedures inhibited the use of the larger fixed wing aircraft. For studies at very low elevation angles, the helicopter became essential when tracked measurements were required (for 1^{o} elevation angle and an altitude of 2000 ft the aircraft range must be 19 n mile).

Antennae The Wessex DMLS horn antenna was mounted on a platform on one side of the aircraft. This starboard mounted antenna was a dual horn identical to that used in the BAC 1-11 radome and the Andover nose and tail positions.

The mounting for this antenna, Fig B25, also contained a Belfast landing lamp to act as a kinetheodolite tracking target. This lamp had two filaments, one of 750 W and one of 500 W. The complete antenna and lamp mounting could be rotated through 90° in azimuth to provide a sideways-looking installation for orbital flight tests.

B.5 Airborne data recording

Both analogue and digital recording systems were used for the collection of flight trials data. The prime purpose of the analogue recording system was to provide real time feedback of data to the flight test observers. In addition, the recordings were valuable in the assessment of discrete events such as multi-path effects. Although the quantity of accuracy data required for MLS assessment made basic digital recording essential, the use of an independent analogue system proved invaluable.

Analogue recording The capacity of the system was limited to that of a single 18-channel ultra-violet recorder. A signal matrix system using hard-wired plug-in circuit boards was provided for selection of the required signal combinations. Table B1 lists the possible parameters for the FDM DMLS and Table B2 lists the parameters for the TDM system trials.

Table B1

FDM DMLS angle receiver analogue recorder parameters

	Plessey receiver	STL receiver
AGC 1 (forward azimuth)	×	×
AGC 2 (elevation)	×	×
AGC 3 (back azimuth/TDM)	×	×
AGC 4 (data)	×	×
Modulation depth 1 (forward azimuth)	×	×
Modulation depth 2 (elevation)	×	×
Modulation depth 3 (TDM)	×	×
Modulation depth 4 (data)	×	×
Deviation 1 (forward azimuth)	×	×
Deviation 2 (elevation)	×	×
Deviation 3 (back azimuth)	×	×
Overall flags (forward azimuth)	×	×
Overall flags (elevation)	×	×
Overall flags (back azimuth)	×	×
Radio altimeter		
Kine synchronisation pulses		
Event mark		

79052

Table B2

TDM DMLS angle receiver analogue recorder parameters

AGC raw time-multiplexed
AGC azimuth (demultiplexed)
AGC elevation (demultiplexed)

Function identity decode (azimuth)
Function identity decode (elevation)

Angle deviation (azimuth)
Angle deviation (elevation)

System flag (azimuth)
System flag (elevation)

Radio altimeter
Kine synchronisation pulses
Event mark

Tracking facility synchronisation on analogue records The pulse signal controlling the synchronous shutter operation of the tracking kinetheodolites was frequency modulated onto a UHF carrier for transmission to the aircraft. The pulse modulation was in the form of a dual-tone serial word giving tracking system frame number. Complete synchronisation was obtained by relating the recorded pulses to the frame numbers of the kinetheodolite synchronisation pulses transmitted. By using the serial word modulation after decoding, a two-level synchronisation pulse was generated for recording purposes, from which frame number synchronisation was readily obtained.

Digital recording[13] Digital recording was necessary for rapidly varying quantities, such as azimuth bearing during an orbit. Also, the shear magnitude of data precluded the use of analogue trace reading as the method of recovery. A digital recorder capable of handling the angle information plus the necessary tracking synchronisation would have been a minimum requirement. It was, however, decided to use a digital recorder capable of handling raw Doppler output, demanded angle and deviation from demanded angle, for approach azimuth, elevation and missed approach azimuth, for each of two receivers, which, for FDM DMLS, could be any combination of two Plessey receivers and one STL receiver. In addition, such quantities as flags, AGC and modulation depth could be converted to digital form and recorded. Range data and kinetheodolite frame number could also be recorded as digital quantities. Full details of the ADR are given in Ref 13. The recording system was based on 12-bit data words and a listing of the application to the FDM system is given in Tables B3 and B4.

Table B3

DMLS airborne digital recorder word listings

Word		No. per frame
1-18 (1A-18A)	DMLS A } see Table B4	1 each
19-36 (1B-18B)	DMLS B }	1 each
37	Range (bits 1-12)	2
38	Range (bits 13-15) and range rate	2
39	Range flags and synchroniser	2
40	Marker word	16
41-42	Kiné frame number	1 each
43-48	Overall flags (6 words), front azimuth, elevation, back azimuth	1 each (3 for each Rx)
49	AGC 1A, front azimuth	1
50	AGC 2A, elevation	1
51	AGC 3A, back azimuth	1
52	AGC 4A, data	1
53	AGC 1B, front azimuth	1
54	AGC 2B, elevation	1
55	AGC 3B, back azimuth	1
56	AGC 4B, data	1
57	Modulation depth 1A, front azimuth	1
58	Modulation depth 2A, elevation	1
59	Modulation depth 3A, back azimuth	1
60	Modulation depth 4A, data	1
61	Modulation depth 1B, front azimuth	1
62	Modulation depth 2B, elevation	1
63	Modulation depth 3B, back azimuth	1
64	Modulation depth 4B, data	1
65	Angle deviation 1A, front azimuth	1
66	Angle deviation 2A, elevation	1
67	Angle deviation 3A, back azimuth	1
68	Angle deviation 1B, front azimuth	1
69	Angle deviation 2B, elevation	1
70	Angle deviation 3B, back azimuth	1
71	Altimeter	1
72	Elevation (RAE/STL)	1
73	Field/frame synchroniser	1
74	Frame count	1
75	Field count/cal/doc data	1
		92

79052

Table B4

Format of words 1-18 (each receiver)

word / bit	1	2	3	4	5	6	7	8	9	10	11	12	13	14	15	16	17	18
1	MSB1 F, Az	MSB13 F, Az Bearing	12	MSB1 B, Az	MSB13 B, Az Bearing	12	MSB1 Elev	13	12	Search (1)	MSB1 Planar	13	MSB1 Planar	13	MSB1 B, Az	11	Aux Az Flag search	MSB1 Data
2	2 Bearing	MSB1 F, Az	13	2 Bearing	MSB1 B, Az	MSB13	2 Bearing	MSB1 Elev	13	Flags Track (MOD depth) (1)	2 F, Az	MSB1 Az Aux	2 Elev	MSB1 El Aux	2 Angle	F, Az Angle process flag	Aux Az Flag track	2
3	3	2 Dev	MSB1 or 7 F, Az	3	2 Dev	MSB1 or 7 B, Az	3	2 Dev	1 or MSB7 Elev	Process quality	3 Angle	2 Bearing	3 Angle	2 Bearing	3	El angle process flag	Aux Az Flag quality	3
4	4	3	2 or 8 angle	4	3	2 or 8 angle	4	3	2 or 8 angle	F, Az L-R (1)(0)	4	3	4	3	4	B, Az angle process flag	Aux Az Flag up / down	4
5	5	4	3 or 9 demand	5	4	3 or 9 demand	5	4	3 or 9 demand	Search (1)	5	4	5	4	5	-	-	5
6	6	5	4 or 10	6	5	4 or 10	6	5	4 or 10	Flags Track (MOD depth)	6	5	6	5	6	1 channel	TDM Sync MSB	6
7	7	6	5 or 11	7	6	5 or 11	7	6	5 or 11	Process quality	7	6	7	6	7	2	TDM Sync LSB	7
8	8	7	6 or 12	8	7	6 or 12	8	7	6 or 12	B, Az L-R (1)(0)	8	7	8	7	8	3 Select	Aux El Flag search	8
9	9	8	Demand ident 1-6(0) or 7-12(1)	9	8	100/200 m^2 (0) (1) ident	9	8	-	Search (1)	9	8	9	8	9	4	Aux El Flag track	9
10	10	9	-	10	9	5Hz source ident INT(0) EX(1)	10	9	-	Flags Track (MOD depth) (1)	10	9	10	9	10	5	Aux El Flag quality	10
11	11	10	-	11	10	MSB Rec ident	11	10	-	Process (0)	11	10	11	10	11	6	Aux El flag L-R	11
12	12	11	-	12	11	LSB	12	11	-	Elev up / down (1)	12	11	12	11	12	7	-	12

Rec ident STL 0,0 - Plessey 0,1 and 1,1 (STL variant) For STL rec words 1-10 only

Appendix B

For the TDM system the original design concept was to use a serial data output. As the prime use of the digital data was recording for data analysis, it was decided that much time could be saved by restructuring the receiver output to look similar to that used in the FDM system. As the relative timing of the TDM azimuth and elevation was not a fixed quantity, the FDM slot A was used for TDM azimuth and the independent FDM slot B for TDM elevation.

B.6 Field test requirements

The field tests of the DMLS FDM and TDM equipments at RAE Bedford were based on the requirements in Attachment B to ICAO State letter SP20/1 - 75/58, dated 3 July 1975. These requirements were in the main generated at the London meeting of ICAO WGA in September 1974. In general, the full set of tests was carried out for the FDM system, as this formed the data base for the system submission to ICAO, while only a sub-set of tests was carried out for the TDM equipment. The following sub-sections describe the tests and the methods proposed for their execution at the time of preparation of the trials programme. The text relates specifically to the FDM system siting.

B.6.1 Flight coverage tests

In all cases the aim was to measure coverage with the minimum of extrapolation. Due to differences in aircraft fit, it was necessary to take into account RF losses due to different antenna types, sites and feeder lengths. Also, due to the limitation on maximum range of the kinetheodolites, coverage flights were not normally tracked and reliance was placed on normal navigation, airfield radar and the DMLS to specify the aircraft position.

Approach azimuth coverage The approach azimuth sub-system radial flights used to determine sub-system coverage are mapped in Fig B26. All coverage radial flight paths were from a range of 32 n mile and at an altitude of 2000 ft or 20000 ft. The radials extend beyond the $\pm 40^{\circ}$ ICAO operational requirements to a hardware system design specification of 60° to either side of the runway centreline. An orbital flight covering $\pm 60^{\circ}$ about the runway centreline at an altitude of 2000 ft and 22 n mile range was also required. This is drawn in Fig B27, which summarises orbital flight paths for approach azimuth tests by including those necessary for accuracy measurements.

Elevation coverage The elevation sub-system was sited so that it could be used for evaluation of both the primary elevation function and the flare role. Radial flight paths used to test the elevation sub-system coverage are set out in Fig B26, previously described for approach azimuth sub-system coverage.

Similarly, the coverage orbital path drawn in Fig B27 was also used to test elevation sub-system coverage.

Another coverage test specifically required for the flare guidance role is outlined by Fig B28. This details an approach path along the runway centre-line, starting at an initial altitude of 800 ft dropping to 150 ft at a range of 610 m (2000 ft) from the runway threshold and continuing at 150 ft above the runway surface.

Missed approach azimuth coverage The radial flight paths required to test the missed approach azimuth coverage are detailed in Fig B29. As the coverage tests at an altitude of 2000 ft were similar to those required to ascertain missed approach azimuth accuracy, they were extended to a range of 10 n mile instead of the 5 n mile specified in LWP/12, to avoid flight duplication. Low level, 500 ft altitude, tests remained at a starting range of 5 n mile.

B.6.2 Flight accuracy tests

Many of the DMLS accuracy flight tests were complemented by ground dynamic and static tests described in section B.6.4 and B.6.5. The flight tests described in the following sections for each DMLS sub-system were in many ways complementary and include performance measurements of the other sub-systems taken at the same time. The mutual co-existence of the DMLS sub-systems were, therefore, demonstrated as far as possible in all of the test flying.

Approach azimuth accuracy Approach azimuth sub-system accuracy orbital flight tests at ranges of 6 n mile and 22 n mile were included with coverage orbital requirements in Fig B27. These paths were continuous throughout 360^{o} in azimuth around the sub-system in order to check for false course information that may be directly radiated or reflected from within the coverage sector.

Accuracy radial paths required are shown in Fig B30. The complete approach azimuth sub-system coverage of $\pm 60^{o}$ about the transmitter boresight was probed at altitudes of 20000 ft and 3000 ft from a range of 20 n mile. In addition, $\pm 15^{o}$ about the runway centreline was studied at an altitude of 2000 ft from 10 n mile range in 5^{o} increments. Finally, as drawn in Fig B31 a series of conventional runway centreline approaches to land were necessary. These were made at a typical glidepath angle of 3^{o}.

Elevation accuracy Where possible, evaluation of the elevation sub-system in its conventional and flare guidance roles was achieved by common flight paths. Many of the elevation test paths required were similar to those

outlined for assessment of the approach azimuth sub-system and were accomplished jointly.

Elevation sub-system radial test paths for accuracy assessment are shown in Fig B32. The radial flight paths were complemented by vertical ascents, shown in Fig B33, from 100 ft at a range of 2.5 n mile from the runway threshold. Although nominally vertical, some forward airspeed was essential to allow aircraft control. For a climb to an altitude of 5000 ft, taking approximately 5 min, a typical required forward airspeed of 10 kn shortened the ground range from 2.5 n mile to approximately 1.5 n mile in still air.

Accuracy on the approach path was tested by conventional and STOL-type approaches shown in Fig B34, where glidepath angles of 3^{o} and 6^{o} were specified.

Finally, a series of orbital flight paths are detailed in Fig B35. These paths were at ranges of 20 n mile and 4 n mile and covered altitudes from 2000 ft to 10000 ft. In addition to information on accuracy, any false signals outside the DMLS elevation sub-system coverage were identified or assessed.

Missed approach azimuth accuracy Missed approach azimuth sub-system accuracy was primarily assessed by flying the radial paths shown in Fig B36, at constant altitudes of 2000 ft and 5000 ft. To supplement these measurements an orbital path, Fig B37, at an altitude of 2000 ft and a range of 7 n mile, was flown to provide a continuous accuracy test throughout the system coverage, or to provide information on any false course signals that might have been generated outside the coverage limits.

B.6.3 Multipath and shadowing tests

In accordance with the recommendations in Attachment B to ICAO State letter SP20/1 - 75/53, the tests were designed to include multipath from existing buildings, from reflecting screens, from aircraft on the ground and in the air, from propeller modulation and from a repeater, and shadowing by other aircraft. On the Bedford airfield, additional shadowing was produced by the humped runway.

An important point to be established in multipath tests was the relative levels of direct and indirect signals. The commutated nature of the Doppler MLS signal meant that AGC measurements on the angle coded signal did not give a true indication of the relative levels. It was, therefore, arranged to transmit an additional C-band CW signal from a dummy element in the approach azimuth array. This single element had the same radiation pattern as that of the azimuth angle array elements, and AGC measurements on this signal could give a true indication

of the direct-to-indirect signal ratio. A similar transmitter could also be used at a point close to the elevation array. This facility, an outcome of using an FDM format, which enabled the level of multipath signal to be determined at the same time as the angle measurements were made, meant that multipath measurements could be made in well authenticated conditions.

Reflecting screens Two reflecting screens were manufactured from basic wooden frames covered by 1 cm (0.5 in) steel mesh, and supported by a tubular steel framework. The screens were 6.4 m (21 ft) square and were towable on small wheels. One of the screens is shown in Fig B38.

Repeater dishes Multipath could be produced by receiving the direct signal at an offset angle, applying a suitable amplification and re-radiating towards the test aircraft. The schematic arrangement is shown in Fig B39. The power gain needed to give equal direct and indirect signals was given by

$$A = \left(\frac{4\pi}{G\lambda} \frac{R_1 R_2}{R_3} \right)^2$$

where R_1, R_2, R_3 are the distances from transmitter to repeater, repeater to receiver and transmitter to receiver respectively, G is the gain of the transmitting/receiving antennae and λ the wavelength. This value neglects any differences in ground reflection effects over the two paths, but it does give a reasonable idea of the amplification needed. A photograph of the repeater dishes is shown in Fig B40. The actual multipath levels achieved could be measured by using the C-band CW AGC.

The numbering of tests follows that of Attachment B to ICAO State letter SP20/1-75/53, dated 3 July 1975. The tests are shown in tabular form in Table B5.

B.6.4 Ground dynamic tests

Ground dynamic tests were a useful adjunct to the ground static and the flight tests, particularly for investigating the level of multipath signals during flare and roll-out.

The ground static tests described in section B.6.5 gave a measure of any bias errors at the ground test positions defined in Attachment B to ICAO State letter SP20/1-75/53, with no externally generated multipath signals present. However, measurements at these discrete test positions did not give the full story, since the presence of any multipath signal was likely to give a spatially

Table B5

Multipath and shadowing tests

Test No.	Description	Method	Position of interfering source	Remarks
1	Approach azimuth multipath at roll out	a) Screens b) Repeater	76 m (250 ft), 152 m (500 ft) North of centreline In front of Tx	CW data Tx to give multipath level
2	Approach azimuth multipath at threshold	a) Screens b) Repeater	76 m (250 ft), 152 m (500 ft) North of centreline In front of Tx	CW data Tx to give multipath level
3	Approach azimuth multipath at decision height	a) Screens b) Repeater	76 m (250 ft), 150 m (500 ft) North of centreline In front of Tx	CW data Tx to give multipath level
4	Elevation multipath at threshold	Repeater	Right 15 m (50 ft) Forward 61 m (200 ft)	False threshold 305 m (1000 ft) forward of Tx
5	Elevation multipath on glideslope	Repeater	Right 15 m (50 ft) Forward 61 m (200 ft)	False threshold 305 m (1000 ft) forward to Tx
6	Flare multipath at threshold	Repeater	Right 45.75 m (150 ft) Forward 183 m (600 ft)	True runway threshold used
7	Flare multipath in flare region	Repeater	Right 47.75 m (150 ft) Forward 183 m (600 ft)	True runway threshold used
8	Approach azimuth shadowing at threshold	Taxying Comet IV	Turn off in front of forward azimuth Tx	Test aircraft 1-2 n mile from threshold at turn off
9	Elevation shadowing at threshold	Screens	Aircraft 'hold' position to south of runway to shadow false threshold	No suitable taxyway to use aircraft
10	Flare shadowing at threshold	Screens	Aircraft 'hold' position to shadow true threshold	No suitable taxyway to use aircraft
11	Aircraft multipath reflection on approach azimuth	Parked Comet IV	North of test runway near 27 threshold	CW data transmitter to give multipath level
12	Over flight of approach azimuth transmitter	Comet IV on take-off	Over Tx	Test aircraft 1-2 n mile from threshold at overfly
13	Transmission through propeller	HS 748 as interfering aircraft	On subsidiary runway for approach azimuth, on taxyway north of test runway for elevation	Test van with horn aerial
14	Reflection from propeller	HS 748 as interfering aircraft	On subsidiary runway for approach azimuth on taxyway north of test runway for elevation	Test van with omni-aerial

varying bias error, which was best detected by a dynamic test. The test needed to be made slowly enough to be considered quasi-static, *ie* errors should not be reduced by any motion averaging, which could be investigated separately. In order to relate any angle bias errors to multipath levels, it was necessary to estimate the latter, and this was done by transmitting a separate C-band CW signal from the data transmitter. AGC recordings of this signal during the dynamic tests then gave a measure of the multipath level.

Approach azimuth The ground dynamic tests of the approach azimuth guidance signals consisted of test vehicle runs along the runway centreline at speeds of approximately 20 n mile/h. The signals were received via a horn antenna at heights varying between 1 m (3 ft) and 10 m (33 ft) above runway surfaces. The true angular position of the horn antenna was determined by following the centreline of the runway as closely as possible (estimated to be better than 0.3 m (1 ft) displacement), or by tracking and recording the horn position, using the kinetheodolites.

The normal airfield environment was investigated by recordings taken with no additional reflectors or repeaters installed. Reflecting screens or repeater sources were then installed and the measurements repeated, for different angular settings of screen or repeater, different repeater amplifications and different antenna heights. These measurements were made in conjunction with the flight multipath tests in order to determine the optimum settings needed to produce the maximum multipath effects in the required regions, *eg* decision height, threshold, flare region and roll out. The multipath levels were measured independently during the flight tests, however, and were not dependent on the ground measurements.

Missed approach azimuth The vehicle runs along the runway centreline were repeated for the missed approach azimuth system, but purely for the normal airfield environment (*ie* no additional reflector or repeater). The transmitter format could be varied, however, and the effect of differing numbers of main array and reference array elements investigated.

B.6.5 MLS ground static tests

Scope As for flight and ground dynamic tests, ground static test procedures were extracted from Attachment B to ICAO State letter SP20/1-75/53, dated 3 July 1975. Apart from recommending specific test points and measurements, it was also required that test point positions were cross-calibrated with the range tracking system employed. To comply with this request, test points

were laid down according to SP20/1 recommendations and then surveyed by the kinetheodolite system.

In addition to ensuring accuracy and consistency between flight and ground measurements, such a survey provided confidence in the accuracy of the range tracking system. Knowing that certain positions such as the approach azimuth and missed approach azimuth array centres were well defined in relation to the runway centreline allowed an immediate range instrumentation check.

For example, the approach azimuth and missed approach azimuth array centres were positioned to be on the extension of the runway centreline. Cartesian coordinates of the approach azimuth with respect to the missed approach azimuth sub-system were measured by the kinetheodolite survey as 3426.28 m (11241.10 ft), 0.071 m (0.22 ft), 6.55 m (21.50 ft) in X, Y and Z respectively; where the X axis defined the direction of the runway centreline. The difference of 0.071 m (0.22 ft) in the Y coordinate was within the tolerances accepted for array siting. In practice, this error resulted in 0.001^{o} misalignment between the DMLS array centres and the runway centreline and this check strongly supported claims made for the kinetheodolite system surveying accuracy.

To support elevation, approach azimuth and missed approach azimuth static test points, a selection of fixed airfield reference points, Fig B42 were also surveyed by the kinetheodolite system. These were used as calibration/check reference objects for any further surveying measurements that were made, thus continuing the consistency of results taken through all measurements.

Where test points were required on grassed areas, a concrete slab was let into the turf to identify the position and its fixed height level without fear that this might be disturbed by airfield services such as grass cutting.

Approach azimuth static tests The layout of the approach azimuth sub-system test points is shown in Fig B43. The points catered for height probes of the DMLS radiation at both ends of the runway and for measurements out to the ICAO coverage requirement of 40^{o} to either side of the array boresight.

The measurements necessary at each of the test points are summarised in Table B6 and the exact test point locations are given by the kinetheodolite survey in Table B7. It should be noted that the monitor test point, F9, chosen for convenience close to the elevation sub-system, was well below line-of-sight from the array due to the runway hump. This is emphasised in Fig B44, which gives approach azimuth line-of-sight minimum height above ground level for the runway length.

Missed approach azimuth static tests Missed approach azimuth sub-system static test point layout is shown in Fig B45. They were very similar in principle to those used for approach azimuth assessment, but covered only 20^{o} to either side of the runway centreline. Required measurements are summarised in Table B8 and the test point positions measured by kinetheodolite survey are listed in Table B9. Apart from test point B6, line-of-sight from the missed approach azimuth array centre was maintained at each point to ground level.

Elevation static tests The DMLS elevation sub-system was sited on the Bedford airfield so that both conventional elevation performance requirements and those for flare guidance could be evaluated with a single transmitter. The test point layout shown in Fig B46 combined conventional approach test points and those required specifically for flare guidance. It should be noted that test point E6, at an azimuth angle of -45^{o} with respect to the array boresight, was outside the nominal elevation sub-system coverage of $\pm 40^{o}$ due to the sub-system displacement of 152 m (500 ft) from the runway centreline. Table B10 lists the measurements required at each of the test points and Table B11 gives the kine-theodolite surveyed test point locations.

Monitoring and stability tests Long-term monitoring tests were to be made over a period of at least 2 weeks during which the output from an airborne receiver located at a common point was to be analysed. This was to be compared with the outputs of any field monitors incorporated in the ground equipments.

Table B6

Approach azimuth static test measurements

Test point	Mast height (ft)		Height increment (ft)	Test Duration (s)	Remarks
	Maximum	Minimum			
F1 F2	20	5	5	>30	
F4	21	5	2	>30	
F5	30	5	2	>30	
F6 F7 F8	70	5	2	>30	
F9	20		-	{ 5 min 24 h }	Stability tests
F3 F - 40° thro' F + 40°	20		-	>30	

Note: Values in this and the following tables are all given in feet as this was the unit used in kiné programmes and in the ICAO test requirement document.

Table B7

Approach azimuth test point positions

(Surveyed by kinetheodolite pair)

Test point	X (ft)	Y (ft)	Z (ft)	RGND (ft)	: (deg)	- (deg)
F1	1001.46	-0.58	0.21	1001.46	-0.0329	0.0117
F2	2004.32	-0.30	-4.82	2004.32	-0.0084	-0.1371
F3	2518.80	0.05	-7.36	2518.80	0.0010	-0.1673
F4	8734.42	-0.41	-16.29	8734.42	-0.0027	-0.1068
F5						
F6	10738.85	-0.09	-23.16	10738.85	-0.0005	-0.1235
F7	10739.10	-75.16	-23.40	10739.36	-0.4010	-0.1248
F8	10739.24	74.88	-23.71	10739.50	0.3995	-0.1265
F9	8578.89	466.14	-16.02	8591.54	3.1101	-0.1068
F - 40°	2631.59	-2206.66	-1.21	3434.33	-39.9807	-0.0201
F - 32°	2601.24	-1623.45	-0.15	3066.27	-31.9685	-0.0027
F - 24°	2575.85	-1146.11	-2.28	2819.32	-23.9863	-0.0462
F - 18°	2573.29	-823.22	-5.31	2701.76	-17.7399	-0.1125
F - 12°	2551.42	-537.15	-6.57	2607.35	-11.8887	-0.1443
F - 8°	2537.69	-354.77	-6.92	2562.37	-7.9583	-0.1546
F - 6°	2530.14	-264.33	-6.92	2543.91	-5.9641	-0.1557
F - 4°	2525.55	-176.95	-6.85	2531.74	-4.0077	-0.1549
F - 2°	2522.27	-87.53	-7.01	2523.79	-1.9874	-0.1590
F - 1°	2521.90	-43.51	-7.20	2522.28	-0.9883	-0.1634
F + 1°	2516.68	44.42	-7.70	2517.07	1.0111	-0.1752
F + 2°	2514.50	88.32	-7.86	2516.05	2.0115	-0.1789
F + 4°	2507.42	176.14	-8.32	2513.60	4.0182	-0.1895
F + 6°	2503.16	262.36	-8.82	2516.87	5.9833	-0.2007
F + 8°	2497.88	349.81	-9.33	2522.25	7.9719	-0.2118
F + 12°	2463.34	523.42	-9.82	2518.33	11.9959	-0.2233
F + 18°	2475.00	804.24	-9.03	2602.39	18.0012	-0.1987
*F + 24°	2462.56	1094.52	-7.70	2694.84	23.9634	-0.1637
*F + 32°	2434.04	1545.88	-6.70	2883.45	32.4200	-0.1331
*F + 40°	1817.66	1518.39	-3.70	2368.42	39.8738	-0.0895
R_1	256.11	-0.47	-2.59	256.11	-0.1040	-0.5783
R_2	10738.85	-0.09	-23.16	10738.85	-0.0005	-0.1235
R_4	286.28	-0.15	-2.53	286.28	-0.0290	-0.5053
R_5	10764.46	-0.36	-22.99	10764.46	-0.0019	-0.1223
R_6	9688.30	646.09	18.77	9709.82	3.8152	0.1107
R_7	3496.32	-1927.57	35.60	3992.46	-28.8685	0.5108
R_8	933.72	895.59	38.20	1293.80	43.8057	1.6910

* Not seen by kinetheodolite pair; surveyed figures given

Table B8

Missed approach azimuth static test measurements

Test point	Mast height (ft)		Height increment (ft)	Test duration (s)	Remarks
	Maximum	Minimum			
B1 B2	20	5	5	30	
B4	21	5	2	30	
B5 B6 B7 B8	70	5	2	30	
B9	20		-	{5 min 24 h}	Stability tests
B3 B - 20° thro' B + 20°	20		-	30	

79052

Table B.

Missed approach azimuth test point positions

(Surveyed by kinetheodolite pair)

Test point	X (ft)	Y (ft)	Z (ft)	RGND (ft)	: (deg)	- (deg)
B1	-1003.82	-0.16	0.08	1003.82	-0.0091	0.0046
B2	-2007.09	-0.08	3.53	2007.09	-0.0023	0.1008
B3	-2506.69	-0.18	5.22	2506.69	-0.0041	0.1193
B4	-8950.76	-0.30	15.08	8950.76	-0.0019	0.0965
B5	-9953.21	-0.22	20.59	9953.21	-0.0013	0.1185
B6	-10954.83	0.08	18.98	10954.83	0.0004	0.0993
B7	-9952.90	-75.22	21.19	9953.18	-0.4330	0.1220
B8	-9952.55	75.22	20.10	9952.83	0.4330	0.1157
B9	-2662.22	466.36	5.49	2702.75	9.9361	0.1164
*B - 20°	-1898.54	-693.95	1.00	2021.39	-20.0783	0.0283
*B - 16°	-2195.13	-632.66	3.00	2284.48	-16.0775	0.0752
B - 12°	-2290.92	-486.76	4.42	2342.06	-11.9955	0.1081
B - 8°	-2371.56	-333.03	5.11	2394.82	-7.9936	0.1223
B - 6°	-2408.77	-253.19	4.59	2422.03	-6.0030	0.1085
B - 4°	-2445.19	-171.00	4.58	2451.16	-4.0040	0.1071
B - 2°	-2475.47	-86.03	4.69	2476.96	-1.9904	0.1085
B - 1°						
B + 1°	-2516.11	43.63	5.02	2516.48	0.9934	0.1143
B + 2°	-2534.29	88.74	4.86	2535.84	2.0054	0.1098
B + 4°	-2556.16	178.84	4.70	2562.40	4.0021	0.1051
B + 6°	-2594.89	272.76	5.14	2609.18	6.0006	0.1129
B + 8°	-2628.92	369.54	5.56	2654.76	8.0014	0.1200
B + 12°	-2697.04	573.53	5.90	2757.34	12.0052	0.1226
B + 16°	-2793.45	801.09	4.78	2906.04	16.0016	0.0942
*B + 20°	-2774.74	1010.54	5.00	2953.03	20.0113	0.0970
R_1	-10985.00	-0.24	18.92	10985.00	-0.0013	0.0987
R_2	-502.26	0.14	-1.65	502.26	0.0154	-0.1882
R_4	-10954.83	0.08	18.98	10954.83	0.0004	0.0993
R_5	-476.65	-0.13	-1.48	476.65	-0.0156	-0.1779
R_6	-1552.81	646.31	40.27	1681.94	22.5981	1.3715
R_7	-7744.79	-1927.34	57.10	7981.00	-13.9746	0.4099
R_8	-10307.39	895.81	59.70	10346.24	4.9671	0.3306
R_9	-1434.96	605.82	32.70	1557.59	22.8890	1.2027
R_{10}	-1415.17	721.36	15.36	1588.41	27.0096	0.5540

* Not seen by kinetheodolite pair; surveyed figures given

79052

Table B10

Elevation static test point measurements

Test point	Mast height (ft)		Height increment (ft)	Test duration (s)	Function
	Maximum	Minimum			
E1	70	3	1	30	EL1
E2					EL1
E3					EL1/EL2
E4					EL1
E5					EL1
E6					EL2
E7					EL2
E8					EL2
E9					EL1/EL2
E10					EL2
E11					EL2
E12					EL2
E13					EL2

Table B11

Elevation test point positions

(Surveyed by kinetheodolite pair)

Test point	X (ft)	Y (ft)	Z (ft)	RGND (ft)	ϕ (deg)	θ (deg)
E1*	500.00	0	-15.72	500.00	0	-1.800
E2	1002.06	1.76	-17.39	1002.06	0.100	-0.994
E3	1634.13	0.76	-19.02	1634.06	0.026	-0.667
E4	777.50	-649.53	-15.43	1013.11	-39.875	-0.872
E5	555.59	461.67	-17.61	722.37	39.725	-1.396
E6	504.07	-500.64	-14.34	710.44	-44.804	-1.156
E7	1005.17	-500.61	-16.01	1122.93	-26.475	-0.817
E8	1632.76	-500.57	-18.15	1707.77	-17.044	-0.609
E9	2134.32	-500.27	-19.88	2192.17	-13.192	-0.519
E10	2616.63	-501.14	-22.47	2664.19	-10.842	-0.483
E11	1633.01	-375.05	-18.90	1675.52	-12.935	-0.646
E12	1633.55	-249.61	-18.69	1652.51	-8.688	-0.648
E13	1633.90	-124.46	-19.01	1638.63	-4.356	-0.664
R_2	2134.69	-500.25	-20.04	2192.52	-13.189	-0.524
R_5	2159.93	-500.54	-19.71	2217.17	-13.047	-0.509
R_6	1083.77	145.91	22.05	1093.55	7.667	1.155
R_9	1201.63	105.42	13.94	1206.24	5.014	0.662
R_{10}	1221.41	220.96	-2.87	1241.23	10.254	-0.132

Notes: * 1) Not seen by kinetheodolite OP1; surveyed figures given

2) MLS coordinates used with elevation array centre as origin

79052

A STAN 3B glide path
B Doppler elevation (FDM)
C Doppler azimuth (FDM)
D STAN 37 localizer
E Kinetheodolite
F Doppler back azimuth (FDM)
G Colocated Doppler azimuth and elevation (TDM)
H Doppler azimuth (TDM)
J Alternate sites
Doppler elevation (TDM)

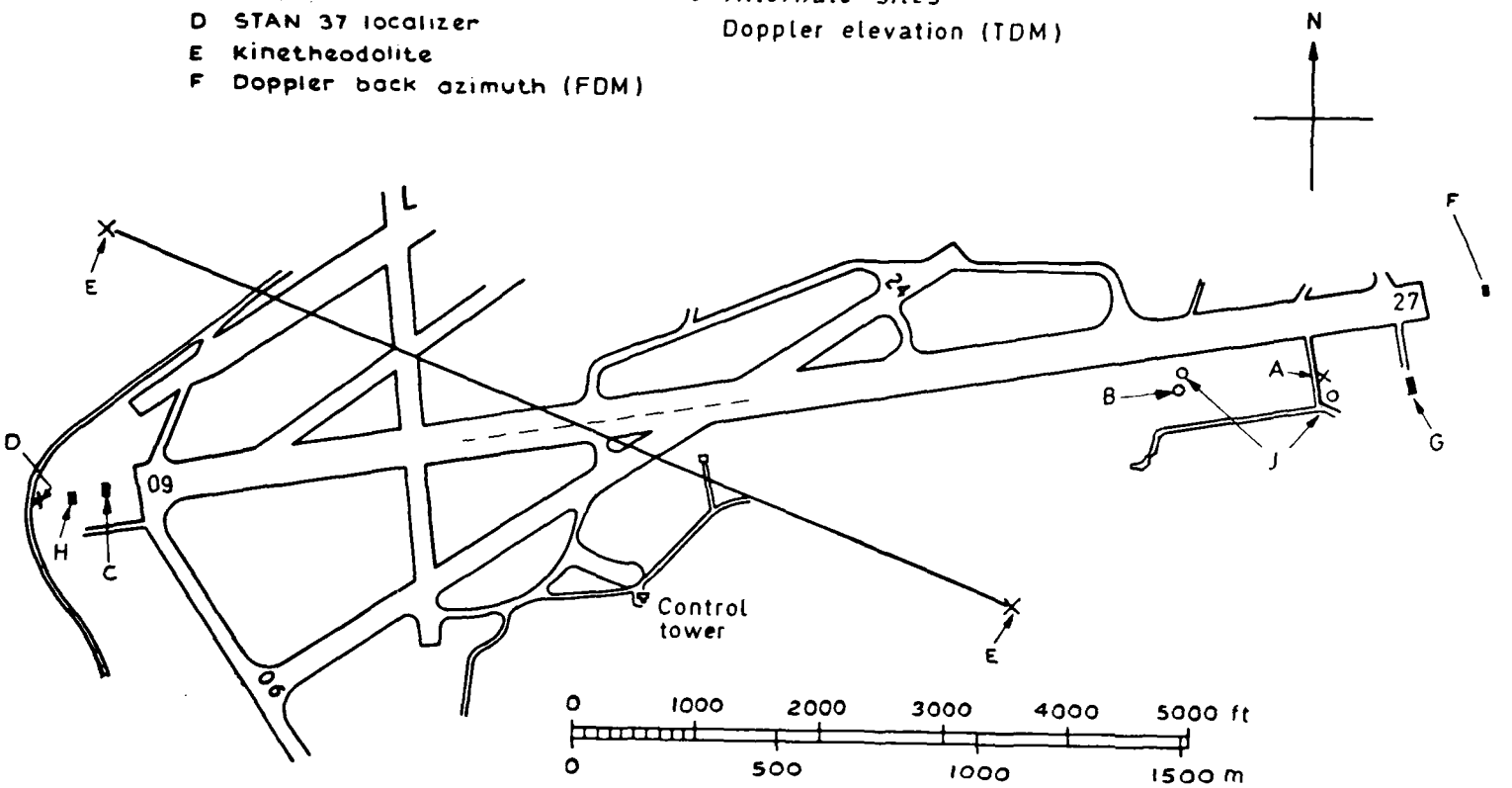

Fig B1 Kinetheodolite position — Bedford airfield

Fig B1

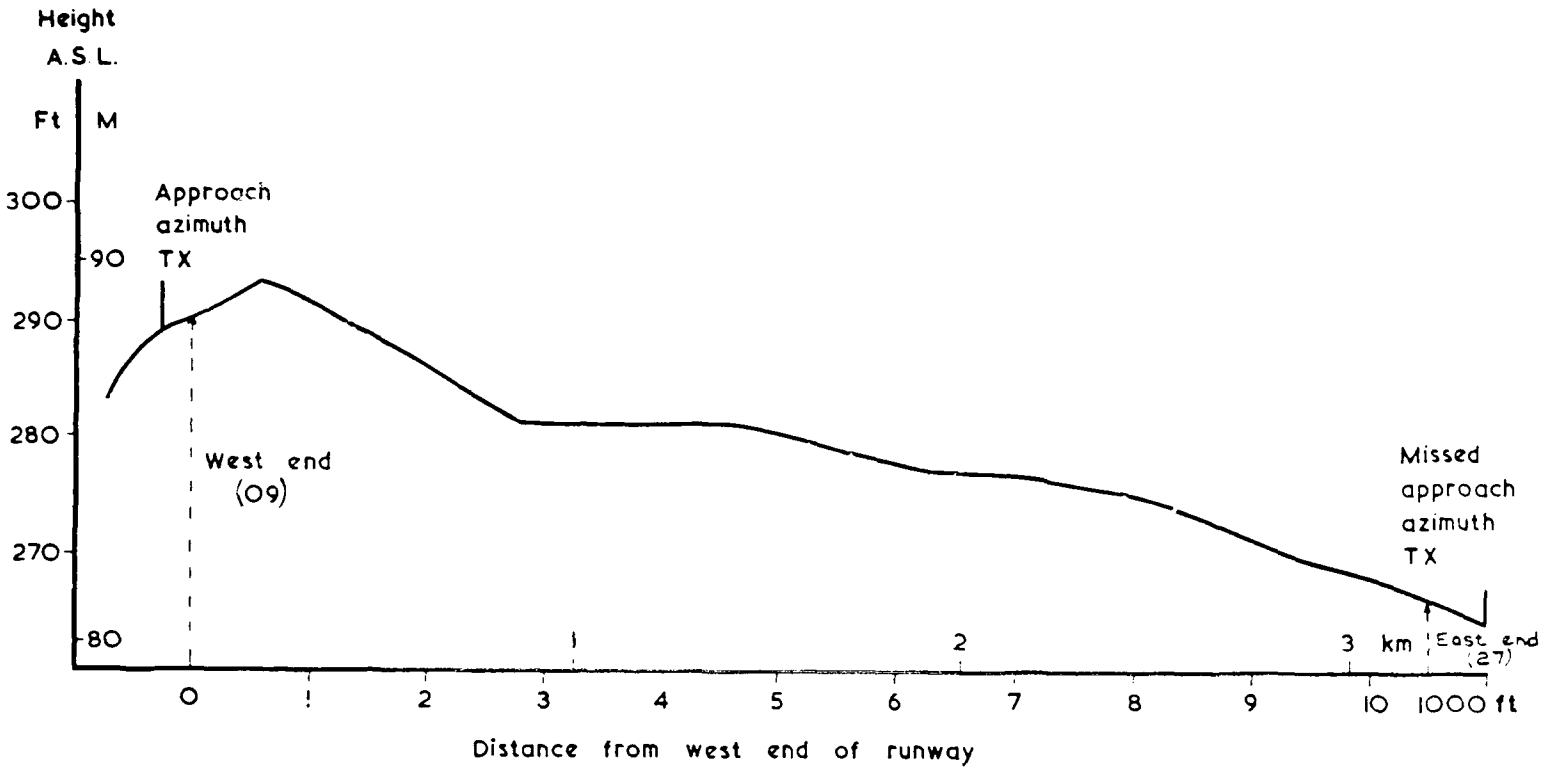

Fig B2 Test runway profile

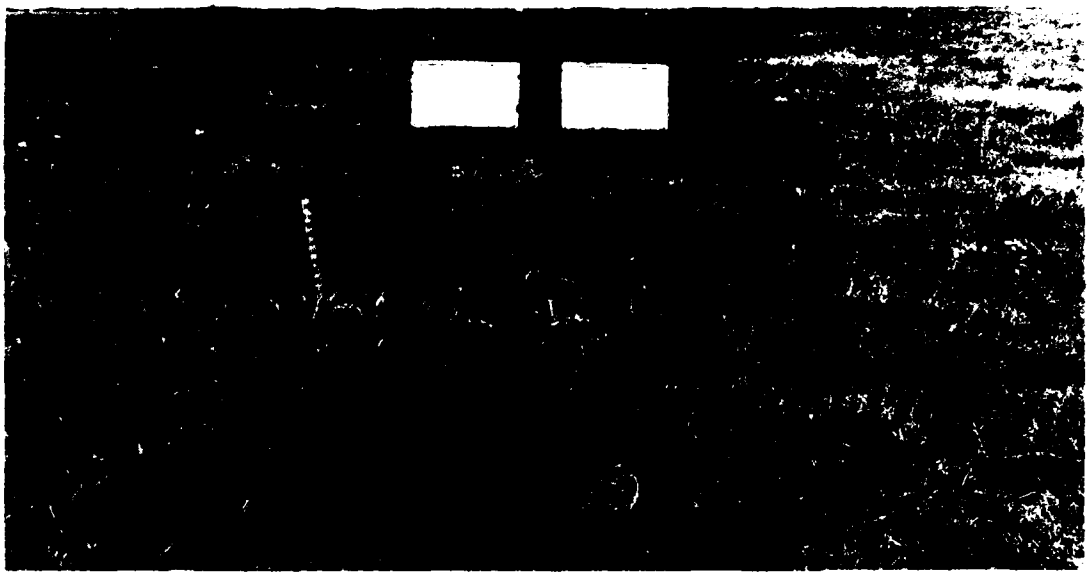

Fig B3 View from approach azimuth along runway

Fig B4

TR 79052 C15536

Fig B4 Kinetheodolite installation

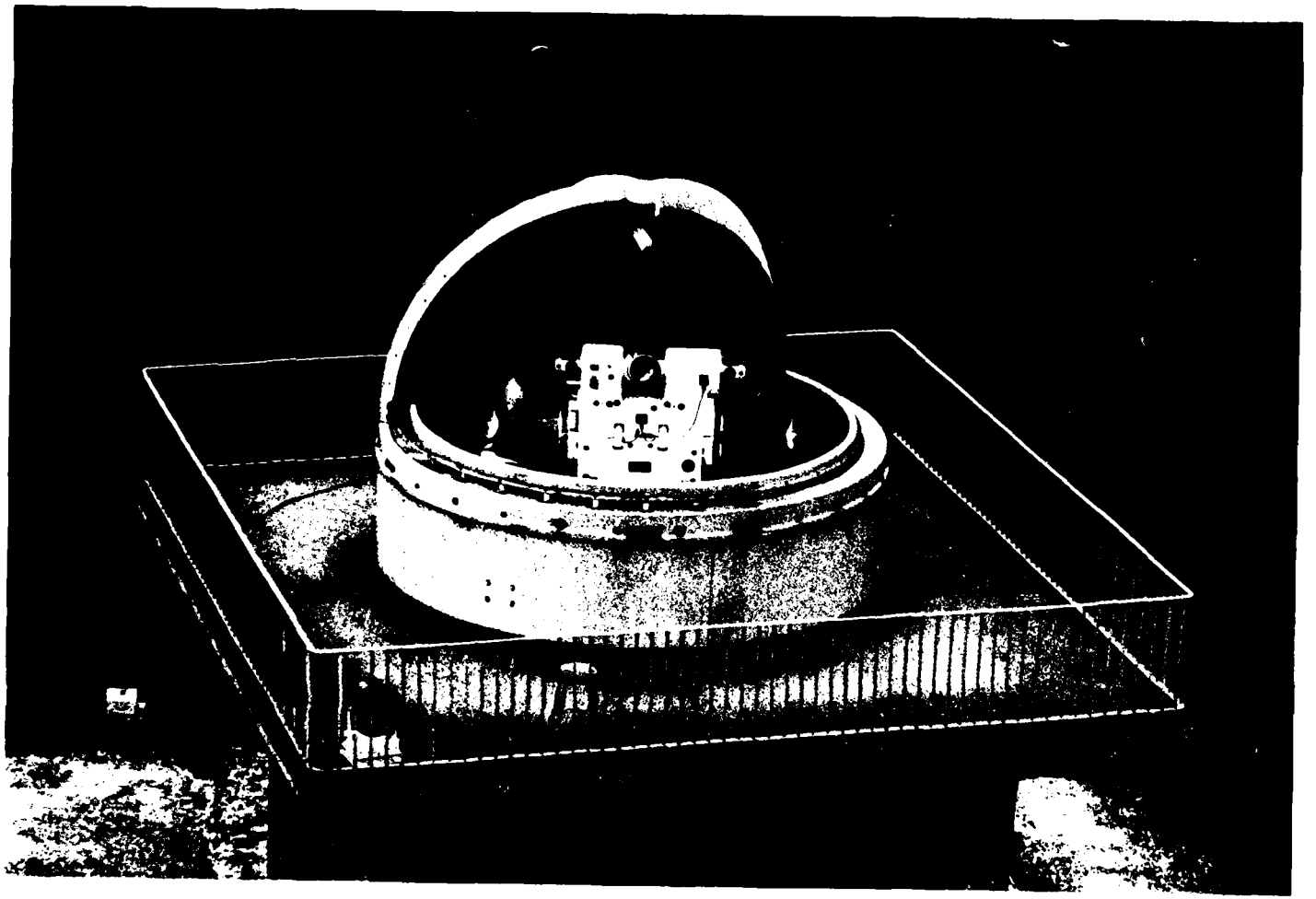

Fig B5 Kinetheodolite camera in operation

Fig B5

Fig B6

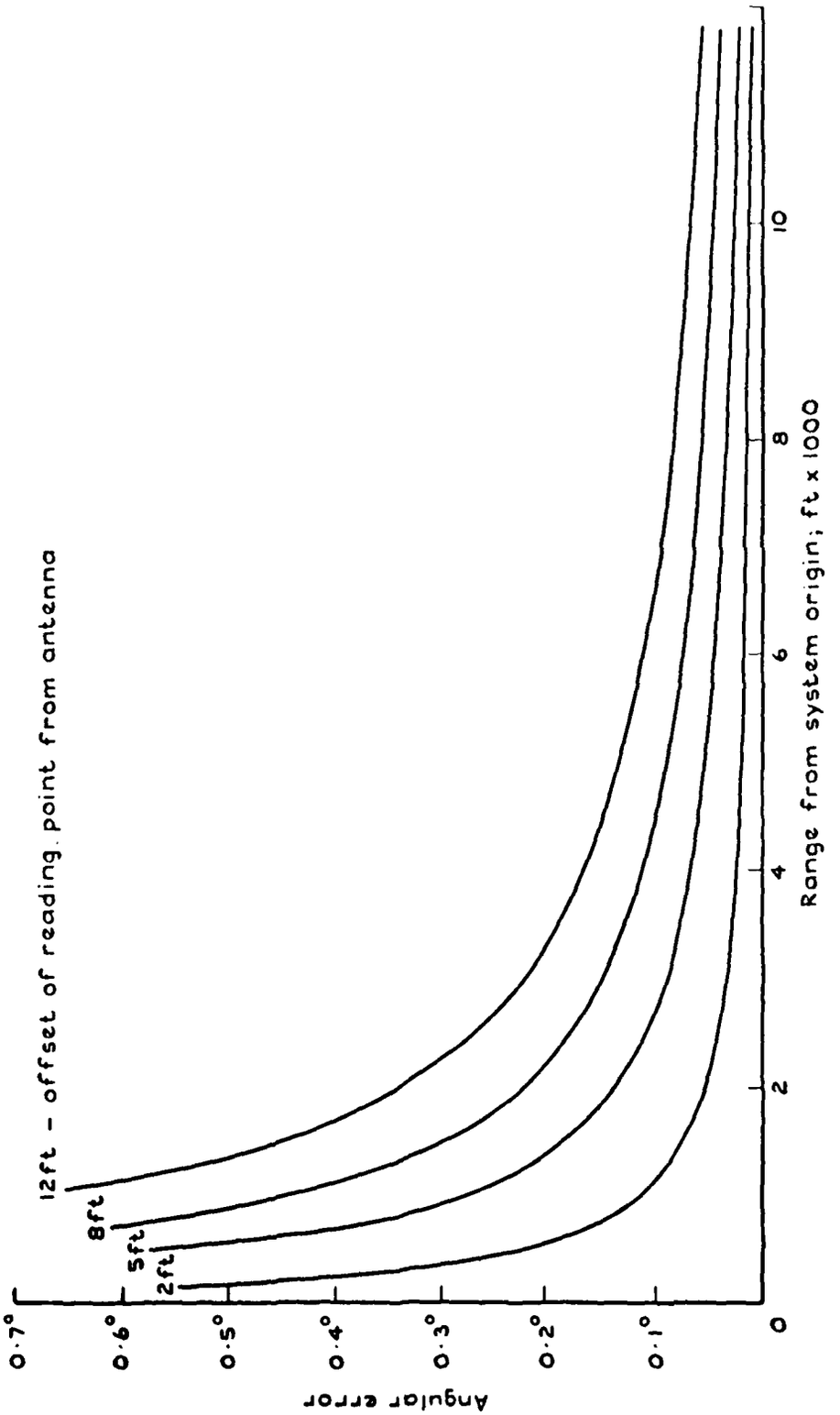

Fig B6 Errors due to displacement of aircraft reading point

TR 79062

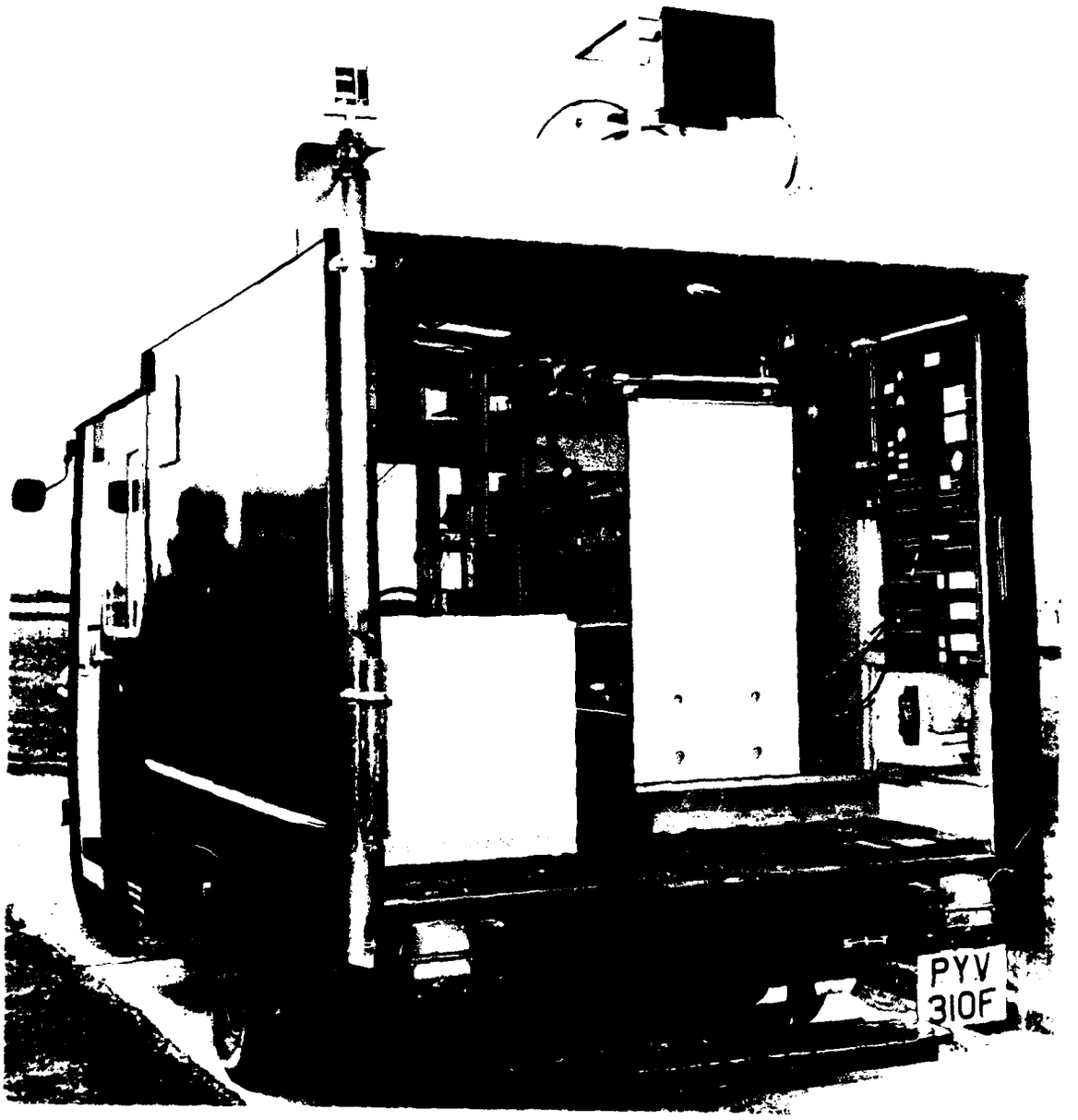

TR 79062 C15538

Fig B7 Test van external view

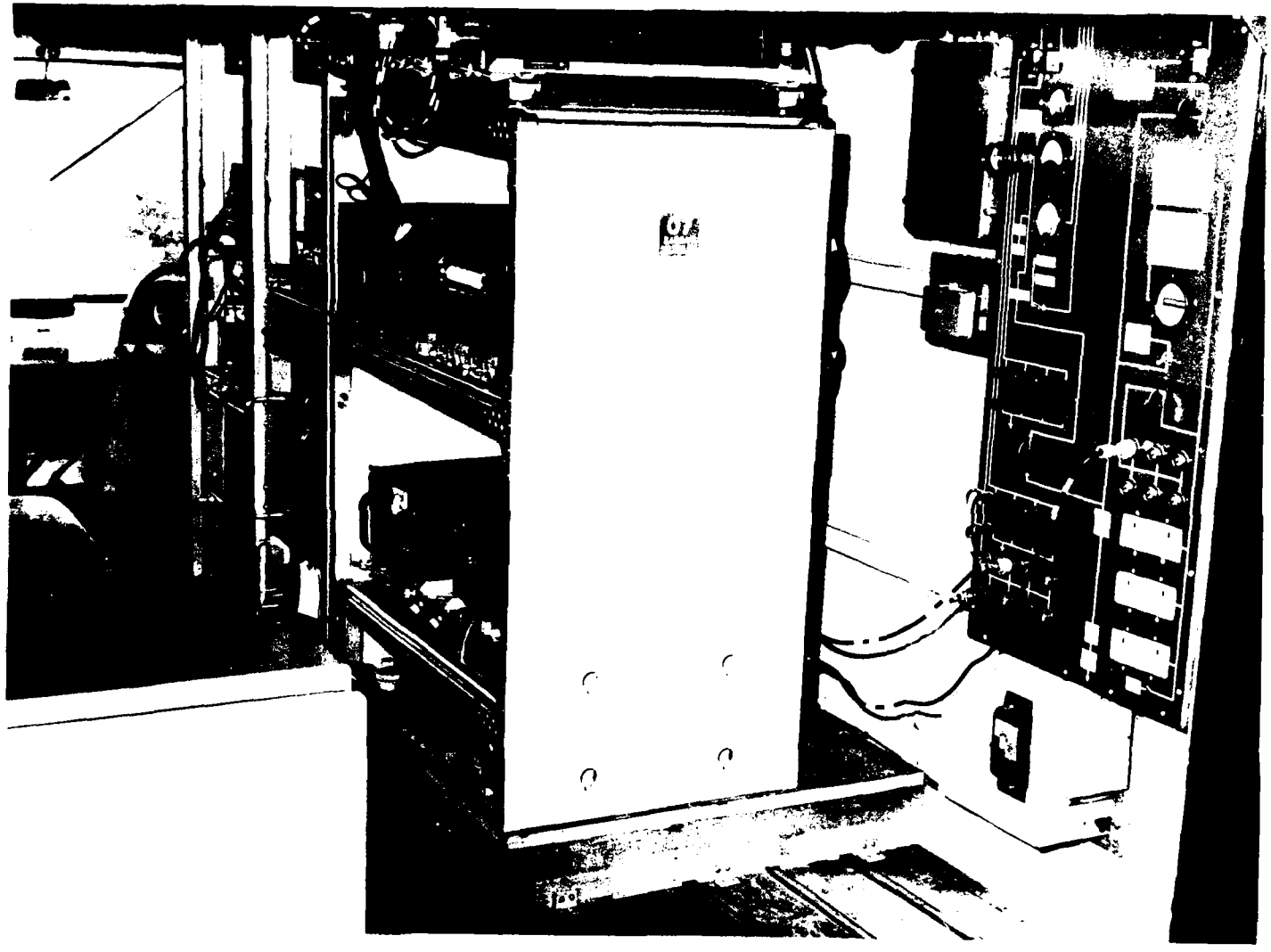

Fig B8 Test van internal view

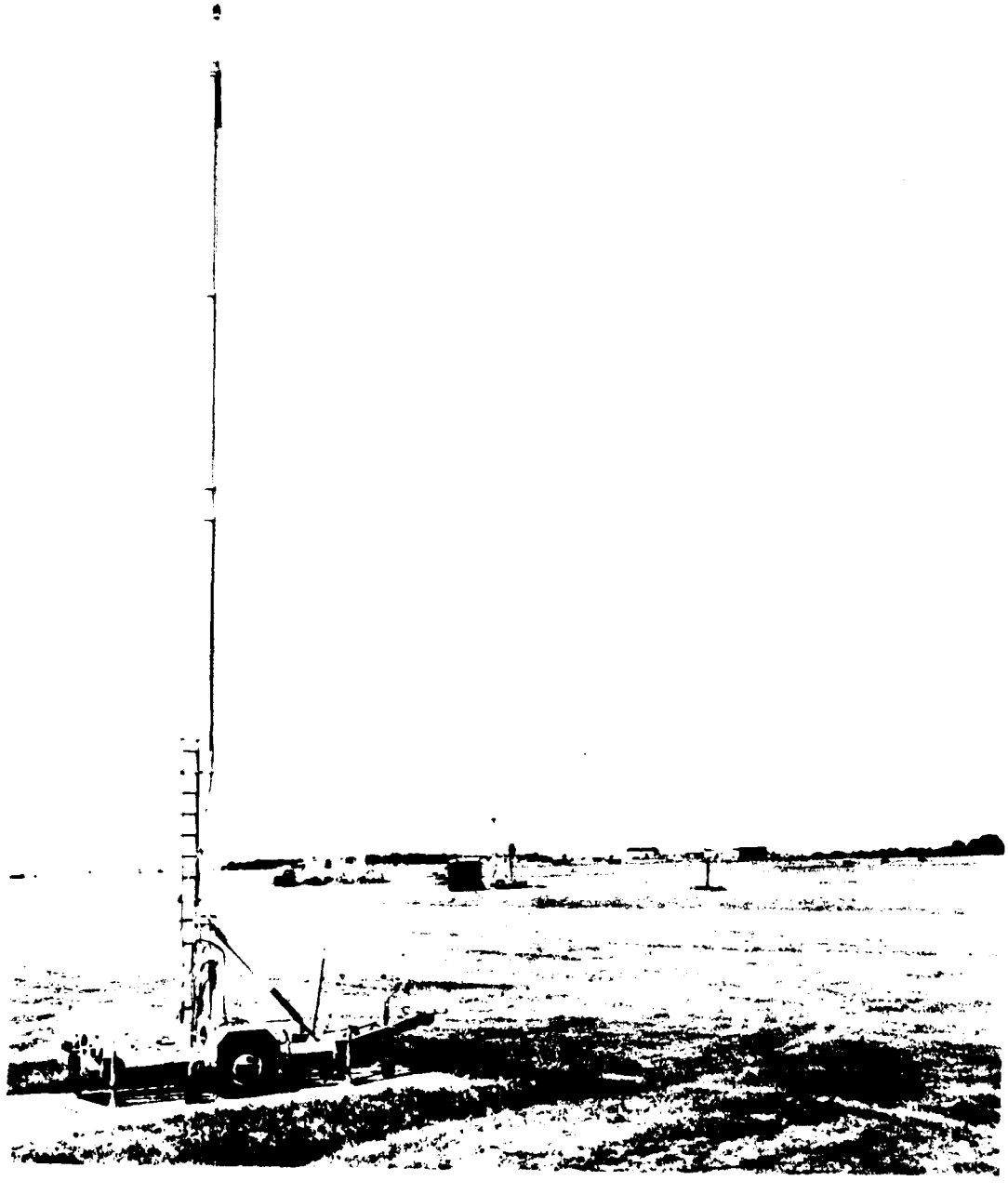

TR 79052 C15540

Fig B9 22m (70ft) telescopic mast

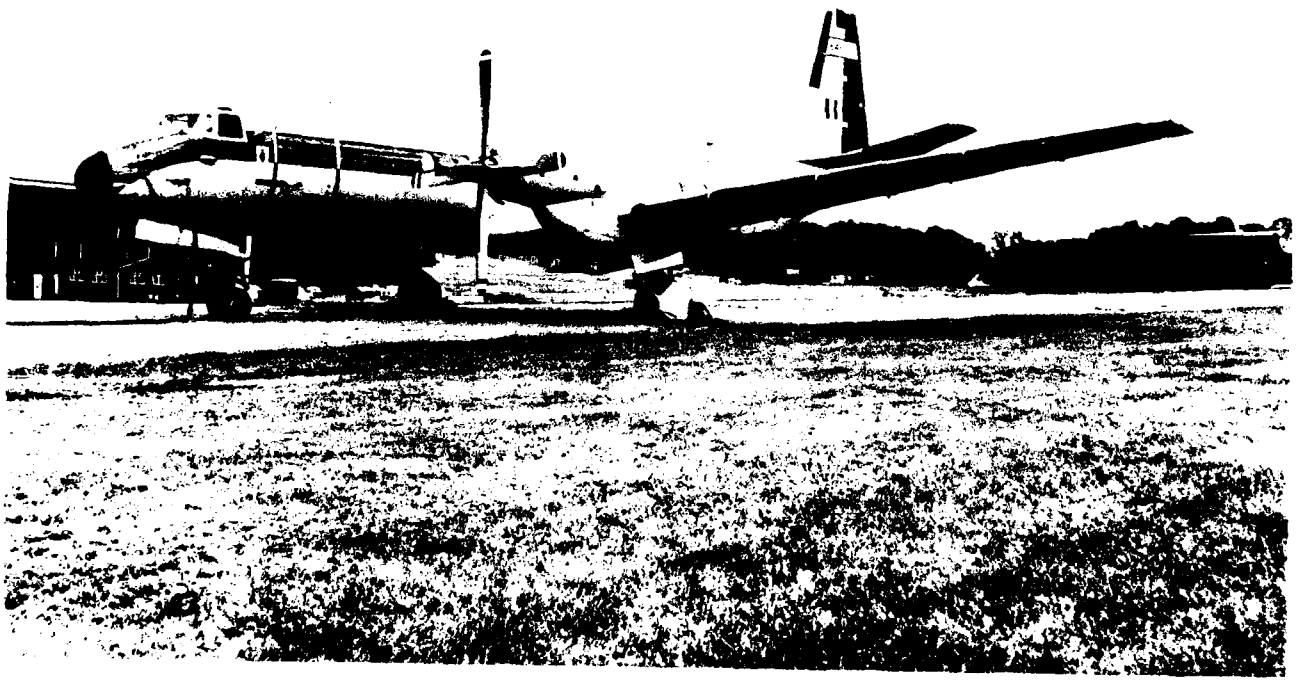

Fig B10 HS Andover

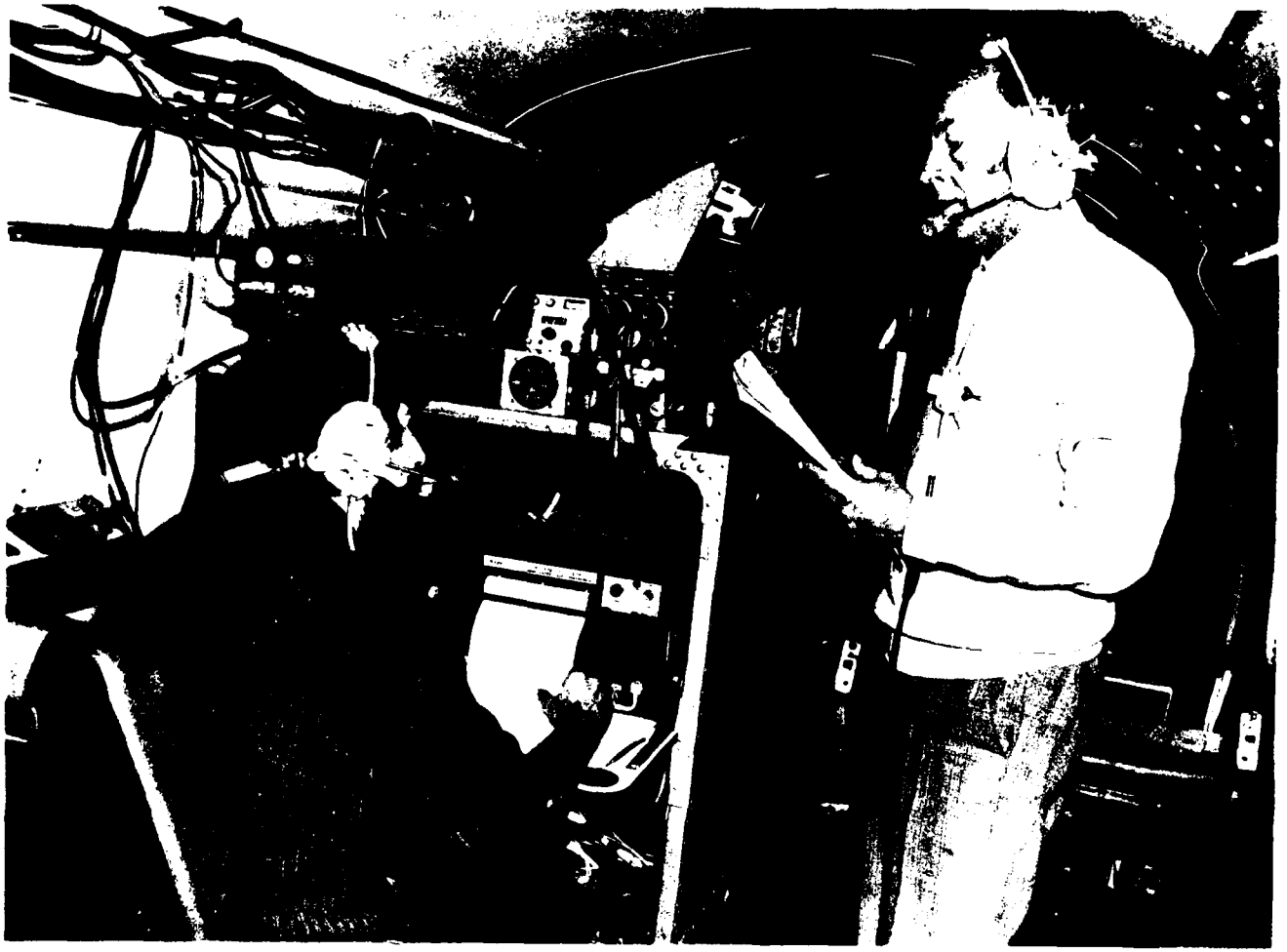

Fig B11 Receiver test rack in Andover

Fig B11

Fig B12

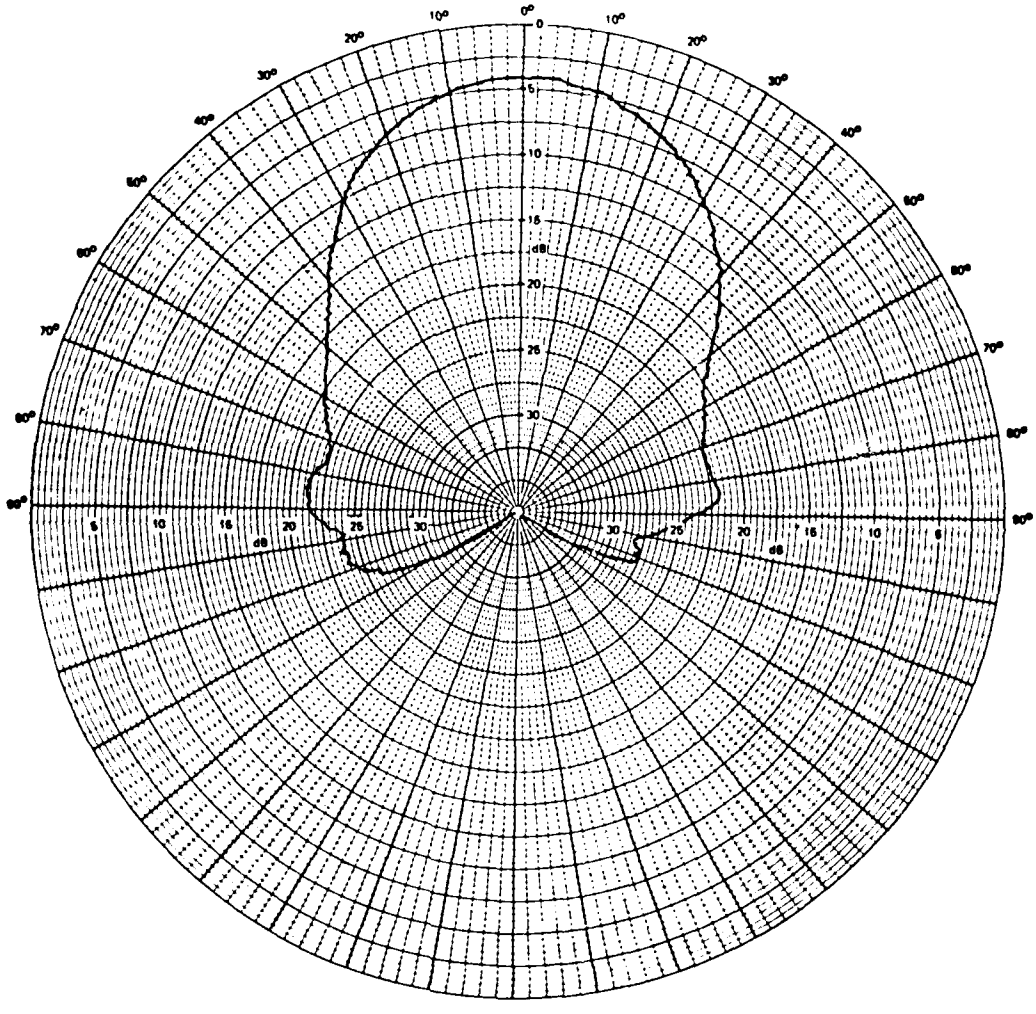

Fig B12 Elevation radiation pattern small horn in Andover nose cone

TR 79062

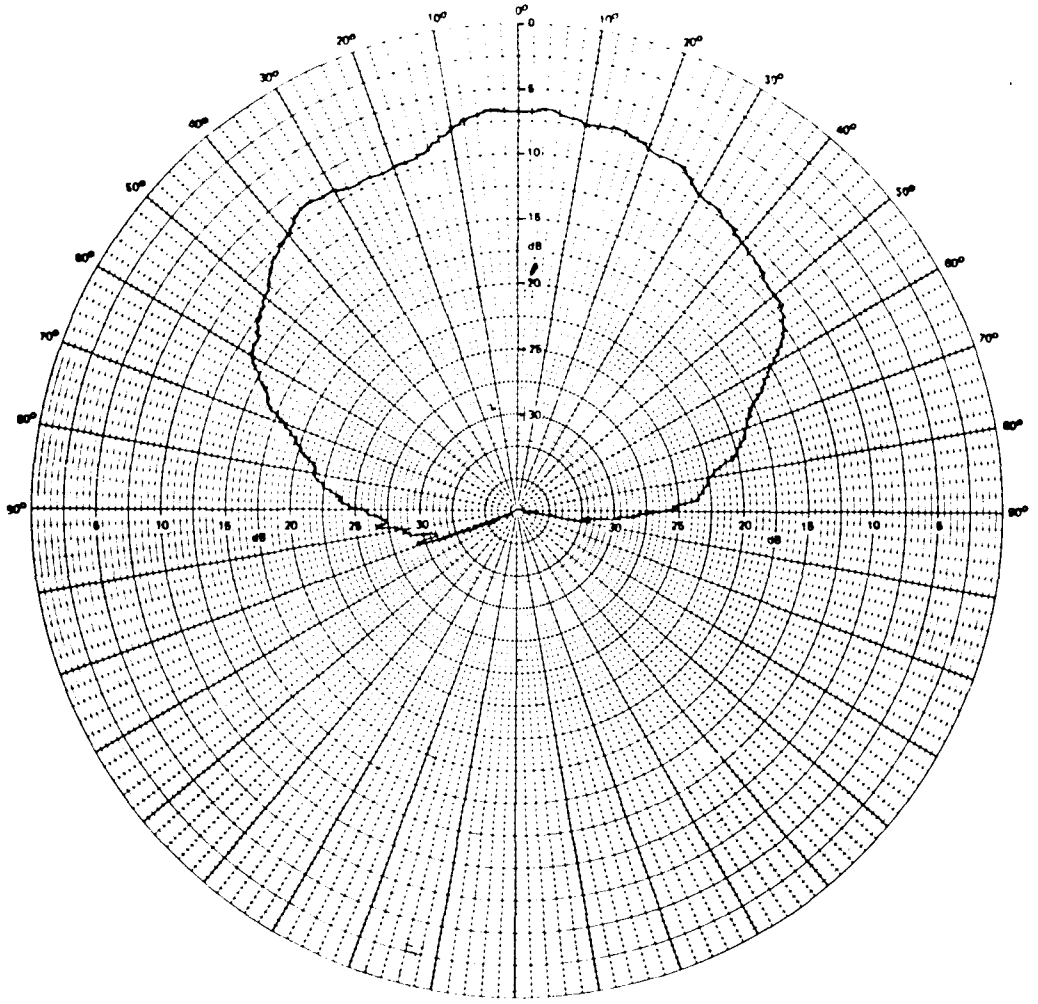

TR 79052

Fig B13 Azimuth radiation pattern small horn in Andover nose cone

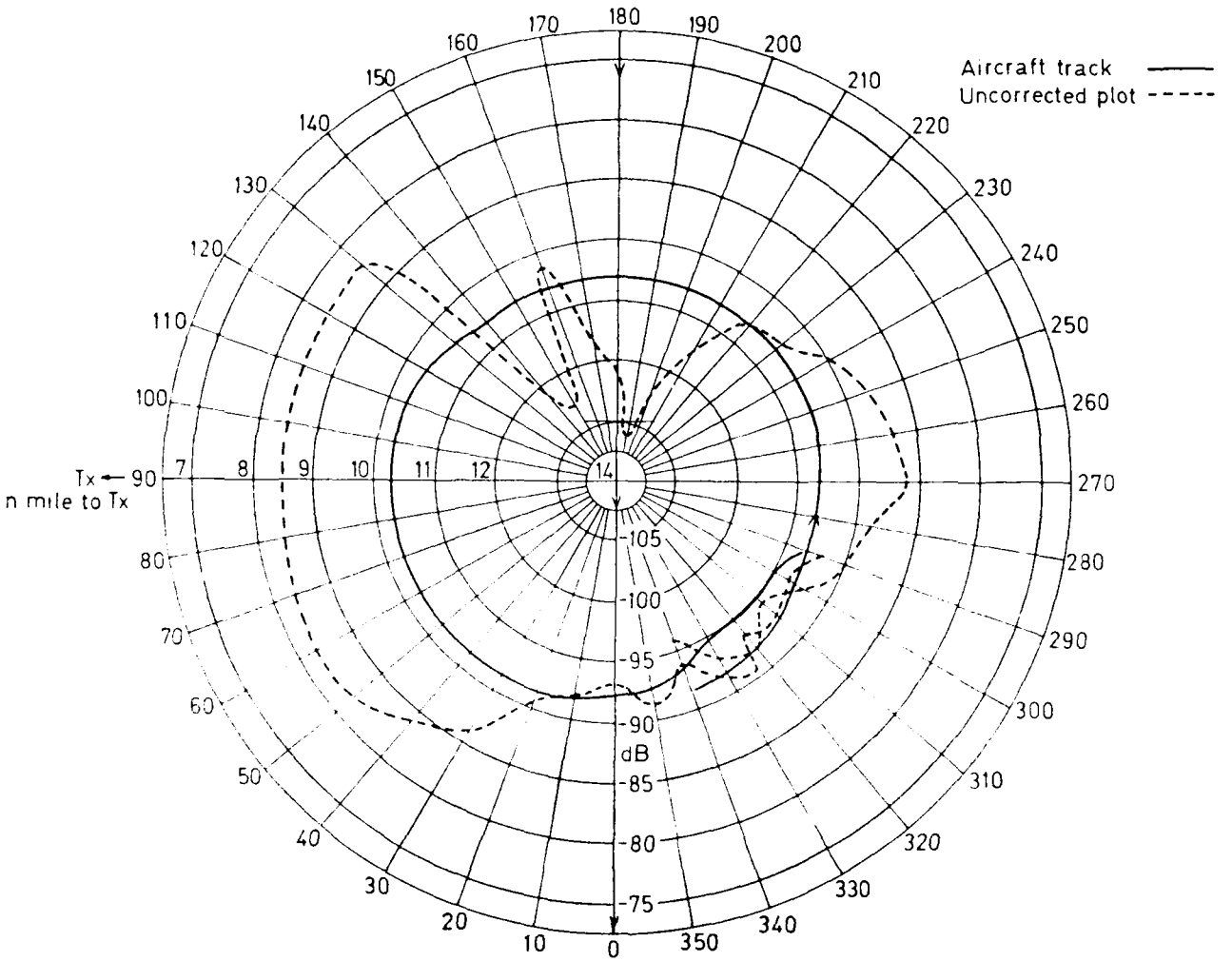

Fig B14a Polar plot of aircraft track and uncorrected signal level

This plot includes unquantified signal level variations due to the effect of ground reflections on the resultant received signal at low elevation angles (1.3° to 2.3°)

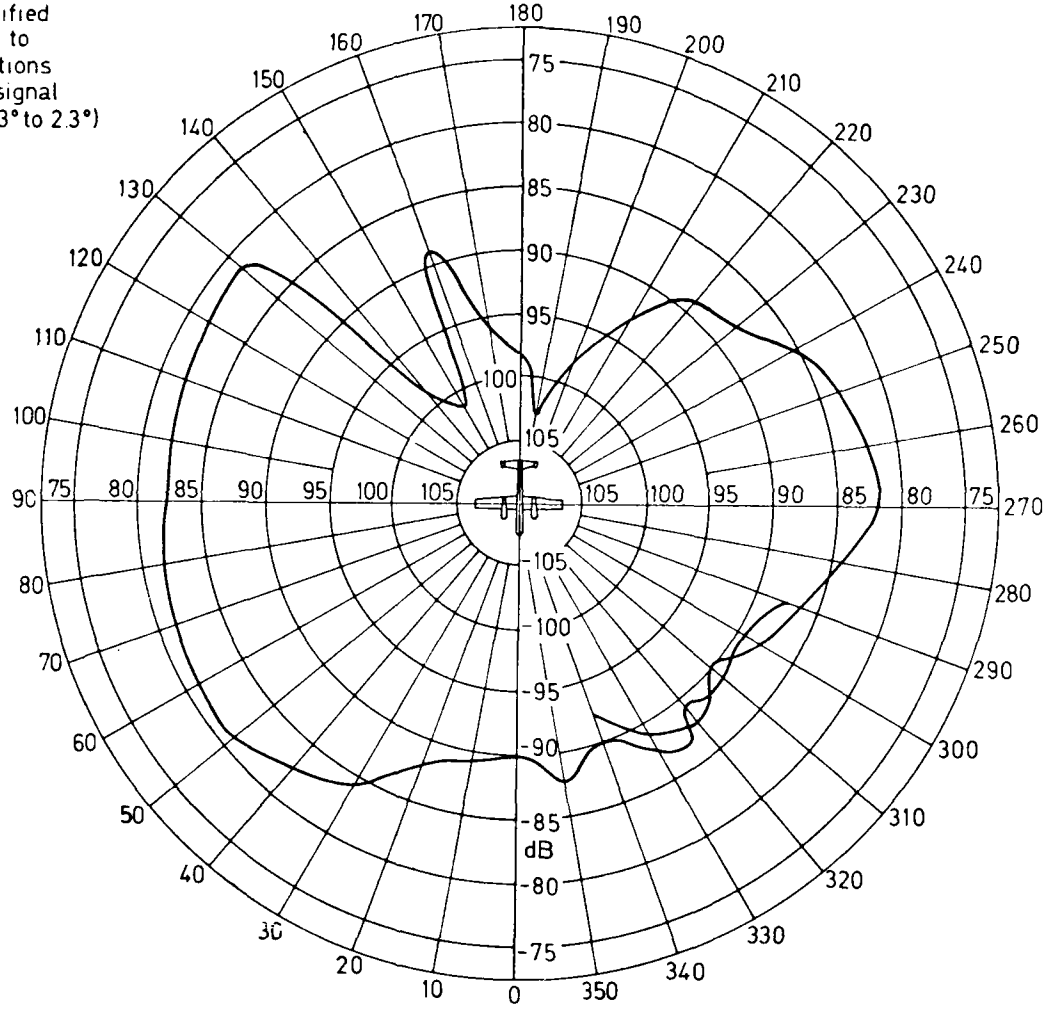

Fig B14b Polar plot of signal level received by DMLS aerial on XS646. Corrected for range variations 24.1.78

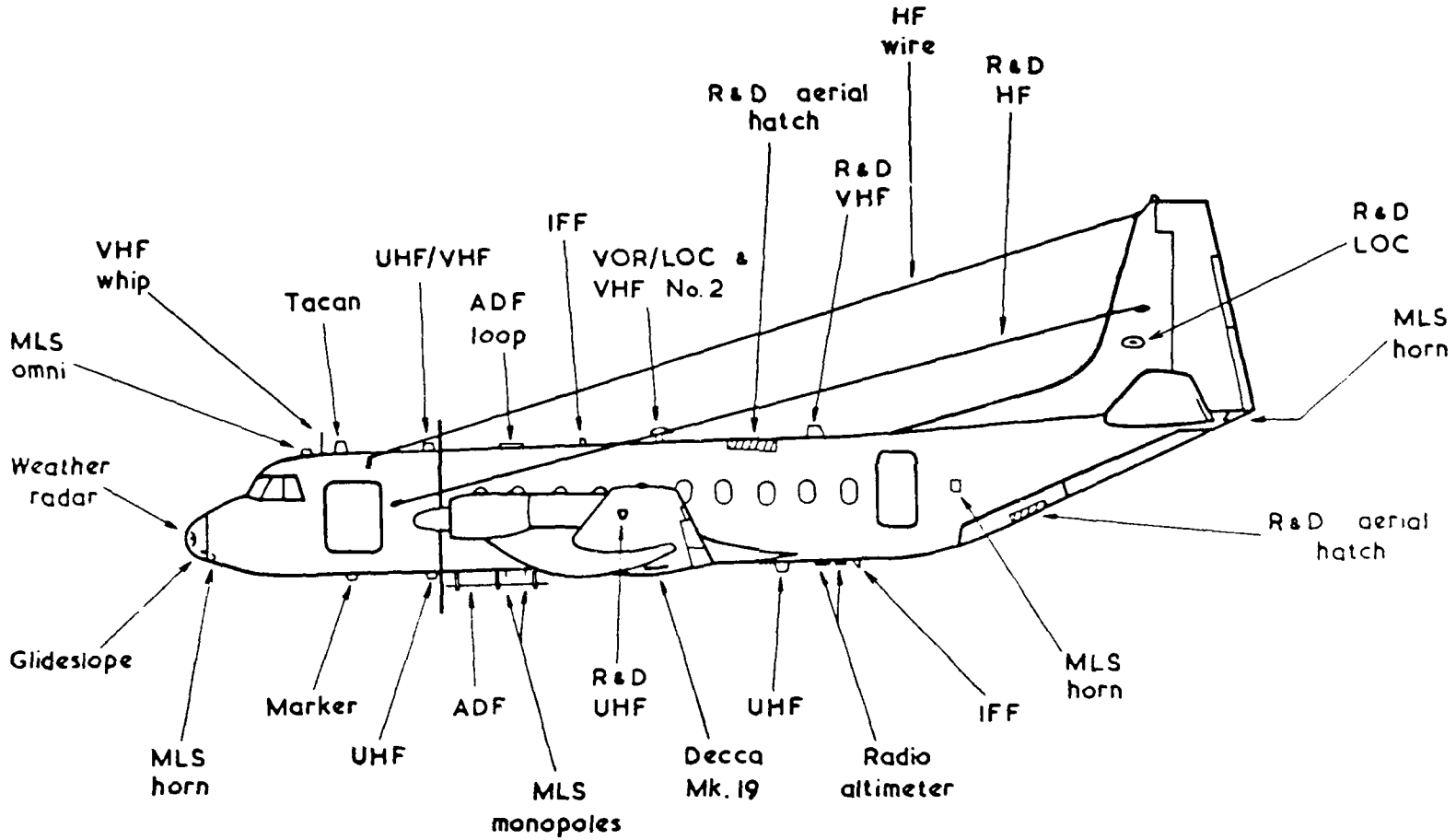

Fig B15 Andover antenna layout

TR 79052

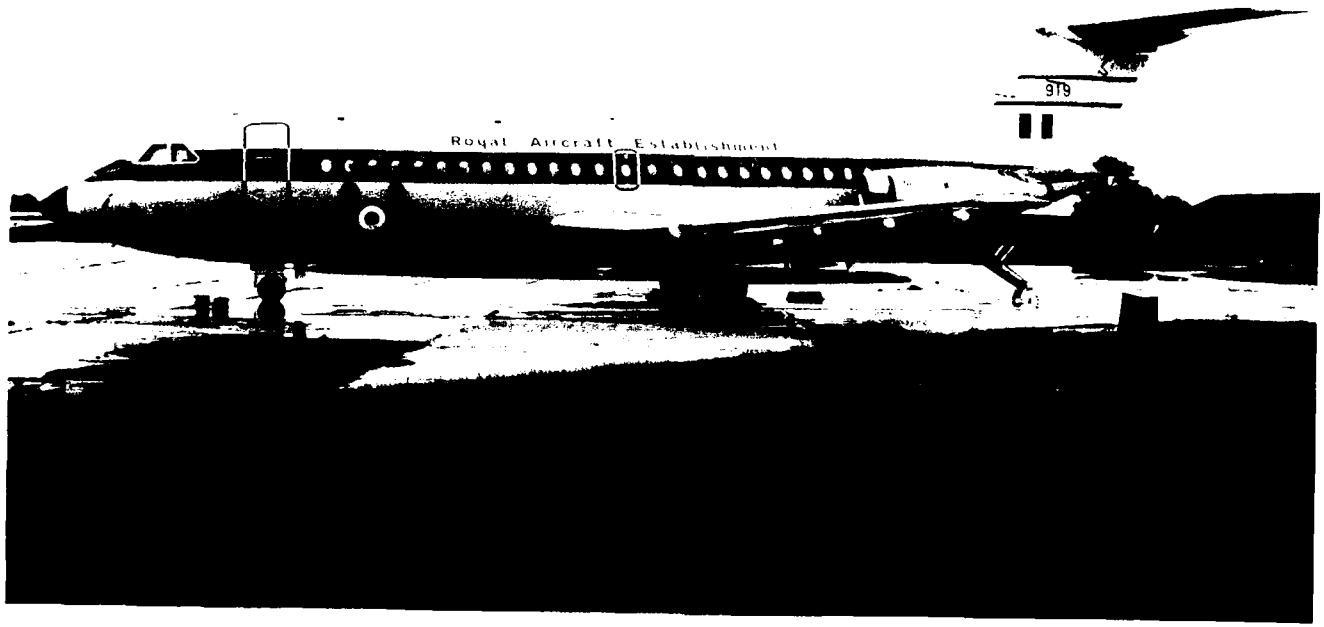

Fig B16 BAC 1-11

Fig B16

Fig B17

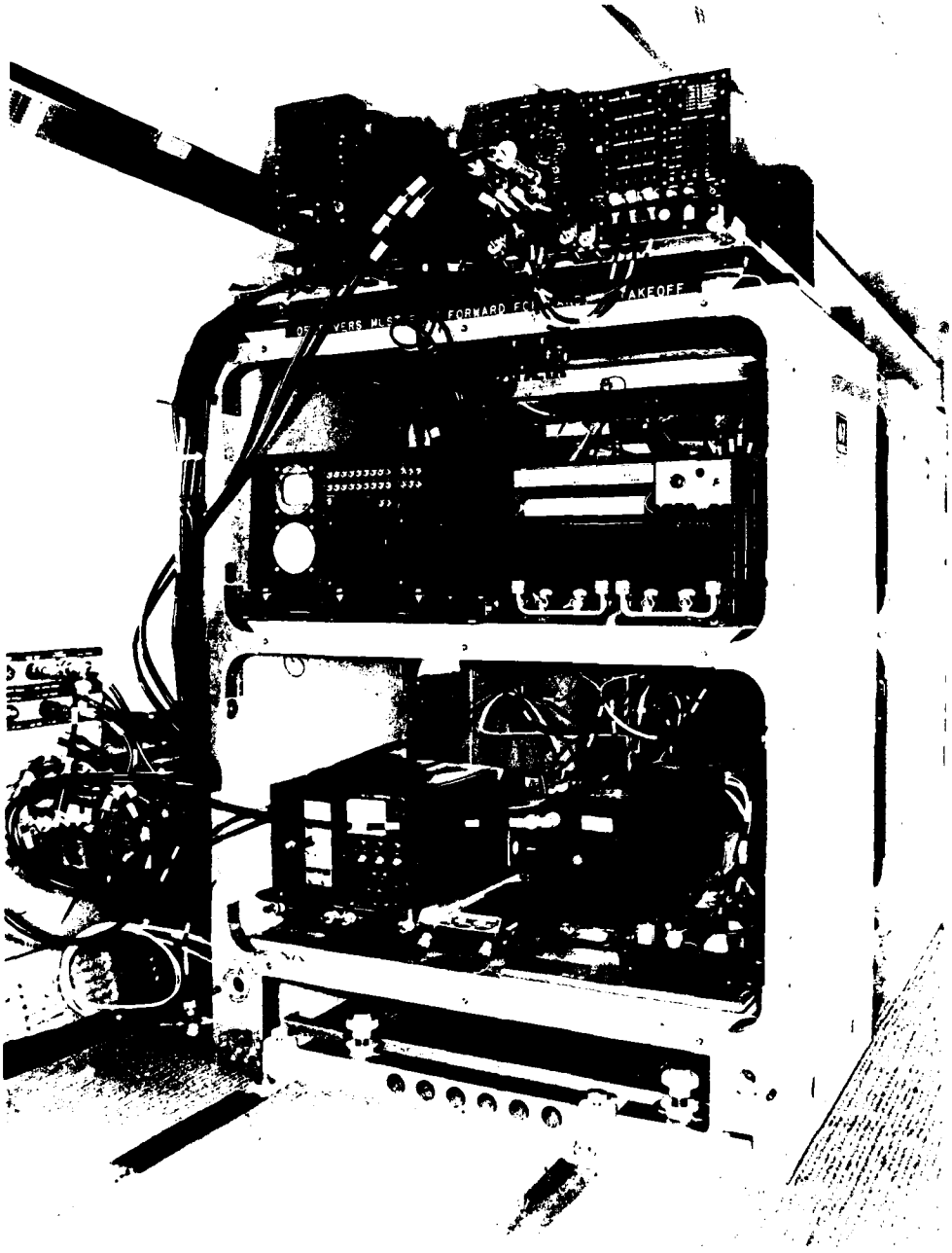

Fig B17 Receivers and analogue recorder BAC 1-11

TR 79052 C15544

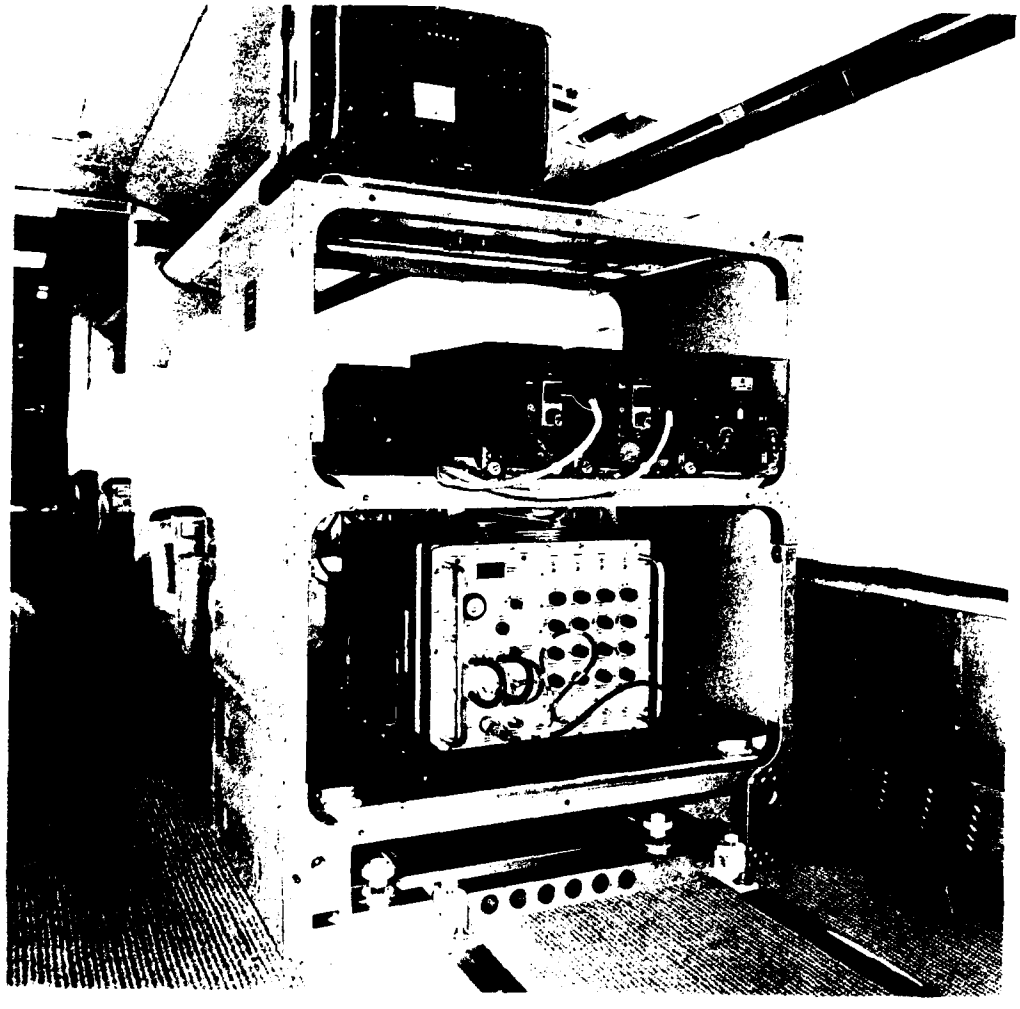

TR 79052 C15545

Fig B18 Digital recorder and receiver test set BAC 1-11

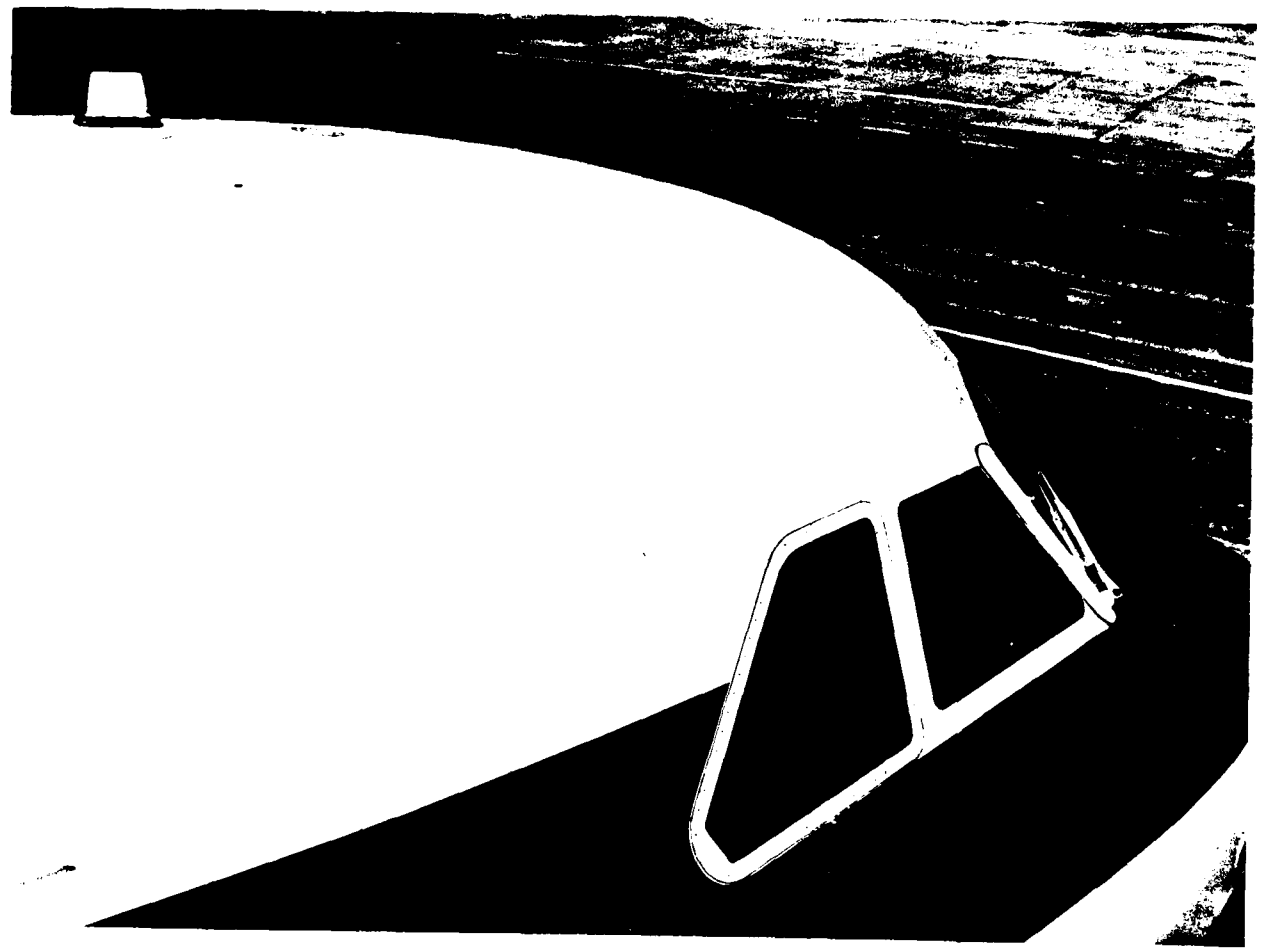

Fig B19 Omni antenna on BAC 1-11

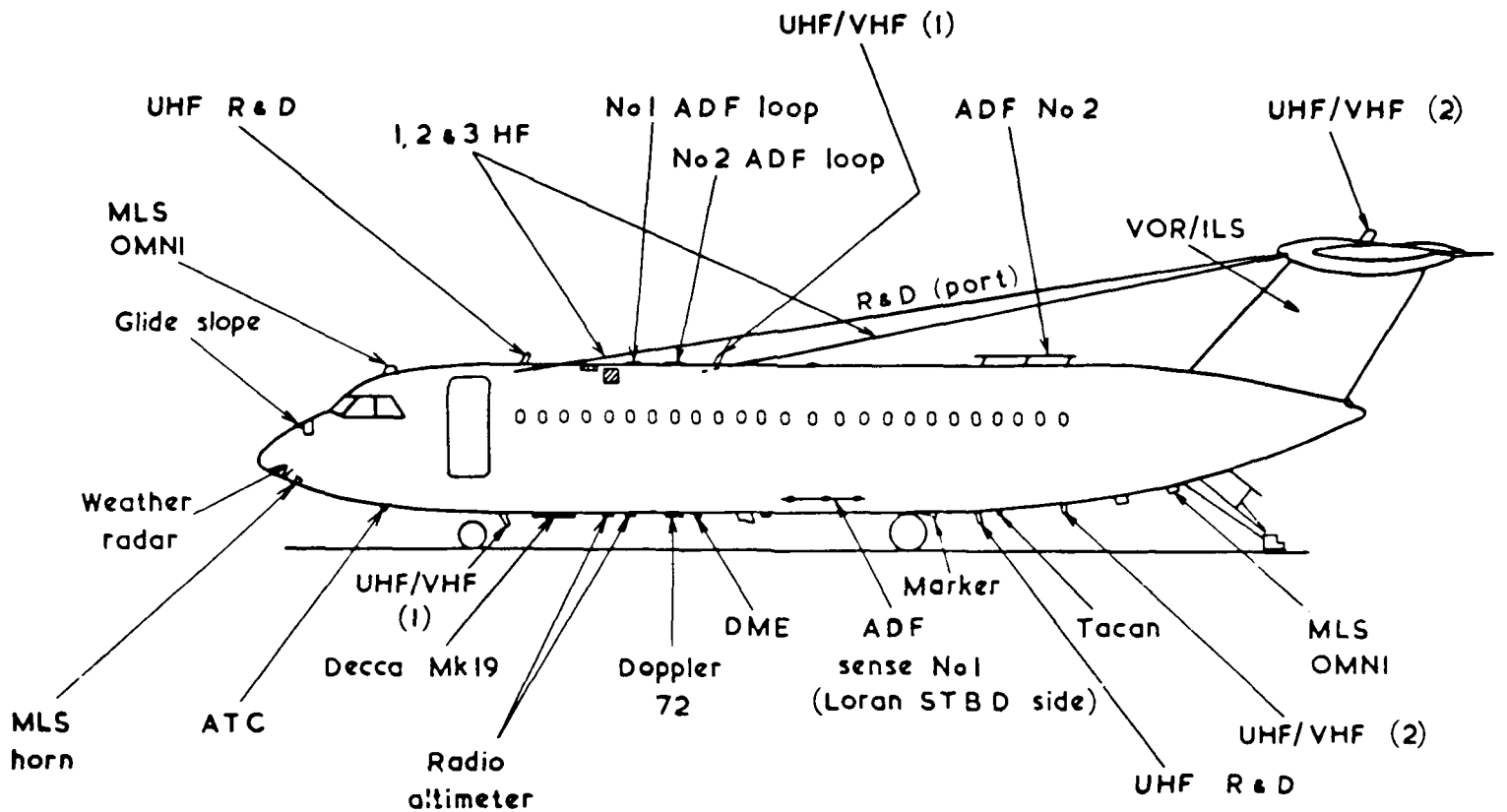

Fig B20 BAC 1-11 antenna layout

Fig B20

Fig B21

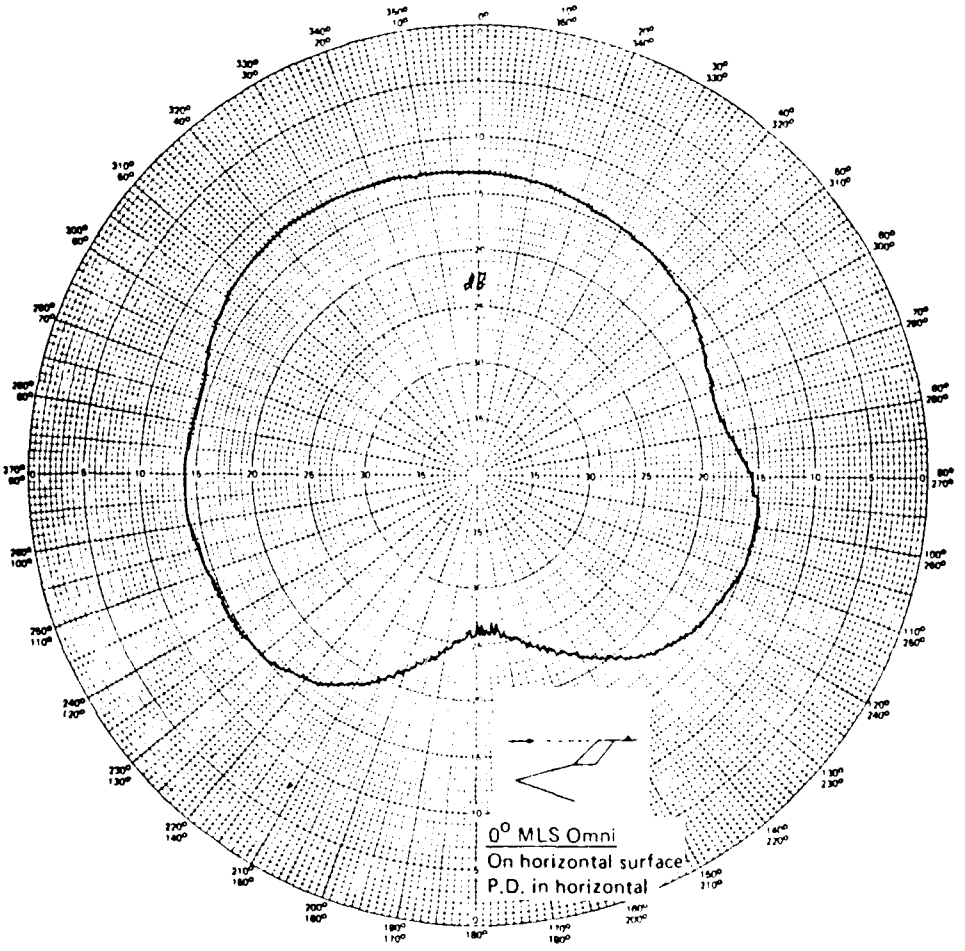

TR 79052

Fig B21 BAC 1-11 upper omni antenna radiation pattern

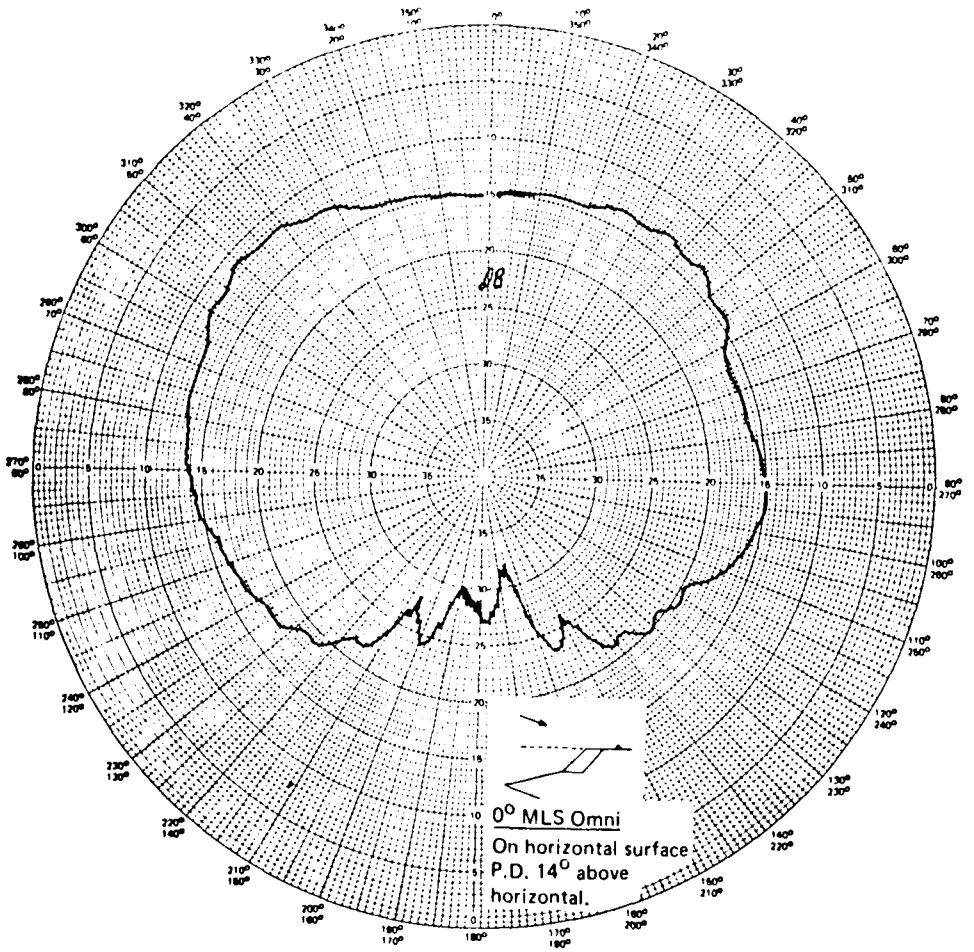

TR 79052

Fig B22 BAC 1-11 upper omni antenna radiation pattern

Fig B23

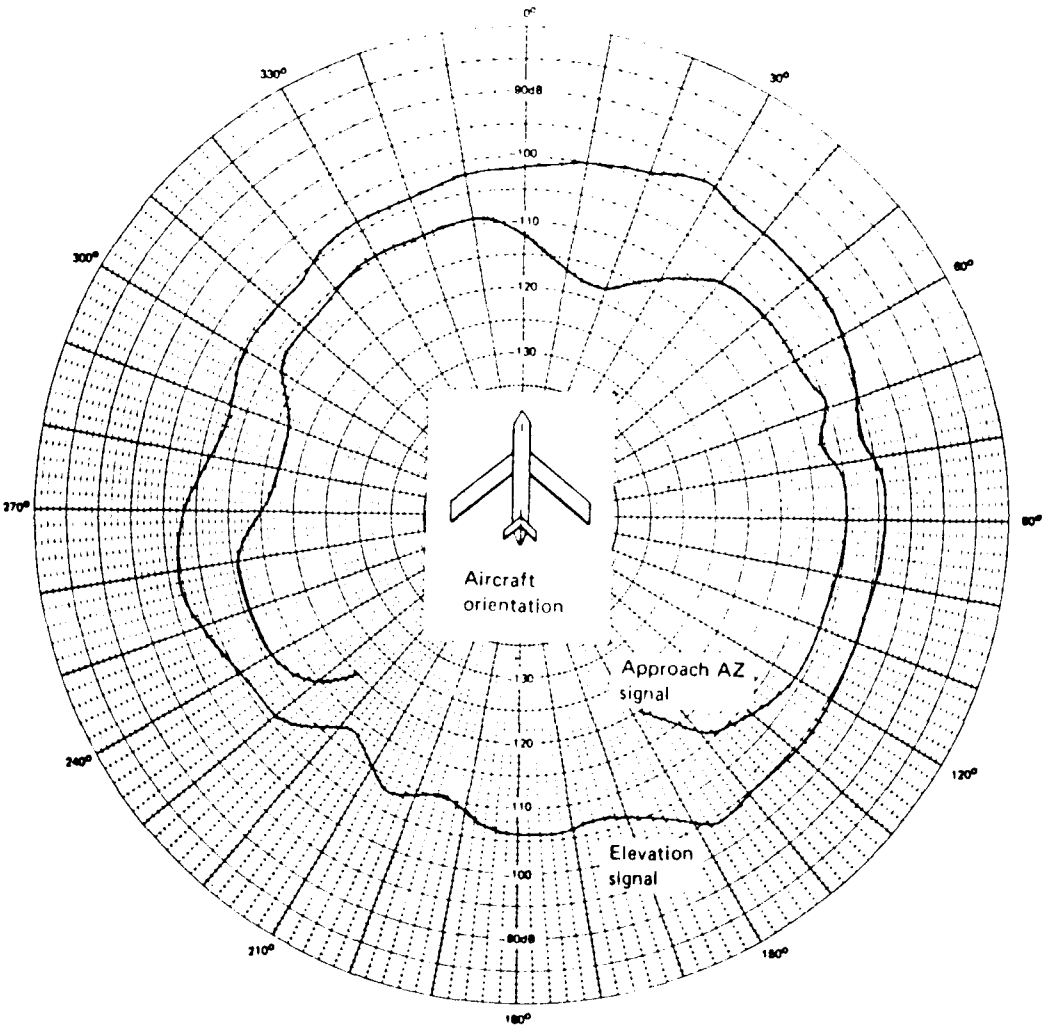

TR 79052

Fig B23 BAC 1-11 upper omni radiation pattern (orbit 1)

Fig B24 Wessex helicopter

Fig B24

AD-A085 478 ROYAL AIRCRAFT ESTABLISHMENT FARNBOROUGH (ENGLAND) F/G 17/7
CONTRIBUTIONS TO THE UK MICROWAVE LANDING SYSTEM RESEARCH AND D--ETC(U)
MAY 79 J M JONES
UNCLASSIFIED RAE-TR-79052-VOL-1 DRIC-BR-73155 NL

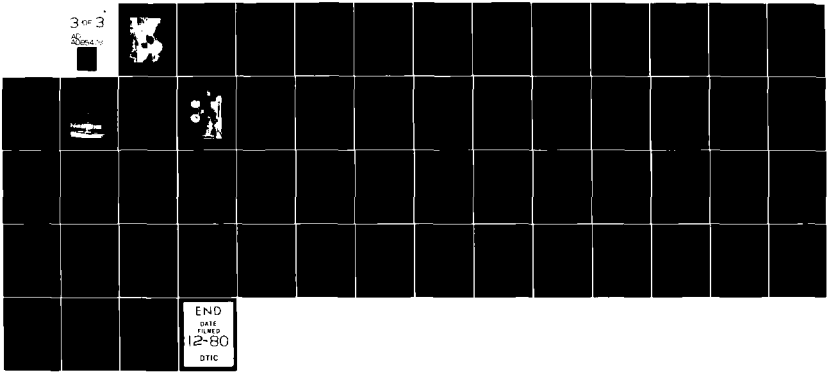

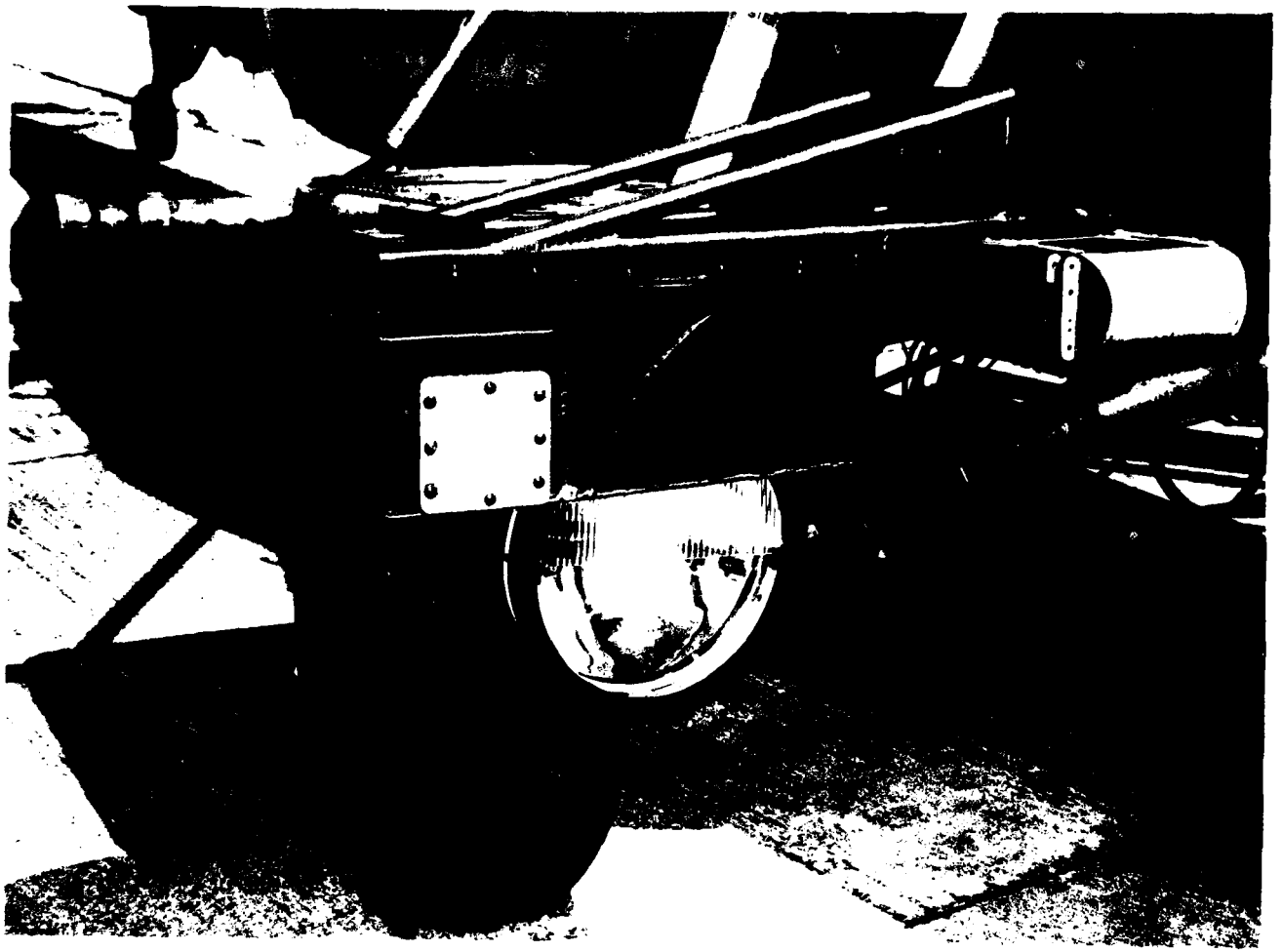

Fig B25 *Wessex antenna mount and tracking lamp*

Path	a	b	c	d	e	f	g
Altitude ft	2 000	2 000	2 000	2 000	2 000	2 000	2 000
		20 000	20 000	20 000	20 000	20 000	

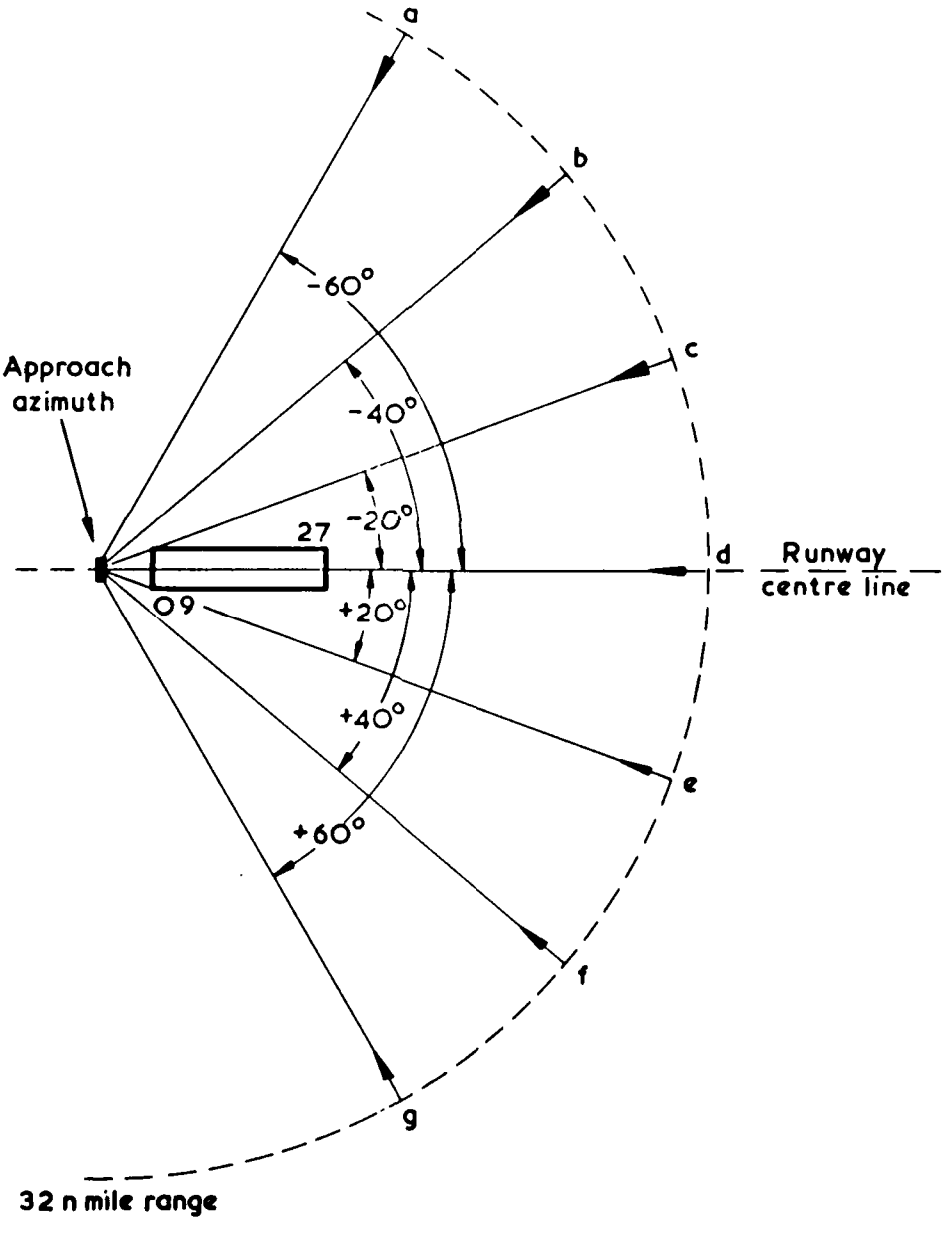

TR 79062

Fig B26 Coverage — approach azimuth and elevation radial flight paths

Fig B27

Test	Path	Altitude ft
Coverage	a	2000
Accuracy	b	10000
	c	2000

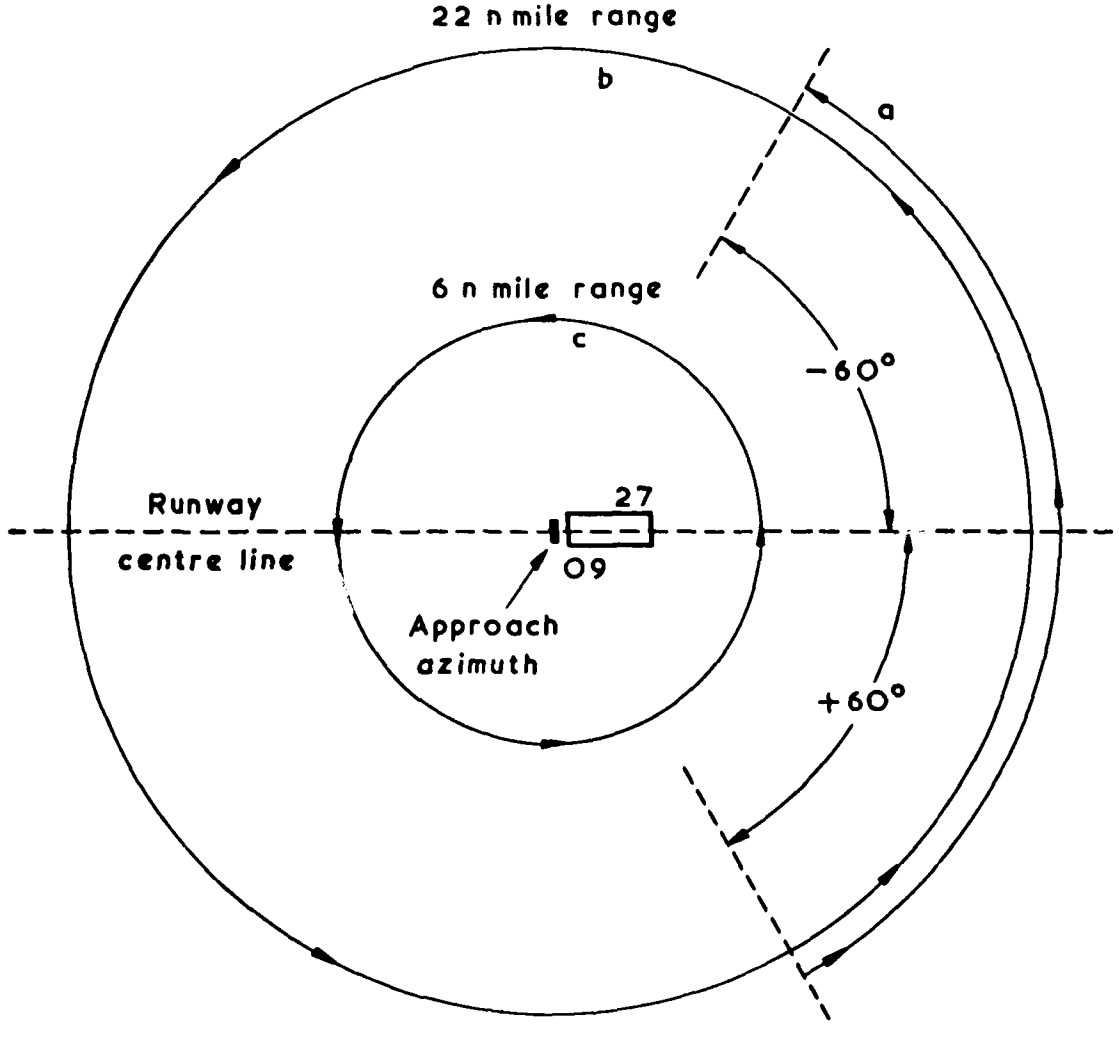

Fig B27 Coverage and accuracy — approach azimuth orbital flight paths

Test	Height above runway, S
Coverage	150 ft
Accuracy	100 ft

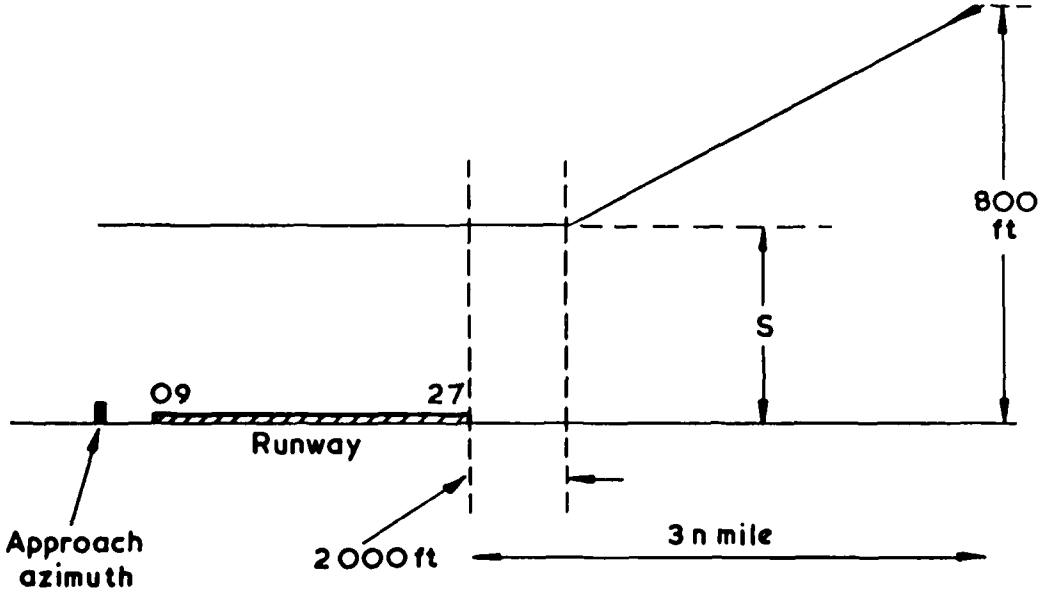

TR 79052

Fig B28 Flare elevation approach flight paths

Fig B29

Path	a, b, c, d, e	f, g, h, i, j, k	ℓ
Altitude ft	2 000		
		500	
			5 000

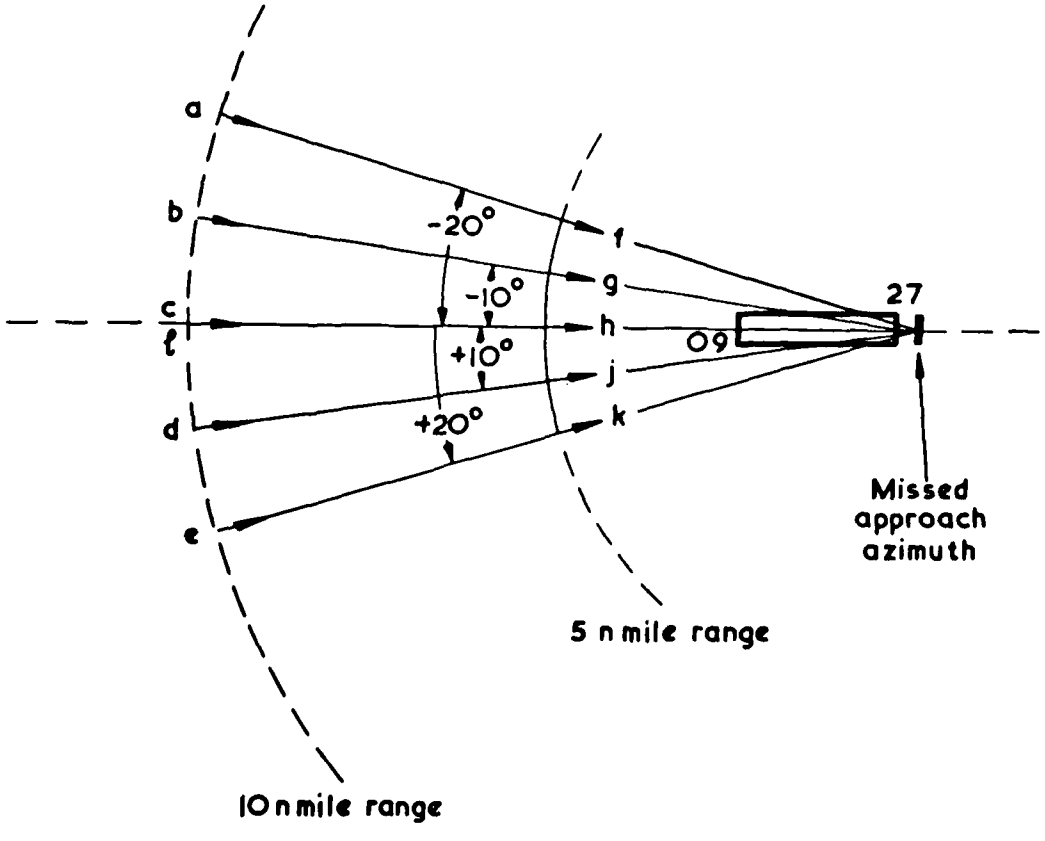

TR 79052

Fig B29 Coverage — missed approach radial flight paths

Path	a	b	c	d	e	f	g	h, j, k, ℓ, m, n
Altitude ft		20 000		20 000		20 000		
	3 000	3000	3 000	3 000	3 000	3 000	3 000	
								2 000

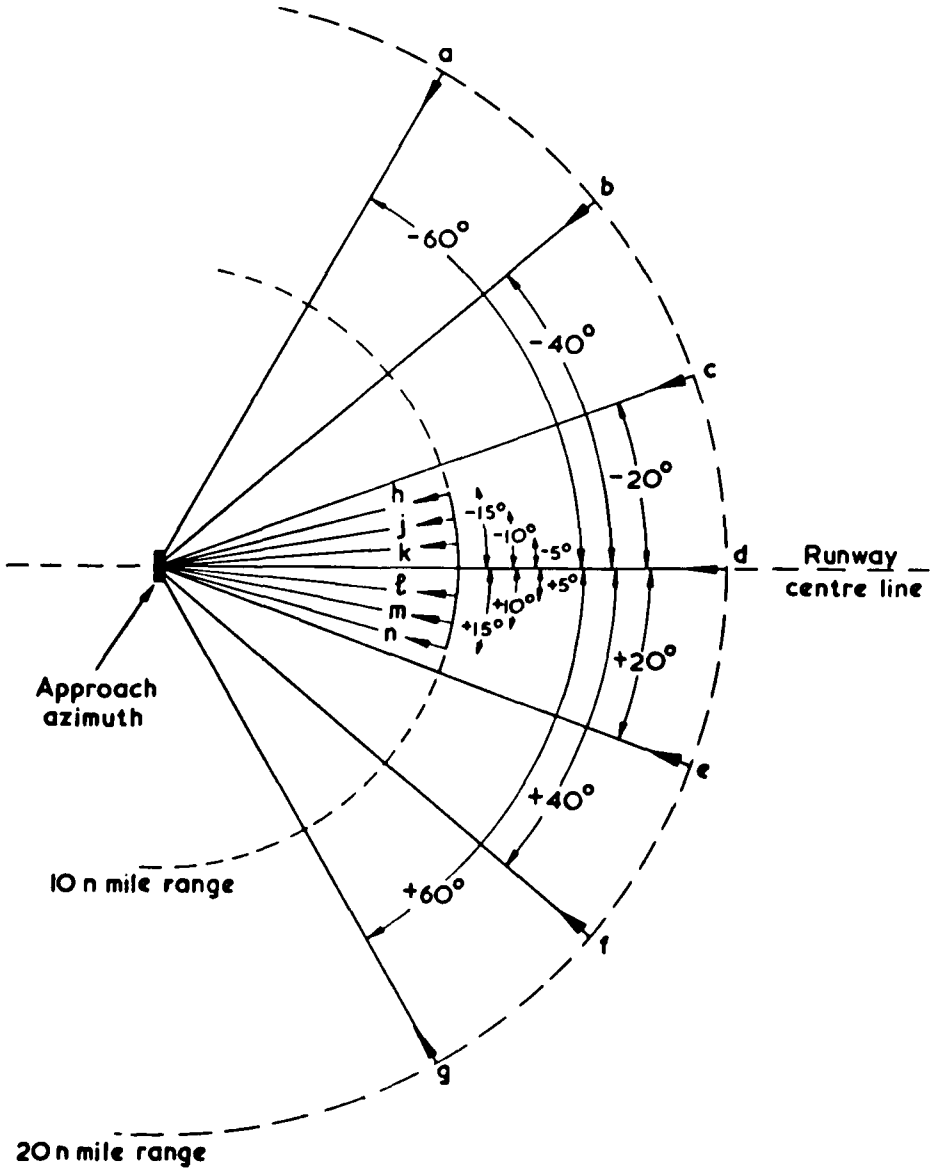

Fig B30 Accuracy – approach azimuth radial flight paths

Fig B31

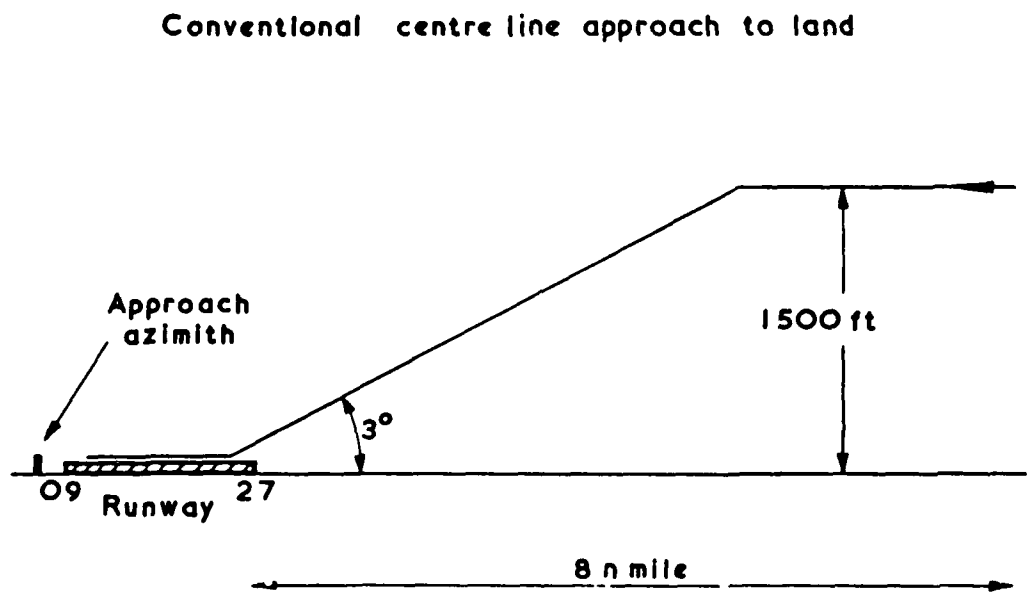

TR 79052

Fig B31 Accuracy – approach azimuth conventional flight path

Fig B32

Path	a, b, c	d, e, f, g, h
Altitude ft	20 000	
		2000

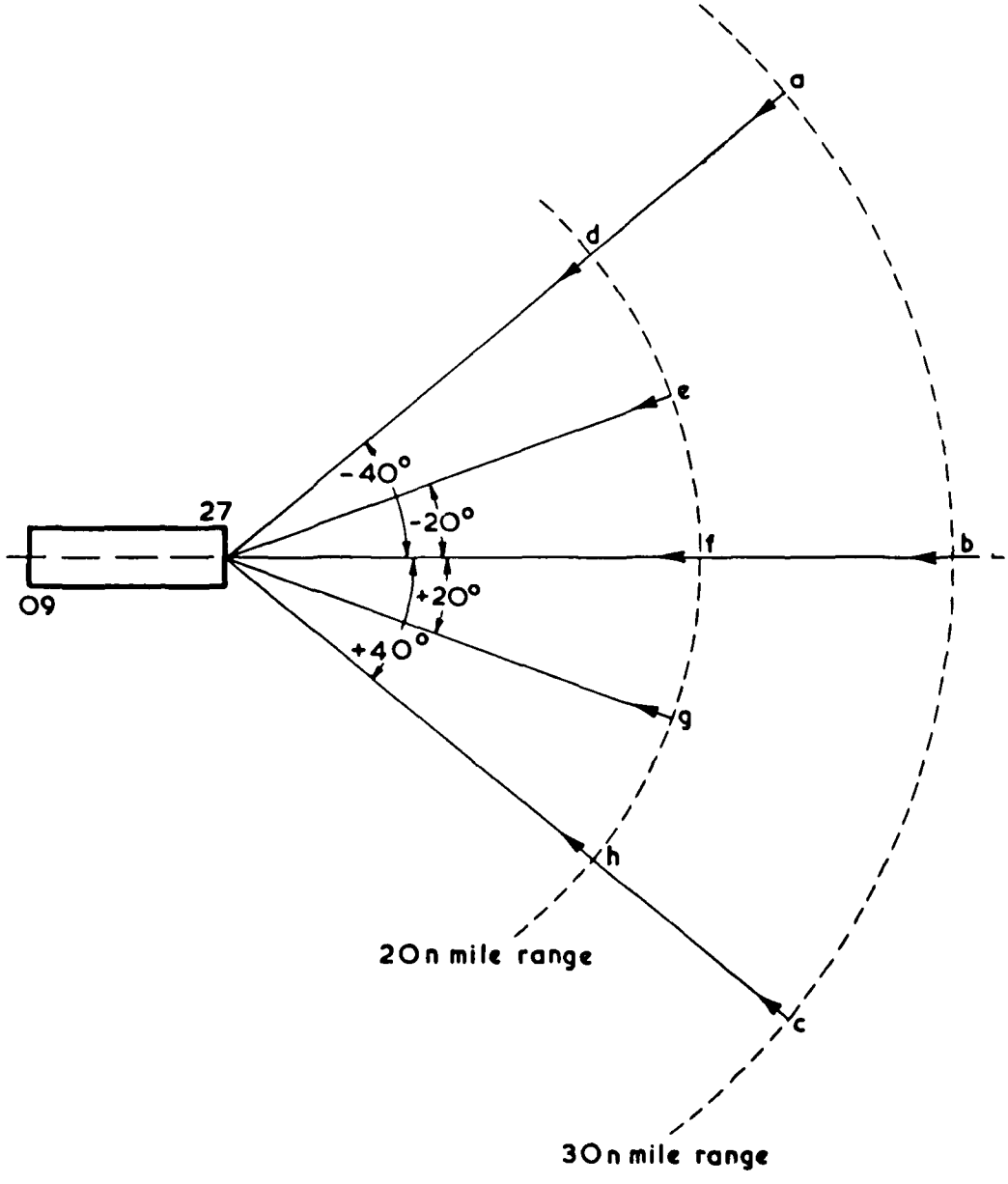

TR 79052

Fig B32 Accuracy — elevation radial flight paths

Fig B33

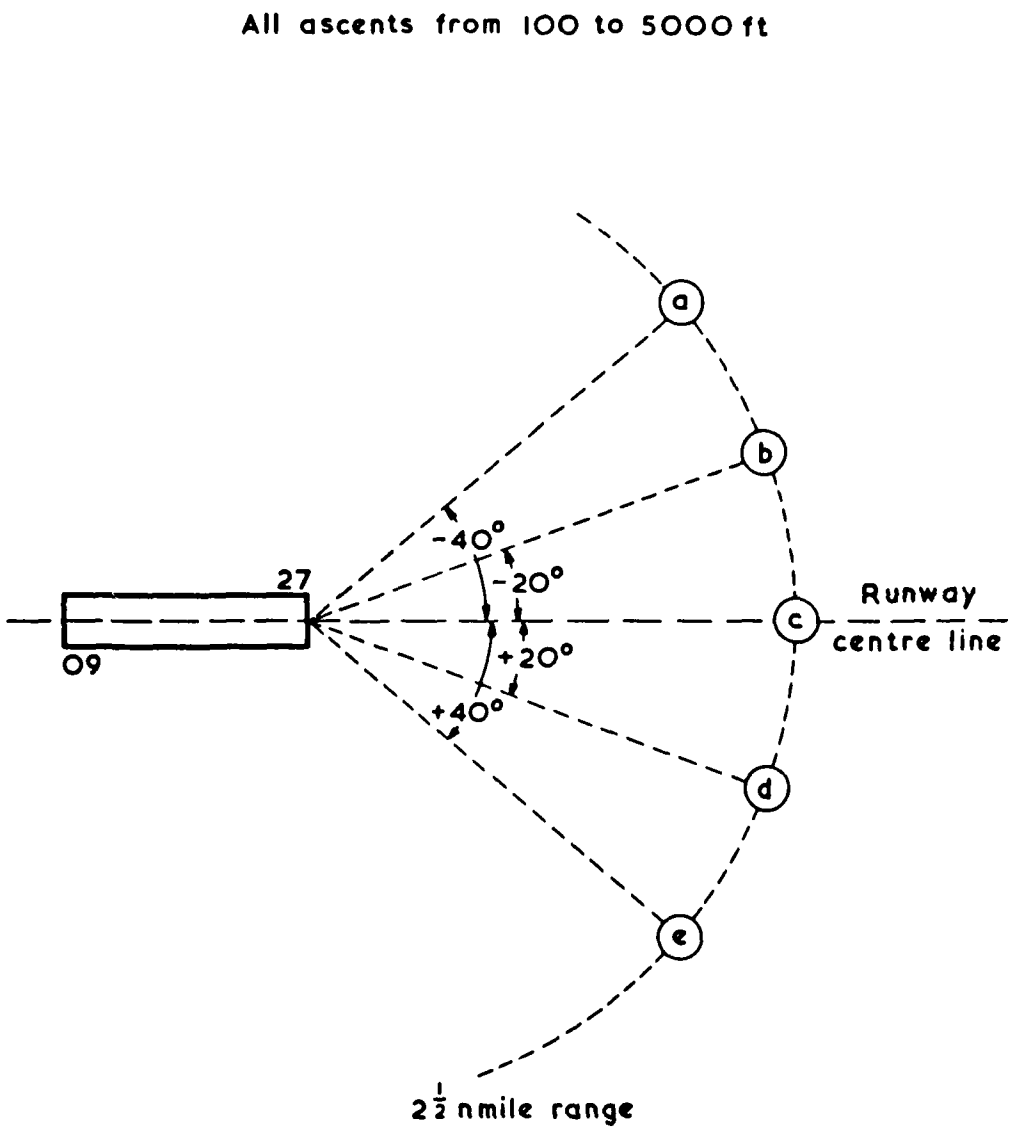

Fig B33 Accuracy — elevation ascent flight paths

Touch and go centre line approaches at 3° and 6°

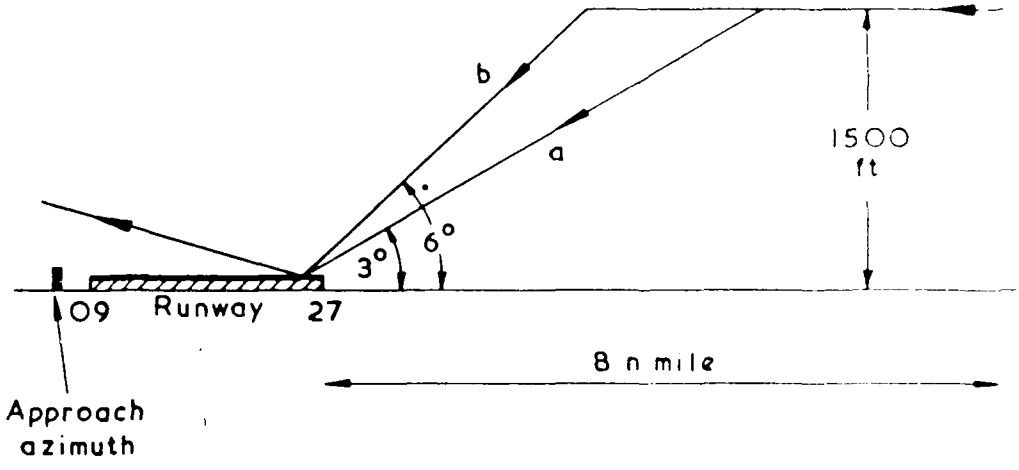

Fig B34 Accuracy – elevation approach flight paths

Fig B35

Path	a	b
Altitude ft	10 000	
		6 000
		4 000
		2 000

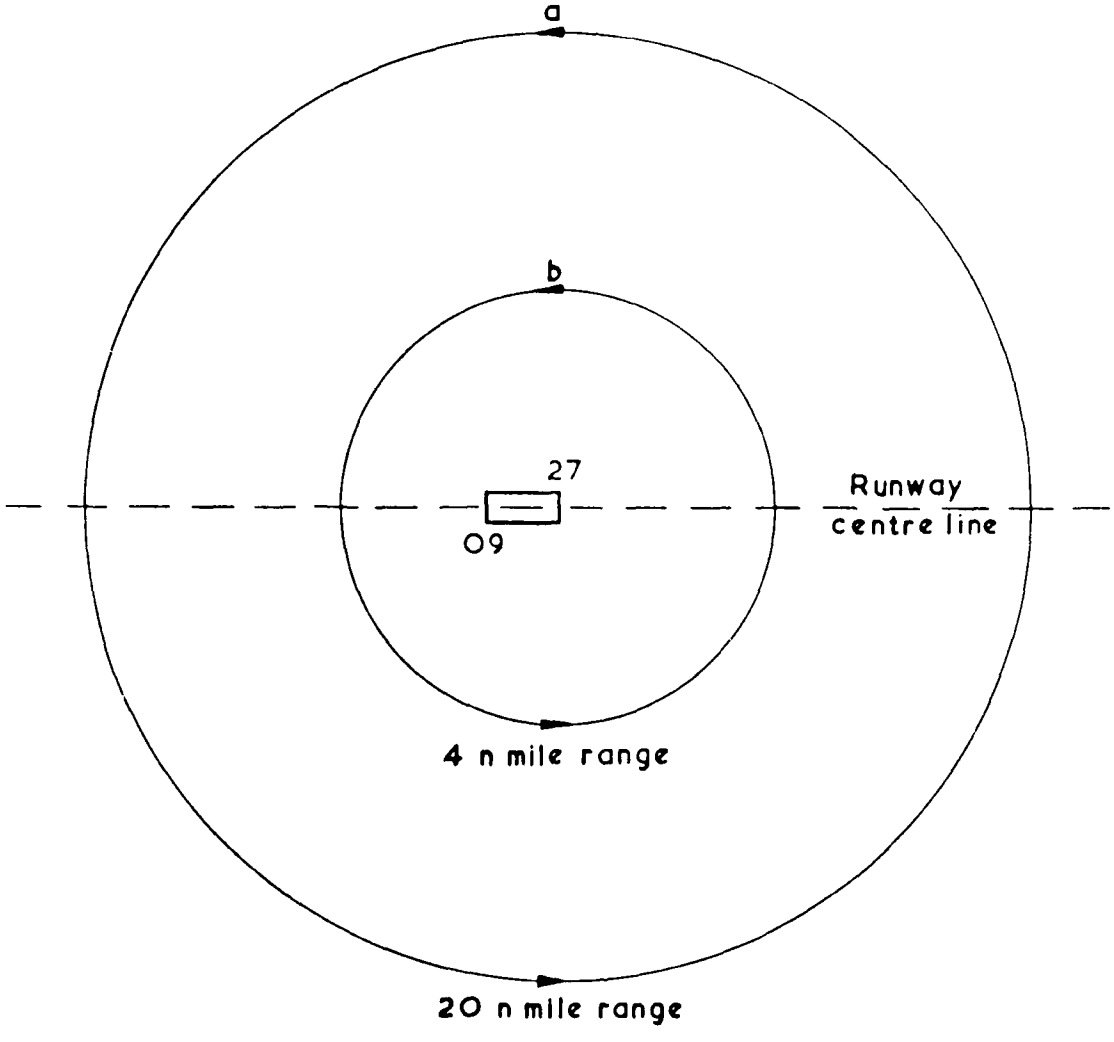

TR 79052

Fig B35 Accuracy – elevation orbit flight paths

All paths at 2 000 ft constant altitude
Path e also at 5 000 ft constant altitude

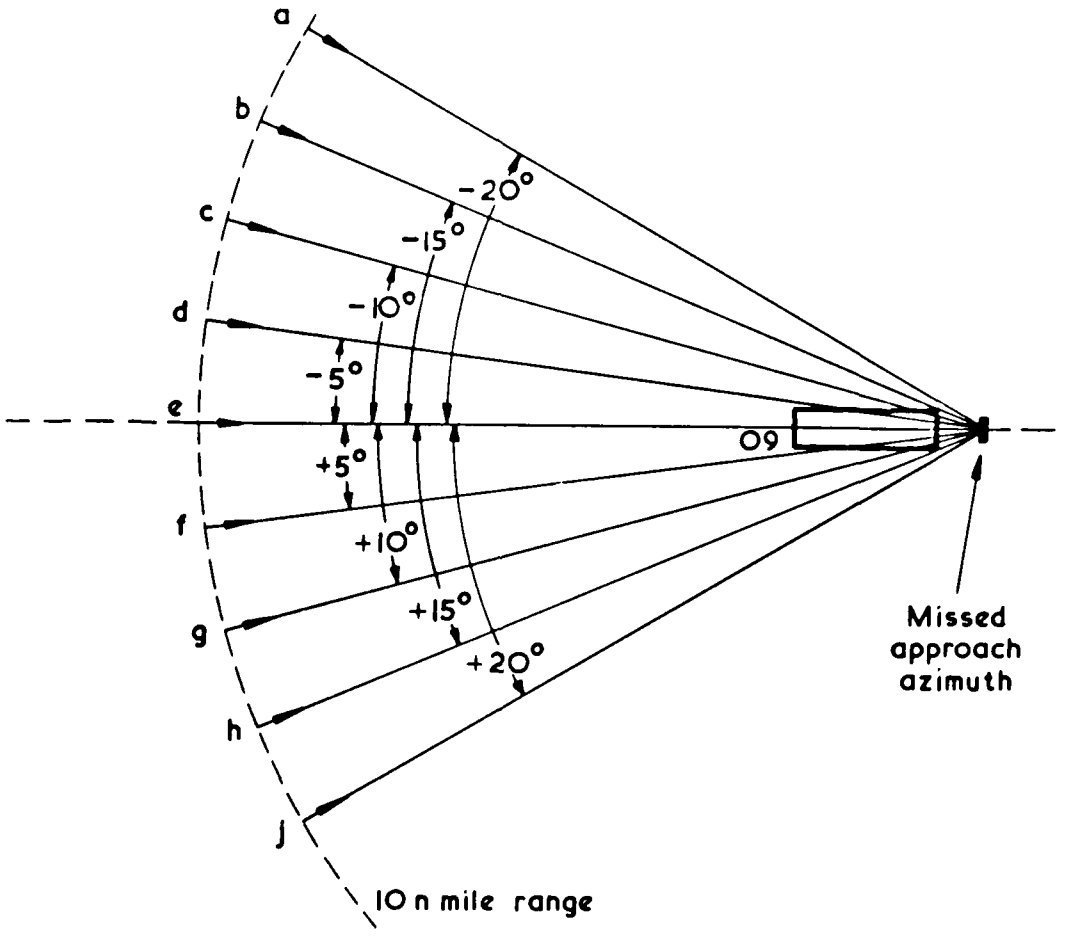

TR 79052

Fig B36 Accuracy — missed approach azimuth radial flight paths

Fig B37

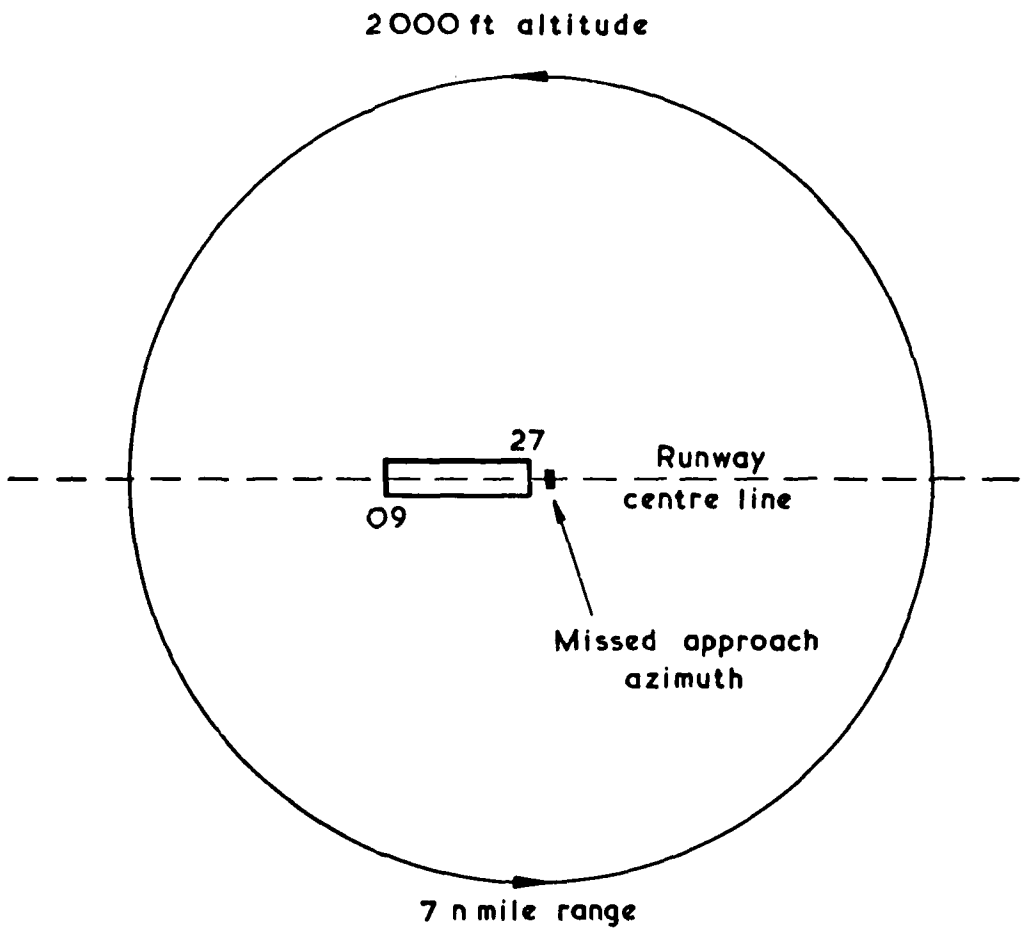

TR 79052

Fig B37 Accuracy – missed approach azimuth orbit flight paths

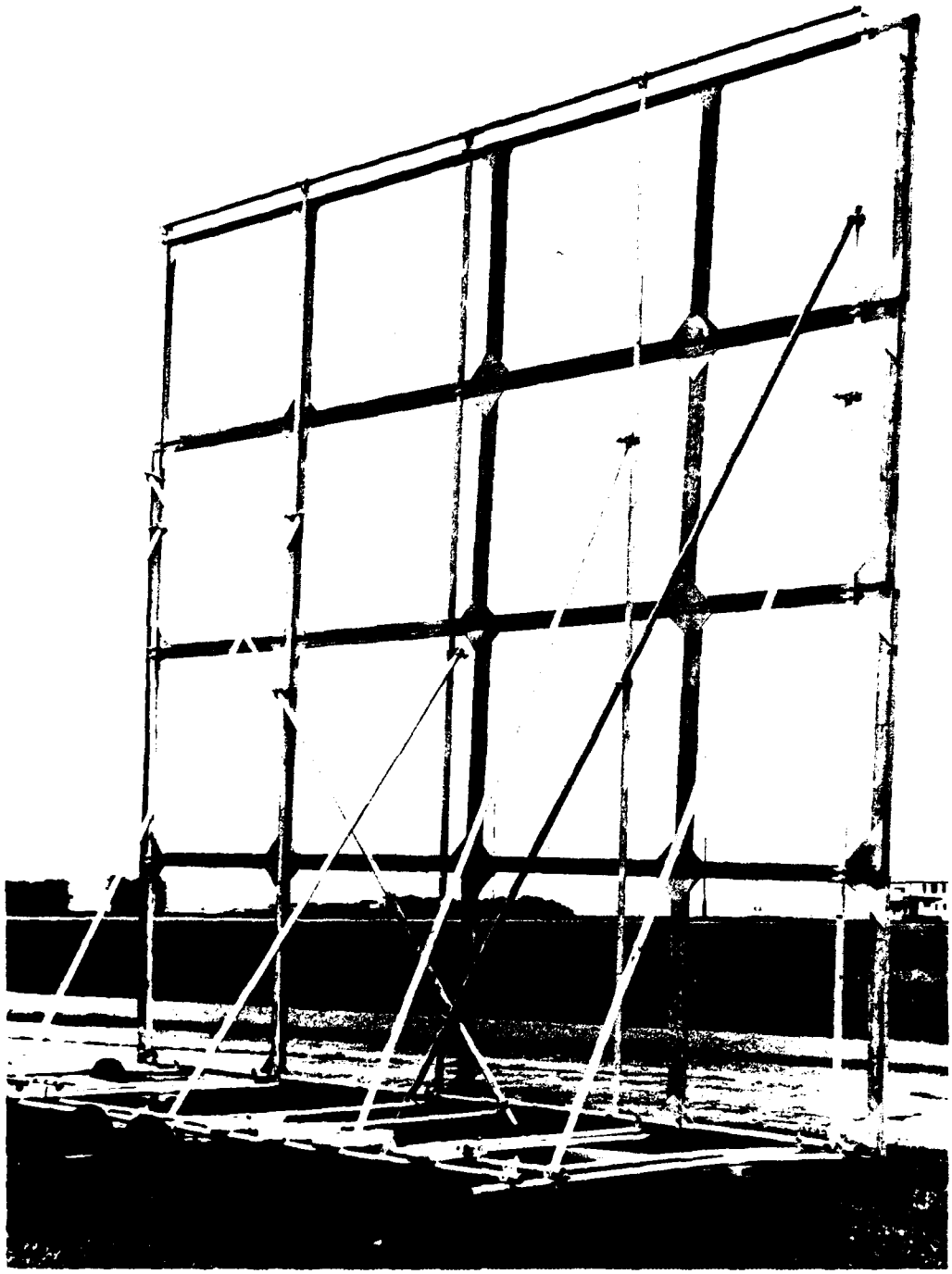

TR 79052 C15549

Fig B38 Multipath screen

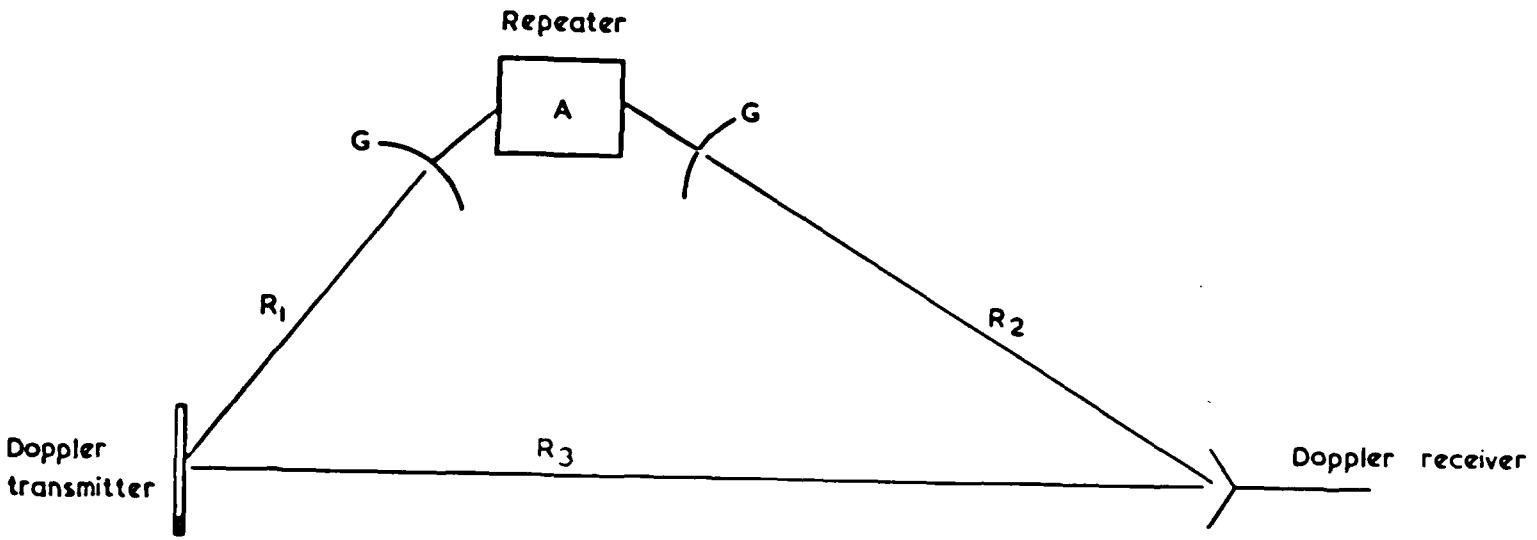

Fig B39 Schematic arrangement of repeater dishes

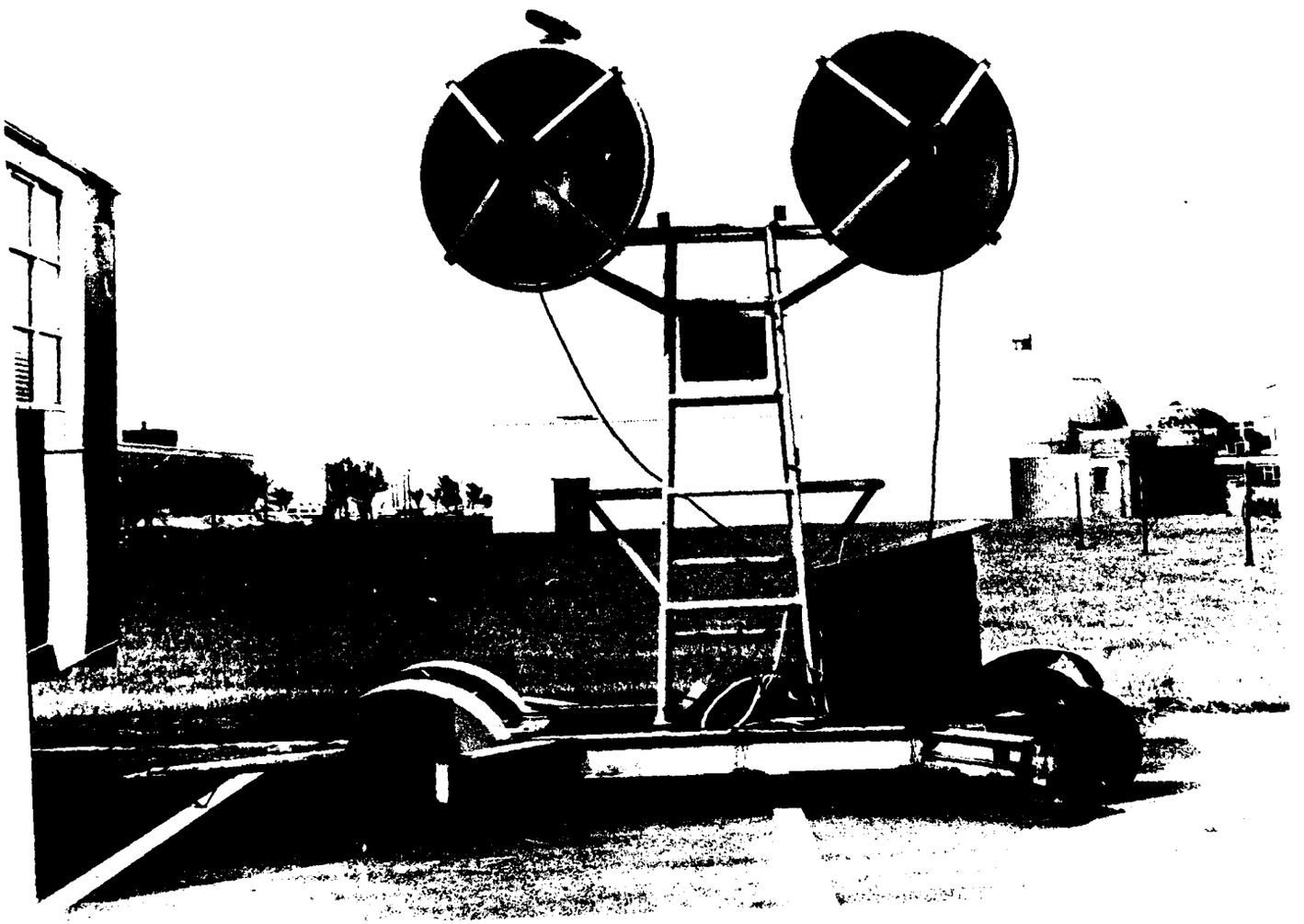

Fig B40 Repeater antennas

Fig B40

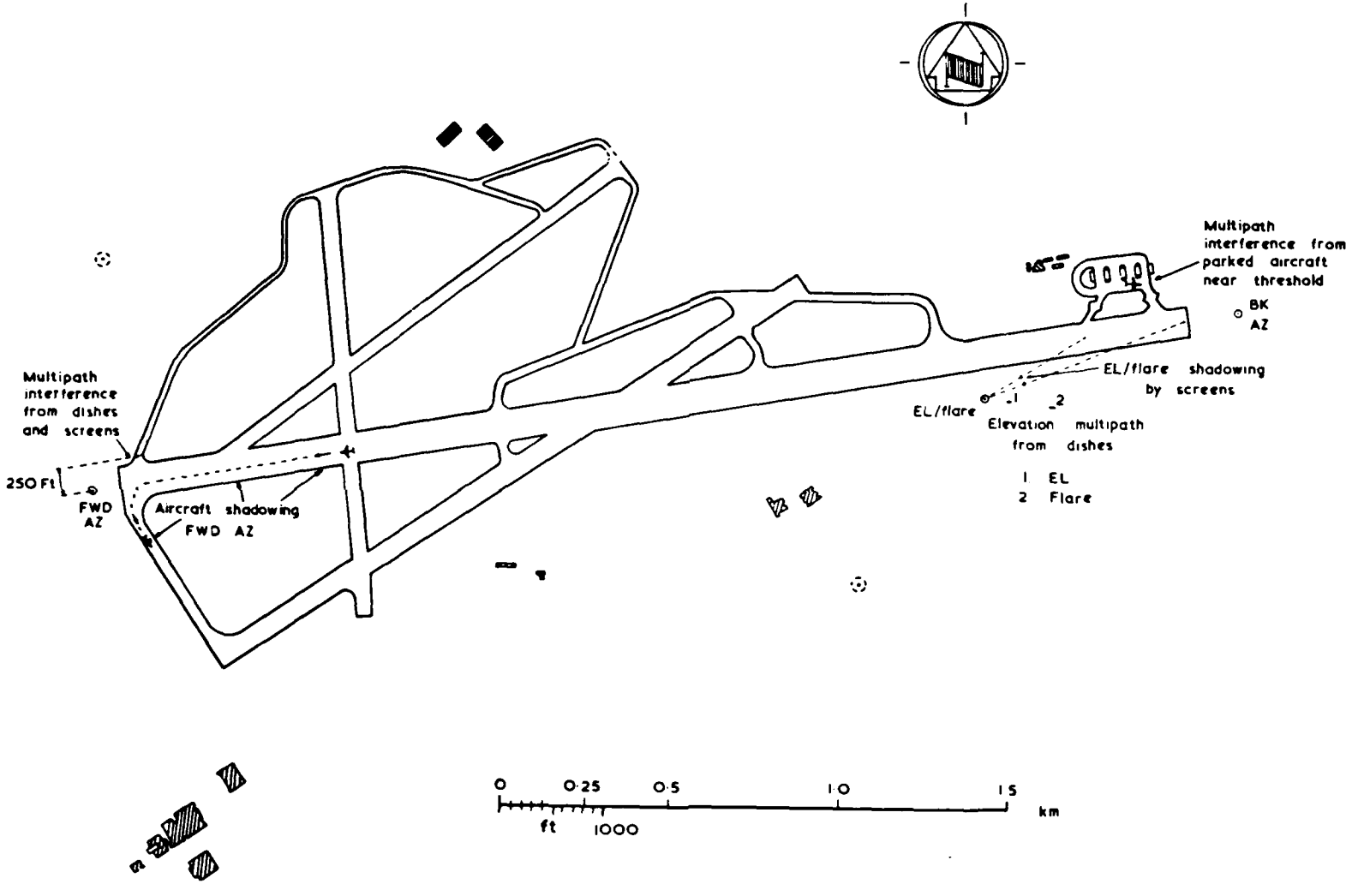

Fig B41 Test site plan showing multipath layout

A STAN 38 glidepath
B Doppler elevation
C Doppler azimuth
D STAN 37 localizer
E Kinetheodolite
F Doppler back azimuth

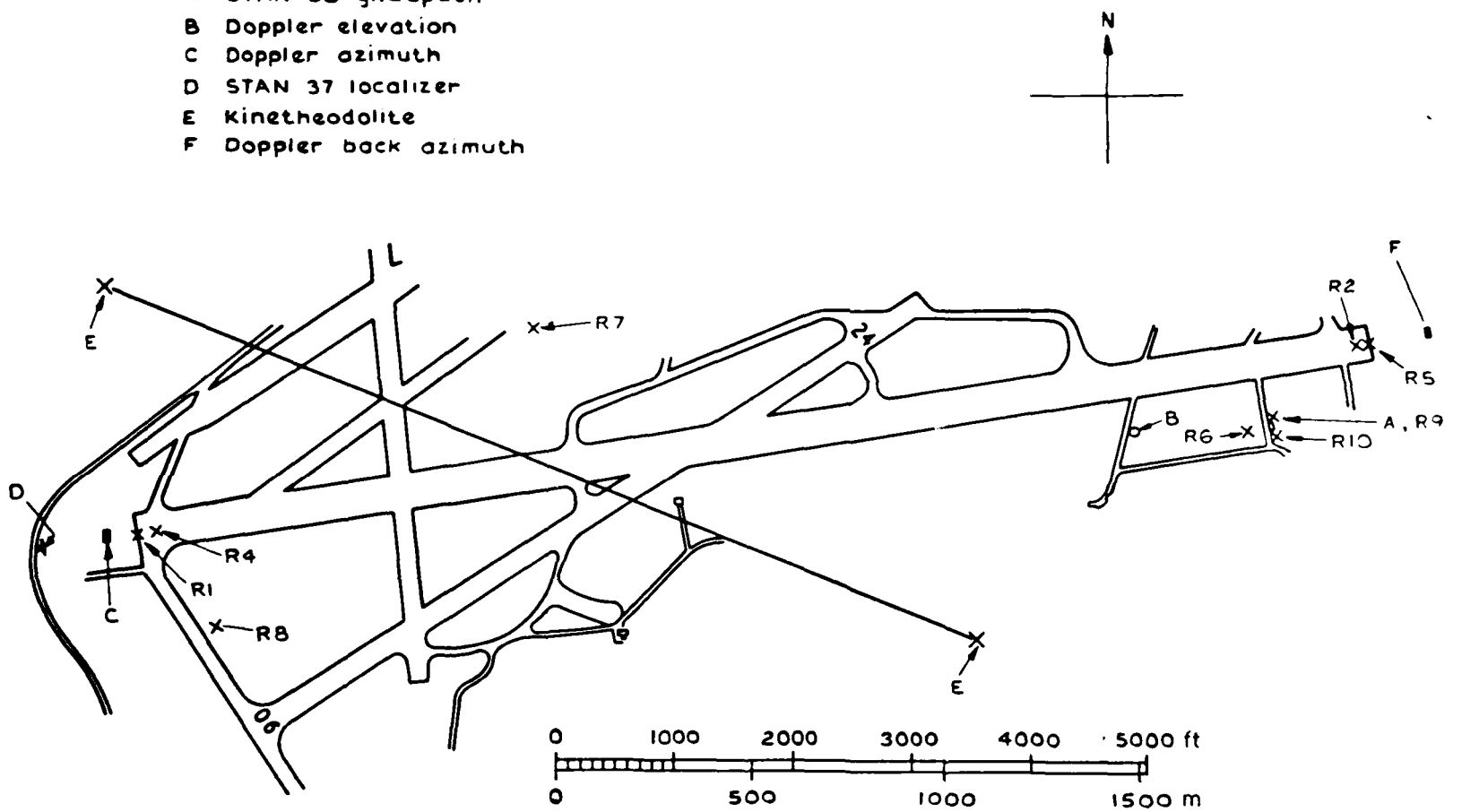

Fig B42 Static test reference point layout

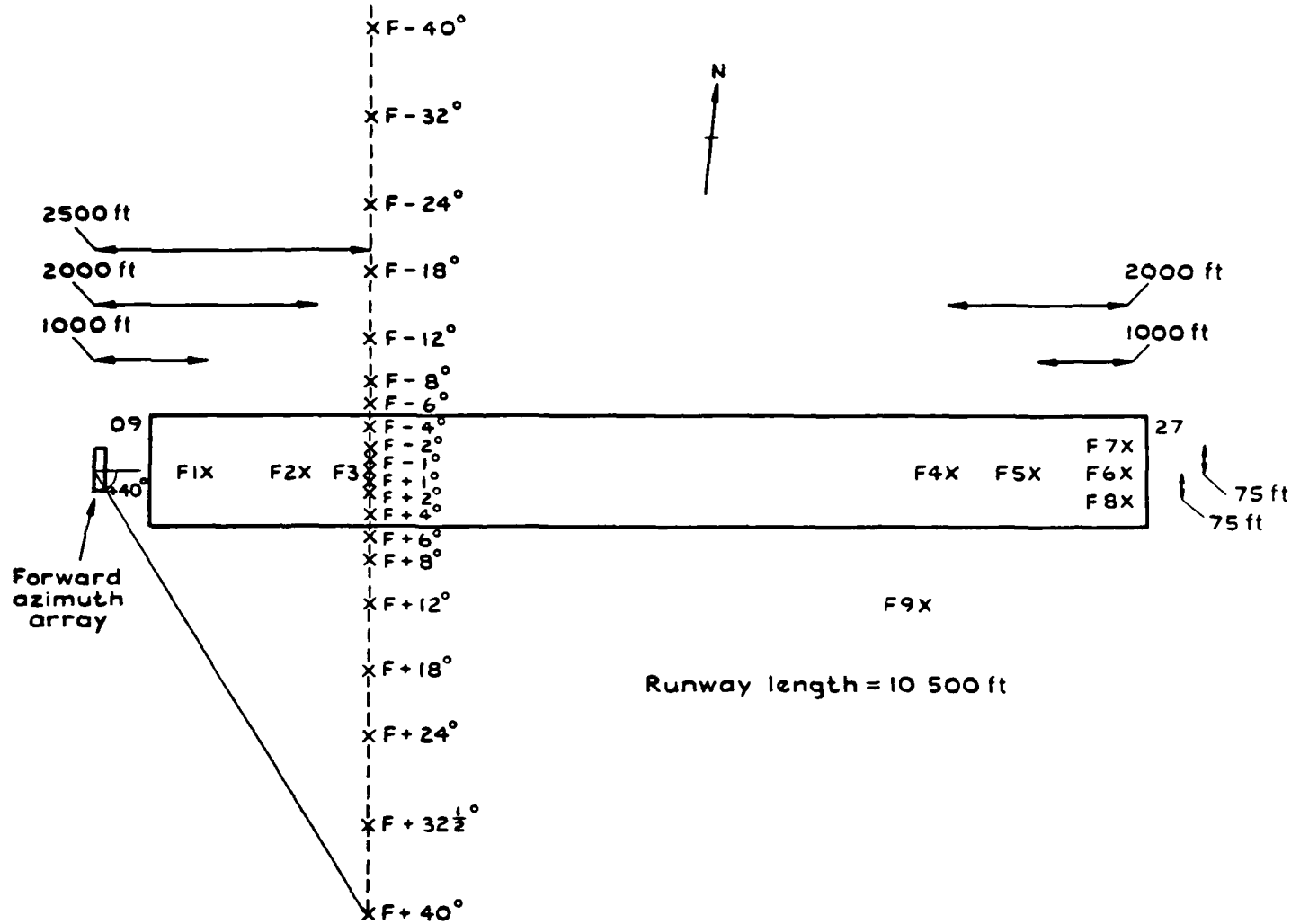

Fig B43 Approach azimuth static test point layout

TR 79052

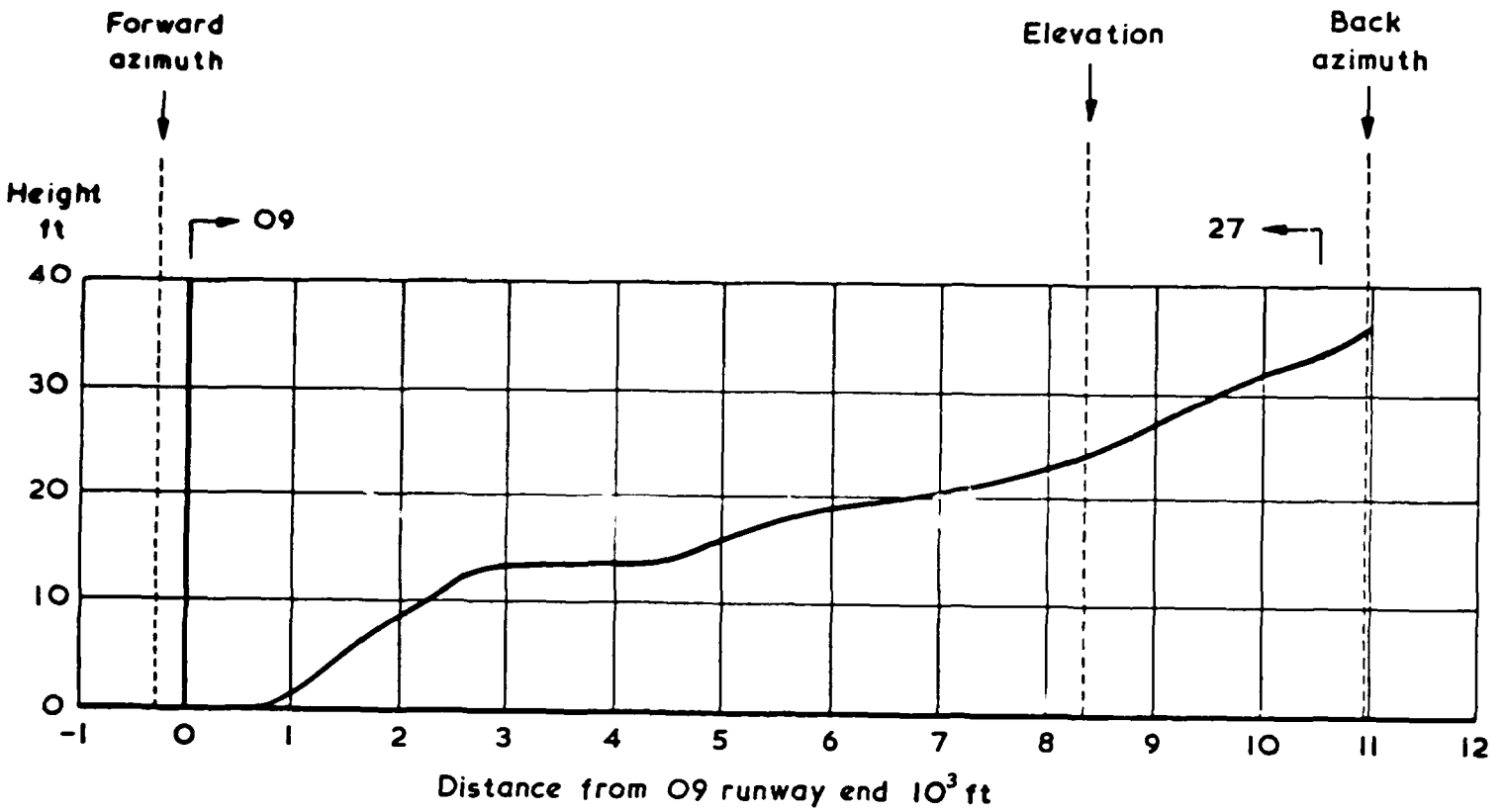

Fig B44 Approach azimuth minimum line of sight heights above local ground level

Fig B44

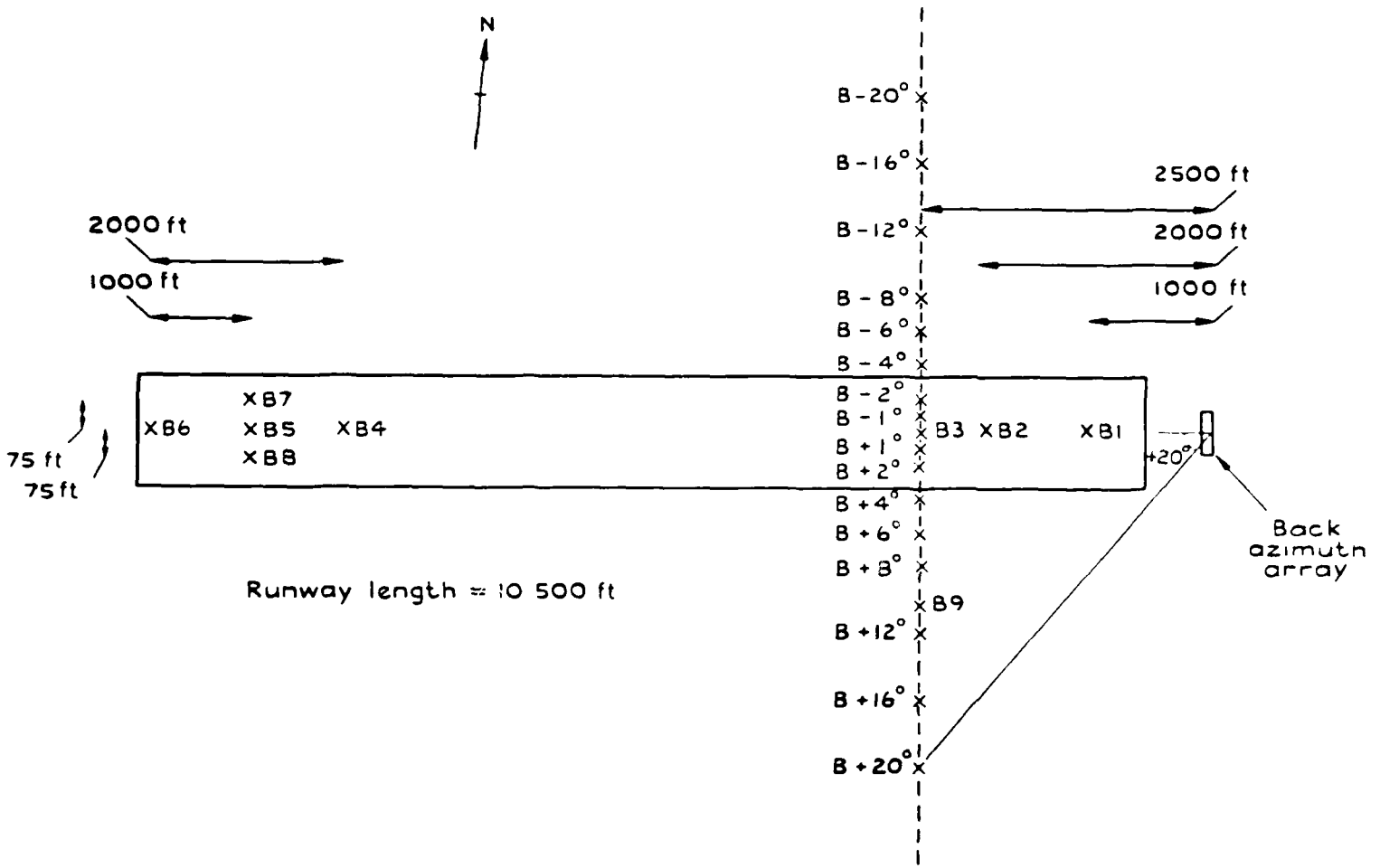

Fig B45 *Missed approach static test point layout*

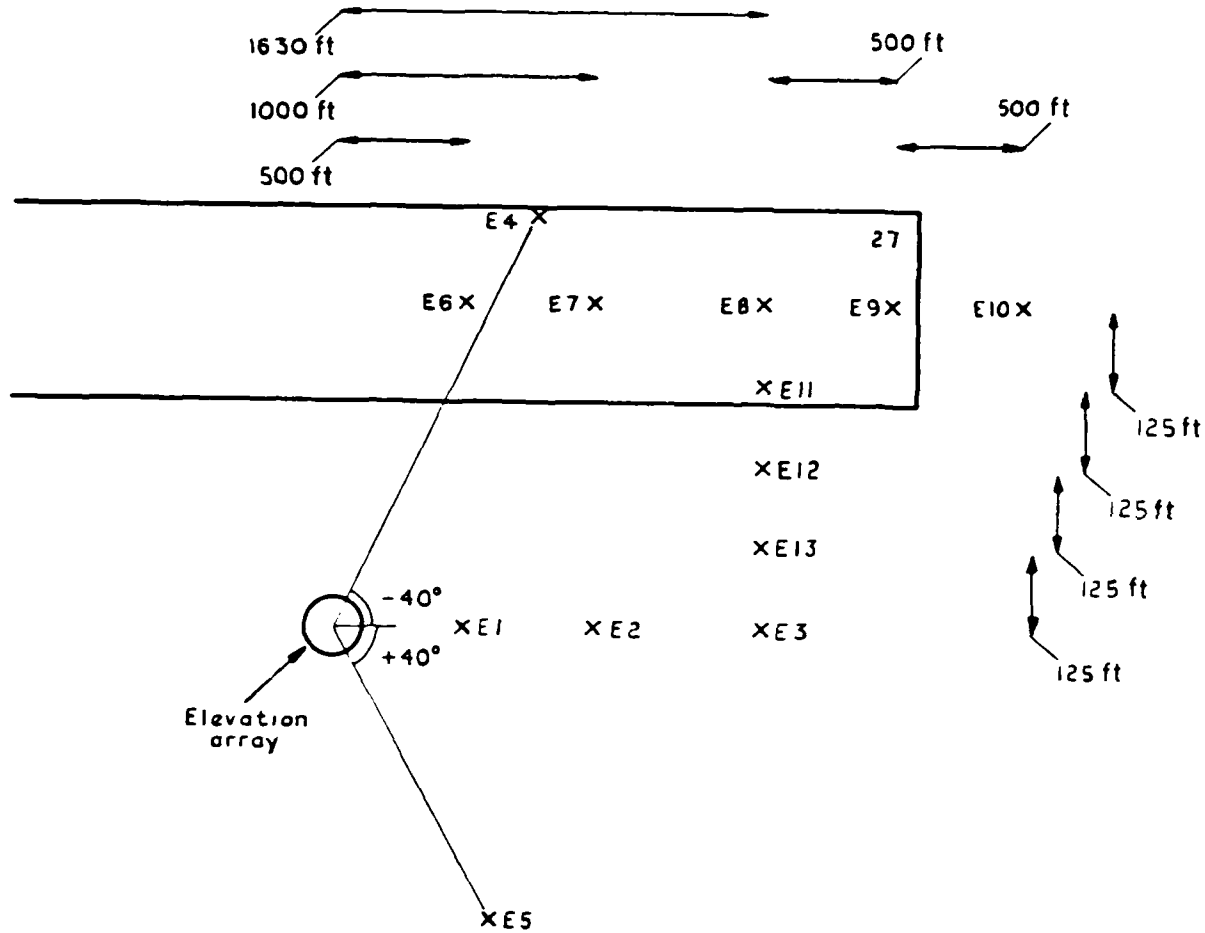

Fig B46 *Elevation static test point layout*

Fig B46

Appendix C

DATA REDUCTION TECHNIQUES AND STATISTICAL ANALYSIS METHODOLOGY

C.1 Introduction

This Appendix discusses the data recording techniques with particular relation to error sources and outlines the methods of data reduction, merging with tracking information and statistical analysis.

Sections C.2 to C.6 are concerned with angle data, whilst section C.7 discusses the recording of other relevant MLS information.

C.2 Analogue angle data recording

C.2.1 General

Similar analogue recording installations were provided in the ground test van and the aircraft. A general description of these systems is given in Appendix B. For ground measurements this was the prime recording system. For airborne measurements the analogue system was provided for 'quick look' and back up to the digital recording system.

C.2.2 Ground based measurements

Most FDM ground test information was recorded on a 7in wide analogue ultra-violet trace recorder, and, as the range of angle deviations at any test point was small, the following recording sensitivities were used:

(a) Approach azimuth and missed approach azimuth, 0.185° per 2 cm, which gave a 2 mm deviation per bit change of 0.0185° in the receiver angle output.

(b) Elevation, 0.0926° per 2 cm, which gave a 2 mm deviation per bit change of 0.00926° in the receiver angle output.

The paper was run at a speed of about 5.5 mm/s, which allowed clear identification of individual output up-dates.

The sources of possible error in the actual recording process were:

(a) Digital-to-analogue (D/A) converter errors in the receiver output, *ie* non uniform bit size.

(b) Recorder galvanometer zero errors and linearity errors.

79052

The D/A errors were a combination of bit size tolerance and zero offset and over the required dynamic range were less than ±0.25 bit. The system was

calibrated before each test run to eliminate sensitivity and zero errors and was checked at the end of each run to ensure it had remained stable.

For the TDM system ground measurements, a general recording sensitivity of 0.005^{o}/mm was employed.

C.2.3 Airborne measurements

In the airborne analogue recording, allowance had to be made for significant deviation about the nominal flight path, whilst a reasonably high sensitivity was desirable to show the general noise level and the presence of any discrete events.

For the FDM system the following sensitivities were selected with a paper speed of 5.5 mm/s:

(a) Approach and missed approach azimuth 0.185^{o} per 10 mm giving coverage to $\pm 1.3^{o}$ about the selected angle offset.

(b) Elevation 0.0926^{o} per 10 mm.

For the TDM system a general value of 0.1^{o} per 10 mm was used for azimuth and elevation.

C.2.4 Trace reading

For analysis of ground based measurements the analogue traces were read on a specialist trace reading machine coupled to an automatic card punch. The traces were read with a scale factor of 20 units/mm. Long experience with this type of machine has shown that trace reading errors were generally contained within ±5 units. In general the analogue information could be correctly re-quantised in the computer without loss of accuracy. It has been general policy to take all airborne angle data from the digital recorder. In an ideal situation a second digital recorder would have been available for the ground measurements.

C.3 Digital recording

The airborne digital recording system is described in Appendix B and Ref 13. This system recorded all relevant parameters from the airborne MLS receivers and necessary auxiliary data from the tracking system and flight observers. We were concerned here primarily with the recording of basic angle output data. The actual recording and playback process was protected by the use of standard parity checks. Errors could arise due to incorrect interrogation by the digital recorder system of the receiver output highway or from noise

pick up. These errors had a very low probability of occurrence and were identified by making a computer parity check between the digital angle output and the digital deviation output. Thus the MLS angle information derived from the digital recorder represented an undistorted history of the MLS receiver output with a high degree of confidence.

C.4 Tracking information

The basic reference system for all accurate measurements made in the evaluation of the UK Doppler Microwave Landing System was the optical kinetheodolite range tracking facility[11], Fig C1. The kinetheodolites were linked by cable to a central processing centre which gave a direct computer feed for on-line tracking in addition to providing synchronisation between the cameras. To achieve the full system accuracy and eliminate instrument operator tracking errors, film was taken for all MLS measurements. This procedure also allowed the detailed subsequent analysis of any outlying tracker data that occurred.

C.4.1 Sources of inaccuracy[12]

Here we are concerned with the errors that were expected in the data from the tracking system. The kinetheodolites were always used in the off-line mode, using film reading to retrieve the basic tracking data, which was then not contaminated by kinetheodolite operator target tracking errors. There were six basic possible sources of error remaining:

(a) Errors between the actual kinetheodolite telescope elevation and azimuth pointing angles and the values recorded on the film.

(b) Errors in the film reading of aircraft offset from the kinetheodolite telescope pointing angle (film frame centre).

(c) Errors arising from imperfect correction for a physical offset of the aircraft tracking lamp from the aircraft antenna due to yaw and pitch motion of the aircraft.

(d) Errors due to atmospheric refraction.

(e) Errors resulting from timing uncertainty between kinetheodolite shutter operation and the MLS receiver measurement period.

(f) Errors close to the system baseline due to the resolution of the kinetheodolite solution computer program.

79052

Errors in (a) were minimised by the mounting structures used for the Contraves instruments. By photographing range reference objects prior to each trial, absolute values for telescope pointing angles were maintained with confidence.

Film reading errors were probably the most significant source of inaccuracy, even when using a definite target such as the aircraft lamp provided for the MLS trials. The film reader resolution was sufficient to make this error very small, but it was found that the machine operator could not in practice align the reader to this resolution; moreover, the operator would make the alignment accurately on the perceived target centre which might be noticeably different between operators. This generated a bias error up to three times the value of the reading error standard deviation. Reading bias was minimised by having the same operator read both tracking data and the range reference objects (also lights) taken before the trial.

Where possible the aircraft tracking lamp was mounted close to the receiving antenna to minimise tracking errors due to aircraft attitude. In addition, a fixed correction for height difference, assuming normal flying attitude, was applied in the computer program used for the analysis of results. This program also corrected for aircraft yaw by estimating it from the velocities in the X and Y coordinates obtained from the kinetheodolite solution. No correction was made for drift or changing pitch during the flare manoeuvre. The errors due to displacement of the aircraft reading point from the antenna are considered in Appendix B.

The kinetheodolite solution program included a refraction correction ε_R, assuming a standard atmosphere, defined by the equation:

$$\varepsilon_R \simeq 23 \times 10^{-8} + \cos\theta(1 - 0.52 \times 10^{-5} r \sin\theta) \quad ,$$

where θ is the target elevation angle and r is the slant range.

Fig C2 shows that this correction was normally small, but became significant at long range. It should be noted that the C-band MLS radiation also suffered refraction during propagation through the atmosphere; no compensation was made, however.

The kinetheodolite shutter pulse together with the frame identification number was transmitted to the aircraft on a UHF data link. For data processing economy the kinetheodolite film was read at a 1 Hz rate, although film was taken at a 5 Hz rate. In the results analysis computer program linear interpolation was used between successive kinetheodolite data points, which were provided with no smoothing, to generate a 5 Hz update of aircraft position. Interpolation within each resulting 200 ms period using kinetheodolite derived velocities was

then used to produce data for aircraft position at the end of each MLS receiver measurement period to a relative timing of 6 ms. Synchronisation between receiver output and tracking data was therefore maintained to a few milliseconds and this source of error was correspondingly small. A flywheel within the results analysis program was incorporated to cater for any transient corruption of frame identification that occurred in the synchronising UHF data link.

As the kinetheodolite telescope pointing angles closely approach the system baseline, the limit of precision of the solution computer program had inadequate word length to achieve the desired accuracy. The effects of this, coupled with the basic angle errors magnified by the unfavourable geometry for points close to the baseline, may be seen on the ground static and ground dynamic approach azimuth sub-system test results, and on azimuth flight roll out data. This, however, was an unusual condition and applies only to near ground level measurements close to the baseline.

Although it is difficult to quantify the sources of error individually, operation of the tracking facility over several years has shown that by using the off-line film reading method errors considerably less than 10" (1σ) were consistently achieved for both elevation and azimuth telescope pointing angles. It was further observed that system errors were predominantly biases, the short term tracking error noise being low.

C.4.2 Cartesian coordinate error contours

As seen in the previous section, errors in tracking were predominantly due to film reading and uncertainty in the measurement of the kinetheodolite telescope position. It has been found by experience over several years' operation that the telescope elevation and azimuth angles are measured with confidence to better than 10" (1σ), equivalent to 0.00278°. This value was used to produce the contours given for the cartesian coordinate errors in Figs C3 through C7.

Figs C3 to C5 give the X, Y and Z coordinate errors respectively in the horizontal plane at zero altitude. The errors are presented in plan on a ±20 n mile grid about the airfield, with the runway positions drawn in the centre of each figure. Due to the rotation of the coordinates from the kinetheodolite baseline to the runway direction, the contours are not symmetrical about the instrument baseline.

79052

X and Y coordinate errors varied slowly as the altitude increased. At 610 m (2000 ft) altitude the errors computed were virtually identical with those

obtained at zero altitude. At 3050 m (10000 ft) a small degradation was observed. This is shown for the error occurring in the X and Y coordinates in Figs C6 and C7 respectively.

C.4.3 Polar coordinate accuracy

As it was necessary to produce polar coordinates to evaluate the MLS performance, it is advantageous to see the tracking system accuracy in this form. Fig C8 gives the kinetheodolite facility 1σ error for the measurement of azimuth angle on the boresight of the approach azimuth sub-system (runway centreline). Except at positions very close to the kinetheodolite baseline, where the error was large and unpredictable, it is seen that the system accuracy is more than adequate for proper assessment of the approach azimuth sub-system. The error is seen to be approximately 0.002^{o} (1σ) for ranges above 2 n mile from the approach azimuth antenna (i.e. at all aircraft positions further than the runway threshold). The error, except for very close ranges, did not vary significantly with change in aircraft altitude. The range measurement error (1σ) given in Fig C9 shows a more marked change, as expected, at high aircraft altitudes. Accuracy was also adequate for the MLS evaluation, being only approximately 0.2% of the range at 20 n mile distance.

The elevation angle error (1σ) along the elevation sub-system boresight is given in Fig C10. Although of slightly greater magnitude than the azimuth error previously presented, it is seen to be perfectly adequate being approximately 0.003^{o} (1σ) for an aircraft approach down to 1 n mile range from threshold and rising to approximately 0.005^{o} (1σ) at threshold.

The calculations made to present Figs C8 to C10 include the uncertainty in the measurement of the approach azimuth and elevation sub-system antenna centres and, therefore, represent the total errors of the kinetheodolite facility.

C.4.4 Close range surveying errors

It is also necessary to consider the close range accuracy of the kinetheodolite facility to assess its performance when used as a surveying tool for the location of ground static test positions. This applied in particular to the elevation sub-system and its associated test points as these measurements were all made at short range. The critical parameter for this sub-system was clearly the location of the test points on the Z axis (vertical). The elevation sub-system antenna centre, being the origin used for MLS sub-system test, was measured to an accuracy of 0.0302 (0.099 ft) standard deviation in the vertical. Since the elevation test points were all closely spaced in the same region of

the airfield as the elevation antenna, they would have been surveyed by the kine-theodolite installation to approximately the same accuracy. By taking the root-sum-square value of the vertical displacement errors of locating the elevation antenna centre and the test point considered, the vertical displacement error (1σ) that will be made in locating the test point with respect to the elevation antenna was 0.043 m (0.14 ft). As the test points vary in range from 152 m (500 ft) to 812 m (2664 ft) from the elevation antenna the accuracy of elevation angle measurement made with respect to this varied from 0.016° (1σ) at the closest test point to 0.003° (1σ) at the furthest.

C.5 Merging of MLS and tracking data

C.5.1 Digital recording system

When using the digital recorder[13], which was the prime form of airborne recording, the actual kiné frame number was transmitted to the aircraft on a UHF data link and recorded directly on the digital recorder together with a pulse coincident with the operation of the camera shutter. The recorder tape information was transferred to a type compatible with an ICL 1900 series computer and then merged with data from the tracking information tape. In the event of data link drop outs, when the shutter pulses were not available, the merging continued with the shutter pulses estimated by a 'flywheel' process until the pulses were received again. The recorder format included absolute timing information relating the kiné shutter pulse to the receiver counting period to an accuracy of 6 ms. In the merging process the kiné data was interpolated with respect to the update time of the receiver output stores. The relative timings are illustrated in Fig C11. From Fig C11 it can be seen that in the hybrid FDM/TDM format there was an inherent delay of 100 ms in the availability of the angle information; this delay was effectively the average value over the 200 ms measurement period. As this delay was inherent in the hybrid FDM/TDM format, no compensation was made, except as stated below. In the TDM format the longest measurement period was 50 ms, giving an output delay of 25 ms. The magnitude of any angle error resulting from these delays depended on the rate of change of angular position of the aircraft. Plots of error as a function of rate of change of angle are given in Fig C12 for the two signal formats. From Fig C12, it can be seen that the effects were small, for a normal radial flight profile, except for the elevation system at high angles and short ranges, and for the azimuth system when passing close to the array, where high rates of change of angle were obtained.

C.5.2 Ground measurement information - dynamic

Dynamic ground information recorded in the test van was processed in exactly the same way as airborne digital recorded data.

C.5.3 Ground measured information - statics

The 10 s samples of static data derived from the analogue records were initially recorded on punched card together with the relevant survey data. This information was then processed in a computer to give the statistical analysis and output format called for by AWOP Working Group A. Some static monitor information was recorded digitally.

C.6 Data reduction and analysis[14]

C.6.1 General

The overall flow diagram of the complete data processing system is shown in Fig C13. The data analysis which is detailed below, followed the general requirements laid down by AWOP Working Group A at the September 1974 and February 1975 meetings. The basis for all statistical analysis was the raw unfiltered error signal defined as

$$e = P_{system} - P_{reference} ,$$

where P_{system} was the MLS measured value at time t, and $P_{reference}$ was the reference value at time t. The latter was either a survey point or given by the tracking system.

In all of the statistical calculations it was assumed that the error was due to the MLS only, *ie* perfect reference values were assumed. Where errors were known to exist in the reference system, their effects are discussed in the relevant results section. As the basic update rate of the DMLS FDM and TDM equipment was 5 Hz, the error signals were used directly for statistical purposes with *no* filtering or averaging.

The censoring criteria suggested by WGA were interpreted and applied to the FDM results as follows:

(i) When the difference between the mean of the previous five values and the current measurement was greater than 0.2°, the previous value replaced the measurement.

(ii) When consecutive points were censored, the second to fifth points inclusive were each compared with the mean of previous five (including censored

values) and replaced by the mean if the difference exceeded 0.2^{o}. A break in the data sequence occurred if a sixth point exceeded the criterion. To start a run the first five points were lost in producing a running mean. Each censored point was flagged by a T at the top of the graph.

(iii) In the TDM system a rate limit of 0.2^{o} per update was incorporated in the receiver processor.

C.6.2 Analysis of each sample of data

For the purpose of basic statistical analysis a standard sample of 50 consecutive data points was used, giving a measurement period of 10 s.

C.6.2.1 Mean of a sample

The mean of the measurement was defined as

$$m = \frac{1}{50} \sum_{i=1}^{50} e_i$$

where e_i was the error value of the ith data point in the measurement. The mean m gave an estimate of the bias error in the region of the measurement.

C.6.2.2 Standard deviation of a sample

A measurement of the error noise was given by the standard deviation of the measurement defined as

$$s = \sqrt{\frac{1}{49} \sum_{i=1}^{50} (e_i - m)^2}$$

C.6.2.3 Percentiles

A measure of the distribution of the error values contained in one measurement sample was given by the limits within which 95 per cent of the individual error values fell, *ie* the 2.5 and 97.5 percentiles. All the error points of a measurement sample were ordered according to their magnitude, and cumulative frequencies were assigned to these magnitudes. If e_1 was the smallest value in the sample, e_2 the second smallest, ... e_{50} the largest, then each error value e was associated with a cumulative probability of $(i + 0.5)/50$. None of the e_i were associated with the value of 2.5 or

97.5 per cent so it was necessary to interpolate. If P_j and P_k were the associated probabilities nearest to the desired level P and e_j and e_k the corresponding measurements ($P_j < P < P_k$), then percentiles were evaluated by

$$e_p = (e_k - e_j) \frac{(P - P_j)}{P_k - P_j} + e_j \quad ,$$

referring to Fig C14. This method preserved the symmetry about the central 50 per cent value so that, if the data were symmetric about some central value, the 2.5 and 97.5 percentiles would have been equally spaced about that value.

C.6.3 Treatment of repeated or lumped measurements

The results from a series of measurements within one flight segment or a coverage volume as appropriate could be gathered together to give the following lumped parameters. If k was the number of samples, then the overall mean was

$$M = \frac{1}{K} \sum_{i=1}^{k} m_i$$

and the standard deviation of the individual mean was

$$S = \sqrt{\frac{1}{K - 1} \sum_{i=1}^{k} (m_i - M)^2} \quad ;$$

this gave an indication of the bias spread within the segment or volume. A root-mean-square (rms) noise value could also be determined as S_0 , where

$$S_0^2 = \frac{1}{K} \sum_{i=1}^{k} S_i^2 \quad .$$

This gave a good indication of the guidance noise from a series of measurements within a segment or volume independent of the bias term.

Also of interest was the standard deviation of all the single data points with respect to the flight segment mean, which was defined as S_T , where

79052

$$S_T^2 = \frac{1}{50K - 1} \sum_{i=1}^{50K} (e_i - M)^2 \quad .$$

This gave an indication as to the consistency of the basic data throughout each flight segment.

C.6.4 Treatment of multipath results

Dynamic multipath data was processed through a number of standard filters in order to isolate, to some extent, the effects of the MLS signal on actual aircraft movement (path following error), control motion noise and rate noise.

These effects were determined by passing the time error records through the standardised filters, which were based on a wide range of existing aircraft response properties. The three filter transfer functions were:

(a) Path following error

$$H(s) = \frac{\omega_n^2}{S^2 + 2\omega_n S + \omega_n^2}$$

where $\omega_0 = 0.64\ \omega_n$.

(b) Control motion noise

$$H(s) = \frac{S}{S + \omega_1} \frac{\omega_2}{S + \omega_2} \quad .$$

(c) Rate effects

$$H(s) = \frac{S}{S + \omega_3} \frac{\omega_4}{S + \omega_4} \quad .$$

The critical frequencies are defined in Table C1.

Table C1

Critical frequency for multipath filters

Function	Critical frequencies rad/(s Hz)					
	ω_0	ω_n	ω_1	ω_2	ω_3	ω_4
Azimuth	0.5-0.08	0.78-0.12	0.3-0.05	10-1.59	2-0.32	4-0.64
Elevation	1.5-0.24	2.34-0.37	0.5-0.08	10-1.59	2-0.32	4-0.64
Flare	2.0-0.32	3.13-0.50	0.5-0.08	10-1.59	2-0.32	4-0.64
Range	2.0-0.32	3.13-0.50	0.5-0.08	10-1.59	2-0.32	4-0.64

For simulator measurements relevant to motion averaging these filters have been implemented in analogue form, while for analysis of the results of dynamic ground and flight multipath data the filters have been implemented in a digital form.

Before filtering, the data was edited to eliminate any blemishes due to faults in the recording and tracking system (*eg* parity errors on the magnetic tape). Small gaps, of not more than five points, caused by such events were bridged by linear interpolation. (This was the only case in which 'manufactured' data was used.) Then all points, for which the MLS receiver flag was on, were deleted; after that any sequences of less than six consecutive points were removed. The remaining sequences of points were censored, as described elsewhere, and then filtered for path following error, control motion noise and rate noise.

AWOP Working Group A suggested the following recurrence relations for the digital filters:

(a) For path following error

$$Y_n = \left\{\omega_n^2T^2\left(X_n^2 - 2X_{n-1} + X_{n-2}\right) + \left(8 - 2\omega_n^2T^2\right)Y_{n-1} - \left(4 - 4\omega_nT + \omega_n^2Y^2\right)Y_{n-2}\right\}\Big/\left(4 + 4\omega_nT + \omega_n^2T^2\right) ,$$

where X_1, X_2, ..., were successive error values, sampled at intervals T, and Y_1, Y_2, ..., were successive filtered values.

79052

(b) For control motion noise

$$Y_n = 2\omega_2 T(X_n - X_{n-2}) + \left(8 - 2\omega_1\omega_2 T^2\right)Y_{n-1} - \left(4 - 2\omega_1 T - 2\omega_2 T + \omega_1\omega_2 T^2\right)Y_{n-2} \Big/ \left(4 + 2\omega_1 T + 2\omega_2 T + \omega_1\omega_2 T^2\right) .$$

(c) For rate noise the same equation was applied with ω_3 and ω_4 instead of ω_1 and ω_2 .

There was a pitfall here. It would have been natural to set T equal to the data interval, 0.2 s, and then have taken successive experimental differences as the X_n . However, the highest critical frequency ($\omega_2/2\pi$) was 1.59 Hz, uncomfortably close to the filter response around ω_2 to be somewhat inaccurately implemented. In fact, T = 0.2 s was too long an interval for use in the given equations.

We cannot say how inaccurate they would have been without making some assumption as to how the data was interpolated between the measured values. We assumed that the filter input was held constant during each 0.2 s period, [illegible] a 'sample and hold' waveform. It would have been possible to have set T as small as we pleased and to have used the above recurrence relations, filling in the X values as required. This would have been an unintelligent use of a computer, since with the assumed interpolation rule there were recurrence equations which were perfectly accurate and used the original 0.2 s period. These were

For path following error:

$$Y_n = AX_n + BX_{n-1} + CY_{n-1} + DY_{n-2} ,$$

where $A = 1 - (1 + a)e^{-a}$

$B = (a + e^{-a} - 1)e^{-a}$

$C = 2e^{-a}$

$D = -e^{-2a}$

$E = -e^{-2a}$

$a = \omega_n T$.

For control motion noise:

$$Y_n = A(X_n - X_{n-1}) + BY_{n-1} + CY_{n-2} \quad ,$$

where $A = a_2\left(e^{-a_1} - e^{-a_2}\right)\Big/(a_2 - a_1)$

$B = e^{-a_1} + e^{-a_2}$

$C = -e^{-(a_1+a_2)}$

$a_1 = \omega_1 T$

$a_2 = \omega_2 T$.

For rate noise, the same formulae apply with ω_3, ω_4 instead of ω_1, ω_2 .

These were the equations actually used, with T = 0.2 s.

To start off the iteration it was necessary to preset the values of X_{n-2}, Y_{n-1} and Y_{n-2} . The simplest procedure would have been to set these to zero; in general this would have caused an initial transient whose longest time constant was $(1/\omega_2) \triangleq 3.3$ s .

To minimise the transient, X_{n-2}, Y_{n-1} and Y_{n-2} were set equal to the mean of the first data values, X_1 to X_5 . This amounted to assuming that the filter input had been constant at this value for an infinite time. The same starting procedure was used following gaps in the data, when these gaps were more than 1 s; there was no memory of prior sections.

C.7 Associated information

The associated MLS information consisted of receiver flag signals, signal strength etc. Flag signals were on/off in nature and needed no calibration with respect to recording. Signal strength information was obtained from the receiver automatic gain control voltage, which was calibrated using a special purpose RF test set. All the associated information was recorded on the digital recorder and a suitable selection relevant to each flight was recorded on the analogue recorder. In general, signal strength information was derived from the analogue recorder for coverage measurements and from the digital recorder for multipath plots.

Receiver AGC was calibrated before each test series, experience has shown the stability to be within ±2 dB over normal trials temperature changes. Signal

strength traces could be read to an absolute accuracy of ±2 dB and a relative accuracy between two levels of ±1 dB.

C.8 Presentation of results

The presentation of results followed the requirements of AWOP Working Group A. In particular, care was taken to maintain the standard scale factors adopted by the Working Group. Where a choice of presentation was permitted, the form giving greatest clarity was adopted.

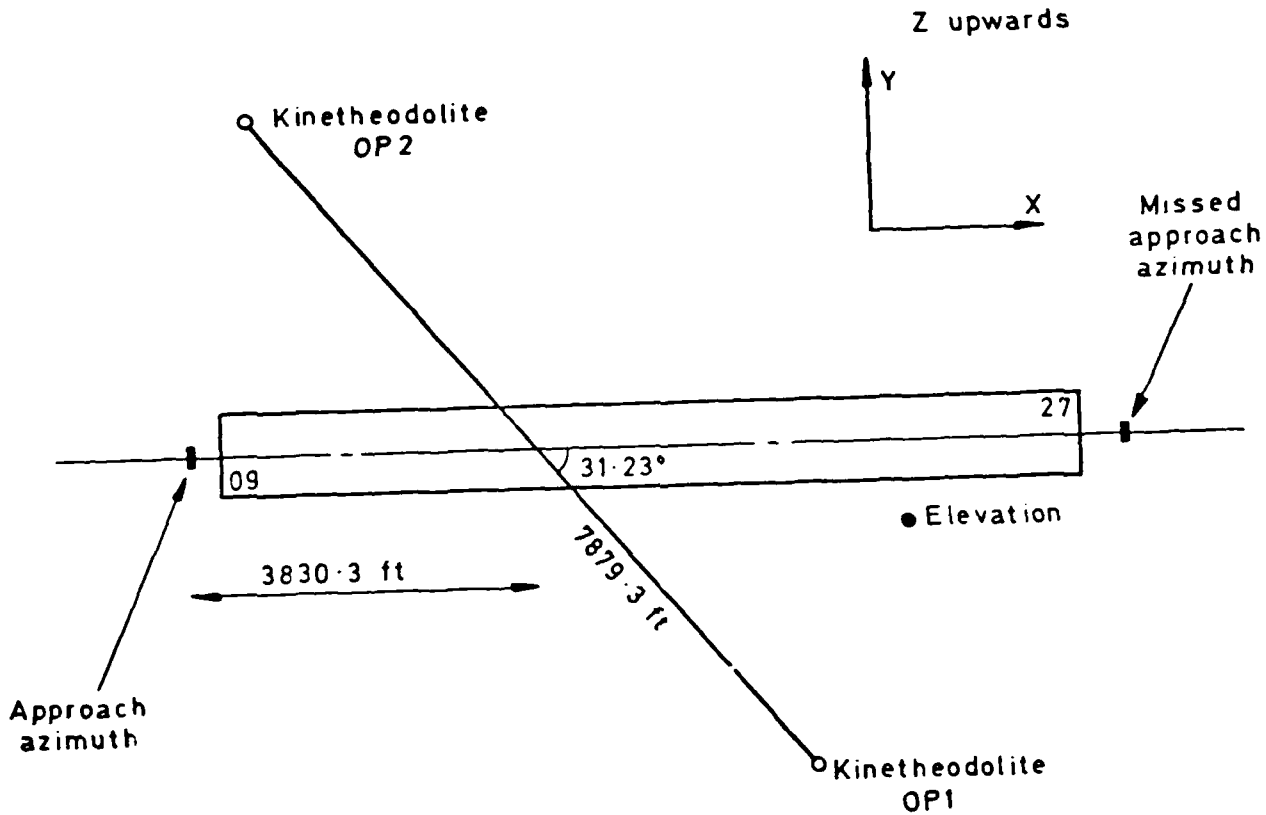

Fig C1 Kinetheodolite facility geometry

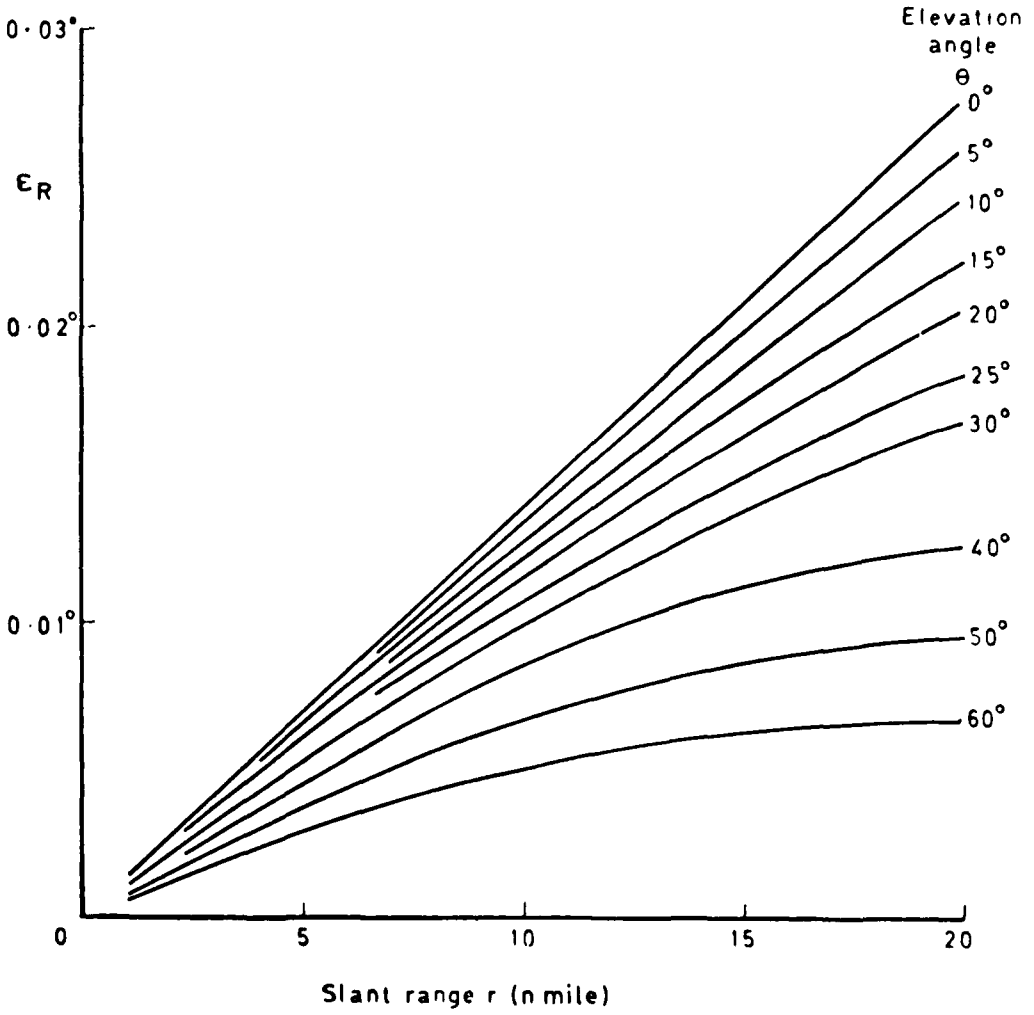

Refraction error, $\varepsilon_R \simeq 23\times10^{-8} + \cos\theta\,(1-0{\cdot}52\, r \sin\theta \times 10^{-5})$

– standard atmosphere, 10°C, 1013 millibars

TR 79062

Fig C2 Optical refraction error

Fig C3

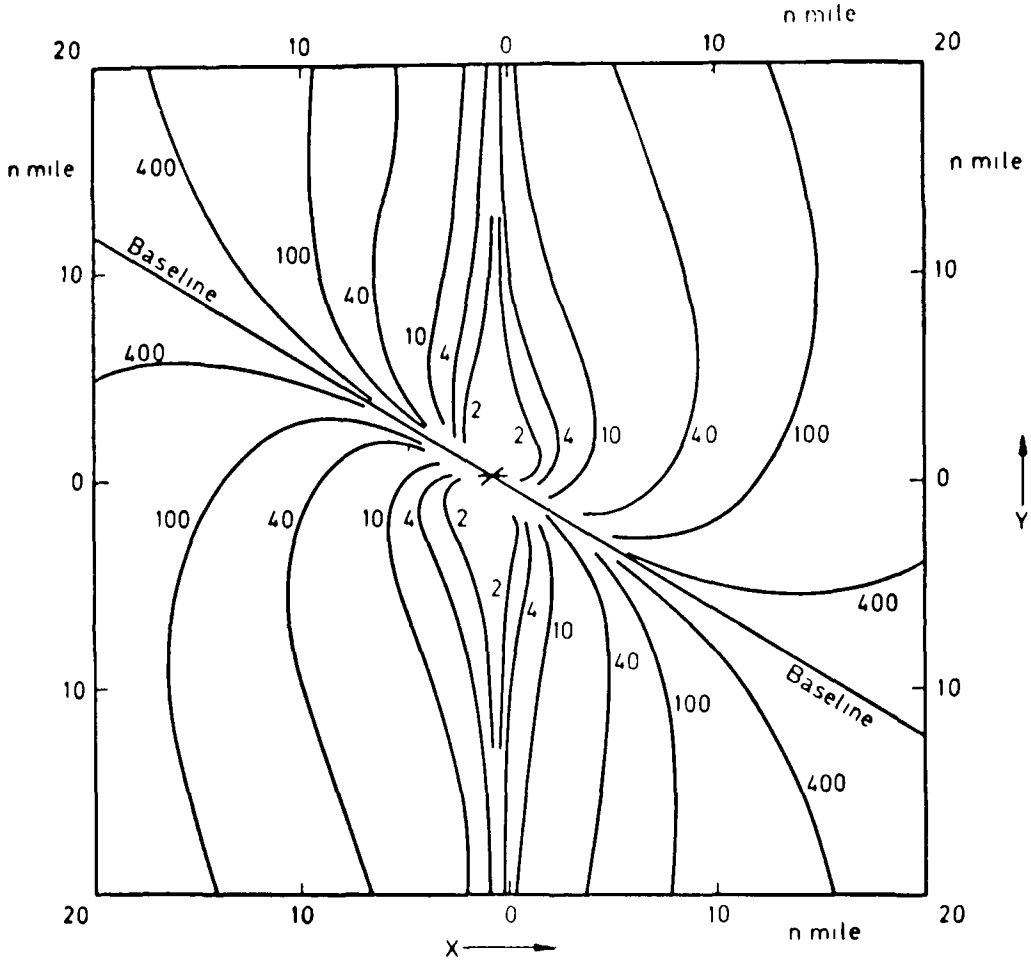

X coordinate error in ft
Error plan given in the horizontal plane at zero altitude, centred on elevation subsystem

TR 79052

Fig C3 Kinetheodolite X coordinate error contours

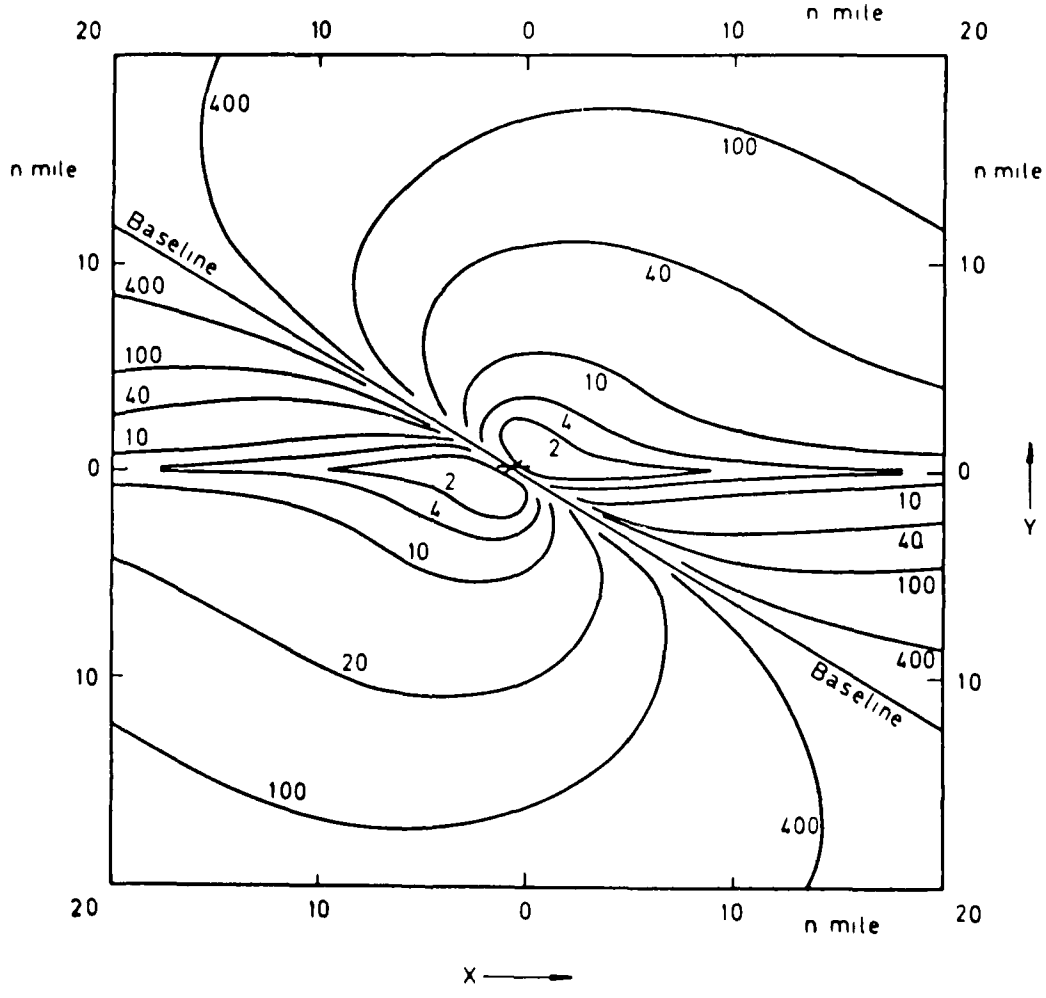

Y coordinate error in ft

Error plan given in the horizontal plane at zero altitude, centred on elevation subsystem

TR 79052

Fig C4 Kinetheodolite Y coordinate error contours

Fig C5

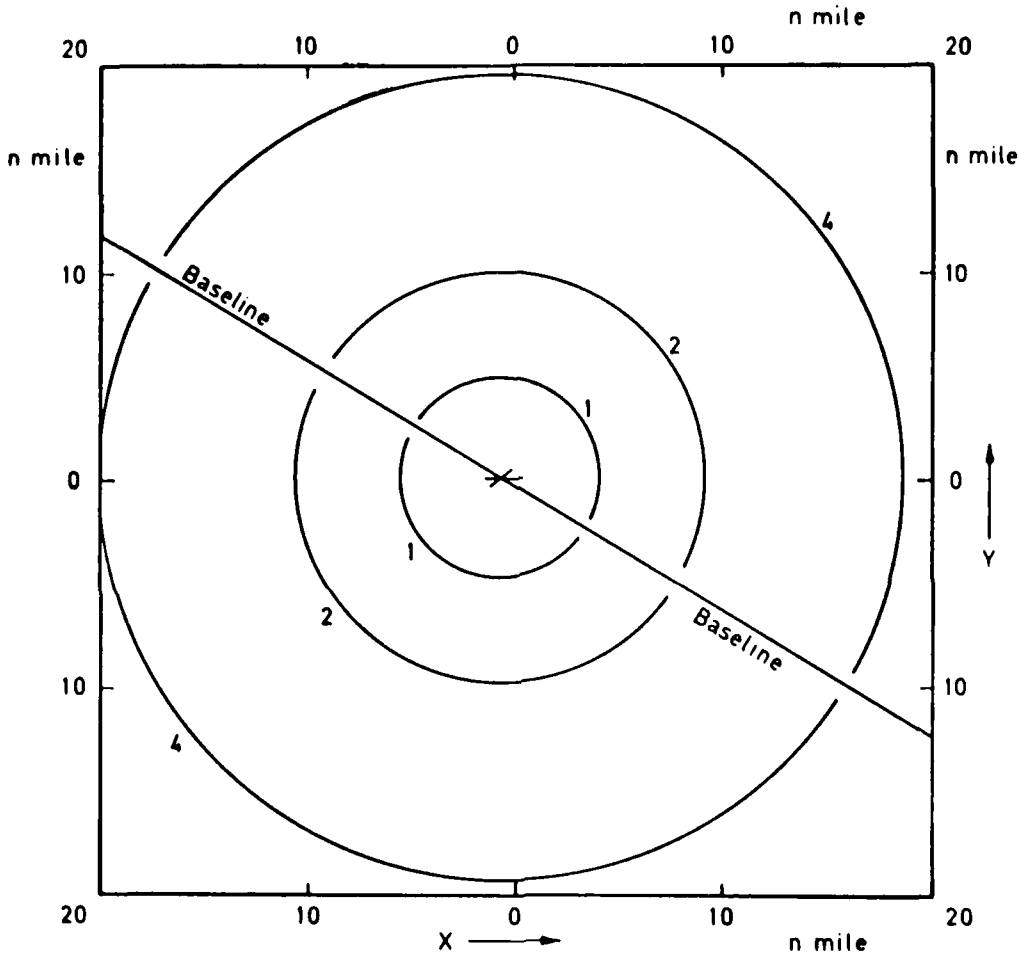

Z coordinate error in ft

Error plan given in the horizontal plane at zero altitude, centred on elevation subsystem

Fig C5 Kinetheodolite Z coordinate error contours

TR 79052

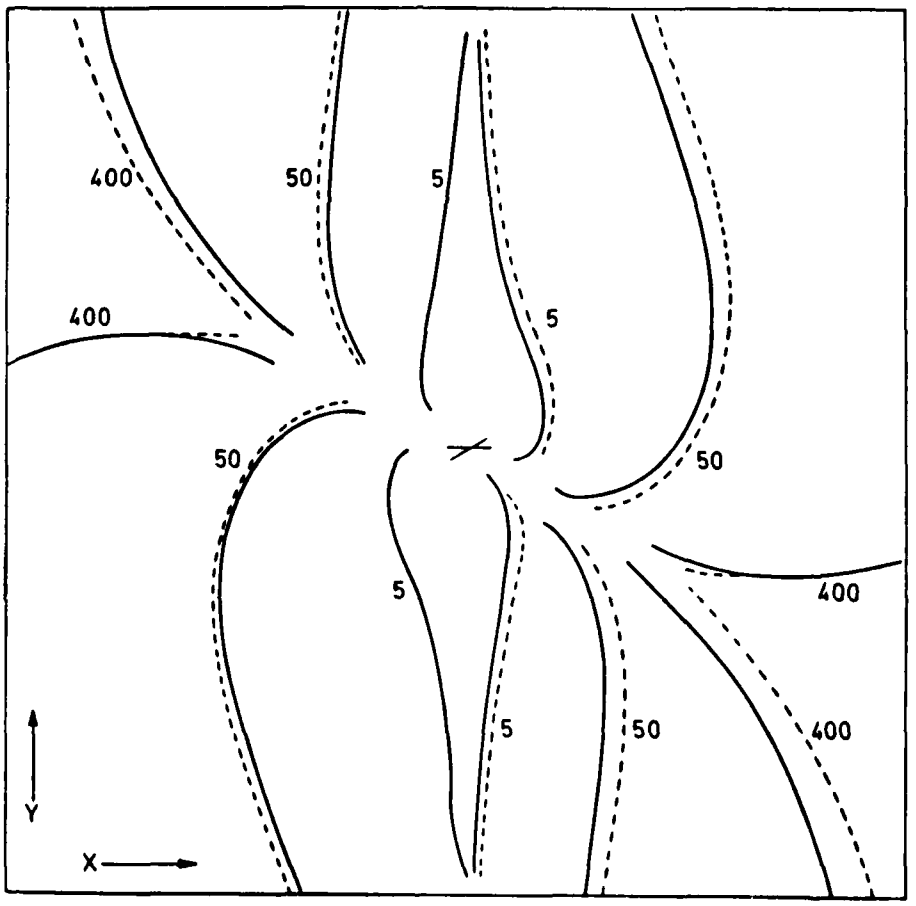

X coordinate error in ft

Error plan for 40 n mile square given in the horizontal plane, centred on elevation subsystem

——— Error at zero altitude

– – – – – Error at 10000 ft altitude

TR 79052

Fig C6 Kinetheodolite X coordinate error contours

Fig C7

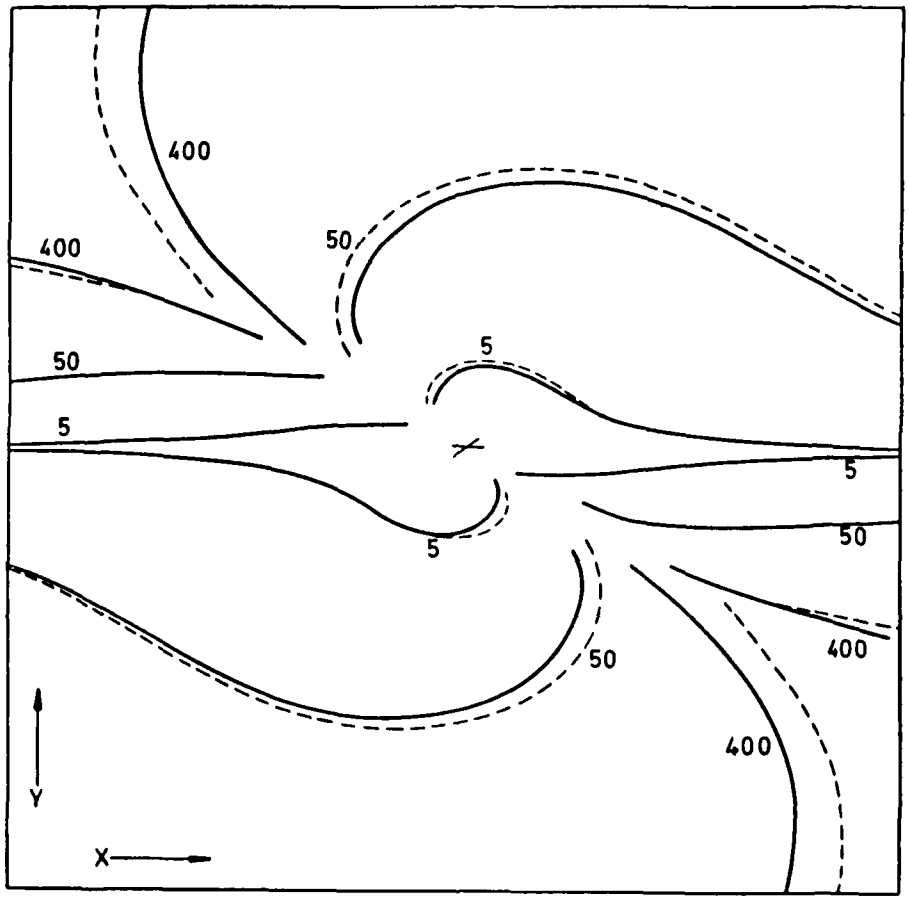

Y coordinate error in ft

Error plan for 40 n mile square given in the horizontal plane, centred on elevation subsystem

——— Error at zero altitude

– – – – Error at 10 000 ft altitude

Fig C7 Kinetheodolite Y coordinate error contours

TR 79052

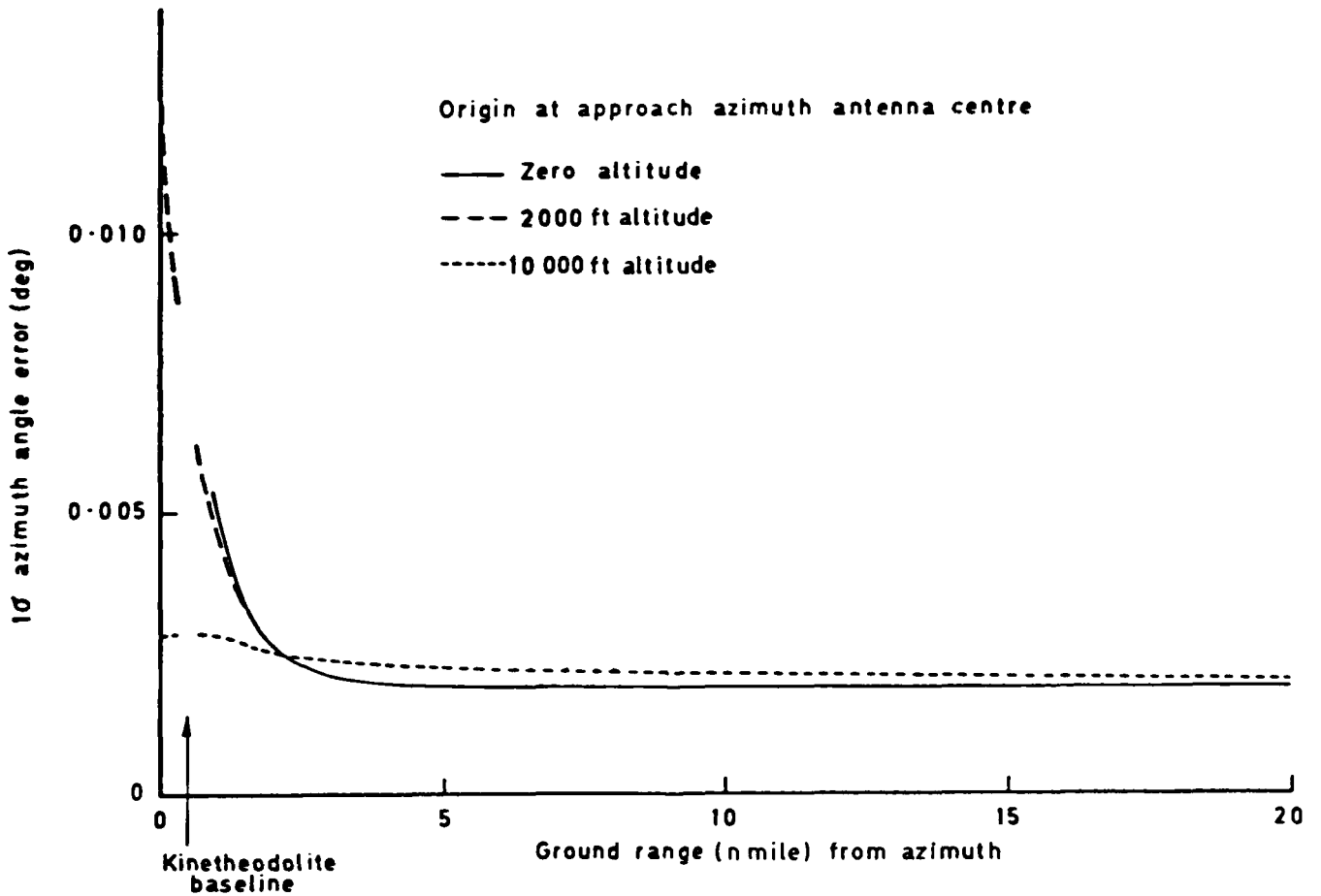

Fig C8 Kinetheodolite facility azimuth error on approach azimuth boresight

Fig C8

Fig C9

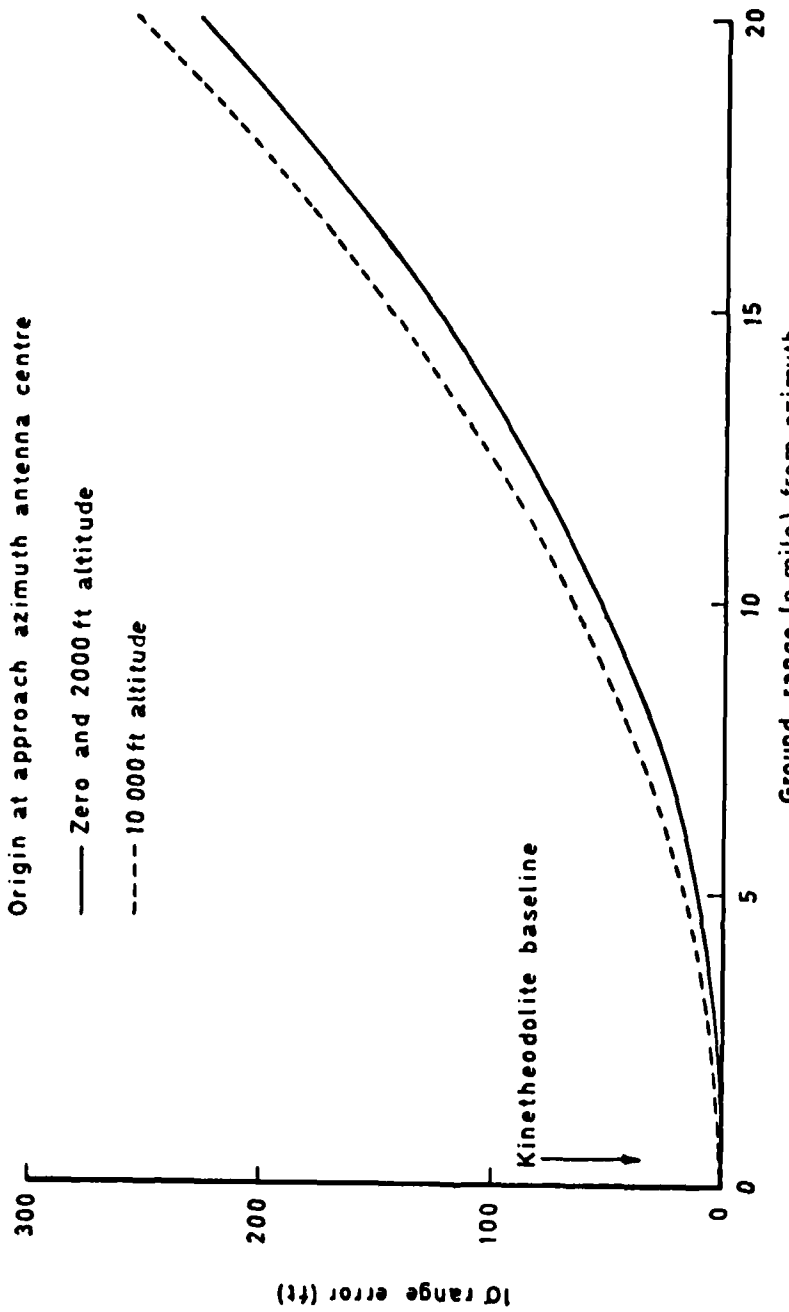

Fig C9 Kinetheodolite facility range error on approach azimuth boresight

TR 79052

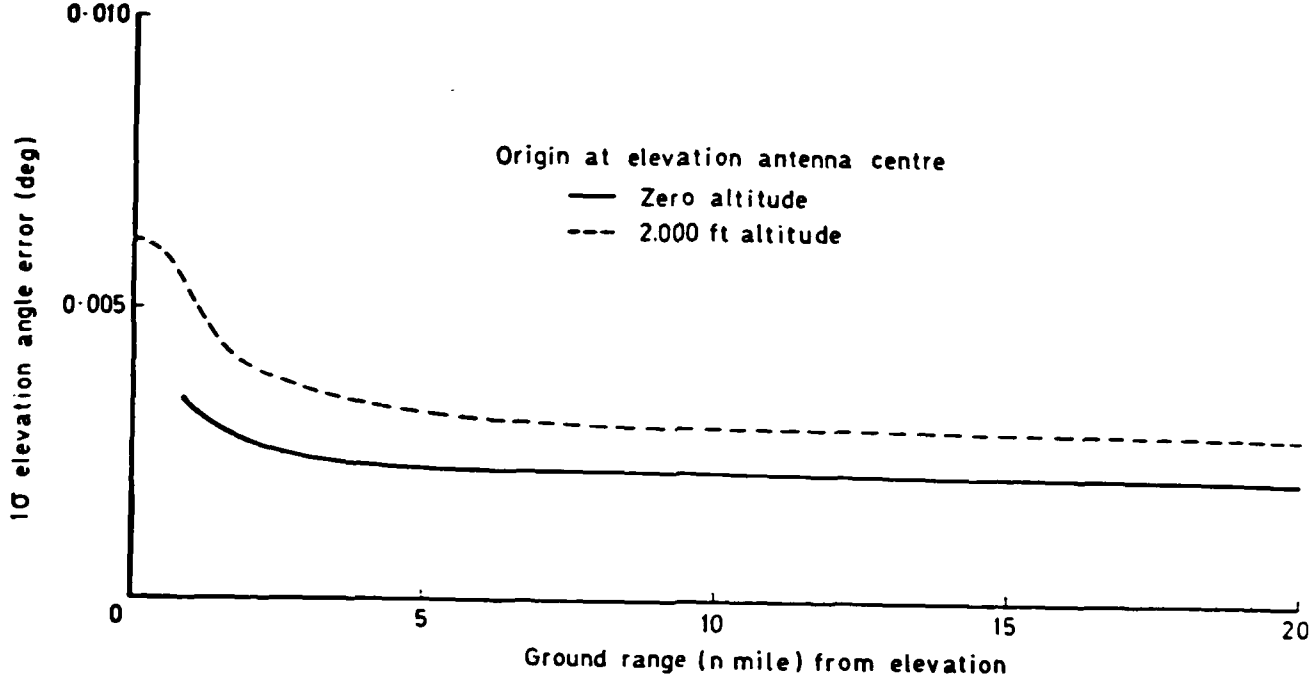

Fig C10 Kinetheodolite facility elevation error on elevation sub-system boresight

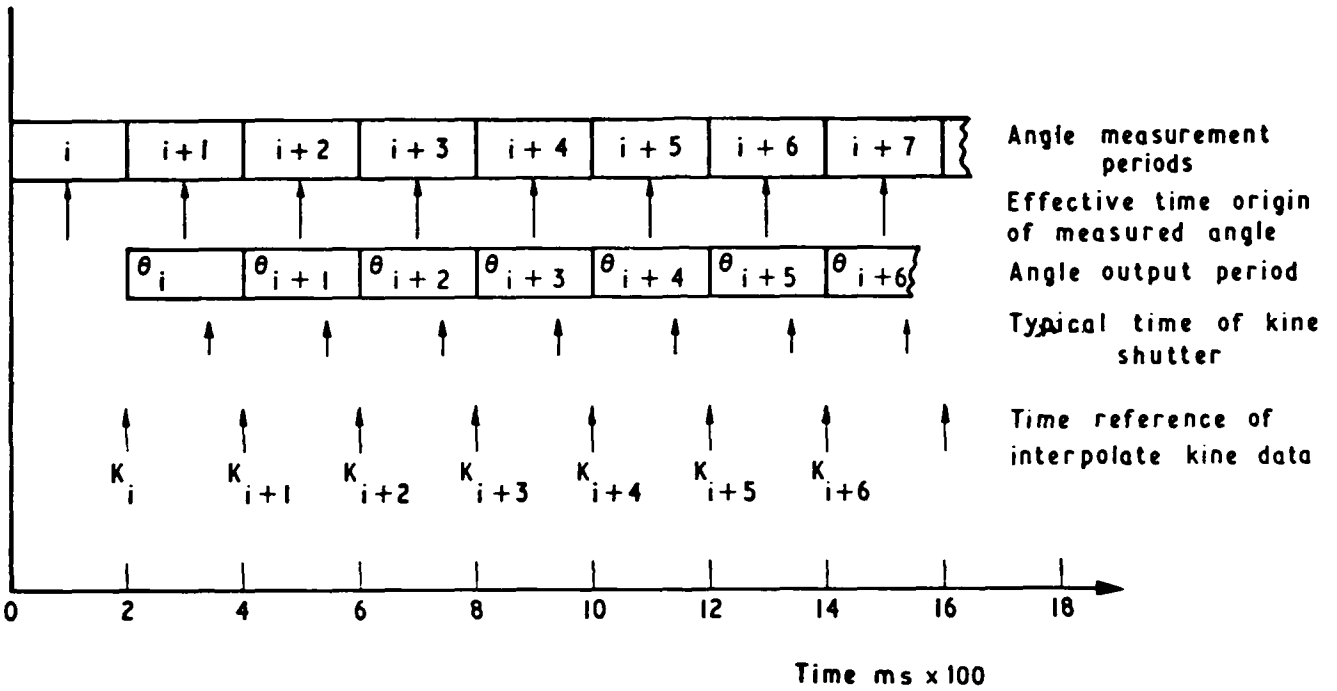

Fig C11 Timing relationships for angle and tracking data

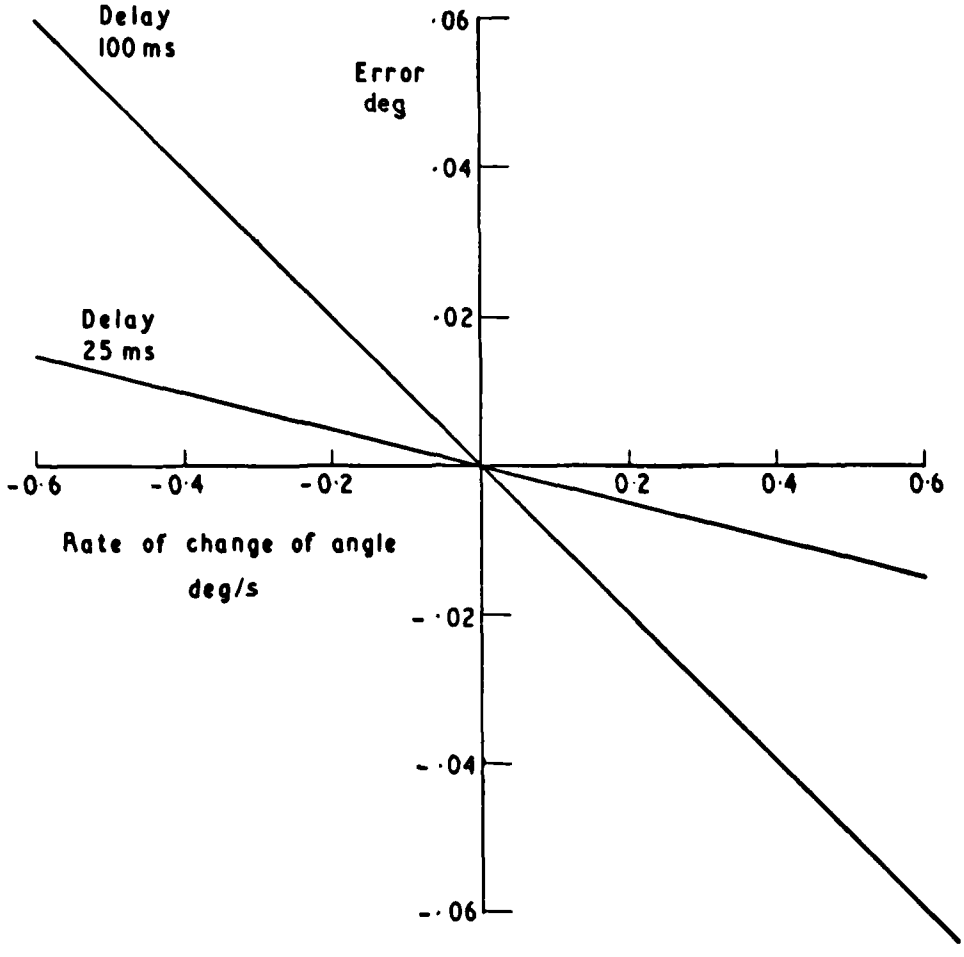

TA 79052

Fig C12 Effects of rate of change of angle

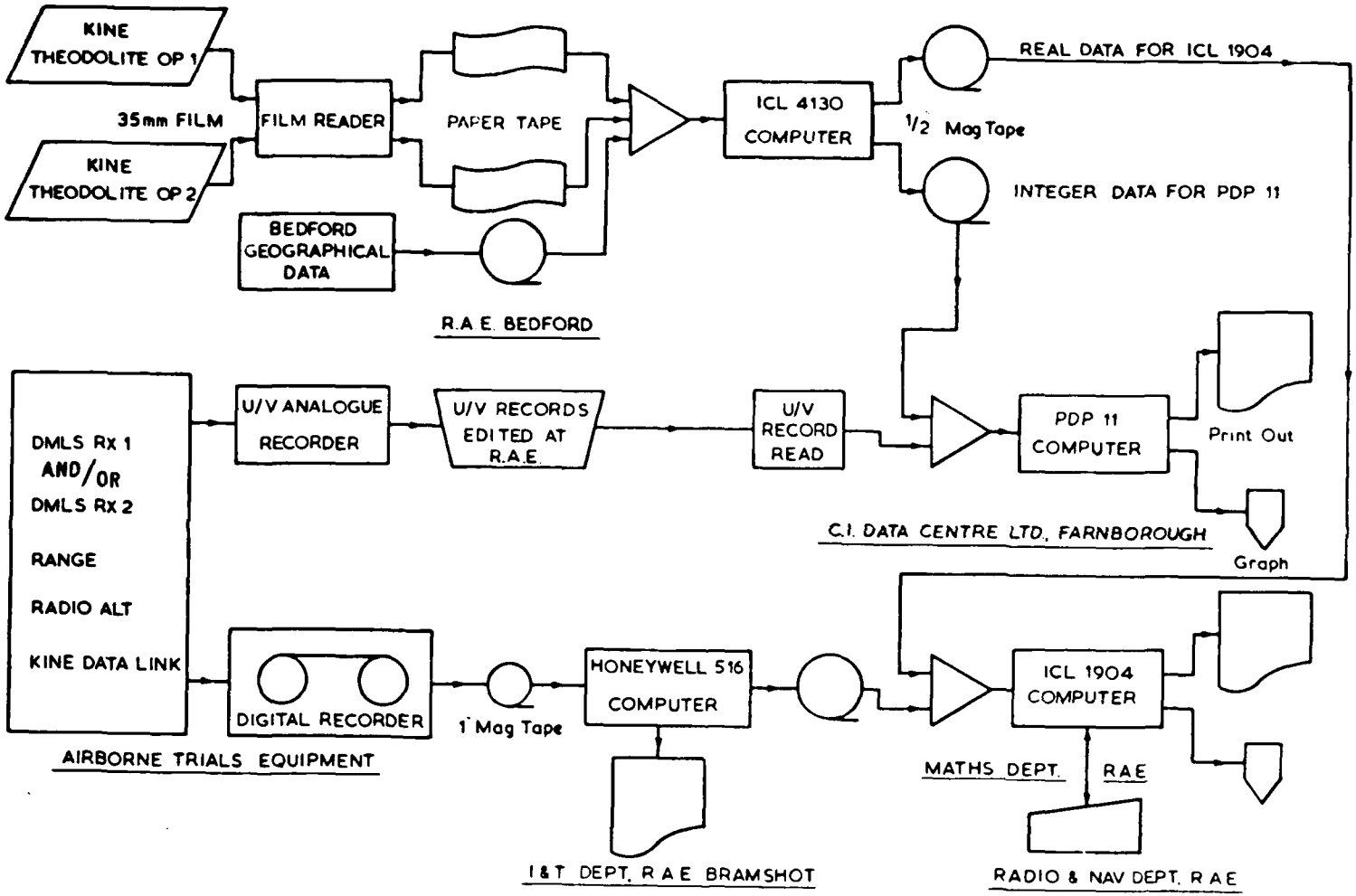

Fig C13 Data processing system diagram

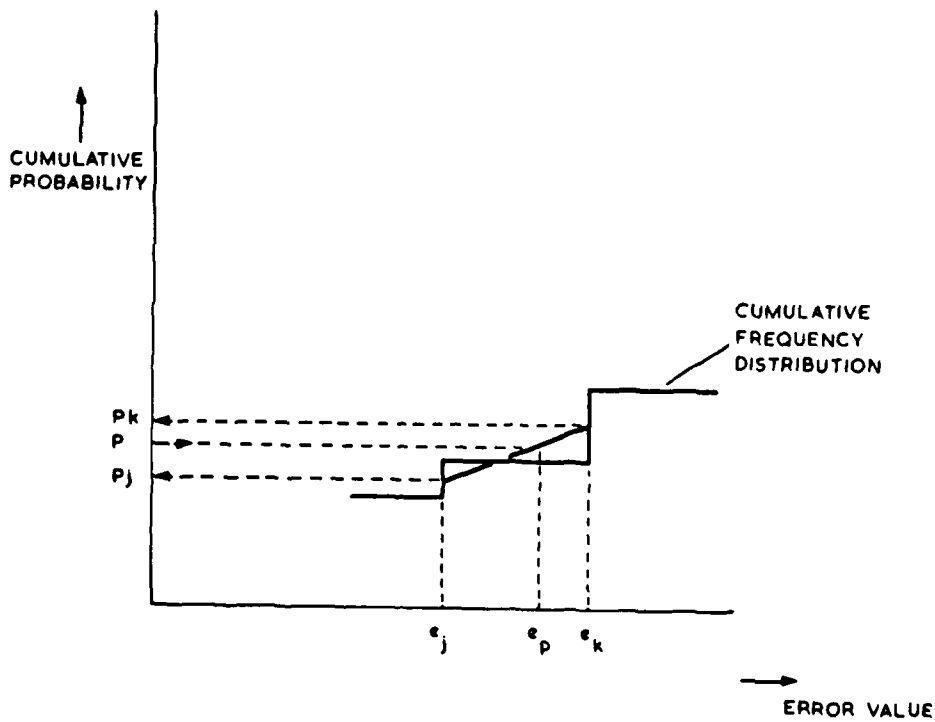

Fig C14 Percentiles estimate

GLOSSARY

AGC	automatic gain control
A/D	analogue to digital
ADF	automatic direction finder
AWOD mtg	All Weather Operations Divisional meeting
AWOP	All Weather Operations Panel
BAz	missed approach azimuth
CAA	Civil Aviation Authority
C band	5 GHz band
C/STOL	conventional/short take off and landing
D/A	digital to analogue
DME	distance measuring equipment
DMLS	Doppler microwave landing system
DPSK	differential phase shift keyed
El	elevation
FAA	Federal Aviation Authority
FAz	approach azimuth system
FDM	frequency division multiplex
FI	function identity
ICAO	International Civil Aviation Organisation
ILS	instrument landing system
Ku band	15 GHz band
MGA	minimum guidance altitude
OCI	out of coverage indication
OR	operational requirement
RAM	random access memory
RF	radio frequency
TDM	time division multiplex
TRSB	time reference scanning beam
TWA	travelling wave amplifier
VCO	voltage controlled oscillator
VOR	VHF omni range
VRPS	variable ratio power splitter
WGA	Working Group A

LIST OF SYMBOLS

a	spacing between TDM azimuth array and radome
b	spacing between TDM elevation reference element and the commutated array
B_N	a missed approach azimuth ground test point
C	velocity of propagation in air
d	physical distance of reference element from the end of the commutated array
D	d/λ
e	MLS error at a given measurement time
E	number of elements in the commutated array
E_N	an elevation system ground test point
F_D	Doppler frequency shift
F_e	'end fire' Doppler frequency
F_0	offset frequency
F_N	approach azimuth ground test point
h	height of a measurement point or the aircraft above local ground
I	length difference between simulated array cables
L	physical length of the array
L	length of array in wavelength
L_{EFF}	actual array length used for correlation in the correlation processor
m	mean of 50 consecutive error values
N	number of scans in a measurement period
R	range of measurement point
R_1	distance of aircraft from the reference antenna
R_2	distance of aircraft from the first element in the array
V	average velocity of commutation of the signal along the array
V_c	cable velocity constant
v	velocity of the aircraft
X,Y,Z	cartesian coordinates of position, X along the runway, Y orthogonal to the runway direction, and Z vertical
λ	operating frequency wavelength
θ	angle subtended by the aircraft at the array with relation to the array normal
ρ	reflection level of a multipath signal

79052

LIST OF SYMBOLS (concluded)

σ	standard deviation of a set of measurements
ω	angular frequency
ω_A	array signal angular frequency
ω_R	reference signal angular frequency
ω_0	offset frequency = $(\omega_A - \omega_R)$

REFERENCES

No.	Author	Title, etc
1	-	Doppler microwave landing guidance system. Proposal submitted by the UK to the International Civil Aviation Organisation, November 1975
2	J.M. Jones	Microwave landing system trials at Brussels National Airport, June 1977 and January 1978. RAE Technical Report (to be issued)
3	P.L. Gibson	Trials of the Doppler microwave landing system at London (Gatwick) Airport. RAE Technical Report 78124 (1978)
4	R. Matthews	Microwave landing system trials at Kristiansand, Norway, 1977, 1978. RAE Technical Report (to be issued)
5	D. Walker	Trials of the Doppler microwave landing system at Manchester International Airport, October/November 1977. RAE Technical Report 78144 (1978)
6	R. Matthews	Performance assessment trials of the Doppler microwave landing system at Berne Airport. RAE Technical Report (to be issued)
7	P.L. Gibson D. Walker	Comparative trials of the Doppler microwave landing system and the time reference scanning beam microwave landing system at the John F. Kennedy International Airport, New York. RAE Technical Report (to be issued)
8	R.B. Lumsden	Automatic landing trials at Berne (Belp) Airport using DMLS guidance. RAE Technical Report (to be issued)
9	R.B. Lumsden	Doppler microwave landing system trials at Tehran (Mehrabad) Airport January to February 1978. RAE Technical Report (to be issued)
10	R.B. Lumsden	Doppler MLS trial at Montreal (Dorval) Airport, April 1978. RAE Technical Report (to be issued)

REFERENCES (concluded)

No.	Author	Title, etc
11	J. Benjamin G.E.J. Peake (editors)	Contributions to the UK microwave landing system study (Phase I). RAE Technical Report 74050 (1974)
12	R. Matthews	Kinetheodolite system operational accuracy: Bedford runway 27. RAE Technical Report (to be issued)
13	G.E.J. Peake	Digital recording and processing of Doppler microwave landing system data. RAE Technical Memorandum Rad 1063 (1974)
14	P.W. James	Data processing for the UK Doppler microwave landing system trials. RAE Technical Memorandum Rad-Nav 54 (1977)

REPORT DOCUMENTATION PAGE

Overall security classification of this page

UNCLASSIFIED

As far as possible this page should contain only unclassified information. If it is necessary to enter classified information, the box above must be marked to indicate the classification, e.g. Restricted, Confidential or Secret.

1. DRIC Reference (to be added by DRIC)	2. Originator's Reference	3. Agency Reference	4. Report Security Classification/Marking
	RAE TR 79052	N/A	UNCLASSIFIED

5. DRIC Code for Originator	6. Originator (Corporate Author) Name and Location
7673000W	Royal Aircraft Establishment, Farnborough, Hants, UK
5a. Sponsoring Agency's Code	6a. Sponsoring Agency (Contract Authority) Name and Location
N/A	N/A

7. Title Contributions to the UK microwave landing system research and development programme 1974 to 1978

7a. (For Translations) Title in Foreign Language

7b. (For Conference Papers) Title, Place and Date of Conference

8. Author 1. Surname, Initials	9a. Author 2	9b. Authors 3, 4	10. Date	Pages	Refs.
Jones, J.M.	-	-	May 1979	651	14

11. Contract Number	12. Period	13. Project	14. Other Reference Nos.
N/A	N/A		Rad-Nav 79

15. Distribution statement
(a) Controlled by – ADXR R&N
(b) Special limitations (if any) –

16. Descriptors (Keywords) (Descriptors marked * are selected from TEST)
Landing systems. MLS. Microwave landing systems. Radio navigation. Multipath. Microwave propagation.

17. Abstract

In support of the UK MLS programme, Doppler Microwave Landing System (DMLS) equipment operating on both frequency division and time division multiplex formats has been extensively evaluated by means of analysis, ground and flight tests and hybrid simulation. The results of this programme have shown that the use of the Doppler technique leads to simple and reliable equipment with performance well inside the operational requirements. In particular, a full understanding of the possible environmental effects on system performance at 5 GHz has been obtained.

F5910/1

RAE Form A143

END

DATE
FILMED

12-80

DTIC